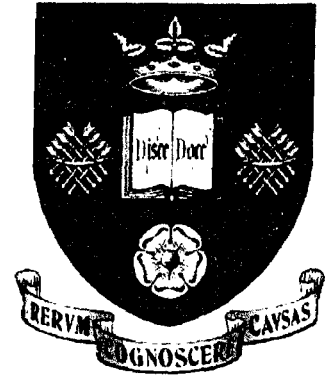


UNIVERSITY OF SHEFFIELD

*Department of Civil and Structural Engineering
& School of Architectural Studies*



**DEVELOPMENT OF A COMPONENT-BASED
MODEL OF STEEL BEAM-TO-COLUMN
JOINTS AT ELEVATED TEMPERATURES**

By Spyros Spyrou

A thesis submitted in partial fulfilment of the requirements for the
degree of Doctor of Philosophy

January 2002

SUMMARY

The response of steel-framed structures to applied loading depends to a large degree on the behaviour of the joints between the columns and beams. Traditionally designers have assumed that these joints act either as 'pinned', with no ability to transmit moments from beam to column, or as 'rigid', providing perfect continuity between the connected members. Advances in analysis, and developments in modern codes of practice, permit designers to account for the real behaviour of steel joints where this is known or can be predicted. Even though experimental studies of joints conducted at many research centres around the world have provided a large bank of test data, the vast number of variables in joints (beam and column sizes, plate thicknesses, bolt sizes and spacing, etc.) often means that data for a specific joint arrangement does not exist. As a result, researchers have turned their attention to ways of predicting the behaviour of such joints. One approach which has gained acceptance is based on the "Component Method" in which overall joint behaviour is assumed to be produced by the responses of its various simpler components.

To date, data on the response of joints at elevated temperatures has been gathered from full-scale furnace tests on cruciform arrangements, which have concentrated exclusively on moment-rotation behaviour in the absence of axial thrusts. However, when steel-framed structures are subjected to fire, the behaviour of the joints within the overall frame response is greatly affected by the high axial forces which are created by restraint to the thermal expansion of unprotected beams. If moment-rotation-thrust surfaces were to be generated this process would require prohibitive numbers of complex and expensive furnace tests for each joint configuration. The alternative, and more practical, method is to extend the Component Method to the elevated-temperature situation.

The basic theme of the Component Method is to consider any joint as an assembly of individual simple components. Each of these components is simply a non-linear spring, possessing its own level of strength and stiffness in tension, compression or shear, and these will degrade as its temperature rises. The main objective of this study was to investigate experimentally and analytically the behaviour of tension and compression zones of end-plate connections at elevated temperatures. A series of

experiments has been carried out and a simplified analytical model has been developed, and this has been validated against the tests and against detailed finite element simulations. The simplified model is shown to be very reliable for this very common type of joint, although similar methods will need to be developed for other configurations. The principles of the Component Method can be used directly in either simplified or finite element modelling, without attempting to predict of the overall joint behaviour in fire, to enable semi-rigid behaviour to be taken into account in the analytical fire engineering design of steel-framed and composite buildings.

CONTENTS

LIST OF FIGURES	viii
LIST OF TABLES	xviii
ACKNOWLEDGEMENTS	xx

CHAPTER 1

Introduction

1.1	Introduction	1
1.2	Structural Fire Protection	2
	1.2.1 Fire Safety Engineering	3
1.3	Background to the Study	4
	1.3.1 Ambient Temperature Semi-Rigid Design Process	5
	1.3.2 Elevated Temperatures Semi-Rigid Design Process	6
1.4	Scope of Research	7
1.5	Thesis Layout	8
1.6	References	10

CHAPTER 2

Beam-to-Column Steel Joints

2.1	Introduction	12
2.2	Global Analysis of Frame Structures	13
2.2.1	Joint Classification	16
2.3	Semi-Rigid Joints at Ambient Temperatures	18
2.4	Semi-Rigid Joints at Elevated Temperatures	20
2.5	“Component Method” at Ambient Temperature	23
2.6	References	27

CHAPTER 3

Test Apparatus for Elevated Temperature Testing

3.1	Introduction	31
3.2	Measurement Devices Used at Elevated Temperature Tests	31
3.3	Development of the Image Acquisition and Processing System	33
3.3.1	Pilot Tests	34
3.3.2	Experimental Results	37
3.4	Development of the Test Programme	39
3.4.1	CCD-Camera and Digital Image Processing	40
3.4.2	Furnace	41
3.4.3	Loading Device	43
3.4.4	Pilot Test to Check the Accuracy of the Image	

Processing Software	44
3.5 Test Procedure at Elevated Temperatures	48
3.6 Discussion	49
3.7 References	50

CHAPTER 4

Tension Zone

4.1 Introduction	52
4.2 Simplified Mathematical Model	54
4.2.1 Failure Mode 1-Bolts Start to Yield after the First Plastic Hinge has Formed	61
4.2.2 Failure Mode 1-Fracture of the Bolts after they Yield	63
4.2.3 Failure Mode 2-Formation of a Second Plastic Hinge at the Bolt Line	65
4.2.4 Failure Mode 2-Yielding of the Bolts after the Second Plastic Hinge at the Bolt Line	67
4.2.5 Failure Mode 2-Fracture of the Bolts after they Yielded	68
4.2.6 Failure Mode 3-Yielding and Fracture of the Bolts	69
4.3 Elevated Temperatures Model	70
4.3.1 Degradation of Steel Strength	70
4.3.2 Degradation of Steel Stiffness	70
4.3.3 Degradation of Bolts at Elevated Temperatures	72
4.3.3.1 Experimental Investigation of Grade 8.8 Bolts at Elevated Temperatures	73

4.4	Experimental Program	76
4.4.1	Phase A-T-stub Configurations	78
4.4.1	Phase B-Tests to Investigate Realistic Configurations	84
4.4.3	Phase C-Investigation Each of Failure Mode in more Detail	90
4.5	Finite Element Analysis	103
4.5.1	Ambient-Temperature Finite Element Analysis	103
4.5.2	Elevated-Temperatures Finite Element Analysis	107
4.6	Discussion	110
4.6.1	Image Acquisition and Processing Technique	110
4.6.2	Test and Theoretical Results	110
4.7	Conclusions	112
4.8	References	113

Chapter 5

Compression Zone

5.1	Introduction	116
5.2	Existing Analytical Models at Ambient Temperature	117
5.2.1	British Standard-BS5950	118
5.2.2	Eurocode 3:Annex J	121
5.3	Experimental Program	126
5.3.1	Experimental Investigation	128
5.4	2D-Finite Element Analysis	130
5.4.1	Finite Element Model	131

5.4.2	Finite Element Results	132
5.4.3	Comparison of Test and Finite Element Results	133
5.5	Simplified Model	137
5.5.1	Analytical Model at Elevated Temperatures	138
5.6	Results and Comments	146
5.6.1	Phase A Test Results	151
5.6.2	Phase B Test Results	155
5.6.3	Phase C Test Results	158
5.6.4	Phase D Test Results	160
5.6.5	Random Specimens Test Results	162
5.7	Conclusions	166
5.8	References	168

CHAPTER 6

Steel Joint Modelling

6.1	Introduction	171
6.1.1	Global Models	172
6.1.2	Mechanical Models	176
6.1.3	Finite Element Analysis	178
6.1.4	Summary of joint modelling techniques and approaches methods	181
6.2	Elevated Temperatures Spring Stiffness Model	182
6.3	Validation of Joint Model	185
6.4	Conclusions	192

6.5	References	194
-----	------------	-----

CHAPTER 7

Steel Joint Moment-Rotation-Thrust Response

7.1	Introduction	199
7.2	Moment-Rotation-Thrust Model	201
7.3	Description of the Finite Element Program Vulcan	204
	7.3.1 Parametric Studies on Sub-Frame Arrangement	205
7.4	Conclusions	211
7.5	References	212

CHAPTER 8

Conclusions and Further Recommendations

8.1	Introduction	214
8.2	Experimental and Analytical Investigation on Components	215
	8.2.1 Instrumentation and Testing Arrangement	215
	8.2.2 Tension Zone	217
	8.2.3 Compression Zone	220
8.3	Joint Modelling and Frame Response	221
8.4	Recommendations for Further Work	222

8.5	References	225
-----	------------	-----

APPENDIX A

Test Apparatus for Elevated Temperature Testing

A.1	Testing Arrangement	227
A.2	Image acquisition and processing system details and specifications	230

APPENDIX B

Geometrical, Mechanical Properties and Test Data for the T-Stub Specimens

B.1	Geometrical Properties	235
B.2	Actual Test Data and Material Properties	246

APPENDIX C

Geometrical, Mechanical Properties and Test Data for the Column Web specimens

C.1	Geometrical, Mechanical and Experimental Data	249
-----	---	-----

LIST OF FIGURES

Figure 2.1	Different types of connections in a building frame	12
Figure 2.2	Joints and connections-single sided joint configuration	13
Figure 2.3	Modelling joints for elastic global analysis	14
Figure 2.4	Typical beam-to-column joints and a diagrammatic stiffness classification	17
Figure 2.5	Strength classification boundaries	17
Figure 2.6	The three zones and their components within an end-plate steel joint	23
Figure 2.7	Application of the component method to a welded joint (after Jaspart)	25
Figure 3.1	The T-stub model used in ambient temperature pilot tests	35
Figure 3.2	Typical deformation of a T-stub specimen at ambient temperature	36
Figure 3.3	Force deflection curve for pilot test No.1	37
Figure 3.4	Force deflection curve for pilot test No. 2	38
Figure 3.5	T-stub specimen at 100°C and at 700°C	39
Figure 3.6	Schematic diagram of the image acquisition and processing system.	41
Figure 3.7	Furnace with the view-ports	42
Figure 3.8	Arrangement for the experimental work.	43

Figure 3.9 Calibration device and a typical measurement image from camera one	44
Figure 3.10 Calibration of the processing system	45
Figure 3.11 Comparison of the real readings with the image processing readings	46
Figure 3.12 Influence of linear sub-pixel division on the accuracy of the readings	47
Figure 4.1 The three zones in an end-plate joint	52
Figure 4.2 T-stub identification and orientation for extended end-plate joint	53
Figure 4.3 Equivalent Column Flange and End Plate T-stubs respectively	55
Figure 4.4 Failure modes for the T-stub flange	56
Figure 4.5 Forces on T-stub assembly	56
Figure 4.6 Detail of a bolt within an end plate to column T-stub connection	59
Figure 4.7 System for calculating the final displacement	63
Figure 4.8 Free body diagram for half of the T-stub flange	65
Figure 4.9 Comparison between bolt and steel Strength Reduction Factors	72
Figure 4.10 Diagram for the instrumentation system adopted for the experiments on Grade 8.8 bolt steel	73
Figure 4.11 Tangential halogen lamp furnace	75
Figure 4.12 Typical test image for Failure Mode 1	76
Figure 4.13 Typical test image for Failure Mode 2	77
Figure 4.14 Typical test image for Failure Mode 3	77
Figure 4.15 Typical T-stub assembly used in Phase A experiments	78

Figure 4.16 Typical distorted images at 570 °C	79
Figure 4.17 Force-deflection curves for test programme AA	80
Figure 4.18 Force-deflection curves for test programme AB	81
Figure 4.19 Force-deflection curves for test programme AC	82
Figure 4.20 Typical image showing Failure Mode 2	83
Figure 4.21 Typical T-stub assembly used in Phase B and C experiments	84
Figure 4.22 Orientation of the cameras	85
Figure 4.23 Force-deflection curves for the column T-stub for test programme BA	86
Figure 4.24 Force-deflection curves for end plate T-stub for test programme BA	87
Figure 4.25 Force-deflection curves for the column T-stub for test programme BB	88
Figure 4.26 Force-deflection curves for end plate T-stub for test programme BB	89
Figure 4.27 Typical image showing Failure Mode 1	91
Figure 4.28 Bolt failure in a combination of shear and tension force	91
Figure 4.29 Image at 650 °C just before bolt failure at 160 kN	92
Figure 4.30 Force-deflection curves for the column T-stub for test programme CA	95
Figure 4.31 Force-deflection curves for the column T-stub for test programme CB	96
Figure 4.32 Force-deflection curves for the column T-stub for test programme CC	97
Figure 4.33 Force-deflection curves for end plate T-stub for test programme CC	98

Figure 4.34 Force-deflection curves for the column T-stub for test programme CD	99
Figure 4.35 Force-deflection curves for end plate T-stub for test programme CD	100
Figure 4.36 Force-deflection curves for the column T-stub for test programme CE	101
Figure 4.37 Force-deflection curves for end plate T-stub for test programme CE	102
Figure 4.38 Finite element discretisation of the T-stub model	104
Figure 4.39 Thickness values of the finite element mesh	105
Figure 4.40 Typical stress-strain curve for the T-stub flange at elevated temperatures according to EC3: Part 1.2	106
Figure 4.41 Force-deflection curves for a column T-stub from Test Group CE	106
Figure 4.42 Von-Misses stresses for a 240kN tension load	107
Figure 4.43 Force-deflection curves for a column T-stub at 410 °C from Test Group CE	108
Figure 4.44 Force-deflection curves for a column T-stub at 660 °C from Test Group CA	108
Figure 4.45 Von-Misses stresses for a 170kN tension load at 660 °C for Test Group CA	109
Figure 4.46 Nut stripping failure mechanism	110
Figure 4.47 Failure modes compared at 505 °C	111

Figure 5.1	Extended endplate joint showing the column web component (shaded)	116
Figure 5.2	Assumed distribution of force for web crushing according to BS5950	119
Figure 5.3	Effective breadth for web resistance in BS5950	120
Figure 5.4	Effective breadth for web buckling resistance in Eurocode 3	122
Figure 5.5	Eurocode 3-Annex J results	125
Figure 5.6	BS5950 results	125
Figure 5.7	Arrangement for compression zone tests	126
Figure 5.8	Column specimen inside the furnace	127
Figure 5.9	Displacement measurement	127
Figure 5.10	Thermocouple positions	128
Figure 5.11	Finite element discretisation of the compression model	130
Figure 5.12	Thickness values used in the finite element mesh	131
Figure 5.13	The stress-strain curves for the column flange and web	132
Figure 5.14	Von-Misses stress distributions for 112,5 kN and 125 kN at 610 °C	132
Figure 5.15	Y-direction (vertical) stress showing the plastic hinges in the flange	133
Figure 5.16	ANSYS and test results at ambient temperature	134
Figure 5.17	ANSYS and test results at 400 °C	134
Figure 5.18	ANSYS and test results at 520 °C	134
Figure 5.19	ANSYS and test results at 610 °C	135
Figure 5.20	ANSYS and test results at 670 °C	135
Figure 5.21	ANSYS and test results at 765 °C	135
Figure 5.22	Column web subjected to patch loads	136

Figure 5.23 Different values of uniform distributed load length c at ambient temperature	137
Figure 5.24 Assumed mechanism of web yielding	138
Figure 5.25 First yielding of the column web	140
Figure 5.26 Effective length of the compressed web	141
Figure 5.27 Second yielding of the system	141
Figure 5.28 Yielding mechanism	142
Figure 5.29 Typical test and Eurocode 3-Annex J results for UC152x152x30	147
Figure 5.30 Test, Equation 5.15 and new Equation 5.16 results for UC152x152x30	148
Figure 5.31 Test, Equation 5.15 and new Equation 5.16 results for UC203x203x46	149
Figure 5.32 Test, Equation 5.15 and new Equation 5.16 results for UC203x203x71	149
Figure 5.33 Test, Equation 5.15 and new Equation 5.16 results for UC203x203x86	149
Figure 5.34 Normalised force against temperature	150
Figure 5.35 Force-deflection curves at 20 °C	151
Figure 5.36 Force-deflection curves at 410 °C	152
Figure 5.37 Force-deflection curves at 500 °C	152
Figure 5.38 Force-deflection curves at 500 °C	152
Figure 5.39 Force-deflection curves at 600 °C	153
Figure 5.40 Force-deflection curves at 610 °C	153
Figure 5.41 Force-deflection curves at 710 °C	153
Figure 5.42 Force-deflection curves at 755 °C	154

Figure 5.43 (a) S-shape buckling deflection and (b) Local buckling deflection of the column web	154
Figure 5.44 Force-deflection curves at 20 °C	155
Figure 5.45 Force-deflection curves at 280 °C	155
Figure 5.46 Force-deflection curves at 400 °C	156
Figure 5.47 Force-deflection curves at 520 °C	156
Figure 5.48 Force-deflection curves at 610 °C	156
Figure 5.49 Force-deflection curves at 670 °C	157
Figure 5.50 Force-deflection curves at 765 °C	157
Figure 5.51 Force-deflection curves at 20 °C	158
Figure 5.52 Force-deflection curves at 535 °C	158
Figure 5.53 Force-deflection curves at 635 °C	158
Figure 5.54 Force-deflection curves at 755 °C	159
Figure 5.55 Test at Ambient Temperatures	159
Figure 5.56 Position of the flange LVDT on the roller	160
Figure 5.57 Force-deflection curves at 20 °C	160
Figure 5.58 Force-deflection curves at 20 °C	161
Figure 5.59 Force-deflection curves at 585 °C	161
Figure 5.60 Force-deflection curves at 650 °C	161
Figure 5.61 Force-deflection curves at 705 °C	162
Figure 5.62 Force-deflection curves at 750 °C	162
Figure 5.63 Force-deflection curves for UC203x203x52 at 610 °C	163
Figure 5.64 Force-deflection curves for UC203x203x60 at 20 °C	163
Figure 5.65 Force-deflection curves for UC203x203x86 at 20 °C	163
Figure 5.66 Force-deflection curves for UC254x254x107 at 20 °C	164
Figure 5.67 Influence of the c value on the UC203x203x46 specimen at ambient temperature	165

Figure 5.68 Influence of the c value on the UC203x203x46 specimen at 610 °C	165
Figure 6.1 Idealised bare-steel spring stiffness model	184
Figure 6.2 Elevated temperature flush end plate joint test arrangement	186
Figure 6.3 Bare steel flush end plate joint detail	187
Figure 6.4 Plan and overall view of the effective T-stub arrangements used for the simplified analysis	188
Figure 6.5 Comparison of the actual test and simplified model results from Al-Jabri fire tests on bare-steel flush end plate joints	189
Figure 6.6 Comparison of ambient temperature model results with Leston-Jone's flush end plate tests	190
Figure 6.7 Comparison of results for 5kNm moment	191
Figure 6.8 Comparison of results for 10kNm moment	191
Figure 6.9 Comparison of results for 15kNm moment	191
Figure 6.10 Comparison of results for 20kNm moment	191
Figure 6.11 Comparison of results for 25kNm moment	192
Figure 7.1 Moment-Rotation and Moment-Rotation-Thrust configuration of a steel joint	200
Figure 7.2 Idealised bare-steel spring stiffness model	202
Figure 7.3 Load-deformation characteristics of the tension and compression zones	202
Figure 7.4 Idealised bare-steel moment-axial force model	203

Figure 7.5 Influence of axial force on rotation behaviour at ambient temperature	204
Figure 7.6 Sub-frame idealisations considered in BS5950	206
Figure 7.7 Testing arrangement	207
Figure 7.8 Flush end plate joint configuration	208
Figure 7.9 Ramberg-Osgood curves at elevated temperatures	208
Figure 7.10 Axial forces in beam at elevated temperatures (Positive=tension)	209
Figure 7.11 Influence of axial force on joint behaviour at 500 °C	209
Figure 7.12 Comparison of frame response when axial forces are considered	210
Figure 8.1 Failure modes for the T-stub flange	218
Figure 8.2 T-stub identification and orientation for extended end-plate joint	218
Figure 8.3 Joint modelling for finite element analysis of frames under fire conditions	223
Figure A.1 (a) Furnace and reaction frame layout (b) Loading device and view ports for the video cameras arrangement	227
Figure A.2 Electric furnace specifications and fabrication drawings	228
Figure A.3 Reaction frame and hydraulic jack fabrication details	229
Figure A.4 Schematic diagram of the image acquisition and processing system	230

Figure B.1 Arrangement of the T-stub specimen	235
Figure B.2 Plan view arrangement of the T-stub specimen	235
Figure B.3 Bolts, Nuts and Washers	236
Figure C.1 Universal Column Section	249

LIST OF TABLES

Table 1.1. Active and Passive measures	2
Table 2.1. Zones within the joint and their components	24
Table 3.1. Mean value, Standard deviation and Standard error with and without	48
Table 4.1. Reduction factors for stress-strain curves of steel at elevated temperatures	71
Table 5.1. Comparison of column web compression resistances (in kN) for a point load (S275 steel)	123
Table 5.2. Different column sections tested at elevated temperatures	129
Table 5.3. Comparison of tests and EC3: Annex J results at ambient temperature	147
Table 6.1. Principal zones within a steel joint	183

Table 6.2. Principal components within the compression and tension zone of a steel joint	188
Table A.1 Monochrome video cameras specifications	231
Table A.2 Frame Grabber specifications	232
Table A.3 C-Mount Lenses specifications	233
Table B.1 Geometrical Properties of specimens for Phase A	237
Table B.2 Geometrical Properties of specimens for Phase B	238
Table B.3 Geometrical Properties of specimens for Phase C	239
Table B.4 Geometrical Properties of specimens for Phase A	241
Table B.5 Geometrical Properties of specimens for Phase B	242
Table B.6 Geometrical Properties of specimens for Phase C	243
Table B.7 Bolt Geometrical Properties for all the specimens	245
Table B.8 Test Data	247
Table B.9 Material Properties	248
Table C.1 Geometrical Data	250
Table C.2 Mechanical Properties	251
Table C.3 Experimental Data	252

ACKNOWLEDGEMENTS

The Author thanks Dr. Buick Davison, Prof. Ian Burgess and Prof. Roger Plank for their supervision and support throughout this research project. Without their guidance and excellent human approach, in difficult times, this project would not have been completed in time. The financial support of EPSRC under a CASE award is gratefully acknowledged.

My special thanks to Jonathan Wood, Shane Smith, Shaun Waters, Glenn Brawn and other technical staff at the University of Sheffield for their advice, comment and continued commitment of time and resources in the development of experimental steel joint component characteristics at elevated temperatures.

Mr. Ahmed Allam is gratefully thanked for his co-operation and valuable support.

The continued encouragement and support of my family, friends, Maria and Antonis will always be remembered.

DECLARATION

Except where specific reference has been made to the work of others, this thesis is the result of my own work. No part of it has been submitted to any University for a degree, diploma, or other qualification.

Spyros Spyrou

Chapter 1

Introduction

1.1 INTRODUCTION

Historically, concern with fire protection has tended to follow the occurrence of disasters, and the main objectives of fire prevention are seen as the protection of life and property^{1,1,1,2}. Noticeable progress has been made in the understanding of structural fire protection since the earliest attempts to implement fire safety. The establishment of the British Fire Protection Committee (BFPC) at the end of the 19th century marks the beginning of a scientific approach to research into structural fire resistance. The first concern when considering structural fire protection was to ensure stability of the structure. However, over the years fire protection has developed into a strategy of which the five main objectives are^{1,1}:

- a) Preventing the initiation of fire
- b) Restricting the growth and spread of fire
- c) Containment of fire within specified boundaries a compartment forming part of a building or the whole building
- d) Provision of means of escape for the occupants of the building, and
- e) The control of fire by automatic devices and by active fire fighting.

The fire protection objectives are fulfilled by taking into account passive as well as active measures. Passive measures are part of the built system and are in operation at all times, whereas active measures come into operation only in the event of a fire. Passive measures include building layout, design and construction, while active measures comprise fire detection and fire control systems.

Table 1.1 below shows the principal active and passive measures.

Table 1.1. Active and Passive measures

<i>Active measures</i>	<i>Passive measures</i>
Detection	Contents and linings
Alarms	Escape provisions
Sprinklers	Compartmentation
Fire fighting	Structural Protection

Looking closer into the structural fire protection, the main objectives are to:

- a) Maintain the integrity of safe areas in a building
- b) Restrict the size of fire and
- c) Prevent the building structure from becoming unstable.

The second is concerned with the division of buildings into smaller compartments to enable an easier control of fire. The third objective has sometimes been considered to be the sole aim of structural fire protection. Retention of structural stability is essential to achieve the other objectives, as it allows an easier control of fire.

1.2 STRUCTURAL FIRE PROTECTION

For steel framed structures the most familiar method of providing adequate structural fire protection is to use some form of insulating material, with the aim of limiting the temperature of the steel so that sufficient strength is retained. This has led to the production of a variety of protective materials for coating, spraying or encasing members^{1.3}.

Building Regulations^{1.4,1.5} require that "*The building shall be designed and constructed so that, in the event of fire, its stability will be maintained for a reasonable period.*" Design codes for the structural fire resistance of steel structures have traditionally adopted a prescriptive approach for determining fire protection requirements^{1.6}, although more recent methods^{1.7,1.8} have introduced means to

calculate periods of fire resistance. These generally relate to isolated elements, and are based primarily on the results of experimental studies.

The provision of fire protection is a costly aspect in the construction of steel structures. Also there are secondary costs associated with time delays because the application of fire protection may hinder the progress of construction. This offsets many of the advantages associated with steel-framed construction.

From an engineering point of view it is more logical to design the structure to withstand fire without protection rather than designing the structure for normal conditions and then applying protection. Therefore in recent years there has been much interest in understanding the response of different structural elements under fire conditions, either in isolation or as a part of a more complete structure. This facilitates the development of new engineering methods of analysis and design taking into account any inherent fire resistance of the structural steel, reducing protection costs and construction time. This new engineering method, which is called Structural Fire Engineering, is a part of Fire Safety Engineering.

1.2.1 Fire Safety Engineering

The rapid changes in how buildings are designed, constructed and used by occupants has created a situation where it is sometimes difficult to satisfy the provisions of fire safety requirements, given in Approved Documents, Technical Standards and Technical Booklets. Increased understanding of the behaviour of elements or frames under fire conditions has led many authorities (e.g. building control, insurance and any other authorities which enforce safety legislations) to acknowledge that improvements in fire safety may now be possible by adopting analytical approaches^{1,9}.

Fire safety engineering is an approach which uses, in the most effective way, all the available methods for preventing, controlling or limiting the consequences of fire. In terms of structural stability, Structural Fire Engineering uses a scientific approach, which ensures that fire resistance is provided where it is needed. There are three stages in the process of achieving safety and cost effectiveness in a Structural Fire Engineering design of a building:

- a) Predicting the heating rate and maximum atmosphere temperature inside the compartment. This involves identifying and assessing the three main parameters which influence the severity of a fire in a given compartment, *fire load* (quantity, type, distribution), *ventilation* (area, height, location) and *compartment* (size-floor area, surface area, shape, thermal characteristics).
- b) Calculating the temperature of the steel member, which depends on the location, the section size and shape, and any protection applied.
- c) Analysing the stability of the structure, which depends not only on the temperature it reaches during a fire but also on the applied load and the effects of any composite action, restraint and continuity from the remainder of the structure^{1,10}.

In light of the foregoing it is clear that designers and developers are looking for the most cost effective solutions, and these solutions could be the result of a better understanding of how the structural frame behaves under fire conditions without any fire protection to its members. In order to construct a frame, joints are necessary to provide continuity to the structure, and hence their behaviour affects the local and/or global behaviour of the structural frame. This conclusion leads to the purpose of the current study, which concerns the behaviour of steel beam-to-column joints in frames under fire conditions.

1.3 BACKGROUND TO THE STUDY

Part of a design process is to analyse a frame to determine its structural usefulness and to compare the predicted behaviour with the required performance in terms of loading and deformation. To construct load-deformation curves for each structure would be desirable, because these would contain all the information necessary for checking the structural behaviour. However such curves are more or less non-linear from the very beginning because of second order geometrical effects and material non-linearities. Later the slope of the curve is further reduced because of local plastification or of some instability phenomena. The situation becomes more complicated as structures contain real joints, which are different from the ideal ones,

hinged and rigid. Ten years ago the concept of using realistic joint behaviour in the design process at ambient temperature, now known as semi-rigid behaviour, first appeared in Eurocode 3.

1.3.1 Ambient temperature semi-rigid design process

Semi-rigid behaviour means that a joint can withstand levels of rotation and moment, in contrast to the “fixed” or “pinned” behaviour usually considered in the design process. This new concept resulted in the realisation that the joint behaviour is a valid part of the whole structural response and should not be ignored in a global frame analysis. Using the semi-rigid characteristics of joints, designers can perform global structural analyses and take into consideration the limit states’ requirements, for both the members and the joints. The new modelling approach is desirable for several reasons, such as:

- a) Engineering efficiency
- b) Precision and accuracy, and
- c) Economics

These reasons gave support for a very comprehensive study (COST Action C1 from 1991 to 1999)^{1,11} which looked into establishing a unified approach for modelling the connection behaviour of joints in engineering structures. In COST Action C1 twenty-three countries participated, and the main objectives were to investigate semi-rigid action experimentally and analytically, and finally propose simplified models for the joint behaviour in each of the material types (concrete, steel, timber and composite). The impact of COST Action C1, especially in the field of steel and composite joints, was to establish code regulations such as EC3 Annex J^{1,12} for steel joints.

In summary, at ambient temperatures extensive experimental data, finite element analysis and simplified models now exist that describe the moment-rotation characteristics for different joint arrangements. Designers, with the help of EC3: Annex J can predict the moment-rotation characteristics for a steel joint, and

introduce this response into a global frame analysis to simulate the real behaviour of the frame.

1.3.2 Elevated temperatures semi-rigid design process

Unfortunately the same cannot be said for joints at elevated temperatures because there is a very small amount of experimental data^{1.13,1.14,1.15} that can help researchers understand the behaviour of joints, in order to develop simplified or analytical models. Also from the Cardington^{1.16} full-scale frame fire tests it was observed that large axial forces were developed in the beams due to restraint to thermal expansion. This observation suggests that it is inadequate to place reliance solely on moment-rotation characteristics of steel joints, as found from furnace tests or numerical modelling.

As a result the modelling of elevated-temperature joint response has not been addressed to date by any design standards or codes. Development of sufficiently accurate methods of predicting joint response will be instrumental in the future use of semi-rigid characteristics for fire limit state design. The number of tests required to define accurately moment-rotation-thrust-temperature characteristics by experimental means is prohibitive, even for a single joint.

The modelling of elevated-temperature joint response may follow one of two paths:

- a) Developing joint models that allow the prediction of elevated-temperature behaviour, following the full range of joint response,
- b) Incorporating degradation characteristics into existing ambient-temperature test data.

In the current study the former approach was adopted, and a simplified model has been derived that predicts the moment-rotation-temperature characteristics for a joint from only its geometrical and mechanical properties. The second approach is attractive, as it would use the extensive ambient temperature data that already exists. The only problem is that these ambient temperature tests do not include the axial forces which can develop at elevated temperatures. However, in both of these

approaches understanding the behaviour of the components within the joint's tension and compression zones is of primary importance.

1.4 SCOPE OF RESEARCH

Design codes do not address properly the behaviour of steel joints at elevated temperatures, due in part to the lack of experimental data. The use of numerical models is also limited, since the degradation of the joint characteristics at elevated temperatures has to be based on empirical relationships postulated either from ambient-temperature tests or from the small amount of elevated-temperature data currently available.

Recent experimental studies^{1.14,1.15} on small-scale joint specimens (exclusively concentrated on moment-rotation-temperature behaviour in the absence of axial thrust due to thermal expansion restraint of the beam) have shown that it is possible to derive moment-rotation characteristics at elevated temperatures. However the large number of tests needed to achieve full moment-rotation-temperature relationships for a single joint demonstrated the inherent difficulty in this approach.

The primary objective of the present investigation is to establish a simplified model that can predict full moment-rotation-temperature characteristics just from the geometrical and mechanical properties of a typical bare-steel joint, which will in principle establish the modelling technique for other types of joints. In order to fulfil the above objective the principles of the "Component Method"^{1.12,1.17} were used. The method considers any joint as a set of individual basic components, resulting principally from the action of tension and compression forces, and then these components are assembled in a way which models their interaction in the joint.

The components within the tension and compression zone were investigated experimentally using a purpose-built testing technique and arrangement. Furthermore, analytical and simplified models were derived which predict the ultimate failure behaviour of individual or groups of components. Finally, a component-based model was developed, and moment-rotation-temperature

characteristics were evaluated and compared against test results^{1.14,1.15} for a typical end plate joint.

The results from such component tests will be of value to other researchers, especially those developing numerical modelling approaches to the behaviour of individual or groups of components at elevated temperatures, aiming to model the overall behaviour of a joint without resort to numerous tests for each type of joint at different temperatures.

On the other hand, when real steel-framed structures are subjected to fire, the behaviour of the joints within the overall frame response is greatly affected by the high axial forces, which are created by restraint to the thermal expansion of unprotected beams. If now moment-rotation-thrust-temperature surfaces were to be generated this process would require prohibitive numbers of complex and expensive furnace tests and unlimited number of component-based model runs in order to predict the overall behaviour of a typical joint configuration. The ultimate goal of this study is to investigate the potential of using the principles of the “Component Method” in a way that the non-linear characteristics of each component can directly be used in either simplified or finite element modelling, without attempting to predict the overall joint behaviour in fire, enabling the semi-rigid behaviour to be taken into account in the analytical fire engineering design of steel-framed and composite buildings.

1.5 THESIS LAYOUT

The thesis consists of eight chapters as described below:

Chapter 2 looks closely into the concepts of “*connection*” and “*joint*” and describes the meaning of “*rigid*”, “*simple*” and “*semi-rigid*” joint action in the context of frame response when analytical methods are considered. A literature review is also presented for the semi-rigid joint action at ambient and elevated temperatures. Finally an introduction to the “*Component Method*” is made.

Chapter 3 describes the testing arrangement, and the development of a displacement measurement technique (image acquisition and processing technique) that was used to investigate experimentally the behaviour of components within a steel joint at elevated temperatures. The advantages of using an image acquisition and processing technique over more conventional methods of displacement measurements are discussed.

Chapter 4 describes the test procedure and results for ten series of tests (tension zone components within a steel joint), where the main objective is to investigate the different ultimate failure modes of T-stub specimens. Also a simplified model is developed which is capable of predicting the ultimate behaviour of these T-stubs at elevated temperatures, and furthermore a 2-D finite element analysis is presented. Finally an experimental investigation of the behaviour of Grade 8.8 bolts under tension forces at elevated temperatures is described.

Chapter 5 continues the experimental investigation into the behaviour of the column web component under transverse compression forces. An analytical investigation and a semi-empirical model are presented for the prediction of the column web component behaviour.

In Chapter 6 a simple component-based model capable of defining the complete range of joint response is described. Comparison is made between the results obtained from the proposed model and those from the bare steel flexible end plate fire tests performed by Leston-Jones^{1,14} and Al-Jabri^{1,15}.

In Chapter 7 the influence of the axial forces developed in a heated beam due to the restraint to thermal expansion on joint response is highlighted. A small 2-D frame finite element analysis is also performed using VULCAN in order to show the influence of these axial forces on the frame response.

Finally, in Chapter 8 general conclusions are drawn, and recommendations for future work are presented.

1.6 REFERENCES

- 1.1 Malhotra, H.L., "*Design of Fire-Resisting Structures*", Surrey University Press, 1982.
- 1.2 Munro, J.R., "*A History of Fire Prevention in Buildings*", The Architect and Surveyor, pp. 17-20, June, 1970, pp. 17-19, August, 1970.
- 1.3 "*Fire Protection of Structural Steel in Buildings*", 2nd Edition, Association of Structural Fire protection Contractors and Manufacturers Limited and the Steel Construction Institute, UK, 1989.
- 1.4 "*The Building Regulations 1991: Approved Document B: Fire Safety*", Department of the Environment, Transport and the Regions 1991.
- 1.5 "*The Building Regulations 2000 Edition: Approved Document B: Fire Safety*", Department of the Environment, Transport and the Regions 2000.
- 1.6 "*BS 449: The Use of Structural Steel in Building*", BSI, London, 1969.
- 1.7 "*BS 5950, Structural Use of Steelwork in Buildings*", Part 8: Code of Practice for fire Resistant Design, BSI, London, 1990.
- 1.8 "*Eurocode 3: Design of Steel Structures, Part 1.2: Structural Fire Design*", European Committee for Standardisation, 1993.
- 1.9 J. Robinson, and J. Dowling, "*Fire Resistance of Steel Framed Buildings*", British Steel, 1997 Edition.
- 1.10 El-Rimawi, J.A., "*The Behaviour of Flexural Members under Fire Conditions*", PhD. Thesis, Department of Civil and Structural Engineering, University of Sheffield, 1989.
- 1.11 "*Control of the Semi-Rigid Behaviour of Civil Engineering Structural Connections*", European Commission, EUR 19244, COST Action C1, Final Report, 1999.
- 1.12 "*EC3: Design of Steel Structures, Part 1.1: Revised Annex J Joints and Building Frames*", (Draft), Document CEN/TC250/SC3 N419E, European Committee for Standardization, 1994.

- 1.13 Lawson, R.M., "*Behaviour of Steel Beam-to-Column Connections in Fire*", *The Structural Engineer*, Vol. 68, No. 14, pp. 263-271, 1990.
- 1.14 Leston-Jones, L.C., "*The Influence of Semi-Rigid Connections on the Performance of Steel Framed Structures in Fire*", Ph.D. Thesis, Department of Civil and Structural Engineering, University of Sheffield, 1997.
- 1.15 Al-Jabri, K.S., "*The Behaviour of Steel and Composite Beam-Column Connections in Fire*", Ph.D. Thesis, Department of Civil and Structural Engineering, University of Sheffield, 1999.
- 1.16 Moore, D.B., and Lennon, T. "*Fire Engineering Design of Steel Structures*", *Progress in Structural Engineering*, Vol. I (I), pp. 4-9, 1997.
- 1.17 Jaspart, J.P., Weynand, K., and Steenhuis, M., "*The Stiffness Model of Revised Annex J of Eurocode 3*", *Connections in Steel Structures III-Behaviour, strength & design*, Proceedings of the third International Workshop, Italy, 1995.

Chapter 2

Beam-to-Column Steel Joints

2.1 INTRODUCTION

“A steel frame structure is a complex assembly of many individual members joined to form a working unit in which component elements are designed to resist the factored loads acting on the structure”.^{2.1}

Structural steel frames usually consist of universal beams and columns assembled together by means of connections at points such as those shown in Figure 2.1. These connections are between columns, beams, column-and-beam and between column-and-foundation.

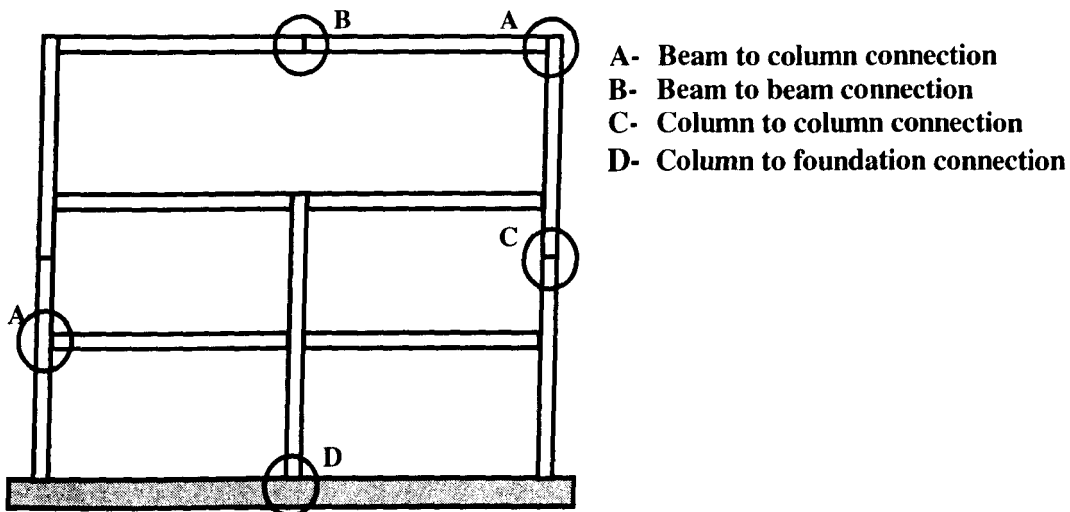


Figure 2.1 Different types of connections in a building frame

As explained by J-P. Jaspart^{2.2} in one of his lectures about designing and analysing joints, with today's understanding of frame response there is a need to define exactly

what is a “*connection*” and what is a “*joint*” within a building frame. A *connection* is defined as “the set of the physical components which mechanically fasten the connected elements”. One considers the connection to be concentrated at the location where the fastening action occurs, for instance at the beam end/column interface in a major-axis beam-to-column joint. When both the connection and the corresponding zone of interaction between connected members are considered together, the wording *joint* is then used (Figure 2.2).

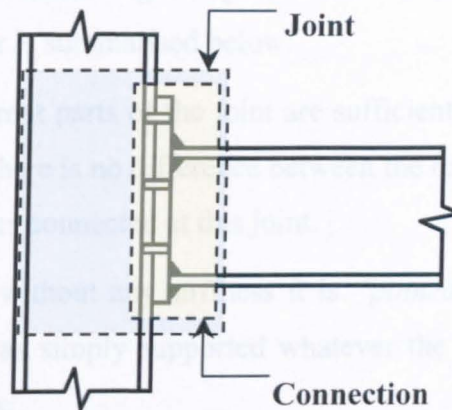


Figure 2.2 Joints and connections-single sided joint configuration

Since frame members and joints are the basic and integrated parts of a steel frame, their behaviour and effects on the overall frame’s performance cannot be ignored in the global analysis of the structure.

2.2 GLOBAL ANALYSIS OF FRAME STRUCTURES

In conventional analysis and design of steel and composite frames, beam-to-column joints are assumed to behave either as “pinned” or as fully “rigid”. Traditionally the engineer has neglected the design and detailing of the actual joint and left this to the fabricator to complete^{2,3,2.4}.

Although the pinned or fixed assumption simplifies significantly analysis and design procedures for the engineer, in practice the actual joint behaviour exhibits characteristics over a wide spectrum between these two extremes. For example, most joints regarded as “pinned” possess some rotational stiffness, whilst joints which are regarded as “rigid” display some flexibility. Based on the above observations, the concept of “semi-rigid” joints has been born and continues to be the subject of research for engineers until today.

The actual meaning of the terms “rigid”, “pinned” and “semi-rigid” and their effect on the structural behaviour is summarised below:

- a) When all the different parts of the joint are sufficiently stiff, the joint is said to be “*rigid*” and there is no difference between the respective rotations at the ends of the members connected at this joint.
- b) When the joint is without any stiffness it is “*pinned*”, and in this case the beam will behave as simply supported whatever the behaviour of the other connected members.
- c) For intermediate “*semi-rigid*” cases, where non-zero and non-infinite stiffness exists, the transmitted moment will result in a difference in rotation Φ between the absolute rotations of the two connected members.

For semi-rigid joints the loads will result in both a bending moment and a relative rotation between the connected members as illustrated in Figure 2.3.

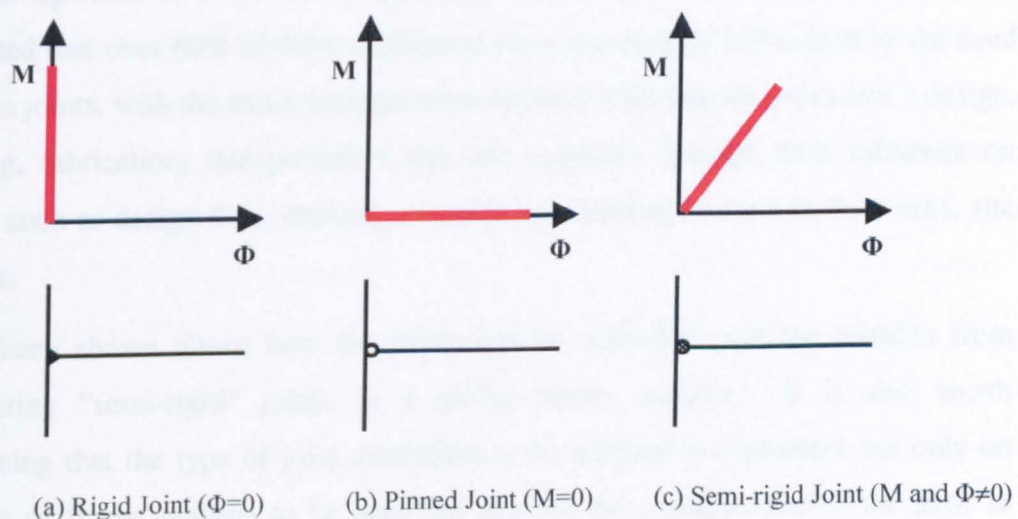


Figure 2.3 Modelling joints for elastic global analysis

The benefits of considering joints as “semi-rigid” are:

- a) Cheaper structures, because by considering “semi-rigid” joints allowances are made for the transfer of moments from the beam to the column, resulting in a reduction in the mid-span bending moment of the beam. Multi-bay frames this allows a reduction in the size of the beam section, with little consequence for the rest of the frame, except in cases where the beam frames into an external column,
- b) Cheaper and more simplified joints compared to rigid joints,
- c) Efficient structures because “semi-rigid” joints provide some restraint against column buckling^{2.5.2.6}.

With recent advances in structural codes and design standards the designer today can predict the behaviour of steel joints by taking into account only the mechanical and geometrical properties of the joint considered. However in order to achieve further reduction in the erection cost of a structural frame, according to Nethercot^{2.7}, there is a very strong need for standardization of the joints so that fabricators can improve and develop their machinery and equipment in order to provide standard joints, hence cheaper fabrication.

According to figures collected by British Steel (now Corus)^{2.7}, for multi-storey construction in the UK, the fabrication costs (the premium charged by fabrication companies to cover all their activities from receipt of information to handover on site) are upwards of 100% of the purchase price of the steel. It has further been estimated that over 60% of these *additional costs* are directly influenced by the need to make joints, with the exact arrangements selected affecting the fabricator’s design, drawing, fabrication, transportation and site expenses through their influence on factors such as design time, drawing complexity, handling of steel in the works, site time etc.

It has been shown above how the joints can be modelled, and the benefits from considering “semi-rigid” joints in a global frame analysis. It is also worth mentioning that the type of joint modelling to be adopted is dependent not only on the type of frame analysis to be used but also on the *classification* of the joint in terms of stiffness, and/or strength, and/or rotation capacity.

2.2.1 Joint classification

The main objective of a classification system is to define appropriate boundaries for behavioural classes of joints as a function of the mechanical properties of the connected members^{2,8}. Classification boundaries provide some guidance for the choice of an adequate and economical joint.

As mentioned above, beam-to-column joints could be classified in terms of stiffness and/or strength or by rotation capacity.

a) Stiffness classification

A joint within a structural steel frame could have a stiffness classification as “rigid”, “semi-rigid” or “flexible”, as shown in Figure 2.4^{2,9,2,10}. By comparing the design joint stiffness to the two extreme stiffness boundaries of “rigid” and “flexible” joints a classification in terms of stiffness can be made.

b) Strength classification

The strength classification simply consists of comparing the joint design resisting moment to “full-strength” and “pinned” boundaries, as shown in Figure 2.5.

c) Rotation capacity classification

Plastic analysis implies not only plastic stress distribution within the cross-section (plastic hinge formation) but also a bending moment redistribution within the structure. To enable the moment redistribution, the sections must be able to undergo sufficiently large rotations before the resistance moment falls below the plastic value^{2,8}. This means that a section or joint must have the ability to go into the plastic region, and possess a certain rotation capacity while maintaining the design moment. This plastic rotation capacity is responsible for the moment redistribution in a system. Required rotation values derived from the system must be compared to available rotation values derived from joint curves^{2,10,2,11}.

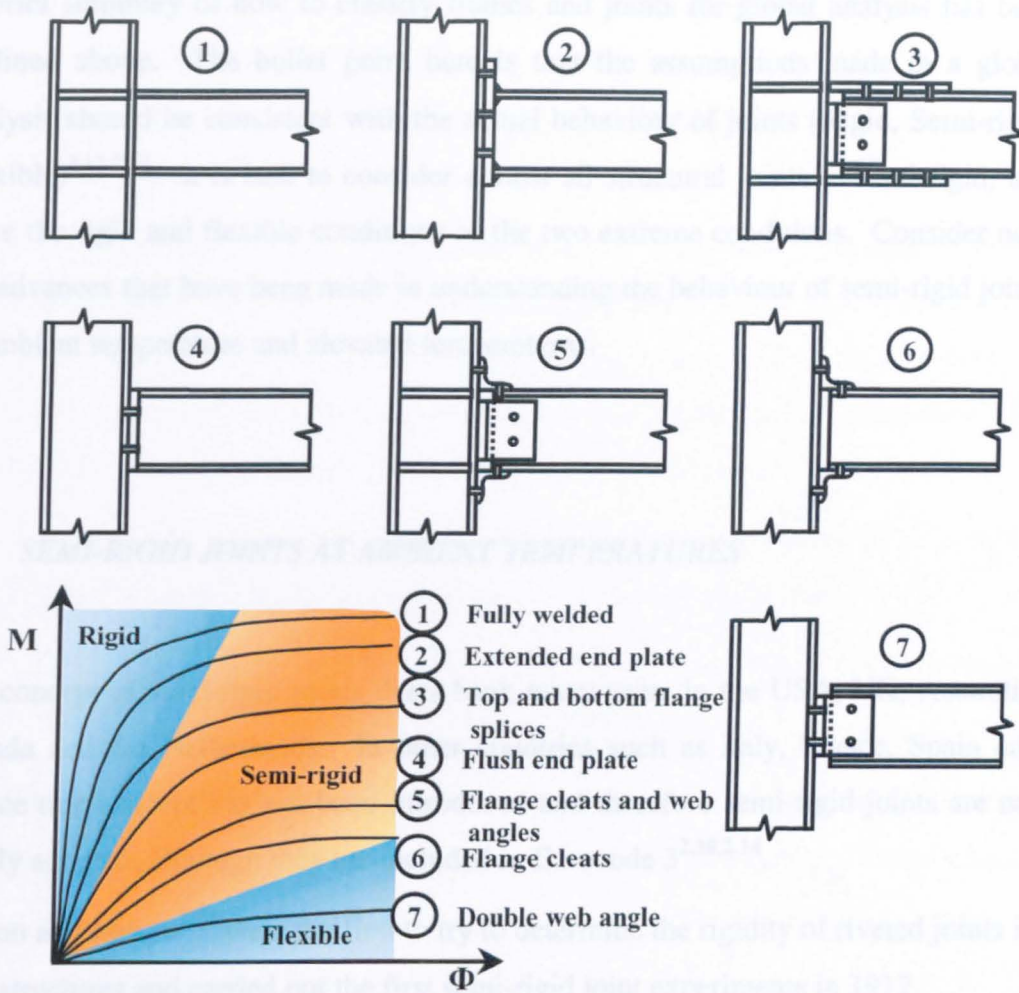


Figure 2.4 Typical beam-to-column joints and a diagrammatic stiffness classification

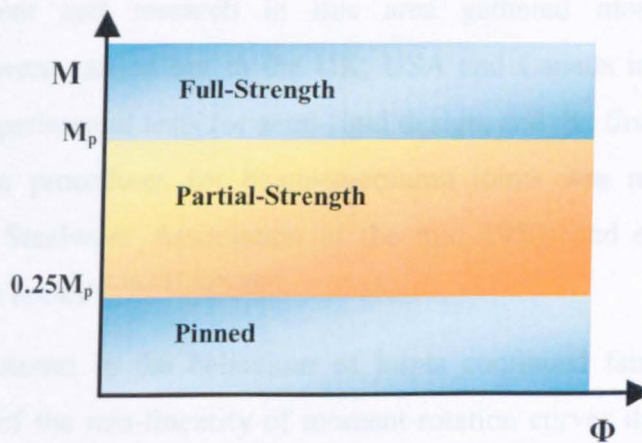


Figure 2.5 Strength classification boundaries

A brief summary of how to classify frames and joints for global analysis has been outlined above. The bullet point here is that the assumptions made in a global analysis should be consistent with the actual behaviour of joints (Rigid, Semi-rigid, Flexible)^{2.12,2.13}. It is best to consider almost all structural joints as semi-rigid, and leave the rigid and flexible conditions as the two extreme conditions. Consider now the advances that have been made in understanding the behaviour of semi-rigid joints at ambient temperature and elevated temperatures.

2.3 SEMI-RIGID JOINTS AT AMBIENT TEMPERATURES

The concept of semi-rigid joints dates back many years in the USA, UK, Australia, Canada and the Netherlands. In other countries such as Italy, France, Spain and Greece this concept has not been introduced and therefore semi-rigid joints are not widely adopted, although they are included in Eurocode 3^{2.10,2.14}.

Wilson and Moore^{2.15} were the first to try to determine the rigidity of riveted joints in steel structures and carried out the first semi-rigid joint experiments in 1917.

According to a historical review on end plate design (prepared by Moore^{2.4}) states that it was not until the 1930s that the need to understand the behaviour of joints became apparent and research in this area gathered momentum. Separate investigations were carried out in the UK, USA and Canada in order to provide a data base of experimental tests for semi-rigid design, and the first attempt to produce a set of design procedures for beam-to-column joints was made by the British Constructional Steelwork Association in the mid 1950s and early 1960s in their series of "Black books"^{2.16,2.17,2.18,2.19}.

The research interest in the behaviour of joints continued fairly slowly until the 1970s because of the non-linearity of moment-rotation curves throughout the entire range of rotations, leading to complexities in modelling.

In 1983, Jones *et al*^{2.20} reviewed the available test data obtained by many researchers concerning the performance of semi-rigid joints and pointed out the need for further investigation into the effect of semi-rigid end restraint on the behaviour of individual

beam-column members and complete frames. Since then many researchers have continued investigating the behaviour of steel joints, but the biggest research breakthrough involving different European countries was performed under the COST^{2.21} Project C1^{2.22}.

COST is the acronym for the French equivalent of "*European Cooperation in the Field of Scientific and Technical Research*". *COST* was the first instrument of European science cooperation going beyond the Community. The *COST Project C1*, was the first in the field of civil engineering. It was established in September 1990 and the objective was to improve knowledge on the behaviour of joints in order to:

- a) Be able to control the level of semi-rigidity in the structures, by developing practical analytical tools, using realistic connection behaviour,
- b) Determine what savings might be achieved using semi-rigid connections and simplifying accordingly the detailing of connections.

COST Project C1 was divided into seven subgroups (working groups) focused on specific topics, of which the most relevant to steel and composite joint behaviour were:

- Working Group 2- Steel and Composite
- Working Group 4- Database
- Working Group 6 - Numerical Simulation

The *COST Project C1* ceased operation in March 1999, but during the nine years of its activity produced about 125 individual projects, four books or conference proceedings, and nearly 400 individual papers and oral presentations.

The main scientific result was a comprehensive approach to structural design including joint design (Fully Integrated Design), in contrast to the past when joint design was done as a separate process.

The more advanced technical result was the participation of the *Cost C1* members in the writing of several chapters of the Eurocodes 3 & 4 (for Steel and Composite Structures) including directly the results of the research^{2.23,2.24}.

In the UK, the code for steel design BS 5950:Part 1^{2.25} does not define any method to determine the joint characteristics, but provides general guidelines to ensure that the joint satisfies the ultimate limit state design criteria. In the early 1990s the Steel

Construction Institute and BCSCA^{2.26,2.27,2.28} published design guides for simple and moment-resisting beam-to-column steel joints. These guides provide a simplified design procedure covering the various forms of joints, and are widely used in practice.

2.4 SEMI-RIGID JOINTS AT ELEVATED TEMPERATURES

During the last 30 years many advances have been made in the design of steel beam-to-column joints at ambient temperature. Over the same period, researchers started to show an interest in the behaviour of steel joints at elevated temperatures. The first experimental fire tests on six different types of joints, ranging from “flexible” to “rigid”, were conducted by CTICM^{2.29} in 1976. The purpose of the tests was to establish the performance of high strength bolts at elevated temperatures, so no attention was given to the actual behaviour of the steel joints. The results showed that due to the deformation of other elements the bolt failure was inevitable.

Then it was the turn of British Steel^{2.30} (1982) to perform elevated-temperature tests on “rigid” moment resisting cleated joints in order to observe their behaviour. Although they carried out only two tests, the conclusion was that bolts and their connected elements could undergo considerable deformation in fire.

The tests carried out by Lawson^{2.31} in 1990, were the first in which research interest moved away from just observing the steel joint’s behaviour at elevated temperatures to actually measuring the behaviour. In total eight tests were carried out, five of them on non-composite beams, two on composite beams and one on a shelf angle floor beam. Three main types of joints have been studied: a) extended end plate b) flush end plate and c) double-sided web cleat. The aim of the programme was to develop a design approach for steel beams taking into consideration the rotational restraint provided by the joint. These tests once more demonstrated that failure of the connecting bolts or welds did not occur, despite relatively large deformations of the joints. Although measurements of moments and rotations were taken, the information recorded was not sufficient to describe the actual moment-rotation characteristics of the joint at different temperatures. To be able to measure moment-

rotation-temperature characteristics, a typical joint arrangement needs to be tested several times at elevated temperatures, with different moment values applied to the joint each time.

That was the primary objective for the experimental work carried out by Leston-Jones *et al.*^{2,32,2.33,2.34,2.35}. In total eleven tests were carried out on (small-scale) flush end plate joints, including two tests at ambient temperature one for bare-steel and one for composite joints. The results confirmed that the joint stiffness and moment capacity decreases with increasing temperature, especially in the range 500 °C to 600 °C. For the first time, a number of moment-rotation curves at different temperatures were derived, describing the full joint response at elevated temperatures.

A follow up to Leston-Jones' work was carried out by Al-Jabri *et al.*^{2.36,2.37}. Leston-Jones' work had concentrated on the behaviour of joints within the lower range of available section sizes (254x102UB22 connected to 152x152UC23) whereas Al-Jabri extended the scope of his work to study the influence of parameters such as member size, connection type and different failure mechanisms. In total twenty tests were conducted (flush and flexible end plate bare-steel joints and flexible end plate composite joints) with five different connection configurations.

The definition of elevated-temperature moment-rotation response is complicated by the introduction of the further variable. In order to define accurately the response of steel joints for the fire limit state, it is necessary to perform research in more detail into the available analytical models, which can be classified (as at ambient temperature) into three main categories:

- 1) Global models,
- 2) Joint modelling by finite elements,
- 3) Component-based models.

Global models involve approaches which are based on fitting mathematical expressions to experimentally obtained data for the joint type considered. Leston-Jones^{2.35} and Al-Jabri^{2.37} have used this type of approach. They have fitted a modified form of Ramberg Osgood equation^{2.34} into their experimental results. The advantage of this approach is that it can give accurate results. On the other hand the main disadvantage is that it could be very expensive and time consuming in performing the actual tests and collecting the data for a wide range of configurations.

Joint modelling by finite elements^{2.38,2.39,2.40} has the advantage that it can provide information on the deformational behaviour of components, accounting also for the effects of their complex interaction. When considering frame analysis, this method could prove to be costly and time consuming.

A component-based model involves identifying the different components within a joint and representing their behaviour in terms of strength and stiffness. Assembling the different components can produce whole ranges of moment-rotation curves. Leston-Jones and Al-Jabri included a component-based model (exclusively concentrated on moment-rotation-temperature behaviour in the absence of axial thrust due to thermal expansion restraint of the beam) in their analysis, based on the ambient-temperature model from EC3 Annex J^{2.41}, by taking into account the degradation of mechanical properties of steel at elevated temperatures according to EC3: Part 1.2^{2.42}. The advantage of this analysis is that it relies on the mechanical and geometrical properties of the joint components. Another advantage is that it is faster and cheaper to apply, provided that the designer understands the behaviour of single components within a joint, which have to be modelled separately. Once this is achieved, the method is capable of predicting the variation in failure modes due to change in the joint geometrical and material properties, as well as loading conditions.

Finally component-based models can easily be implemented into frame analysis programs. To date a very limited research and exploration exists^{2.35,2.37} in the application of the component-based models at elevated temperatures.

One of the objectives of the current study is to examine experimentally and analytically the behaviour of these components at elevated temperatures and finally produce the moment-rotation-temperature characteristics for the joint considered. Furthermore the preparation of a component-based model for joints, at elevated temperatures can be very complex due to the high axial forces that can be developed because of the thermal expansion restraint of the unprotected beams. This can be overcome by using the non-linear behaviour of each component, without attempting to predict the overall joint behaviour, into a simplified or finite element model for the design of frame structures under fire conditions.

A summary of the “*Component Method*” principles (at ambient temperature, EC3 Annex J^{2.41}) is outlined next.

2.5 "COMPONENT METHOD" AT AMBIENT TEMPERATURE

As already discussed, the component-based approach compares favourably with all other analytical methods, since it combines economy with effective and predictive application. The originality of the "component method"^{2,43} is to consider any joint as a set of individual basic components. In the particular case of Figure 2.6, which illustrates a joint with an extended end-plate connection subjected to bending, the joint is divided into the three major zones (tension, shear and compression) and then each zone is divided into the relevant components as shown in Figure 2.6 and Table 2.1 below.

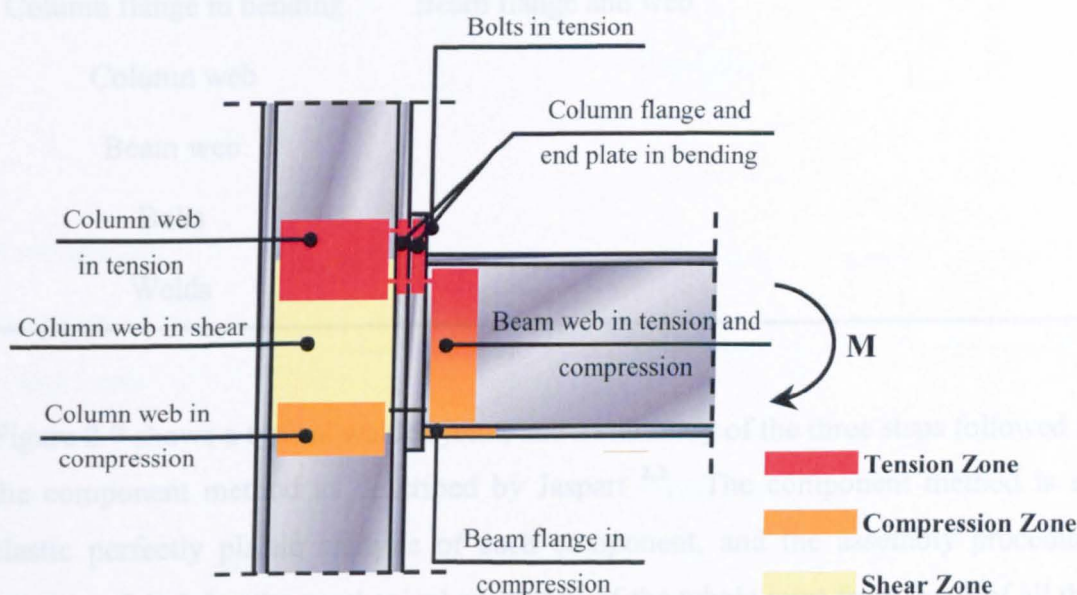


Figure 2.6 The three zones and their components within an end-plate steel joint

Each of these basic components possesses its own level of strength and stiffness in tension, compression or shear.

The column web is subjected to compression, tension and shear stresses simultaneously. This interaction of stresses is likely to decrease the resistance of the individual components. The application of the component method requires the following three steps^{2,2,2,44}.

- a) Identification of the active components in the joint being considered,

- b) Evaluation of the stiffness and/or resistance characteristics for each individual basic component (specific characteristics being initial stiffness and design resistance),
- c) Assembly of all the components and evaluation of the whole joint stiffness and/or resistance characteristics.

Table 2.1. Zones within the joint and their components

Tension Zone	Compression Zone	Shear Zone
End plate in bending	Column web	Column web panel
Column flange in bending	Beam flange and web	
Column web		
Beam web		
Bolts		
Welds		

Figure 2.7 shows a typical welded joint, and a summary of the three steps followed in the component method as described by Jaspart ^{2,2}. The component method is an elastic perfectly plastic analysis of each component, and the assembly procedure consists of deriving the mechanical properties of the whole joint from those of all the individual constituent components. This requires a preliminary distribution of the forces acting on the joint into internal forces acting on the components in a way that satisfies equilibrium.

The advantages of using the “Component Method” in this study is that it provides a tool to predict the behaviour of steel joints without going into an impractical attempt to test the full range of steel joint combinations. Secondly, by predicting the non-linear behaviour of individual components at elevated temperatures they could then be represented as springs which in effect can take the high axial forces in the joint generated by the thermal expansion against restraint to the beams.

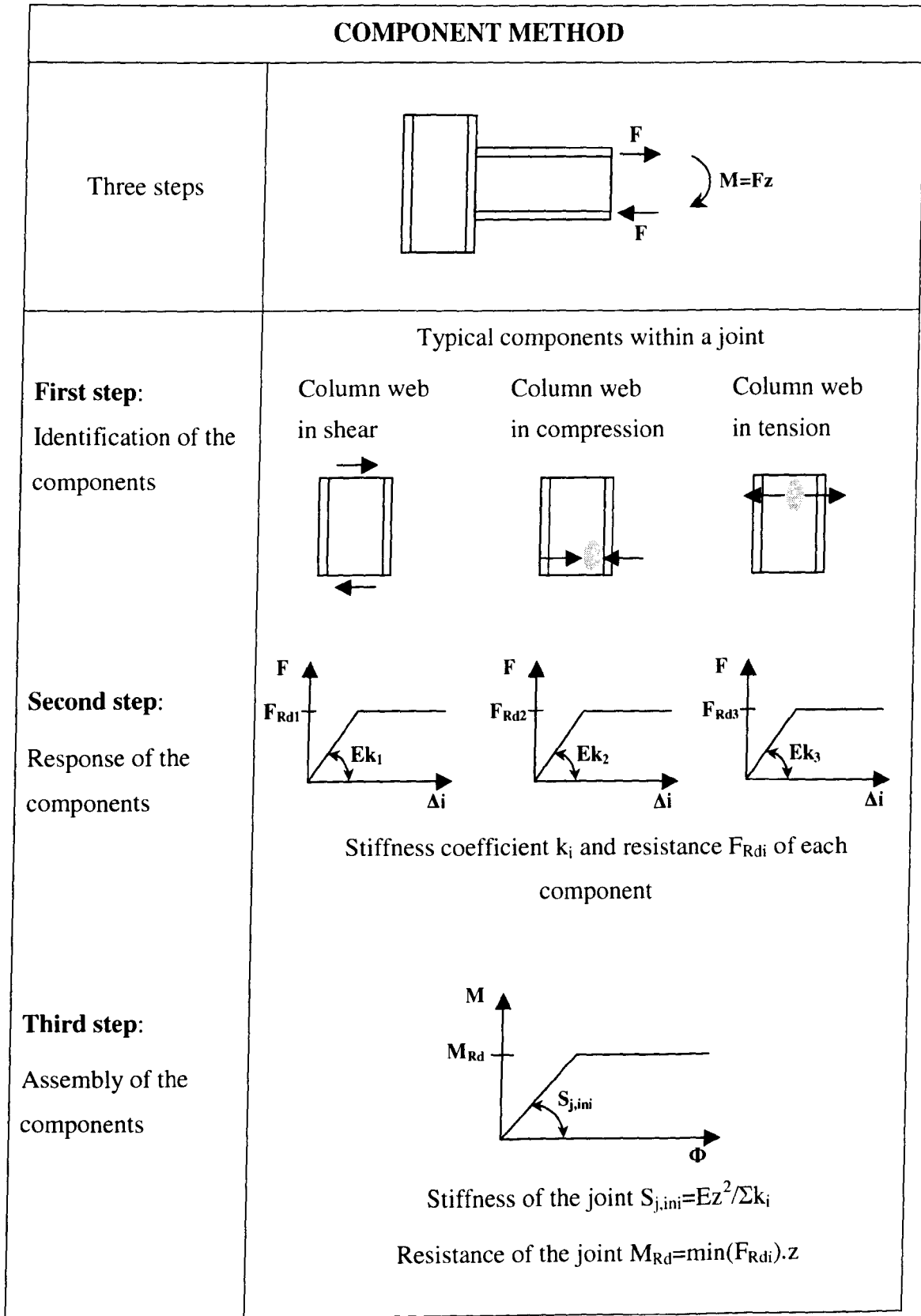


Figure 2.7 Application of the component method to a welded joint (after Jaspart^{2.2})

Because the current study is the first in the field which tries to use the “Component Method” principles at elevated temperatures, the initial task was to experimentally investigate the components or group of components at different temperatures and try to observe and predict the non-linear behaviour of these components in terms of strength and stiffness. To do so a test arrangement was developed in order to perform the component tests at elevated temperatures. The test apparatus and associated instrumentation are described in the next chapter.

2.6 REFERENCES

- 2.1 Liew J.Y.R., White, D.W., and Chen, W.F., "*Limit States Design of Semi-Rigid Frames Using Advanced Analysis: Part I: Connection Modelling and Classification*", Journal of Constructional Steel Research, Vol. 26, pp. 1-27, 1993.
- 2.2 Jaspart, J.P., lecture notes from "*Semi-Rigidity in Connections of Structural Steelworks: Theory, Analysis and Design*", Advance Professional Training, Italy, 1999.
- 2.3 Moore, D.B., "*A Review of Connection Research and Development in the UK*", Connections in Steel Structures III-Behaviour, strength & design, Proceedings of the third International Workshop, Italy, 1995.
- 2.4 Moore, D.B., "*The Design of End-Plate Connections*", Conference on Modern developments in frame and slab structures, Building Research Establishment, UK, 1988.
- 2.5 Anderson, D., Bijlaard, F.S.K., Nethercot, D.A., and Zandonini, R., "*Analysis and Design of Steel Frames with Semi-Rigid Connections*", IABSE Surveys S-39/87, 1987.
- 2.6 Nethercot, D.A., "*Joint Action and the Design of Steel Frames*", The Structural Engineer, Vol. 64, No.12, 1985.
- 2.7 Nethercot, D.A., "*Towards a Standardisation of the Design and Detailing of Connections*", Journal of Constructional Steel Research, Vol.46, No. 1-3, 1998.
- 2.8 Gomes, F., Kuhlmann, U., DeMatteis, G., and Mandara, A., "*Recent Developments on Classification of Joints*", Proceedings an International Conference on "Control of the semi-rigid behaviour of Civil Engineering structural connections", COST C1, Liege, 1998.
- 2.9 "*Structural Connections-Stability and Strength*", Edited by R. Narayanan, Elsevier Applied Science, 1989.
- 2.10 "*Semi-Rigidity in Connections of Structural Steelworks: Theory, Analysis and Design*", Advance Professional Training, Italy, 1999.

- 2.11 Kuhlmann, U., “*Verification Procedure for Rotation Capacity of Joints*”, Document COST C1/WD2/97-24, Innsbruck, September 1997.
- 2.12 Nethercot, D.A., Li, T.Q., and Ahmed, B., “*Unified Classification System for Beam-to-Column Connections*”, Journal of Constructional Steel Research, Vol. 45, No. 1, pp. 39-65,1998.
- 2.13 Hasan, R., Kishi, N., and Chen, W., “*A New Non-linear Connection Classification System*”, Journal of Constructional Steel Research, Vol. 47, pp. 119-140,1998.
- 2.14 “*EC3 (1993), Design of Steel Structures, Part 1.1*”, European Committee for Standardization, CEN, Brussels.
- 2.15 Wilson, W.M., and Moore, H.F., “*Tests to Determine the Rigidity of Riveted Joints in Steel Structures*”, University of Illinois, Engineering Experimentation Station, Bulletin No. 114, Urbana, USA, 1917.
- 2.16 “*Welded Details for Single-Storey Portal Frames*”, BCSA, Publication No.9, 1955.
- 2.17 “*Steel Frames for Multi-Storey Buildings. Some Design Examples to Conform With the Requirements of BS449: 1959*”, BCSA, Publication No.16, 1961.
- 2.18 “*Examples of the Design of Steel Girder Bridges in Accordance with BS153: Parts 3A, 3B and 4*”, BCSA, Publication No.22, 1963.
- 2.19 “*Single Bay Single Storey Elastically Designed Portal Frames*”, BCSA, Publication No.24, 1964.
- 2.20 Jones, S.W., Kirby, P.A., and Nethercot, D.A., “*The Analysis of Frames with Semi-Rigid Connections-A State-of-the-Art Report*”, Journal of Constructional Steel Research, Vol. 3, No. 2, 1983.
- 2.21 The URL of the official COST website is: <http://cost.cordis.lu>
- 2.22 Information about COST Project C1 can be found at <http://info.uibk.ac.at/c/c8/c809/res/cost/>
- 2.23 COST C1, Semi-Rigid Behaviour of Civil Engineering Connections, “*Composite Steel-Concrete Joints in Braced Frames for Buildings*”,

- published by the European Commission, European Cooperation in the Field of Scientific and Technical Research, Brussels, 1997.
- 2.24 Proceedings of the International Conference on “*Control of the Semi-Rigid Behaviour of Civil Engineering Structural Connections*”, COST C1, Liege, 1998.
- 2.25 “*BS 5950 Structural Use of Steelwork in Building: Part 1: Code of Practice for Design in Simple and Continuous Construction*”, British Standard Institution, London, 1985.
- 2.26 “*Joints in Simple Construction Vol. 1: Design Methods*”, SCI-P-105, The Steel Construction Institute and BSCA, 1992.
- 2.27 “*Joints in Simple Construction Vol. 2: Practical Application*”, The Steel Construction Institute and BSCA, 1993.
- 2.28 “*Joints in Steel Construction: Moment Connections*”, The Steel Construction Institute, 1995.
- 2.29 Kruppa, J., “*Resistance on feu des assemblage par boulous*”, Centre Technique Industriel de la Construction Metallique, St. Remy Chevzuese, France, 1976, CTICM Report, Document No. 1013-1, English translation available entitled “*Fire Resistance of Joints with High Strength Bolts*”.
- 2.30 “*The Performance of Beam/Column/Beam Connections in the BS5950: Part 8 Fire Test*”, British Steel (Swindon labs), Reports T/RS/1380/33/82D and T/RS/1380/34/82D, Rotherham, 1982.
- 2.31 Lawson, R.M., “*Behaviour of Steel Beam-to-Column Connections in Fire*”, The Structural Engineer, Vol. 68, No. 14, pp. 263-271, 1990.
- 2.32 Lennon, T., and Jones, L.C., “*Elevated Temperature Moment Rotation Tests*”, Internal Report N135/94, Building Research Establishment, 1994.
- 2.33 Lennon, T., and Jones, L.C., “*Elevated Temperature Composite Connection Moment Rotation Tests*”, Internal Report N65/95, Building Research Establishment, 1995.
- 2.34 Leston-Jones, L.C., Lennon, T., Plank, R.J., and Burgess I.W., “*Elevated Temperature Moment-Rotation Tests on Steelwork Connections*”, Proc. Instn Civ. Engrs Structs & Bldgs, **122**, pp. 410-419, 1997.

- 2.35 Leston-Jones, L.C., "*The Influence of Semi-Rigid Connections on the Performance of Steel Framed Structures in Fire*", Ph.D. Thesis, Department of Civil and Structural Engineering, University of Sheffield, 1997.
- 2.36 Al-Jabri, K.S., Lennon, T., Burgess, I.W., and Plank, R.J., "*Behaviour of Steel and Composite Beam-Column Connections in Fire*", Journal of Constructional Steel Research, Vol. 46, No. 1-3, 1998.
- 2.37 Al-Jabri, K.S., "*The Behaviour of Steel and Composite Beam-to-Column Connections in Fire*", Ph.D. Thesis, Department of Civil and Structural Engineering, University of Sheffield, 1999.
- 2.38 Liu, T.C.H., "*Finite Element Modelling of Behaviours of Steel Beams and Connections in Fire*", Journal of Constructional Steel Research, Vol. 36, No. 3, pp. 181-199, 1996.
- 2.39 Liu, T.C.H., "*Three-Dimensional Modelling of Behaviours of Steel/Concrete Composite Connection Behaviour in Fire*", Journal of Constructional Steel Research, Vol. 46, No. 1-3, 1998.
- 2.40 El-Houssieny, O.M., Abdel Salam, S., Attia, G.A.M., and Saad, A.M., "*Behaviour of Extended End Plate Connections at High Temperature*", Journal of Constructional Steel Research, Vol. 46, No.1- 3, 1998.
- 2.41 "*EC3:Design of Steel Structures, Part 1.1:Revised Annex J Joints and Building Frames*", (Draft), Document CEN/TC250/SC3 N419E, European Committee for Standardization, 1994.
- 2.42 "*EC3:Design of Steel Structures, Part 1.2:General Rules for Structural Fire Design*", (Draft), ENV 1993-1-2, European Committee for Standardization, 1995.
- 2.43 Zoetemeijer, P., "*A Design Method for the Tension Side of Statically Loaded, Bolted Beam-to-Column Connections*", HERON, Vol. 20, No. 1, pp. 1-59, 1974.
- 2.44 Weynand, K., Jaspart, J.P., and Steenhuis, M., "*The Stiffness Model of Revised Annex J of Eurocode 3*", Connections in Steel Structures III-Behaviour, strength & design, Proceedings of the third International Workshop, Italy, 1995.

Chapter 3

Test Apparatus for Elevated Temperature Testing

3.1 INTRODUCTION

When steel-framed structures are subjected to fire their ability to sustain load is severely impaired and the action of the joints is of particular concern. To date, data on the response of joints at high temperatures has been gathered from full-scale furnace tests^{3.1, 3.2, 3.3}. The data bank collected so far is rather small compared to the number of possible steel joint arrangements and the variation in temperatures, but it is clearly impractical to test all the joint arrangements at different temperatures. The application of the "Component Method" has been proposed, but to date there were no component tests at elevated temperatures so the primary task of this research is to perform tests on single components (column webs in compression) or groups of components (T-stubs in tension) at elevated temperatures.

Most of the components are fairly small, so their testing is fairly simple to carry out, taking into account also that they should be loaded uniaxially in tension or compression. The only major problem was that at high temperatures the conventional types of force and displacement measurement devices could not be applied, due to the hostile environmental conditions inside a furnace.

3.2 MEASUREMENT DEVICES USED AT ELEVATED TEMPERATURE TESTS

Several full-scale fire tests on frames have been performed^{3.4} during the last decade or so. The objectives of these tests varied. In some cases they were performed in order to observe the efficiency of fire safety systems installed in a frame, and in other

cases to actually measure maximum steel temperatures and maximum beam deflections. The use of mechanical measurement devices was very limited, and the maximum beam deflections recorded in some tests were mostly taken after the end of the test.

The most comprehensive frame full-scale fire tests were performed at the Building Research Establishment's (BRE) Cardington Laboratory in 1995 and 1996^{3.4,3.5,3.6,3.7}. The tests were carried out on an 8-storey composite steel framed building which had been constructed as a typical multi-storey office building. The programme was jointly coordinated by BRE and British Steel, and was supported by the European Coal and Steel Community and the UK Government's Department of the Environment. Other organizations involved in the programme included TNO Building and Construction Research, Centre Technique Industriel de la Construction Metallique (CITCM), the Steel Construction Institute (SCI) and the University of Sheffield.

The purpose of the tests was to investigate the behaviour of real structures under fire conditions, and to collect data that would allow computer programs for analysing structures under fire conditions to be verified. The data was collected by using numerous thermocouples, strain gauges, displacement transducers and inclinometers. Loads were applied using sandbags and most of the displacement readings were taken by referring the readings to the floor above the actual fire compartment.

Looking at smaller scale furnace tests, such as those performed by Lawson^{3.1}, Leston-Jones^{3.2} and Al-Jabri^{3.3} on steel joints, the instruments used varied from rotation devices such as "dumb-bells" and "inclinometers" to displacement transducers, dial gauges, thermocouples and load control devices.

The rotation devices mentioned above are very sensitive, and accurately measure rotational movements of beam-to-column joints. The main difficulty is in using these devices inside a furnace where the atmosphere temperature could reach temperatures over 900 °C. To overcome this problem the researchers placed inclinometers inside a fire-protected box and at the same time cool air was pumped through the box by means of a compressor.

To allow for possible failure of the inclinometers, displacement transducers were placed outside the furnace. These transducers were connected to the beam flange by

means of quartz rods (which have relatively low thermal conductivity and expansion characteristics). The loads, applied on the beams, were measured using load cells, which were attached to hydraulic jacks outside the furnace.

For the current study, a more robust, reliable and less time and effort consuming measuring device was needed in order to carry out a large number of component tests at elevated temperatures. Another factor, which influenced the choice on the equipment to be used was the need to observe the behaviour of the components under different load and temperature conditions. For these reasons the principles of photogrammetry were investigated as a tool to measure displacements. Additionally real video recordings could be made of the actual behaviour of the components at elevated temperatures.

3.3 DEVELOPMENT OF THE IMAGE ACQUISITION AND PROCESSING SYSTEM

“Photogrammetry is the art, science, and technology of obtaining reliable information from no-contact imaging systems through recording, measuring, analysing and representation” ^{3.8}.

The term of photogrammetry was first used in published work in 1867 ^{3.8} when the art and science of photography itself was still in its infancy. Over the last 80 years the principal application of photogrammetry has been the compilation of maps from aerial photographs. There has been in addition a continuing development of applications of photogrammetric close-range techniques to many other fields such as engineering, architecture, archaeology, medicine, industrial quality control, robotics etc.

In engineering, several papers describe the use of image acquisition and processing techniques, not only at ambient temperature ^{3.9,3.10,3.11} but at elevated temperatures as well ^{3.12,3.13,3.14}. McEntegart ^{3.15} reported that real time analysis of video images is expected to generate exciting possibilities for non-contacting extensometry at ultra-high temperatures (1200 °C-2000 °C).

3.3.1 Pilot tests

In order to assess the capabilities of photogrammetry and the feasibility of using image acquisition and processing techniques at elevated temperatures, two very simple and quick pilot tests were performed.

The objectives of these two pilot tests were to:

- a) Check the viability of imaging techniques for measuring axial displacements under increasing tensile axial force, and compare the displacement readings of a T-stub assembly (discussed in more detail at a later stage) using two different measurement techniques. One technique used conventional linear voltage displacement transducers (LVDTs), and the second used a digital camera. The specimen arrangement is shown in Figure 3.1.
- b) Check that, at elevated temperatures, the images taken contain enough information to measure displacements and/or observe the behaviour of the specimen.

The specimens were made by bolting together two T-stub elements obtained from a rolled I-beam profile (305x165x40UB), steel grade S275, cutting it along the web plane. These T-stubs were connected through the flanges by means of four M12 Grade 4.6 bolts.

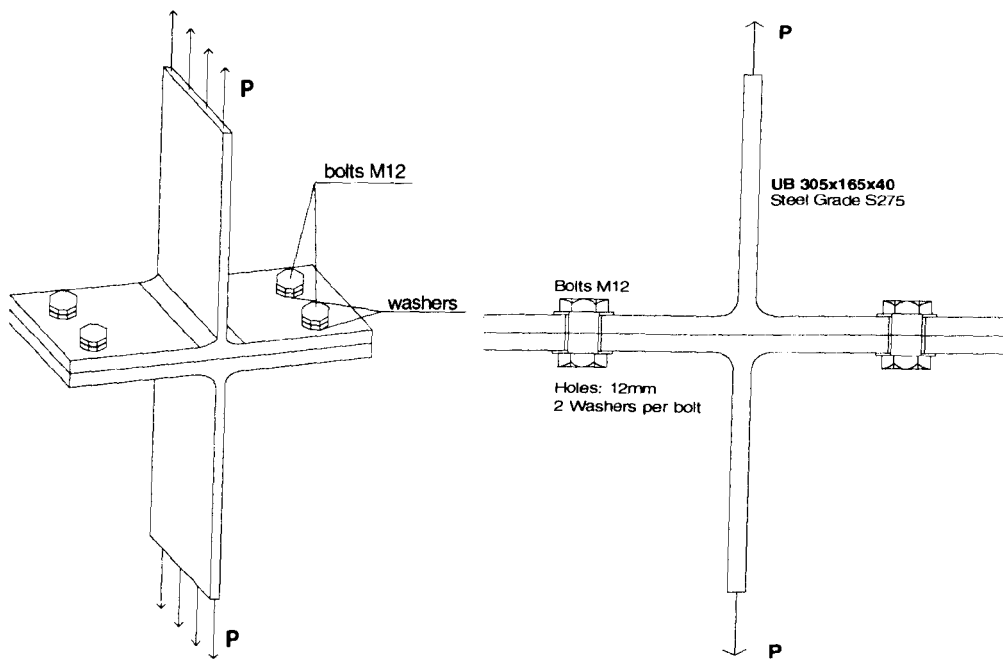


Figure 3.1 The T-stub model used in ambient temperature pilot tests

The specimens were subjected to a tensile axial force applied to the webs by the jaws of a 1000 kN capacity Avery testing machine. As these were pilot tests, readily available equipment—rather than bespoke apparatus—was used to prove the techniques before purchasing more sophisticated cameras and image processing software. The axial displacements were measured in two ways:

1. S8FLP10A^a LVDTs with 38mm length and 10mm mechanical stroke, which provide an electrical signal directly proportional to a linear mechanical movement of the shaft, were attached directly to the specimen. This kind of arrangement gives the opportunity to use electronic logging devices, which can accurately record large amounts of experimental data automatically.
2. A Casio QV-7000SX LCD digital camera was used to capture images of the deflected shape for subsequent analysis using image-processing software. The digital camera was placed on one side of the T-stub assembly at a distance of 300mm.

^a “Sakae”, Techni Measure, www.techni-measure.co.uk

When the test started the experimental data from the LVDT was automatically recorded. The LVDT was connected to an Orion Delta logging system, which recorded all the data, converted the readings into Engineering units, and stored it directly on computer. Using the LCD Digital Camera, pictures had to be taken manually at given load intervals (every 20kN in the elastic region and every 2kN in the plastic region). At the end of the test, the images were analysed using image processing demonstration software in order to give the displacement readings.

The procedure to analyse the images using the software was very simple. Before the tests were carried out, reference horizontal and vertical distances were measured. Using a Vernier gauge, the flange thickness was measured in the vertical direction and the web thickness in the horizontal direction. The next step was to scale these readings according to the initial image. The two edges of the flange on the initial image were identified by eye, and using the mouse the measured distance (10.55mm) was entered. As the picture was already divided into pixels this automatically generated a scaling factor between pixels and millimetres. With this conversion, any vertical distance could be measured simply by picking up with the mouse pointer any two points in the vertical direction. The software counts the number of pixels between the locations and transforms the distance into millimetres. The same procedure was used to scale the horizontal readings.

During loading of the specimens, a number of deflected images were recorded for each test. These were then analysed using the software and the results compared with the measurements obtained from the LVDTs. An image of the T-stub's deflected shape is shown in Figure 3.2.



Figure 3.2 Typical deformation of a T-stub specimen at ambient temperature

3.3.2 Experimental results

The resolution of the recorded image at the time of Test No. 1 was 640x480 pixels. The field of view of the camera was 117mm in the vertical direction and 126mm in the horizontal direction and a total of fourteen images were captured. The relationship between the LVDT readings and the image processing results is shown in Figure 3.3.

It is obvious from Figure 3.3 that there is good correlation between the readings made by the camera with image processing software and the LVDTs. The sensitivity of readings taken from LVDTs was $20\mu\text{m}$. The standard accuracy from the software, for these specific images, was up to $243.75\mu\text{m}$, obtained by dividing the value in the vertical direction (117mm), which is the direction of displacement, by the 480 pixels in that direction. The software, on the other hand, uses linear sub-pixel division in order to interpolate maximum accuracy from the images. Also from Figure 3.3 it can be seen that the LVDT ran out of travel distance at about 4mm. The imaging technique however is capable of reading data over a wide range of deformation.

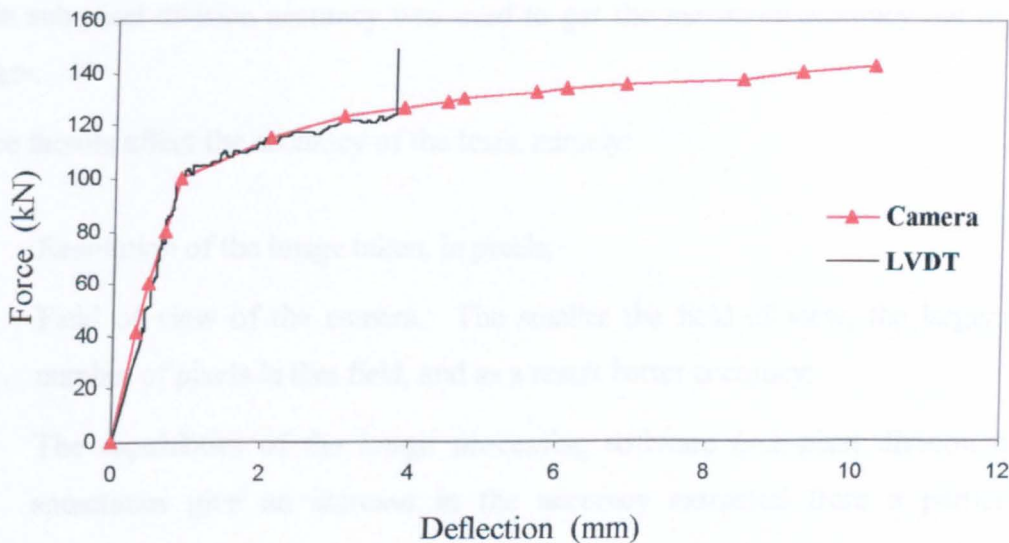


Figure 3.3 Force deflection curve for pilot test No.1

A second test was conducted with the image resolution set at 1280x960 pixels. This time the field of view of the camera was 74mm in the vertical direction and 121mm in the horizontal direction, and a total of twelve images were captured. The relationship between the LVDT readings and the image processing results is shown in Figure 3.4.

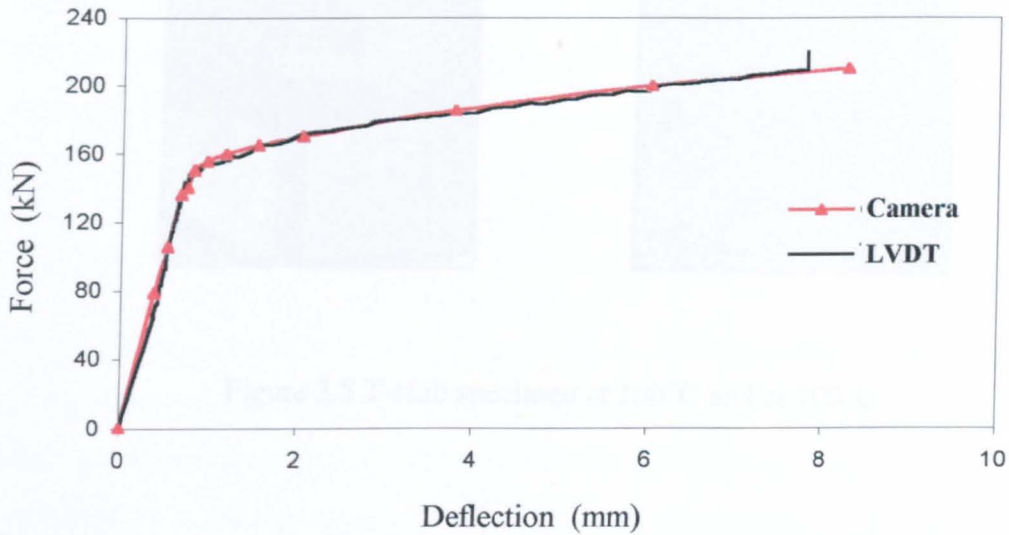


Figure 3.4 Force deflection curve for pilot test No. 2

In this test the implied accuracy obtainable from the software was $77.08\mu\text{m}$, but again sub-pixel division accuracy was used to get the maximum accuracy out of the images.

Three factors affect the accuracy of the tests, namely:

- a) Resolution of the image taken, in pixels;
- b) Field of view of the camera. The smaller the field of view, the larger the number of pixels in that field, and as a result better accuracy;
- c) The capabilities of the image processing software (sub-pixel division may sometimes give an increase in the accuracy extracted from a particular image).

A further concern, which might affect the accuracy of the tests, is the quality of the images taken at elevated temperatures, when above a certain temperature everything inside the furnace is glowing. In order to test this, another pilot test was performed by heating the already deflected T-stub specimens up to 750°C . Figure 3.5 shows

two images of the T-stub specimen inside the furnace, one at 100°C and the other at 700°C.

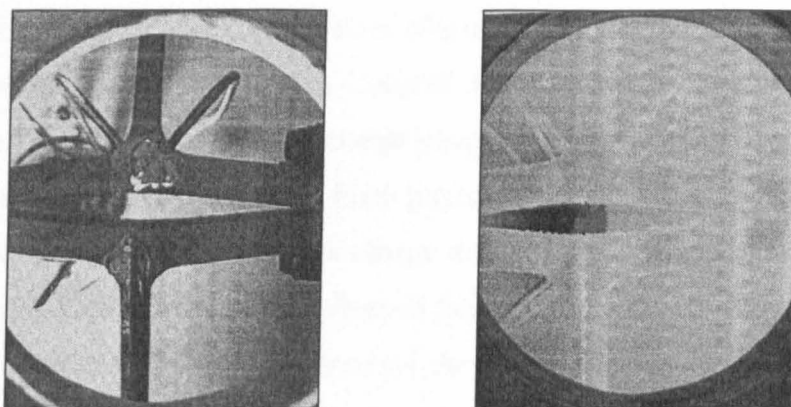


Figure 3.5 T-stub specimen at 100°C and at 700°C

From these images it is clear that well-defined edges are still visible in the image at 700°C, and these can be used to measure the displacement between the deflected flanges.

3.4 DEVELOPMENT OF THE TEST PROGRAMME

Encouraged by the results from the pilot tests it was decided to use imaging techniques in the test programme to find the characteristics of components at elevated temperatures. A specially designed experimental arrangement was constructed, including a furnace and an image acquisition and processing system, and this is described in detail below.

3.4.1 CCD-Camera and Digital Image Processing

Developments in video camera and digital image processing technology have led to the possibility of producing a real-time displacement measurement from a video image. A solid state CCD (Charge-Coupled Device) camera produces the video signal. The CCD is made of many charge-coupled cells, or picture elements, which are arranged in a rectangular array. Each picture element, also called a pixel of the array, converts incoming light into a charge directly proportional to the amount of light received. This charge is then clocked (shifted) from cell to cell, to be finally converted to a video signal that represents the original image as the output of the CCD.

The CCD image sensors are stable and accurate devices, and the resolution for the current tests is selected typically to be of an array of 768x576 individual light-sensitive elements or pixels. The signal from the camera is digitised, stored and processed by a microprocessor in order to locate the position of the optical targets within the image to sub-pixel accuracy.

The above technique measures displacements by tracking two contrasting targets. However, unlike most non-contact optical systems, which measure along one axis, the video extensometer is an area-scan device. Due to this it is possible to track the position of the target more precisely, so that the measurement is less sensitive to target distortion, test-piece lateral movement or bending. In addition, image processing enables the test-piece shape to be monitored continuously and offers the potential for observing the development of surface features.

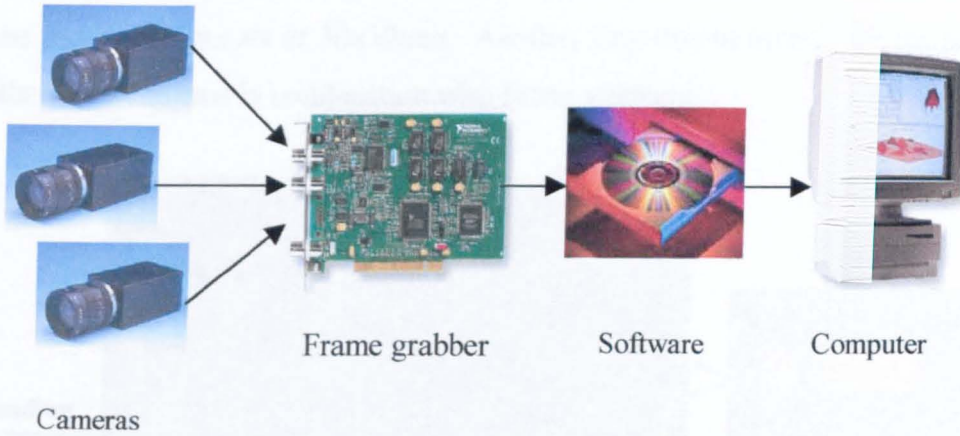


Figure 3.6 Schematic diagram of the image acquisition and processing system.

3.4.2 Furnace

A purpose-built furnace^b, with an internal capacity of 1m³, was commissioned with view-ports to accommodate three video cameras. It was convenient to use an electric fan-assisted furnace in order to avoid any flames within the field of view of the video cameras. The fan also ensures a uniform distribution of atmosphere temperature up to 1100°C. Two view-ports were used to accommodate the three video cameras. One was at the front of the furnace, perpendicular to the axis of loading, facing in the horizontal direction where there is movement of the flanges. The other was at the top of the furnace, facing in the vertical direction (Figure 3.7). The first view-port accommodated two video cameras, one for accurate measurements and the other for general observation of the T-stub distortion. The other view-port accommodated another video camera, again for measurement of the T-stub distortion. There were also two opposed holes in the sides of the furnace to allow a hydraulic jack to apply force to the specimens.

The image acquisition and processing system had to be carefully selected. First, the required accuracy of the deflection measurement was set at 40µm without any sub-pixel division. Then the camera field of view needed to be investigated, depending

upon the position of the video cameras relative to the specimen and the type of lenses to be used; this was set at 30x30mm. Another step was to investigate the resolution of the video cameras in combination with frame grabbers.

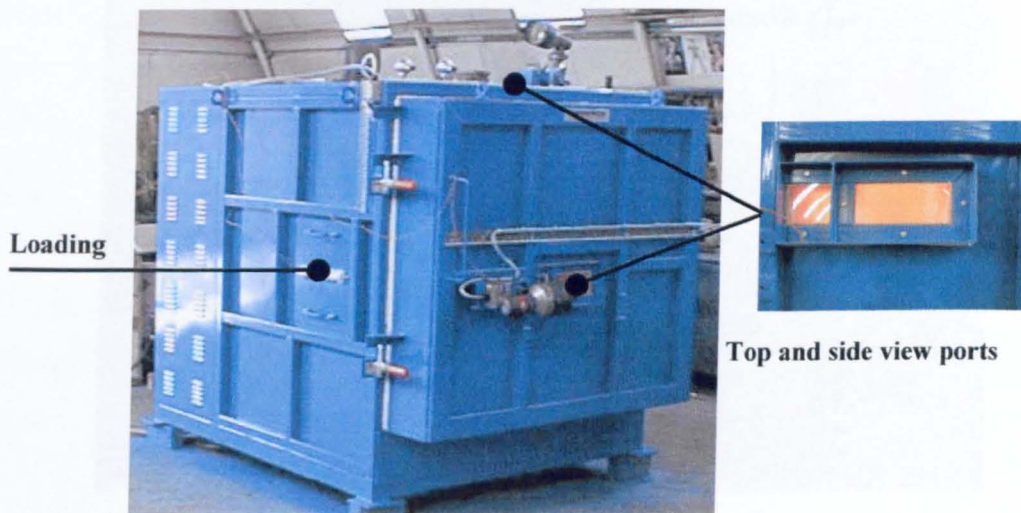


Figure 3.7 Furnace with the view-ports

Three monochrome analogue video cameras, manufactured by JAI (model: CV-M50) and a colour frame grabber, manufactured by Imagenation (model: PXC200) were selected, together giving a capture resolution of 768 x 576 pixels. The Imagenation PXC200 frame grabber features precision video capturing hardware for applications that requires high colour accuracy. Features of the precision hardware design include:

- High colour accuracy
- Image capture resolution up to full-size:768x576 (PAL and SECAM video format)
- Continuous, software initiated and triggered image captures, and
- Four multiplexed composite video inputs.

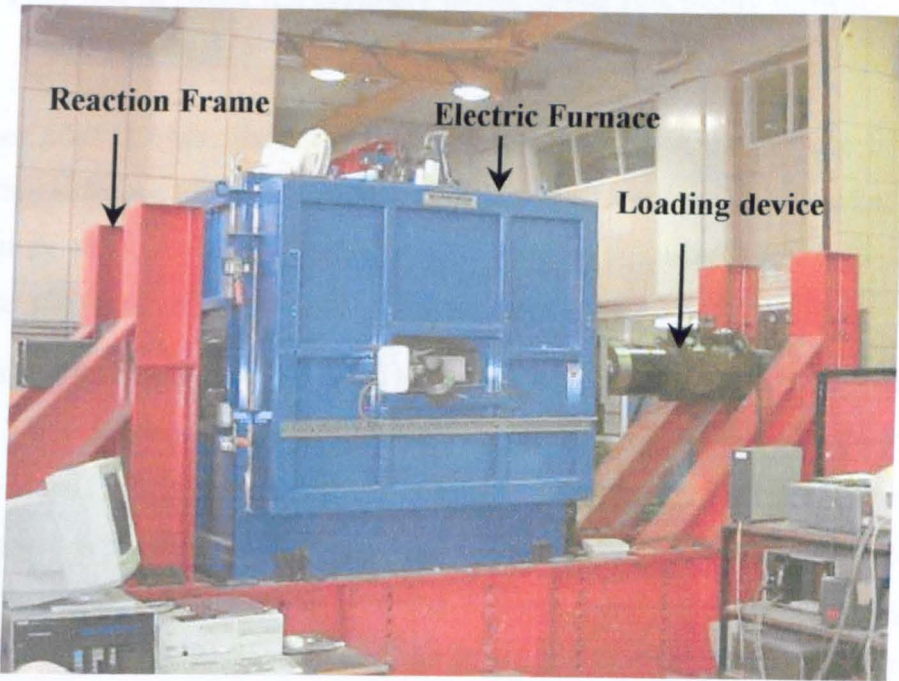


Figure 3.8 Arrangement for the experimental work.

The image processing software was designed to include the change of information in an image from low to high temperatures, and the capability of controlling the sub-pixel division. Figure 3.6 shows a schematic diagram of the image acquisition and processing system and Figure 3.8 the arrangement for the experiments.

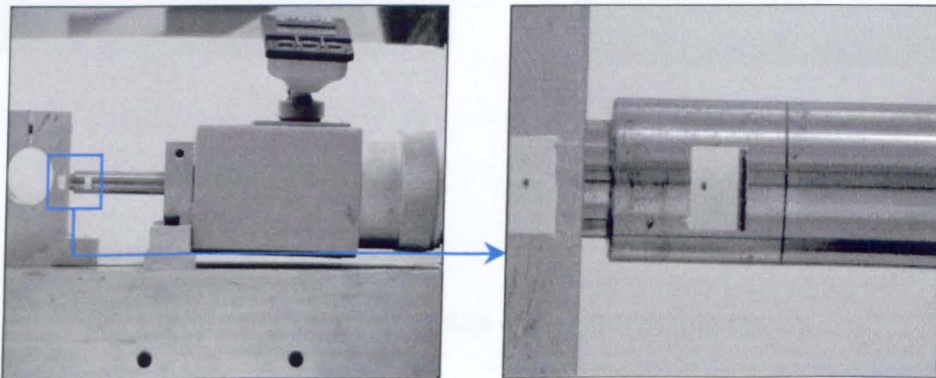
3.4.3 Loading device

The load was applied to the specimen by the use of a 500 kN capacity hydraulic jack, which was attached to a reaction frame outside the furnace. The jack was connected to a Kelsey control device capable of controlling the movement of the hydraulic jack either in load or displacement mode. A fire-protected grabbing device was designed in order to keep the hydraulic jack outside the furnace but at the same time applying the tension or compression forces to the specimen effectively.

3.4.4 Pilot test to check the accuracy of the image processing software

A further pilot test was necessary to check the accuracy of the purpose built image processing software taking into account the lenses which were to be used at elevated temperature tests, and the distance of the cameras from the specimen. Also the influence of a linear sub-pixel division on accuracy was explored.

A digital calibration device was used with accuracy in the displacement readings of $\pm 1\mu\text{m}$. The test procedure was to drive the displacement rod and capture images in 0.50mm steps. The device is shown in Figure 3.9(a) and a typical image used for measurement is presented in Figure 3.9(b). Camera One, used to capture images for measuring the displacements, was placed 850mm away from the targets giving a field of view of 32.74x21.85mm. In order to capture that field of view, a 75mm lens and a doubling extension tube, which effectively transforms the 75mm lens into a 150mm lens, were used.



(a) Calibration device

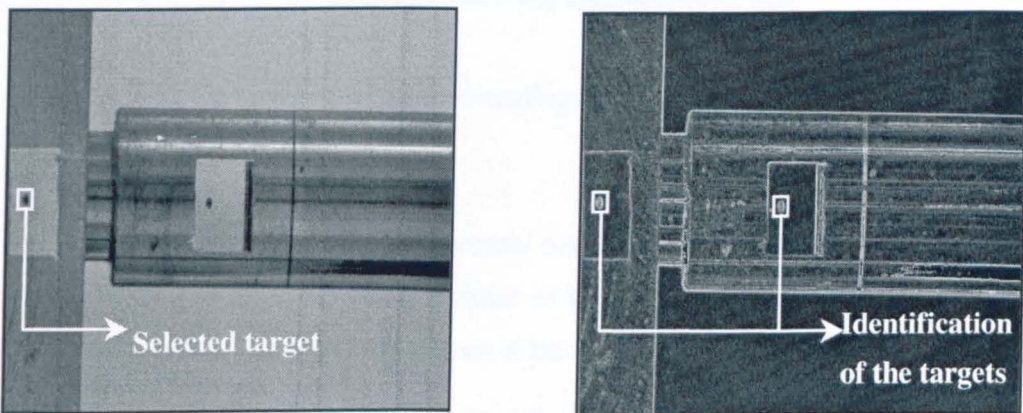
(b) Measurement image

Figure 3.9 Calibration device and a typical measurement image from camera one

On the calibration device a set of targets was placed and the difference between them was measured during the image processing. The targets are the two black dots shown in Figure 3.9(b). The calibration device adjusted the right-hand dot while the left-hand dot remained stationary. The initial displacement of the two dots was measured (13.386mm) and used to calibrate the processing method in order to give

the actual displacement (in millimetres) of the targets when they started moving apart.

The calibration procedure of the processing method first involves the selection of the area of the left-hand side target as shown in Figure 3.10(a). Then an edge detector filter was applied to the image in order to identify the right-hand side target, using the selected area shown in Figure 3.10(b). The distance between the two bottom left-hand corners was calculated in pixels and transformed into millimetres using the calibration reading above (13.386mm).



(a) Left hand-side target

(b) Edge detection filter

Figure 3.10 Calibration of the processing system

According to the above information the accuracy of the software without any sub-pixel division was up to $\pm 42.63\mu\text{m}$ and a total of 20 images were captured.

The results of the real readings compared with the readings from the image processing are shown in Figure 3.11. It is clear that there is a good correlation between the displacement readings.

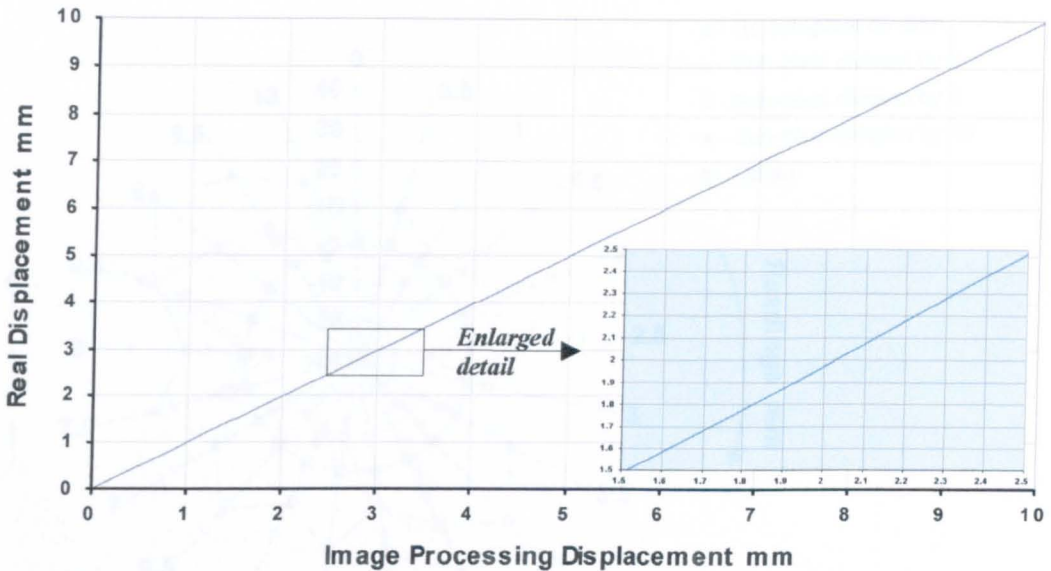


Figure 3.11 Comparison of the real readings with the image processing readings

The largest difference in the displacement readings was 0.038mm without any sub-pixel division. With a sub-pixel division of two, which means linear interpolation between the pixels, the largest difference in the readings was 0.025mm.

Available image processing software specifications suggest that by performing sub-pixel divisions to the captured images the accuracy obtained can be increased. For this reason a further investigation was performed, and Figure 3.12 below shows the results of this investigation.

It is clear by comparing the polygons with the origin (black circle) that there is some improvement in the accuracy by using linear sub-pixel division of two (for the majority of the readings) but the readings do not become more accurate for linear sub-pixel divisions above two.

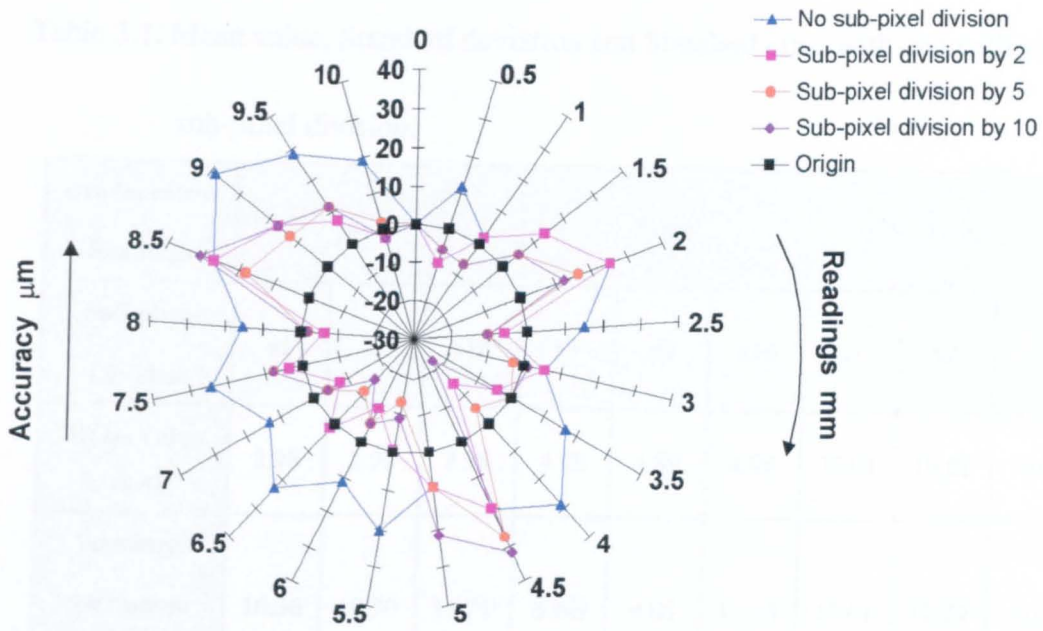


Figure 3.12 Influence of linear sub-pixel division on the accuracy of the readings

However in order to examine the efficiency of the image acquisition and processing system, another set of displacements (3mm, 5mm and 10mm) were measured (twelve times for each), using the same calibration device, and Table 3.1 shows the statistics of this exercise.

The standard deviation is a measure of how widely values are dispersed from the average value (the mean). The higher this becomes the more data points need to be collected in order to be confident that the sample is representative of the population. From the standard deviation values shown in Table 3.1 below it is clear that the displacements measured in the actual tests were accurate enough for the purpose of the current experimental investigation.

The standard error of the mean it is the standard deviation of the sampling distribution of the mean, which again comes out as a very small value.

Table 3.1. Mean value, Standard deviation and Standard error with and without sub-pixel division.

Displacement Readings	3mm			5mm			10mm		
	x1	x2	x10	x1	x2	x10	x1	x2	x10
Mean Value (mm)	2.98	2.98	2.98	4.98	4.99	4.99	10.01	10.01	10.01
Standard Deviation (μm)	10.36	10.30	11.71	8.88	9.05	11.43	12.61	12.89	10.33
Standard Error of sample means (μm)	2.99	2.97	3.38	2.56	2.61	3.29	3.64	3.72	2.98

3.5 TEST PROCEDURE AT ELEVATED TEMPERATURES

The procedure followed during the elevated-temperature tests was first to take the specimens up to the desired temperature and then apply the load. Thermocouples were positioned around the specimens in order to monitor the temperature, and as soon as the specimen reached the desired temperature a load step was applied using the control panel of the hydraulic jack. According to the geometry of each specimen, images were captured at different load steps, sometimes every 1kN in the elastic region, 0.5kN in the elastoplastic region and back to 1kN in the plastic region, and sometimes every 5kN in the elastic, 1kN in the elastoplastic and 2.5kN in the plastic region.

3.6 DISCUSSION

The accuracy of the image acquisition and processing system seems to be adequate. The use of this technique has many advantages in comparison with conventional mechanical instruments and offers a wide range of testing applications and benefits. Some of the benefits of using this technique are:

- a) Direct and non-contacting measurements means that nothing need be attached to the specimen,
- b) Multiple choice of gauge length and operating range because of the flexibility in choosing the field of view for the camera (the limitation here is the resolution of the picture which is dependent on the required accuracy of the measurements),
- c) Used in connection with furnaces (elevated temperatures) or within a hostile environment the video camera can be set some distance away from the test specimen,
- d) The entire testing procedure can be observed on a monitor and even recorded, so it is possible to go back and collect more information by replaying images of the behaviour of the specimen,
- e) The advantage of processing a picture is the availability of information in two dimensions, so it is possible to measure displacements in the transverse direction simultaneously, if necessary,
- f) The system permits comparison of the deflected shapes of the specimen at elevated temperatures with deflected shapes from finite element analysis.

An experimental study of bolted T-stub assemblies (the group of components within the tension zone of a steel joint) is outlined next in order to measure the force-displacement characteristics at elevated temperatures representative of those achieved in building fires. Also a simplified mathematical model has been derived and verified against elevated-temperature test results, thus extending the component approach for use in fire engineering studies.

3.7 REFERENCES

- 3.1 Lawson, R.M., "*Behaviour of Steel Beam-to-Column Connections in Fire*", The Structural Engineer, Vol. 68, No. 14, pp. 263-271, 1990.
- 3.2 Leston-Jones, L.C., "*The Influence of Semi-Rigid Connections on the Performance of Steel Framed Structures in Fire*", Ph.D. Thesis, Department of Civil and Structural Engineering, University of Sheffield, 1997.
- 3.3 Al-Jabri, K.S., "*The Behaviour of Steel and Composite Beam-to-Column Connections in Fire*", Ph.D. Thesis, Department of Civil and Structural Engineering, University of Sheffield, 1999.
- 3.4 Simms I., and Newman, G., "*The Behaviour of Structures in Fire*", Steel Construction Institute lecture notes from the Fire Engineering of Steel Structures Course, University of Sheffield, 1999.
- 3.5 Armer, G.S.T., and Moore, D.B., "*Full-scale Testing on Complete Multi-storey Structures*", Structural Engineer, Vol. 72, No. 2, 1994.
- 3.6 Moore, D.B., and Lennon, T. "*Fire Engineering Design of Steel Structures*", Progress in Structural Engineering, Vol. I (I), pp. 4-9, 1997.
- 3.7 Robinson, J., "*The Cardington Fire Test Programme-Initial Conclusions*", Fire Safety Engineering, Vol. 4, No. 6, 1997.
- 3.8 Information taken from online <http://www.isprs.org/society/history.html>
- 3.9 Coimbra, D., Greenwood, K., and Kendall, K., "*Tensile Testing of Ceramic Fibres by Video Extensometry*", Journal of Materials Science, Vol. 35, pp. 3341-3345, 2000.
- 3.10 Robins, P., Austin, S., Chandler, J., and Jones, P., "*Flexural Strain and Crack Width Measurement of Steel-Fibre-Reinforced Concrete by Optical Grid and Electrical Gauge Methods*", Cement and Concrete Research, Vol. 31, pp. 719-729, 2001.
- 3.11 Collins, T.L.D., Sweeney, J., and Coates, P.D., "*Image Analysis for Strain Measurements in Solid Phase Deformation Studies*", Report from IRC in Polymer Science and Technology, Department of Mechanical and Medical

- Engineering, University of Bradford, 2001,
<http://irc106.irc.brad.ac.uk/irc/techniques/ia/index.html>
- 3.12 Piel, D., and Petersen, C., “*Strain Measurement by Computerized Image Analysis*”, “Strain Measurement at High Temperatures”, Proceedings of a CEC Workshop held at the JRC Petten, Netherlands, 1986.
- 3.13 Gaudig, W., Bothe, K., Bhaduri, A.K., and Maile, K., “*Determination of the Geometric Profile and Stress/Strain State in the Necked Region During Inelastic Deformation at Elevated Temperatures Using a Non-Contact Measurement Technique*”, Journal of Testing and Evaluation, JTEVA, Vol. 24, No. 3, pp. 161-167, 1996.
- 3.14 Bhat, G.K., “*Electronic Speckle Pattern Interferometry Applied to the Characterisation of Materials at Elevated Temperatures*”, American Society for Nondestructive Testing, Material Evaluation, NDT Solutions 1998, <http://www.asnt.org/publications/materialseval/solution/jan98solutions/jan98sol.htm>
- 3.15 McEnteggart, I., “*Contacting and Non-Contacting Extensometry for Ultra High Temperature Testing*”, “Ultra High Temperature Mechanical Testing” Edited by: Lohr, R.D., and Steen, M., Woodhead Publishing Ltd., 1995.

Chapter 4

Tension Zone

4.1 INTRODUCTION

It has been emphasized in the previous chapters that it is important to be able to predict the overall behaviour of beam-to-column joints based on their geometrical and mechanical properties. This can be achieved by means of the so-called component method^{4.1,4.2}, which was introduced in Chapter 2 with reference to the simplest case represented by a fully welded joint. The main objective is to evaluate the stiffness and resistance characteristics of individual or groups of components.

In a bolted joint the major components within the tension zone (Figure 4.1) are the end plate in bending, the column flange in bending and the bolts in tension. All these components are modelled using an equivalent T-stub, i.e., two T-elements connected through the flanges by means of one or more bolt rows as shown in Figure 4.2 below.

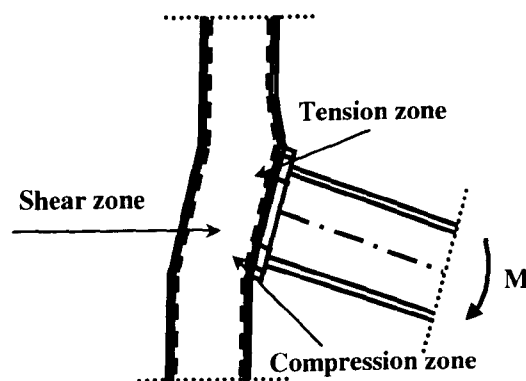


Figure 4.1 The three zones in an end-plate joint

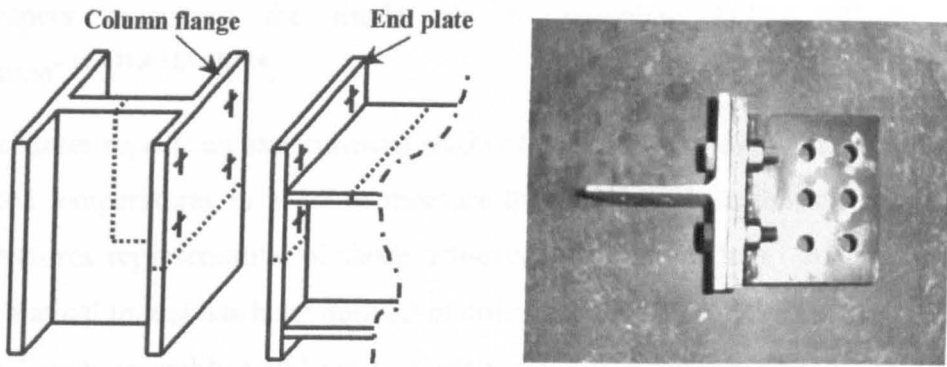


Figure 4.2 T-stub identification and orientation for extended end-plate joint

Early attempts^{4.3} to design end plate connections assumed the column flange to be infinitely stiff and proceeded to estimate the minimum required end plate thickness by calculating the plastic moment capacity using various collapse mechanisms. In the early 1970s researchers realised that the flexibility of the column flanges could affect the behaviour of the connecting tension bolts by inducing prying action. Prying action is the force generated between the contact surfaces of the end plate and the column flange resulting from the resultant tension force and the reaction of the bolts. Zoetemeijer^{4.4} took into account the inter-dependence between these components and produced straight-line yield patterns to represent the failure of both end plate and column flange T-stubs in bending.

Packer and Morris^{4.5} (1977) used curved yield lines to predict the column flange capacity in both stiffened and unstiffened joints. A year earlier Agerskov^{4.6} used the principles of simple bending theory to analyse T-stub behaviour. Based on the same principles Yee and Melchers^{4.1} calculated the elastic stiffness response of the T-stub assembly, but Zoetemeijer's^{4.7} work is of most importance, because contains the basic principles of the component method which is extensively applied today throughout Europe.

Simple bending theory is the basis for the simplified formulae given in Eurocode 3: Annex J^{4.8} and British design guides^{4.9} for calculating the elastic stiffness, and the perfectly plastic ultimate strength of the T-stub assembly. The elasto-plastic response of T-stub assemblies was not one of the primary objectives in the preparation of any design codes or standards, so information is limited to a handful

of papers extending the model up to complete failure of the T-stub specimen^{4.10,4.11,4.12,4.13,4.14}.

This chapter reports an experimental study of bolted T-stub assemblies conducted at elevated temperatures in order to measure the force-displacement characteristics at temperatures representative of those achieved in building fires. Also a simplified mathematical model has been derived in order to predict the elastic-plastic behaviour of the T-stub assemblies and verified against elevated-temperature test results, thus extending the component approach for use in fire engineering studies.

4.2 SIMPLIFIED MATHEMATICAL MODEL

The deformation of each equivalent T-stub assembly (either end plate or column flange such as that shown in Figure 4.3) may be induced by the elastic and plastic flexure of the column flange and end plate, and by the elastic and plastic elongation of the bolts. In Figure 4.3 the effective width (L_{eff}) has been shown, as described by Faella *et al*^{4.15} assuming a 45° spread of the bolt action starting from the washer edge and finishing at $0.8r$ or $0.8a_f\sqrt{2}$ (where r is the root radius of the column flange and a_f the weld thickness for the end plate) from the face of the web.

This assumption leads to effective width values different from those suggested in the current draft of Eurocode 3:Annex J, but for the current study, even though the same assumption was made for the effective width (Faella *et al*.^{4.15}) it happened, for almost all the test cases, that the values were very close to the EC3: Annex J values.

Figure 4.3 Equivalent Column Flange and End Plate T-stub assembly

It is well known that bolted T-stub assemblies can fail according to three possible mechanisms, as shown in Figure 4-4 below.

- First yielding in the T-stub flange, and then yielding at 45 degrees of the column flange (Figure 4.4a).
- Complete yielding of the T-stub flange (Figure 4.4b).

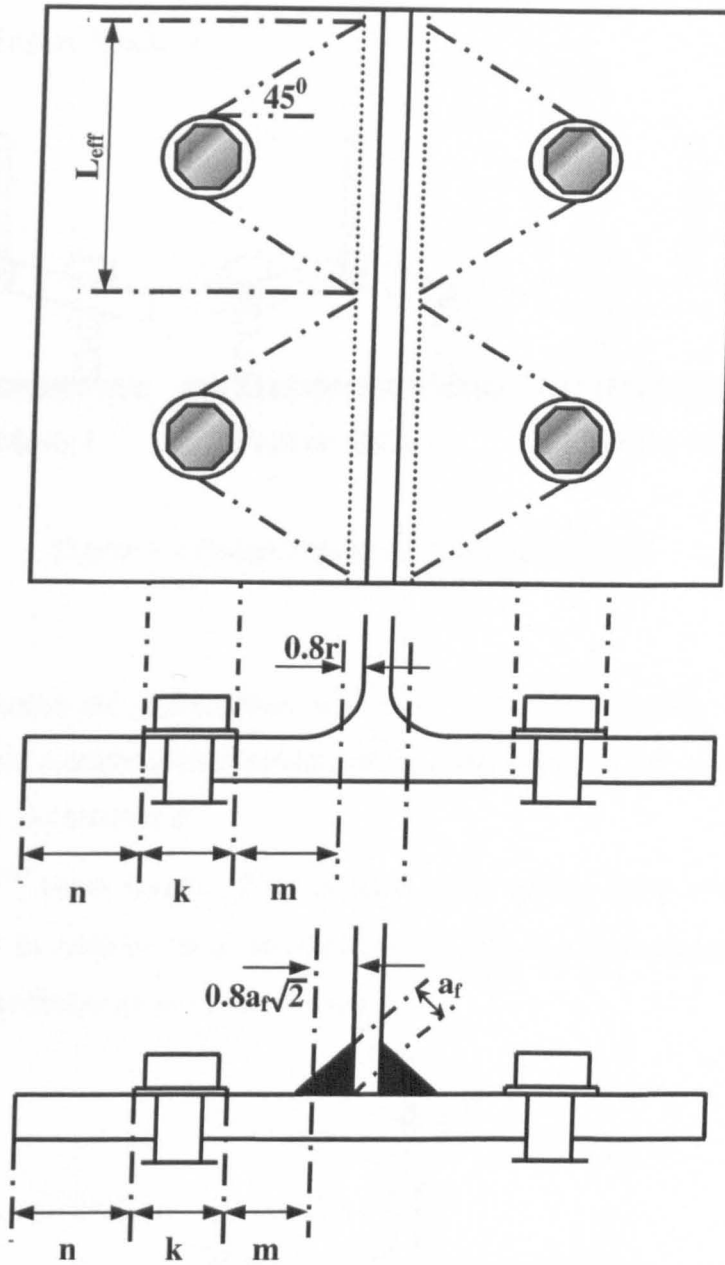


Figure 4.3 Equivalent Column Flange and End Plate T-stubs respectively

It is well known that these T-stub assemblies can fail according to three possible collapse mechanisms, as shown in Figure 4.4 below:

- First yielding in the T-stub flange, and then yielding and fracture of the bolts (Failure Mode 1),
- Complete yielding of the T-stub flange (Failure Mode 2),

- c) The T-stub flange remains elastic and failure occurs due to the fracture of the bolts (Failure Mode 3).

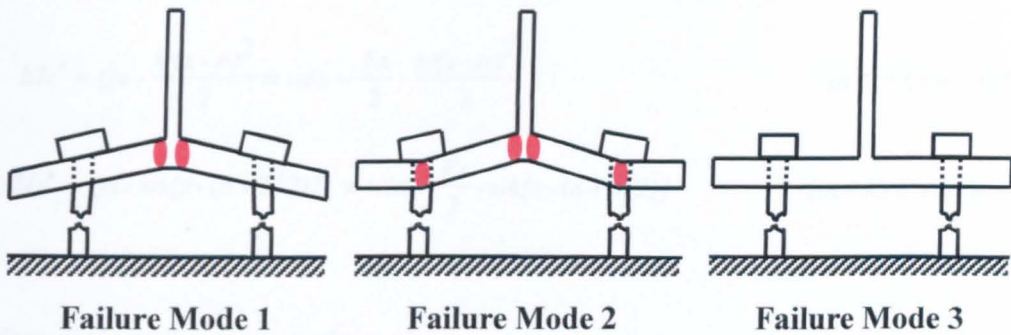


Figure 4.4 Failure modes for the T-stub flange

In order to research the deformation mode, for a T-stub assembly, under various bending moments, a mathematical model has been developed in this study to consider the elasto-plastic deformations.

From classical^{4,16} beam theory, if the tension force acting on a T-stub assembly (Figure 4.5) is F , in order to obtain the deflection δ_{ep} the bending moment expressions in each part of the flange must be determined.

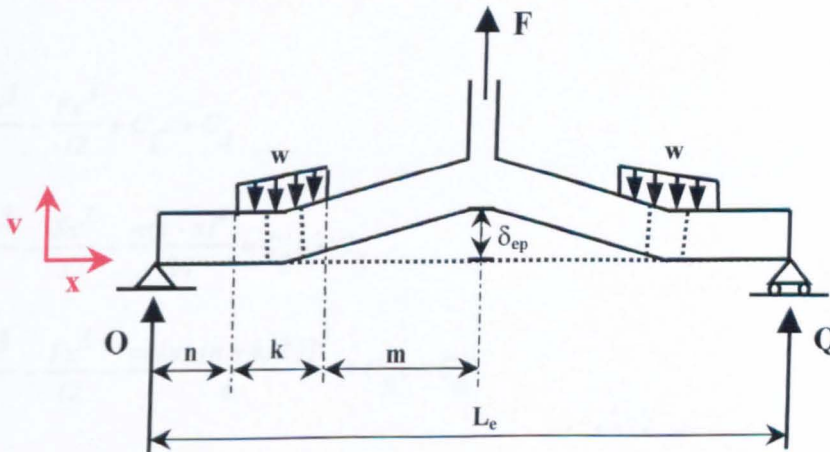


Figure 4.5 Forces on T-stub assembly

The bending moment expressions at the three intervals moving from left to right across the T-stub are:

$$EIv'' = Qx = w_kx - \frac{Fx}{2} \quad (0 \leq x \leq n)$$

$$EIv'' = Qx - \frac{w(x-n)^2}{2} = w_kx - \frac{Fx}{2} - \frac{w(x-n)^2}{2} \quad [n \leq x \leq (n+k)]$$

$$EIv'' = Qx - wk[x - (n+k/2)] = w_kx - \frac{Fx}{2} - wk[x - (n+k/2)] \quad [(n+k) \leq x \leq (n+k+m)]$$

Integration of these equations gives

$$EIv' = \frac{w_kx^2}{2} - \frac{Fx^2}{4} + C_1$$

$$EIv' = \frac{w_kx^2}{2} - \frac{Fx^2}{4} - \frac{w(x-n)^3}{6} + C_2$$

$$EIv' = \frac{w_kx^2}{2} - \frac{Fx^2}{4} - \frac{wk[x - (n+k/2)]^2}{2} + C_3$$

Performing a second integration the deflection equations are:

$$EIv = \frac{w_kx^3}{6} - \frac{Fx^3}{12} + C_1x + C_4$$

$$EIv = \frac{w_kx^3}{6} - \frac{Fx^3}{12} - \frac{w(x-n)^4}{24} + C_2x + C_5$$

$$EIv = \frac{w_kx^3}{6} - \frac{Fx^3}{12} - \frac{wk[x - (n+k/2)]^3}{6} + C_3x + C_6$$

The six constants of integration appearing in the preceding equations can be found from the following boundary conditions:

- a) at $x=0$ the deflection is equal to zero;

- b) at $x=n$ and $x=(n+k)$ the slope and deflection for the two parts of the beam must be equal;
- c) at $x=(n+k+m)$ the slope is equal to zero.

Using the above boundary conditions the constants can be found and the deflection δ_{ep} at $x=(n+k+m)$ can be determined.

$$\delta_{ep} = \frac{FL_e^3}{48EI} - \frac{wk}{EI} \left[\frac{Le^3}{24} + \frac{[m+(k/2)]^3}{6} - \frac{[m+(k/2)]^2 Le}{4} - \frac{k^2 [n+(k/2)]}{24} \right] \quad \dots 4.1$$

Where E is the T-stub flange Young's Modulus; $I = 2L_{eff} t_f^3/12$, L_{eff} is the effective length for the T-stub flange (Figure 4.3); F is the tension force applied to the T-stub; wk is the bolt tension force; and n , k and m are defined in Figure 4.3.

To use the equation above, the bolt force wk needs to be expressed in terms of the T-stub force F . This can be obtained from the compatibility condition requiring that at the bolt line ($x=n+k/2$), the deflection of the T-stub flange must be equal to the bolt elongation. From beam bending theory the deflection at the bolt line $x=n+(k/2)$ can be given by:

$$\delta_{bl} = \frac{F}{EI} \left[\frac{[n+(k/2)]Le^2}{16} - \frac{[n+(k/2)]^3}{12} \right] + \dots \dots \dots$$

$$+ \frac{wk}{EI} \left[\frac{[n+(k/2)]^3}{6} + \frac{k^2 [n+(k/2)]}{24} + \frac{[n+(k/2)][m+(k/2)]^2}{2} - \frac{[n+(k/2)]Le^2}{8} - \frac{k^3}{384} \right] \quad \dots 4.2$$

which should be equal to the bolt elongation given by

$$\delta_{b2} = \frac{wkL_b}{E_b A_s} \quad \dots 4.3$$

Where L_b is the effective length of the bolt (Figure 4.6); E_b is the Young's Modulus of the bolt and A_s is the shaft area of the bolt.

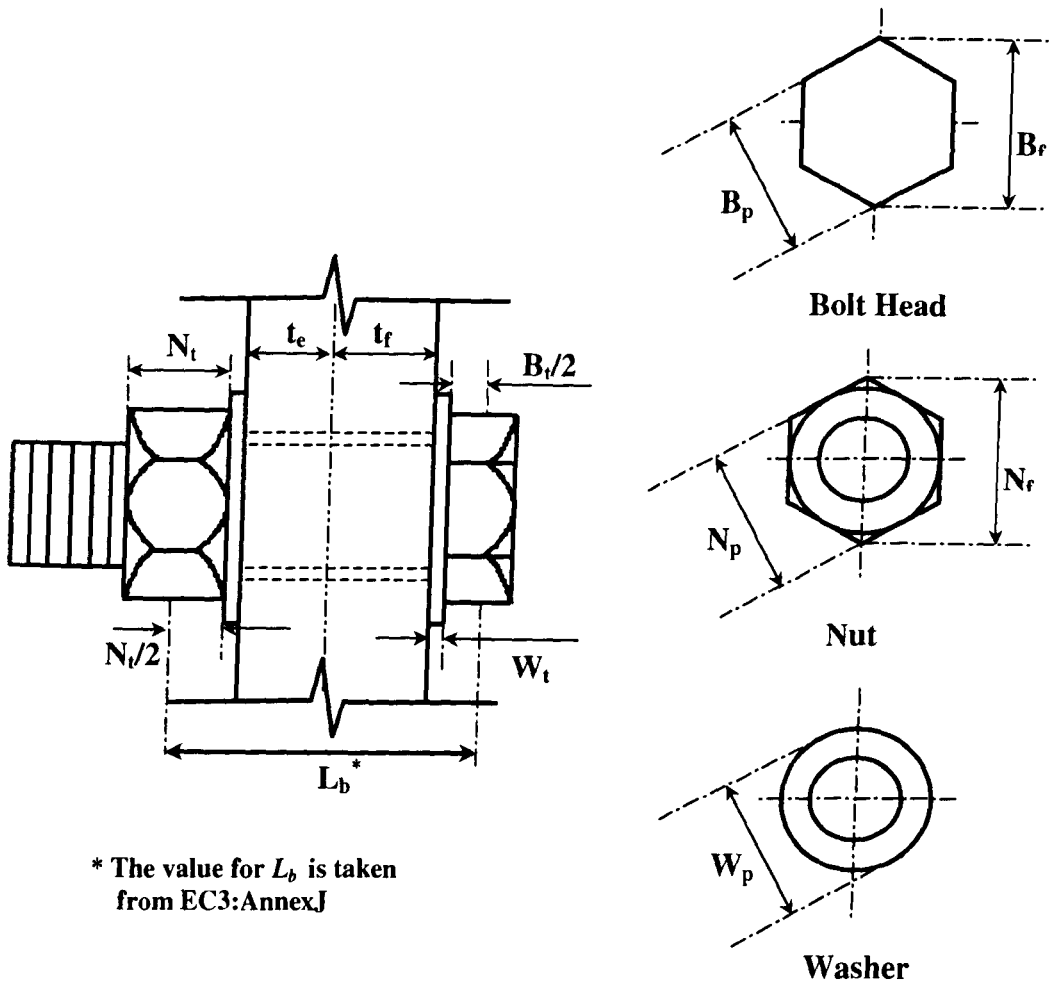


Figure 4.6 Detail of a bolt within an end plate to column T-stub connection

Therefore, from equations 4.2 and 4.3 above, the bolt force wk can be expressed as:

$$wk = \frac{\frac{F}{EI} \left[\frac{[n+(k/2)]Le^2}{16} - \frac{[n+(k/2)]^3}{12} \right]}{\frac{L_b}{E_b A_s} - \frac{1}{EI} \left[\frac{[n+(k/2)]^3}{6} + \frac{k^2 [n+(k/2)]}{24} + \frac{[n+(k/2)] [m+(k/2)]^2}{2} - \frac{[n+(k/2)]Le^2}{8} - \frac{k^3}{384} \right]}$$

...4.4

Further simplification of the formula above gives the bolt force as a ratio ρ of the total T-stub force F .

$$wk = \rho F \quad \dots 4.5$$

And the prying force Q as shown in Figure 4.5 is given by:

$$Q = wk - F = F(\rho - 1) \quad \dots 4.6$$

By substituting equation 4.4 into 4.1 the maximum deflection δ_{ep} in the middle span of the T-stub flange can be written as a function of F .

The next step in the calculation procedure is to determine the magnitude of the total T-stub force F and the position of the first plastic hinge. The first plastic hinge will appear when the maximum bending moment in the T-stub flange exceeds the plastic moment resistance M_p given by:

$$M_p = \frac{(2L_{eff})f_y t_f^2}{4} \quad \dots 4.7$$

Where f_y is the yield stress of the T-stub flange; L_{eff} is the effective length as shown in Figure 4.3 and t_f is the flange thickness.

In order to calculate the tension force in the T-stub flange and the position of the first plastic hinge, the minimum value for the flange forces is taken from equations 4.8, 4.9 and 4.10. These equations represent:

- a) The flange moment in the middle of the T-stub assembly, at $x=(n+k+m)$
- b) The flange moment at the bolt line of the T-stub assembly, at $x=n+(k/2)$
- c) T-stub force due to yielding of the bolts

$$M_f = wk[n + (k/2)] - \frac{F_{fl}(n+k+m)}{2} = M_p \quad \dots 4.8$$

$$M_b = wk[n + (k/2)] - \frac{F_{fl2}[n + (k/2)]}{2} - wk \frac{k}{8} = M_p \quad \dots 4.9$$

$$wk = 2A_s f_{by} = \rho F_{fl3} \quad \dots 4.10$$

Where $M_f = wk[m + (k/2)] - Q(n + k + m)$, $M_b = Q[n + (k/2)] - (wk)k/8$ and f_{by} is the yield stress for the bolt. By substituting $Q = wk - (F_{fl}/2)$ and wk with equation 4.5 the T-stub force F_{fl} can be calculated.

The minimum value of those three T-stub forces will give the total tension force and also the position of the first plastic hinge.

$$F_{fl} = \min[F_{fl1}, F_{fl2}, F_{fl3}] \quad \dots 4.11$$

After the formation of the first plastic hinge, which for Failure Modes 1 and 2 always happens in the middle of the T-stub flange, at $x = (n + k + m)$, a failure may develop in one of the two ways below, and whichever happens first will define the failure mode of the T-sub flange. Either:

- a) The bolts start to yield (Failure Mode 1), or
- b) A second plastic hinge forms in the T-stub flange at $x = n + (k/2)$ (Failure Mode 2)

4.2.1 Failure Mode 1-Bolts start to yield after the first plastic hinge has formed

After the formation of the first plastic hinge, if the bolts start to yield then part of the flange remains elastic and the total T-stub force F_{flb} is given by:

$$M_p = (wk + \Delta wk)[m + (k/2)] - \left[(wk + \Delta wk) - \frac{(F_{fl} + \Delta F_{fl})}{2} \right] (n + k + m) \quad \dots 4.12$$

$$F_{flb} = (F_{fl} + \Delta F_{fl}) = \frac{2M_p + \sum (wk + \Delta wk)[n + (k/2)]}{(n + k + m)} \quad \dots 4.13$$

where $\Sigma(wk + \Delta wk) = 4A_s f_{by}$ and M_{pe} is given by equation 4.7.

The total bolt force and the total prying force are given below as functions of the T-stub force from equation 4.12 above.

$$(wk)_b = wk + \Delta wk = \frac{\frac{(F_{fl} + \Delta F_{fl})}{2} (n+k+m) - M_p}{[n+(k/2)]} \quad \dots 4.14$$

$$(Q)_b = Q + \Delta Q = \frac{\frac{(F_{fl} + \Delta F_{fl})}{2} [m+(k/2)] - M_p}{[n+(k/2)]} \quad \dots 4.15$$

The deflection when the bolts start to yield can be calculated using the same analysis as in the calculation of initial deflection δ_{ep} . In this case though the total bolt and T-stub forces have to be taken into account in the bending moment equations as well as the plastic moment M_p at the middle of the flange, $x=(n+k+m)$. By integrating the bending moment equations twice, the constants can be calculated using the same boundary conditions as before, except at $x=[n+(k/2)]$ where the total bolt deflection is equal to $(\delta_{bl})_b = \delta_{bl} + \frac{\Delta wk L_b}{E_b A_s}$. The total deflection of the T-stub flange at $x=(n+k+m)$ is given below:

$$\begin{aligned} \left(\delta_{ep} \right)_b = \delta_{ep} + \Delta \delta_{ep} = & \frac{(wk + \Delta wk)}{EI} \left[\frac{(n+k+m)^3}{6} - \frac{[m+(k/2)]^3}{6} \right] - \\ & - \frac{(F_{fl} + \Delta F_{fl}) (n+k+m)^3}{2EI} + \frac{A(n+k+m)}{EI} + \frac{B}{EI} \end{aligned} \quad \dots 4.16$$

Where the constants A and B are:

$$\begin{aligned} A = (wk + \Delta wk) \left[\frac{k^3}{384[n+(k/2)]} - \frac{[n+(k/2)]^2}{6} - \frac{k^2}{24} \right] + \frac{(F_{fl} + \Delta F_{fl}) [n+(k/2)]^2}{2} + \\ + \frac{EI \delta_{bl}}{[n+(k/2)]} + \frac{\Delta wk EI L_b}{E_b A_s [n+(k/2)]} \end{aligned}$$

$$B = (wk + \Delta wk) \left[\frac{k^2 [n + (k/2)]}{24} \right]$$

By substituting $(wk + \Delta wk)$ from equation 4.14 into the displacement equation 4.16 the total displacement $(\delta_{ep})_b$ at which the bolts yield can be expressed as a function of the T-stub force $(F_{fl})_b$.

4.2.2 Failure Mode 1-Fracture of the bolts after they yield

After yielding of the bolts, the prying force Q cannot be increased any further and the bolts take any increase of the T-stub force until they fracture. Hence,

$$(\Delta wk)_b = \frac{(\Delta F_{fl})_b}{2} = 2A_s f_{bu} - (wk)_b \quad \dots 4.17$$

$$(\Delta Q)_b = 0 \quad \dots 4.18$$

Where f_{bu} is the ultimate stress of the bolt.

The incremental deflection due to the final incremental force $(\Delta F_{fl})_b$ on the T-stub flange can be calculated using beam theory again, but with the system as shown in Figure 4.7.

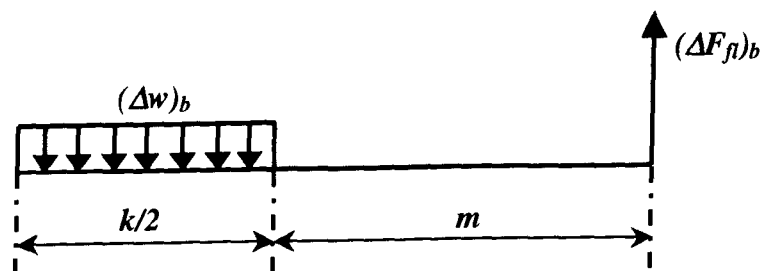


Figure 4.7 System for calculating the final displacement

The bending moment expressions are:

$$EIv'' = -\frac{(\Delta w)_b x^2}{2} \quad [0 \leq x \leq (k/2)]$$

$$EIv'' = -\frac{(\Delta wk)_b [x - (k/4)]}{2} \quad [(k/2) \leq x \leq (k/2) + m]$$

Integration of these equations gives

$$EIv' = -\frac{(\Delta w)_b x^3}{6} + C_1$$

$$EIv' = -\frac{(\Delta wk)_b [x - (k/4)]^2}{4} + C_2$$

Performing a second integration the deflection equations are

$$EIv = -\frac{(\Delta w)_b x^4}{24} + C_1 x + C_3$$

$$EIv = -\frac{(\Delta wk)_b [x - (k/4)]^3}{12} + C_2 x + C_4$$

The four constants of integration appearing in the preceding equations can be found from the following boundary conditions:

- At $x=0$ the deflection $v=(\Delta wk)_b(L_b/E_b A_s)$,
- At $x=k/2$ the slope and deflection for the two parts of the beam must be equal,
- At $x=m+(k/2)$ the slope is equal to zero.

Using the above boundary conditions the constants can be found and the incremental displacement $(\Delta \delta_{ep})_b$ at $x=m+(k/2)$ determined.

$$(\Delta\delta_{ep})_b = \frac{(\Delta F_{fl})_b}{EI} \left[\frac{[m + (k/4)]^2 [m + (k/2)]}{8} - \frac{[m + (k/4)]^3}{24} + \frac{k^3}{1536} + \frac{EIL_b}{2E_{tb}A_s} \right] \quad \dots 4.19$$

Note that E_{tb} is taken as 1.0% of the bolt elastic Young's Modulus E_b (205 kN/mm²). Shi *et al*^{4.10} report that the Tangent Modulus for the bolt should be taken as 5% of the elastic Young's Modulus, and this value is derived from an ambient-temperature finite element analysis. Studies performed at Sheffield University by Theodorou^{4.17} (described later in the chapter in more detail) on Grade 8.8 bolts at elevated temperatures concluded that the value of 1.0% could be used for defining the bolt Tangent Modulus value.

For the T-stub flange, Piluso *et al*^{4.12} performed 12 coupon tests and reported that the Tangent Modulus of the flange (up to ultimate stress) was ranging from 1.0-1.6% of the elastic Young's Modulus. For the current study a value of 1.5% was chosen because it best fits all the experimental results.

4.2.3 Failure Mode 2-Formation of a second plastic hinge at the bolt line

The formation of the first plastic hinge is analysed as described in section 4.2. If a second plastic hinge is formed in the flange at the bolt line, $x=[n+(k/2)]$ the T-stub force F_{fl} can be calculated as shown below:

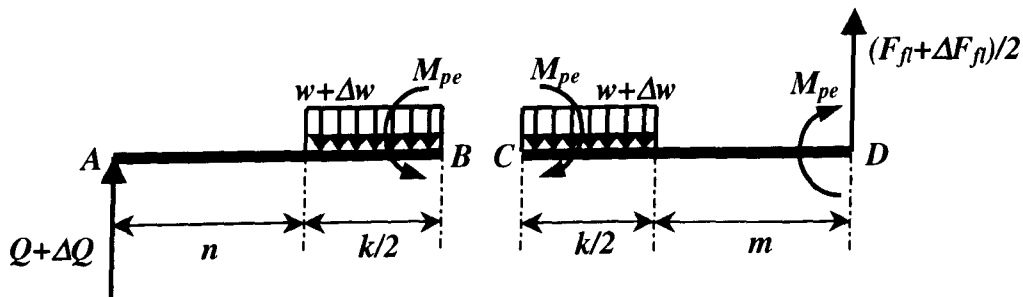


Figure 4.8 Free body diagram for half of the T-stub flange

By taking $\Sigma M_A = 0$ then M_{pe} is equal to:

$$M_p = (wk + \Delta wk)[n + (3k/8)] - \frac{(F_{fl} + \Delta F_{fl})}{2} [n + (k/2)] \quad \dots 4.20$$

and for the other part of the T-stub flange (Figure 4.8), when $\Sigma M_C = 0$ the total force is equal to:

$$(F_{fl})_f = F_{fl} + \Delta F_{fl} = \frac{4M_p + 2(wk + \Delta wk)\frac{k}{8}}{[m + (k/2)]} \quad \dots 4.21$$

Solving equation 4.20 with respect to $wk + \Delta wk$ and substituting into equation 4.21 the T-stub force when the second plastic hinge forms is given by:

$$(F_{fl})_f = F_{fl} + \Delta F_{fl} = \frac{2M_{pe} [2n + (7k/8)]}{[mn + (3km/8) + (3kn/8) + (k^2/8)]} \quad \dots 4.22$$

The bolt force and prying force increments are given by the following formulae:

$$\Delta wk = \frac{\Delta F_{fl}}{2} \left[\frac{[m + (k/2)]}{[n + (k/2)]} + 1 \right] \quad \dots 4.23$$

$$\Delta Q = \frac{\Delta F_{fl}}{2} \left[\frac{[m + (k/2)]}{[n + (k/2)]} \right] \quad \dots 4.24$$

The total bolt force is equal to $(wk)_f = wk + \Delta wk$ and the total prying force is equal to $(Q)_f = Q + \Delta Q$. The deflection at $x = (n + k + m)$ can be calculated using the same bending equations as in the calculation of initial deflection δ_{ep} but this time using the incremental forces. After the second integration the constants can be calculated using the same boundary conditions as before except at $x = n + (k/2)$ where the bolt

deflection according to the incremental bolt force is equal to $\Delta\delta_{bl} = \frac{\Delta wk L_b}{E_b A_s}$. The

incremental deflection $\Delta\delta_{ep}$ of the T-stub flange at $x=(n+k+m)$ is given below:

$$\Delta\delta_{ep} = \frac{\Delta Q}{EI} \left[\frac{(n+k+m)^3}{6} \right] - \frac{\Delta wk}{EI} \frac{[m+(k/2)]^3}{6} + \frac{C(n+k+m)}{EI} + \frac{D}{EI} \quad \dots 4.25$$

in which the constants C and D are given as:

$$C = \Delta wk \left[\frac{k^3}{384[n+(k/2)]} - \frac{k^2}{24} + \frac{EIL_b}{E_b A_s [n+(k/2)]} \right] - \frac{\Delta Q[n+(k/2)]^2}{6}$$

$$D = \Delta wk \left[\frac{k^2 [n+(k/2)]}{24} \right]$$

By substituting equations 4.23 and 4.24 into the equations for constants C and D and then those into equation 4.25 the deflection $\Delta\delta_{ep}$ can be calculated according to the incremental T-stub force ΔF_{fl} .

4.2.4 Failure Mode 2-Yielding of the bolts after the second plastic hinge at the bolt line

After the appearance of the second plastic hinge in the fillet at $x=n+(k/2)$ the prying force Q cannot be increased any further and any increase of the T-stub force is taken by the bolts until they yield. Hence,

$$(\Delta wk)_f = \frac{\left(\Delta F_{fl} \right)_f}{2} = 2A_s f_{by} - (wk)_f \quad \dots 4.26$$

$$\Delta Q_b = 0 \quad \dots 4.27$$

where $(wk)_f = wk + \Delta wk$, f_{by} is the yield stress for the bolt, the total bolt force is equal to $(wk)_{fb} = (wk)_f + (\Delta wk)_f$, and the total T-stub force is equal to $(F_{fl})_{fb} = (F_{fl})_f + (\Delta F_{fl})_f$.

The procedure to calculate the deflection $(\Delta \delta_{ep})_f$ due to the incremental force $(\Delta F_{fl})_f$ is the same as described in section 4.2.1.

$$\left(\Delta \delta_{ep} \right)_f = \frac{\left(\Delta F_{fl} \right)_f}{E_t I} \left[\frac{[m + (k/4)]^2 [m + (k/2)]}{8} - \frac{[m + (k/4)]^3}{24} + \frac{k^3}{1536} + \frac{E_t I L_b}{2E_b A_s} \right] \quad \dots 4.28$$

Where E_t is taken as 1.5% of the flange elastic Young's Modulus E .

4.2.5 Failure Mode 2-Fracture of the bolts after they yielded

The incremental T-stub force, between yielding and fracture of the bolts is given below:

$$(\Delta wk)_{fb} = \frac{\left(\Delta F_{fl} \right)_{fb}}{2} = 2A_s f_{bu} - (wk)_{fb} \quad \dots 4.29$$

$$(\Delta Q)_b = 0 \quad \dots 4.30$$

where f_{bu} is the ultimate stress for the bolt, the total bolt force is equal to $(Wk)_{fb} = (Wk)_{fb} + (\Delta Wk)_{fb}$ and the total T-stub flange force is equal to

$(F_{fl})_{fb1} = (F_{fl})_{fb} + (\Delta F_{fl})_{fb}$. The deflection $(\Delta \delta_{ep})_{fb}$ due to the incremental force $(\Delta F_{fl})_{fb}$ is given by:

$$\left(\Delta \delta_{ep} \right)_{fb} = \frac{\left(\Delta F_{fl} \right)_{fb}}{E_t I} \left[\frac{[m + (k/4)]^2 [m + (k/2)]}{8} - \frac{[m + (k/4)]^3}{24} + \frac{k^3}{1536} + \frac{E_t I L_b}{2 E_{tb} A_s} \right] \quad \dots 4.31$$

Where E_t is taken as 1.5% of the flange Young's Modulus E and E_{tb} is taken as 1.0% of the bolt Young's Modulus E_b .

4.2.6 Failure Mode 3-Yielding and fracture of the bolts

In this failure mode the T-stub flange remains elastic and the bolts cause the failure. The procedure to calculate the force and displacement up to fracture of the bolts is the same as described in section 4.2.5.

The incremental T-stub force is given by equation 4.29 and the displacement is given by equation 4.31. The value for E_{tb} is taken as 1.0% of the bolt Young's Modulus E_b .

4.3 ELEVATED TEMPERATURES MODEL

Steel weakens with increasing temperature, and eventually failure occurs in a member as a result of its inability to sustain the applied load. In order to model the T-stub flange behaviour at elevated temperatures the variation of yield stress and Young's modulus for bolts and for structural steel need to be taken into account.

4.3.1 Degradation of steel strength

Design codes have adopted the concept of “ Strength Reduction Factor-SRF” (which is really a strength retention factor) to present the degradation of material strength at elevated temperatures. This is basically the residual strength of the steel at a particular temperature relative to its basic yield strength at room temperature. At ambient temperature, the stress-strain characteristics of steel are approximately bi-linear with a distinct yield plateau. At high temperatures, however, the stress-strain curves degrade and lose their bi-linear nature, making it difficult to define the exact yield point and elastic modulus.

To overcome the problem a limiting strain is specified and the relationship between strength reduction factor and temperature will depend on the limit chosen. The design codes BS5950: Part 8^{4.18} and EC3: Part 1.2^{4.19} have adopted 0.5%, 1.5% and 2.0% strain limits for the fire limit state. The appropriate limit depends on whether the steel is bare or composite and the strain limit of any protective material used.

4.3.2 Degradation of steel stiffness

The stiffness of steel is defined by Young's (elastic) Modulus, which is the slope of the tangent of the stress-strain curve at zero stress. At elevated temperature the tangent modulus must be used because of the non-linear nature of the curves. However this depends on the proof strain at which the elastic modulus is measured. Therefore, a bi-linear relationship is often used, with the elastic modulus expressed

as function of temperature. The difference in the strength and stiffness reduction factors between the BS5950: Part 8 code and EC3: Part 1.2 is very small.

Table 4.1 shows the Strength Reduction Factors for S275 steel at 2% strain and the Stiffness Reduction Factor taken from EC3: Part 1.2. These are the SRF values used in the mathematical model at elevated temperatures in order to model the behaviour of the T-stub assemblies.

Table 4.1 Reduction factors for stress-strain curves of steel at elevated temperatures

Steel Temperature, θ_s	Reduction factors for yield stress f_y , and Young's modulus E_s , at steel temperature θ_s	
	$k_{y,\theta} = f_{y,\theta} / f_y$	$k_{E,\theta} = E_{s,\theta} / E_s$
20 ⁰ C	1.000	1.000
100 ⁰ C	1.000	1.000
200 ⁰ C	1.000	0.900
300 ⁰ C	1.000	0.800
400 ⁰ C	1.000	0.700
500 ⁰ C	0.780	0.600
600 ⁰ C	0.470	0.310
700 ⁰ C	0.230	0.130
800 ⁰ C	0.110	0.090
900 ⁰ C	0.060	0.0675
1000 ⁰ C	0.040	0.0450
1100 ⁰ C	0.020	0.0225
1200 ⁰ C	0.000	0.000

4.3.3 Degradation of bolts at elevated temperatures

Unfortunately, little is known about the deterioration of bolts in fire and this is insufficiently addressed in design codes. In order to determine the deterioration of the strength of bolts in fire a series of tests was conducted by Kirby^{4,20} on Grade 8.8 bolts which are widely used in steel construction. The bolts suffer a significant decrease in capacity in the temperature range 300°C to 700°C. Based on these results, the following tri-linear relationship has been proposed for the Strength Reduction Factor-SRF describing the degradation of bolt strength at elevated temperatures:

$$\theta_b \leq 300^\circ\text{C} \quad \text{then } \text{SRF} = 1.0$$

$$\theta_b < 300^\circ\text{C} \leq 680^\circ\text{C} \quad \text{then } \text{SRF} = 1.0 - (\theta_b - 300)2.128 \times 10^{-3}$$

$$\theta_b < 680^\circ\text{C} \leq 1000^\circ\text{C} \quad \text{then } \text{SRF} = 0.17 - (\theta_b - 680)5.13 \times 10^{-4}$$

where θ_b is the temperature of the bolt.

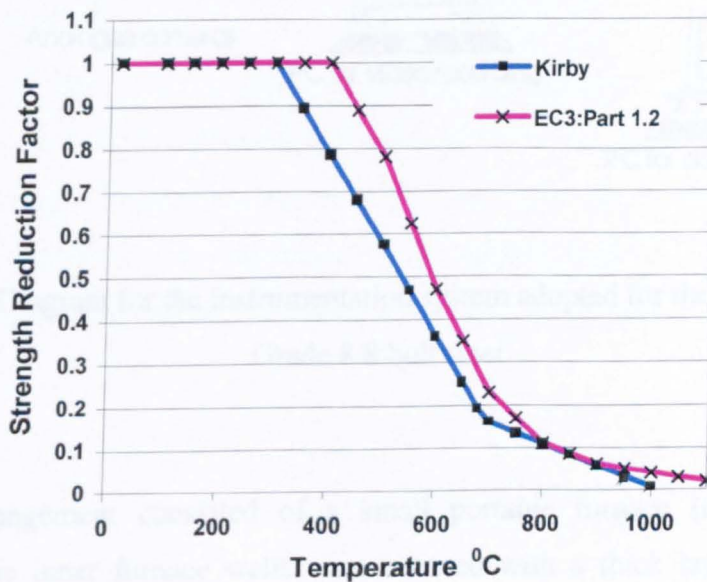


Figure 4.9 Comparison between bolt and steel Strength Reduction Factors

There is no information about the degradation of stiffness for Grade 8.8 bolts at elevated temperatures. For this reason Theodorou^{4.17} carried out a separate study in association with this project in order to study the behaviour of these bolts.

4.3.3.1 Experimental Investigation of Grade 8.8 Bolts at Elevated Temperatures

A number of tensile tests under steady-state heating conditions between 20⁰-1000⁰C were conducted to establish the degradation of stiffness and strength of Grade 8.8 bolts. The intention was to define the mechanical properties in order to understand the overall behaviour of connections and T-stub assemblies. The test arrangement is illustrated in Figure 4.10.

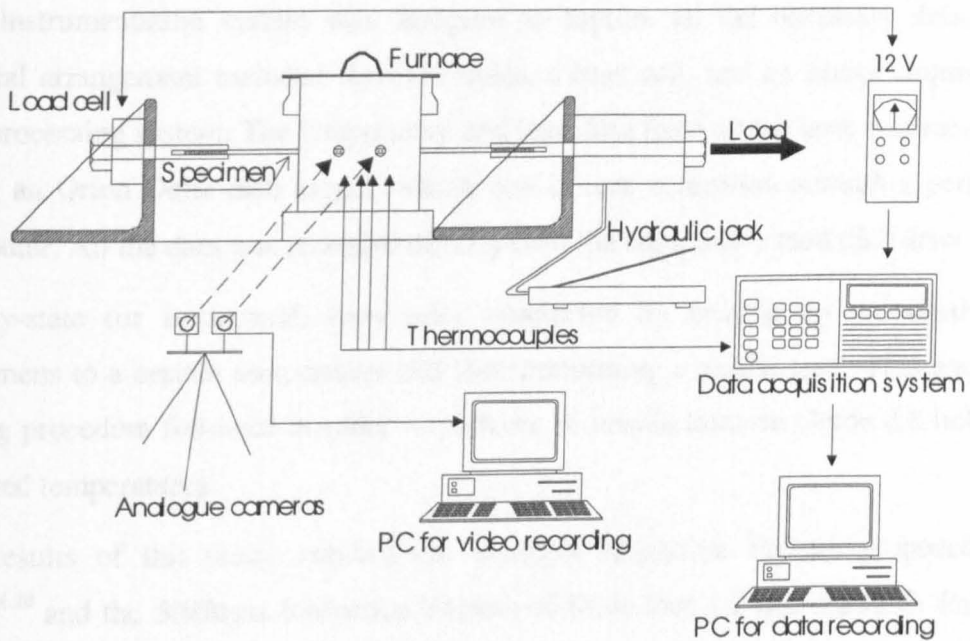


Figure 4.10 Diagram for the instrumentation system adopted for the experiments on Grade 8.8 bolt steel

The test arrangement consisted of a small portable furnace (internal capacity 715cm³). The inner furnace walls were covered with a thick layer of insulating material, to facilitate rapid heating and to keep the temperature inside the furnace constant. A tangential halogen lamp (1000W, 230V) was placed in the upper part of the furnace in order to achieve uniform distribution of the heating and rapid growth

of temperature up to 1000 °C^{4.21}. A general layout of the furnace is illustrated in Figure 4.11. Two slots in the opposite ends of the furnace allowed the loads to be applied to the specimen.

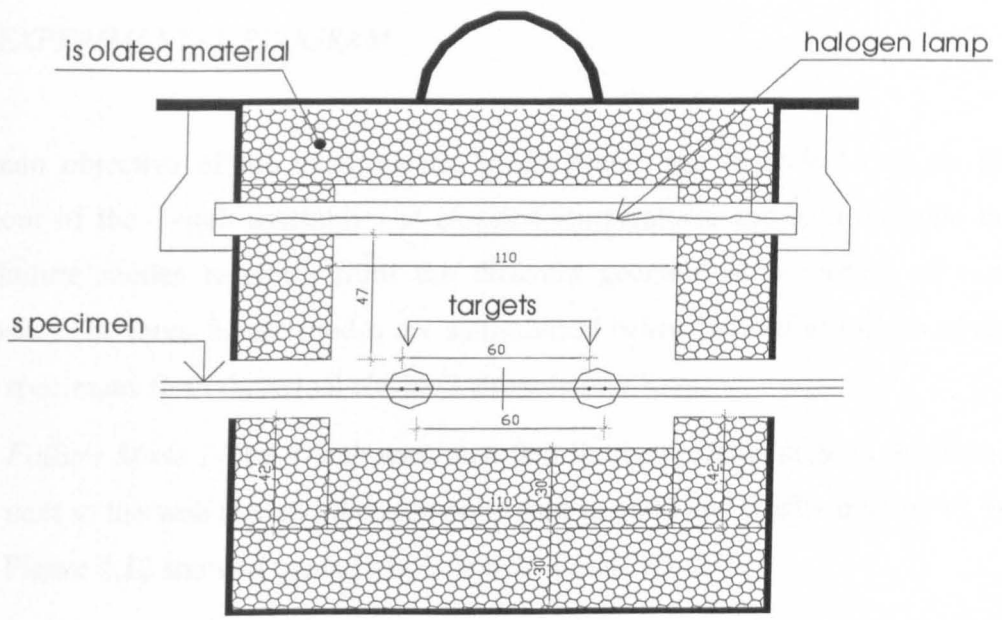
Two equal angles (200x200x16) placed on either side of the furnace provided the reaction frame for the test arrangement. Loads were applied to the specimen via a hydraulic jack loading system. The loads were recorded using a hollow load cell placed between the reaction frame and specimen as shown in Figure 4.10 above.

At the front of the furnace two circular holes, of 15mm diameter, were drilled. These were perpendicular to the axis of loading, facing the specimen axis. These two view-ports were used to accommodate video cameras used for optical monitoring of the specimen and for measuring the strains from the captured images.

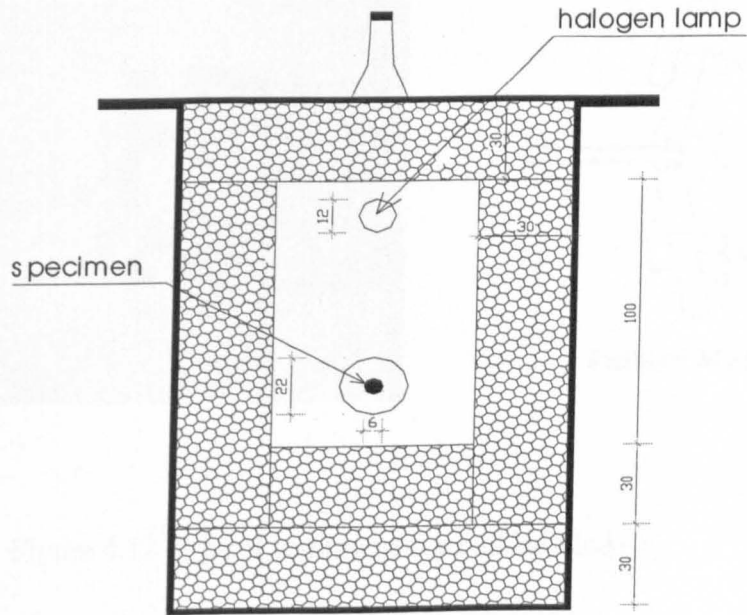
The instrumentation system was designed to capture all the necessary data. The general arrangement included thermocouples, a load cell, and an image acquisition and processing system. The temperature and load data from all the tests was recorded using an Orion Delta data logger, which was in turn controlled through a personal computer. All the data was recorded directly onto the computer's hard disk drive.

Steady-state (or isothermal) tests were conducted by heating up unloaded test specimens to a certain temperature and then performing a tensile test. This was the testing procedure followed in order to perform 16 tensile tests on Grade 8.8 bolts at elevated temperatures.

The results of this study verified the Strength Reduction Factors proposed by Kirby^{4.20} and the Stiffness Reduction Factors of EC3: Part 1.2 and BS5950: Part 8, which are for S275 steel. Furthermore the bolt specimens produced very large strains as the temperature was increased (values ranging from 8-16%). Full details of the test programme and results have been reported by Theodorou^{4.17}.



Cross-S ection of F urnace



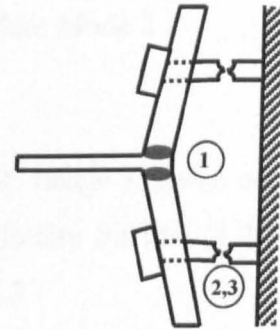
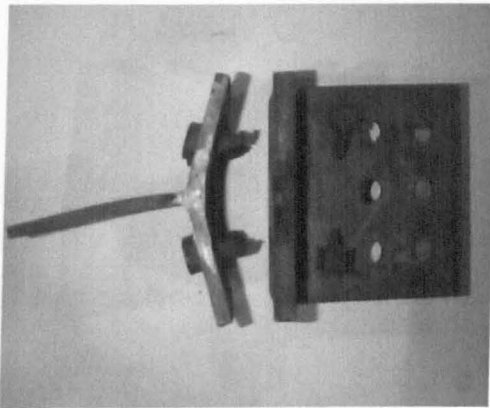
Cross-S ection of F urnace

Figure 4.11 Tangential halogen lamp furnace

4.4 EXPERIMENTAL PROGRAM

The main objective of the experimental investigation was to collect data on the behaviour of the T-stub assemblies at elevated temperatures and to investigate the three failure modes resulting from the different geometrical properties of each specimen. The three failure modes are summarised below, with illustrations of the T-stub specimens from the actual elevated-temperatures tests.

- a) *Failure Mode 1*-The T-stub specimen first forms a plastic hinge in the flange next to the web (1), and then the bolts start to yield and finally fracture (2,3). Figure 4.12 shows a typical test image for failure mode 1.



Failure Mode 1

Figure 4.12 Typical test image for Failure Mode 1

- b) *Failure Mode 2*-The T-stub specimen first forms a plastic hinge in the flange next to the web (1), then it forms another plastic hinge in the flange at the bolt line (2), and then the bolts start to yield and finally fracture (3,4). Figure 4.13 shows a typical test image for Failure Mode 2.

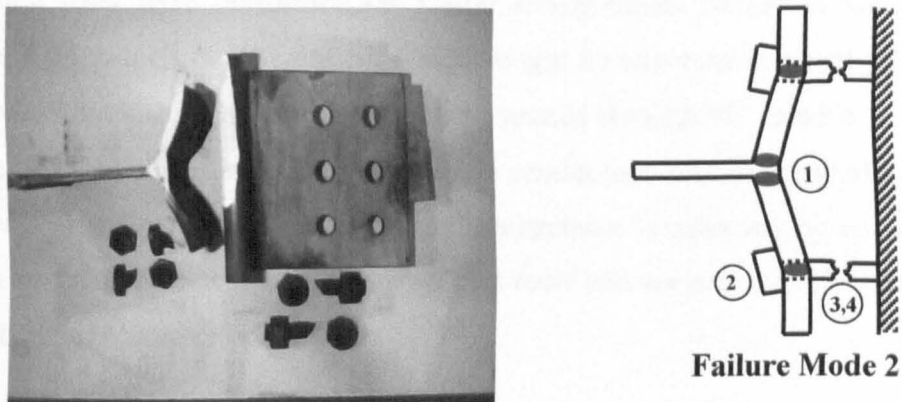


Figure 4.13 Typical test image for Failure Mode 2

- c) *Failure Mode 3*-In this failure mode the T-stub flange remains elastic and essentially flat, but the bolts start to yield and finally fracture (1,2). Figure 4.14 shows a typical test image for Failure Mode 3.

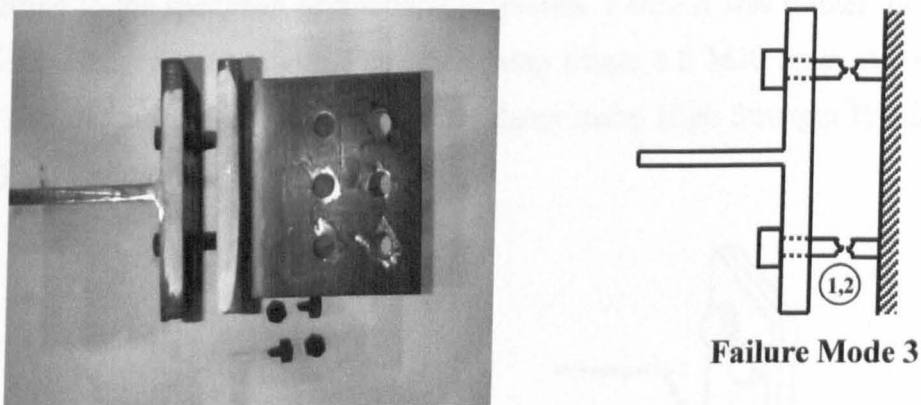


Figure 4.14 Typical test image for Failure Mode 3

A total of 45 T-stub specimen tests were conducted at elevated temperatures divided into three phases (Phase A, B and C). All the geometrical and mechanical properties of each T-stub specimens can be found in Appendix B. Also in Appendix B all the

test data have been included, for example the ultimate tensile force for each test, the number of images taken and the accuracy of the image processing technique.

The first tests were performed on T-stub arrangements similar to that shown in Figure 4.15, which is different from what might be expected in a real joint (Figure 4.2) which would have one of the T-stubs rotated through 90° relative to the other. However this is the arrangement that other researchers around the world have used for tests at ambient temperature. This arrangement is achieved by connecting the flanges of the specimens by one or two bolt rows and keeping the orientations of the T-stubs in the same direction.

4.4.1 Phase A-T-stub configurations

The initial phase (*Phase A*) included twelve tests and the arrangement of the T-stub elements, with the positions of the thermocouples, is shown in Figure 4.15 below. The thermocouples, (type K, 3mm in diameter and 2.0m long), were placed in position by drilling 3mm holes at the root radius (No 1 and 3) and in front and at the back of each T-stub flange (No 2 and 4).

According to the specimen geometrical properties, *Phase A* was further divided into three sub-categories (*AA* with four tests using Grade 8.8 M20 bolts, *AB* with five tests, and *AC* with three tests, both of the latter using High Strength Friction Grip-HSFG M16 bolts).

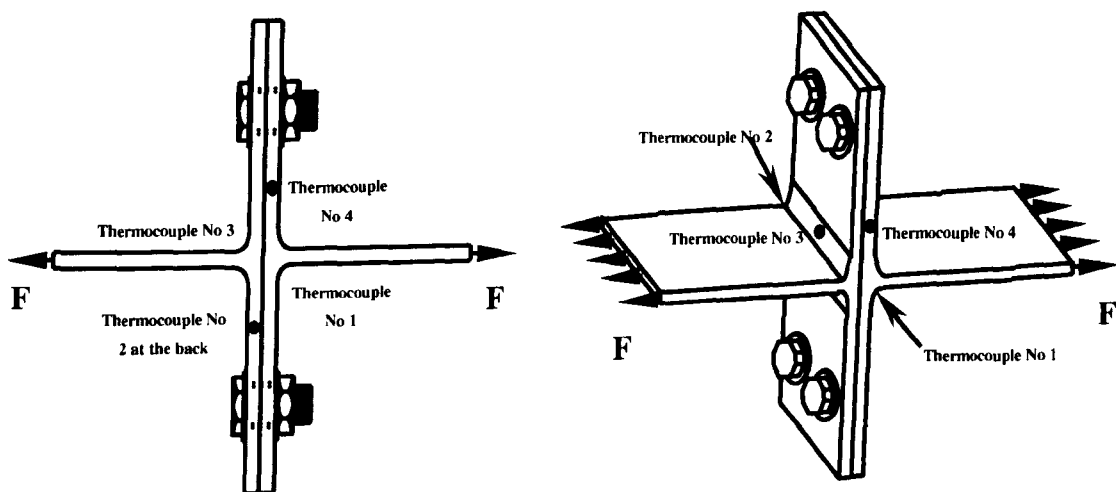
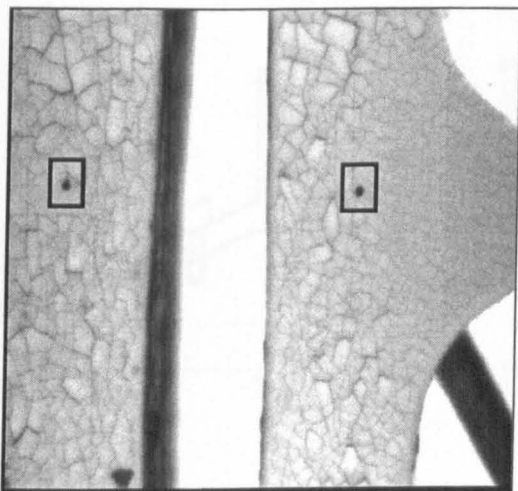
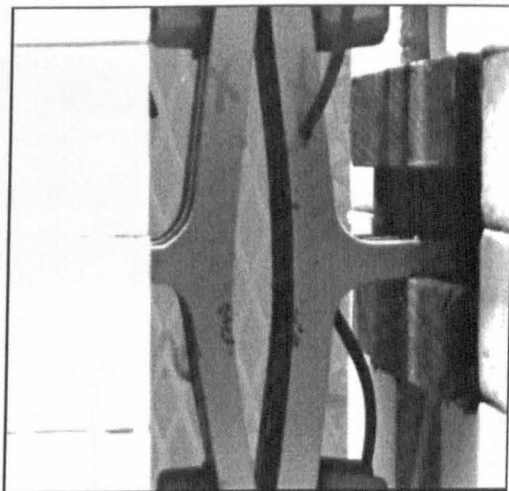


Figure 4.15 Typical T-stub assembly used in *Phase A* experiments

The tests were carried out using two video cameras placed in the front view-port of the furnace. The first camera captured images for accurate displacement measurements and the other for general observation of the T-stub distortion. Typical distorted images at 570 °C taken from the two cameras are shown in Figure 4.16.



(a) Image from first camera



(b) Image from second camera

Figure 4.16 Typical distorted images at 570 °C

The targets used to measure displacements are shown (boxed) in Figure 4.16(a). They were made using a 0.5mm drill and the distance between them was measured using a Vernier calliper, before placing the specimen in the furnace.

4.4.1.1 Test results and comments

The test results compared with the mathematical model results are presented in Figures 4.16-4.18 for Test Groups AA, AB and AC respectively.

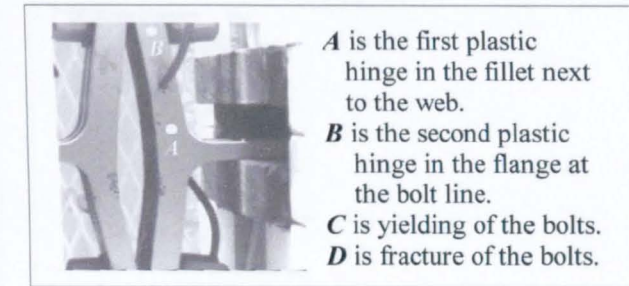
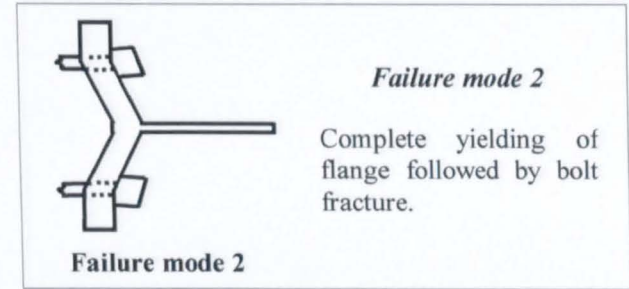
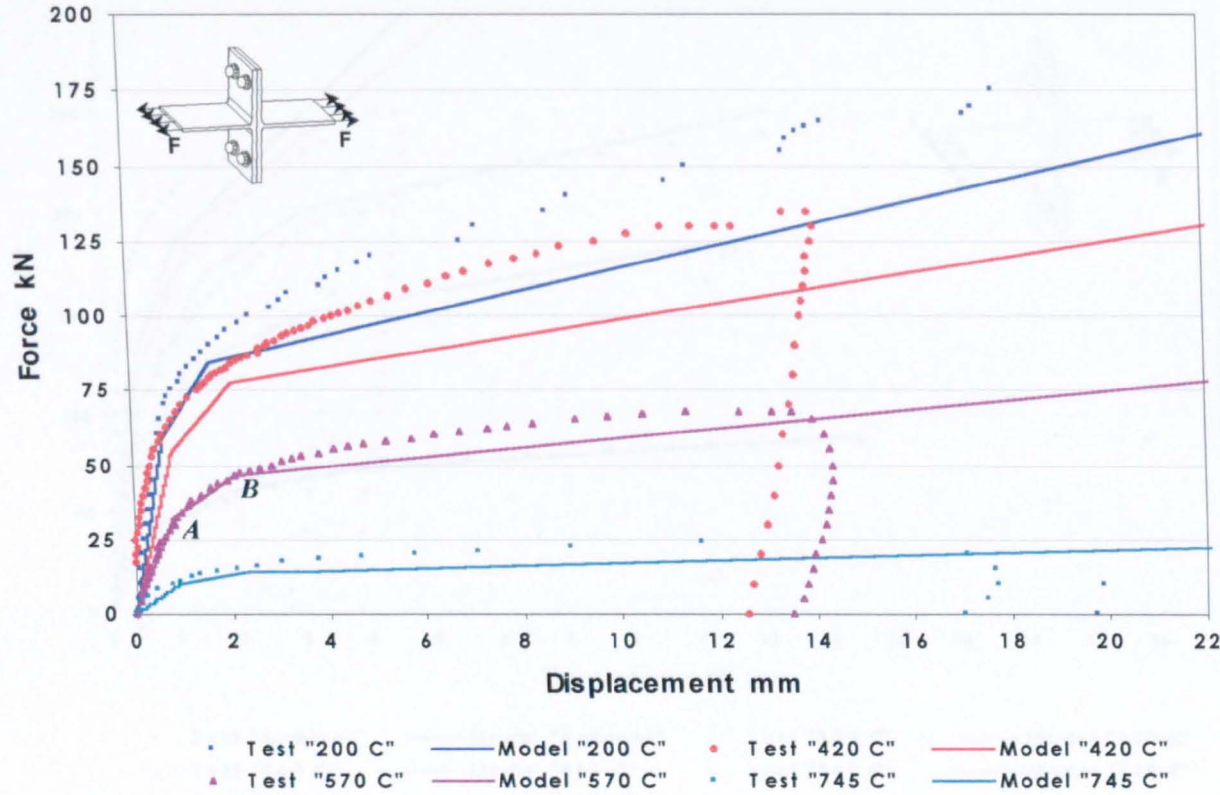


Figure 4.17 Force-deflection curves for test programme AA

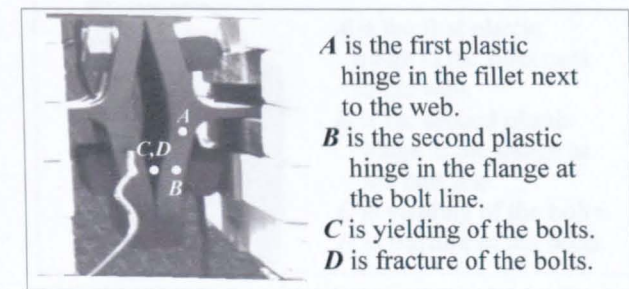
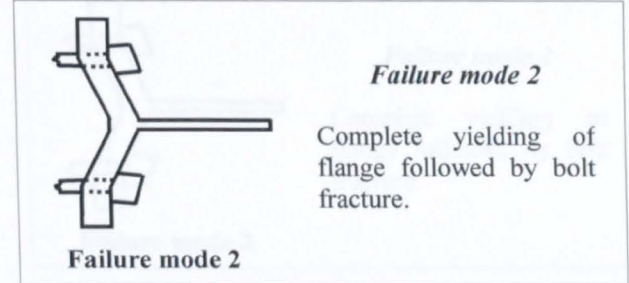
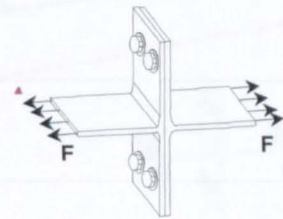
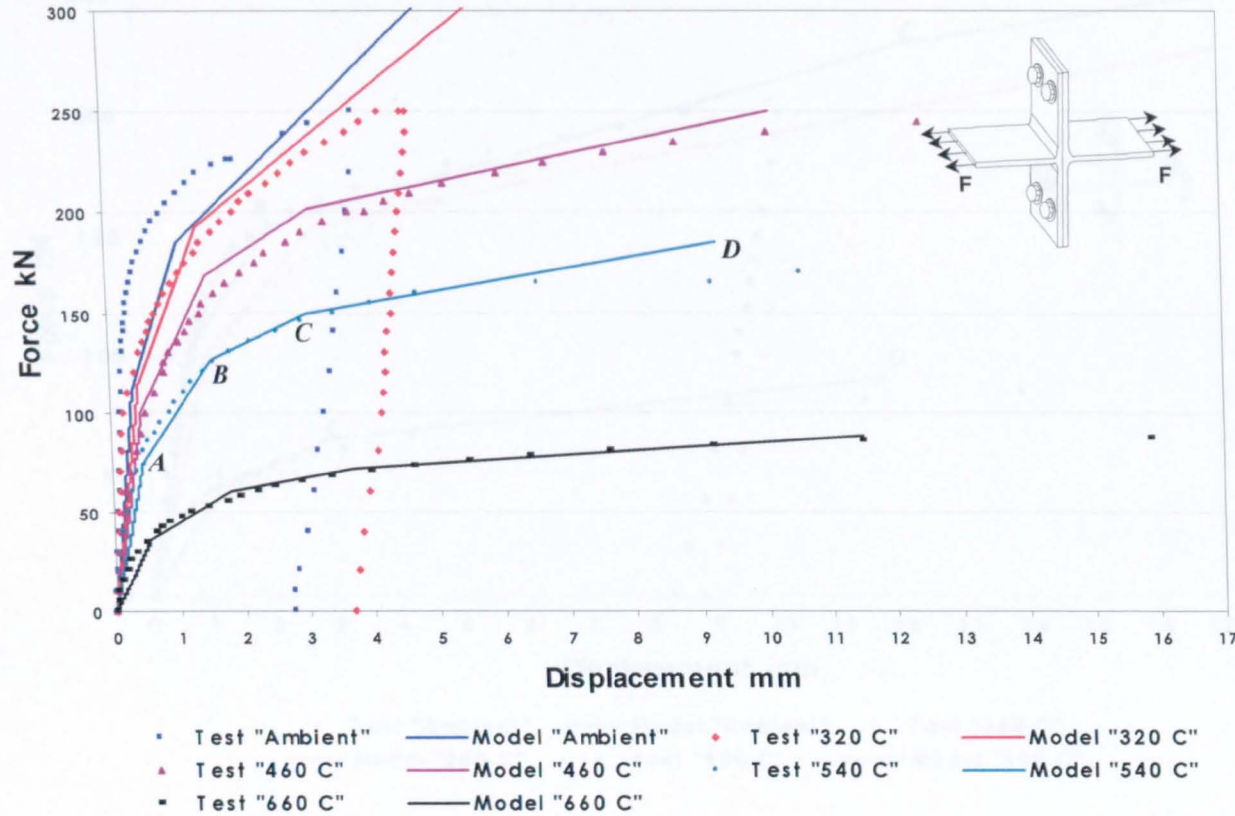


Figure 4.18 Force-deflection curves for test programme AB

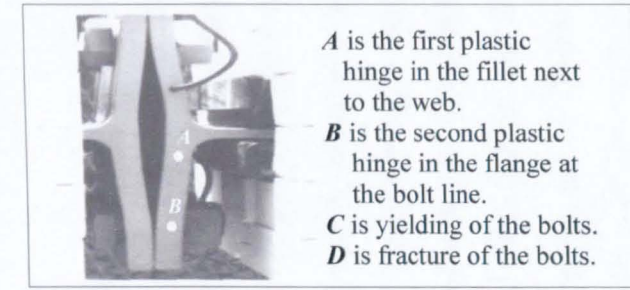
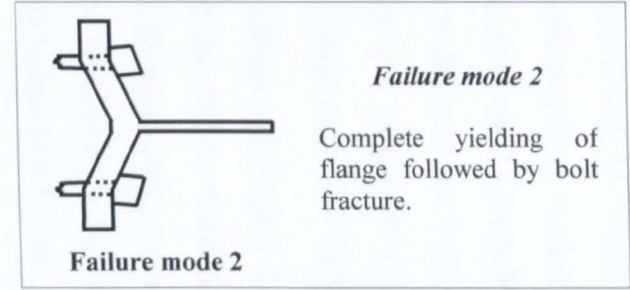
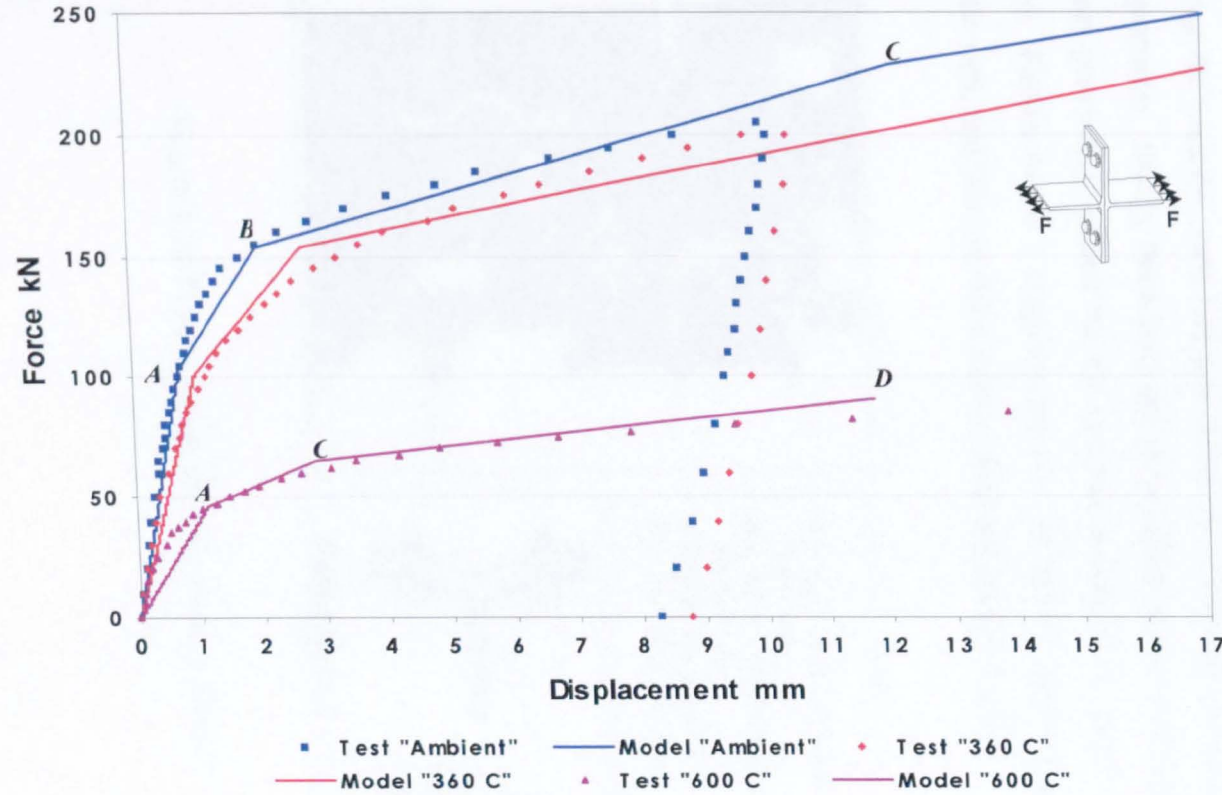


Figure 4.19 Force-deflection curves for test programme AC

For the *Test Group AA* (Figure 4.17) the simplified model analysis suggests that the failure mode would be complete yielding of the T-stub flange and then yielding and fracture of the bolts (Failure Mode 2). Instead, the actual failure mode consisted of complete yielding of the T-stub flange and then some kind of shear failure of the T-stub flange was suspected to follow. The reason for this was that the bolts (M20) were quite large compared to the T-stub flange thickness (9.50mm).

For *Test Group AB* (Figure 4.18) a different bolt size (M16) was used in order to verify that the failure mode predicted from the simplified model, as in *Test Group AA*, could be reasonably modelled. During these tests, Failure Mode 2 occurred and this can be verified by a typical image (Figure 4.20) taken during one of the tests at 460 °C just before bolt failure.

Test Group AC used the same bolt size (M16) but a different geometry for the flange T-stub specimen. During these tests the same failure mode occurred, as for the two test phases previously, except for the last test at 600 °C in which Failure Mode 1 happened. Failure Mode 1 suggests that the first plastic hinge forms in the flange next to the web, and then the bolts start to yield and finally fracture.

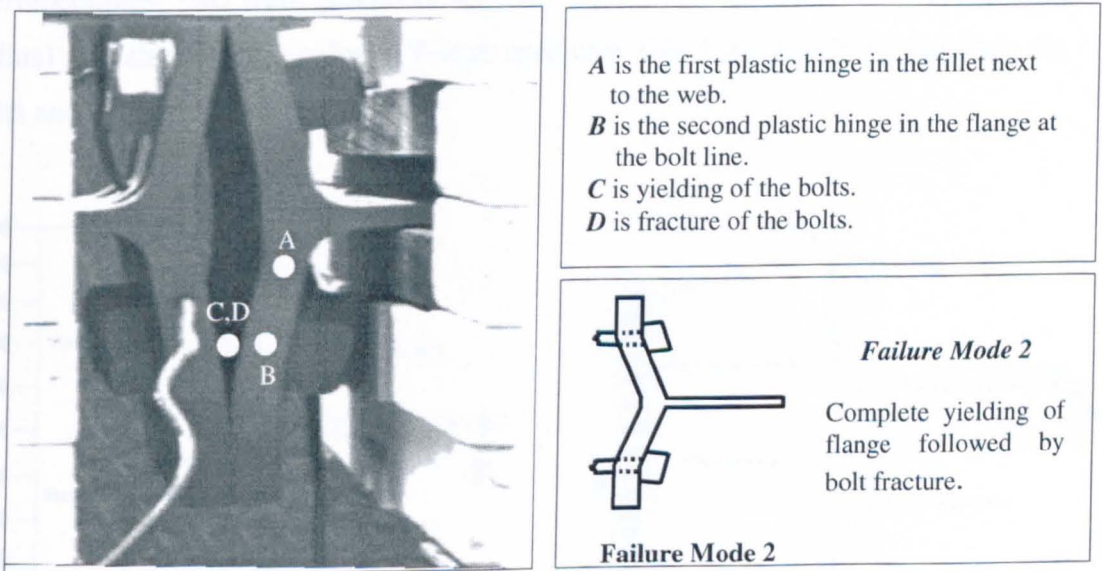


Figure 4.20 Typical image showing Failure Mode 2

The initial observations at the end of *Phase A*, were that the experimental arrangement (including furnace, loading device and image acquisition and processing technique) seemed to be reliable and efficient, permitting testing at a rate of one test per day.

Comparing the simplified mathematical model results with the actual test results demonstrated clearly that the model could predict the failure mode (only Failure Mode 2 occurred during these tests) with an acceptable accuracy in terms of strength and stiffness.

4.4.2 Phase B-tests to investigate realistic configurations

At the end of *Phase A* it was decided that a new arrangement for the T-stub specimens (Figure 4.21) should be investigated in order to examine the real behaviour of the tension zone within realistic beam-to-column joints. Another objective was to investigate further the three different failure modes across a range of plate thicknesses and bolt sizes. Figure 4.21 also shows the position of the thermocouples; two were placed in the end plate (No.3 in front and No.4 in root radius) and three in the column T-stub specimen (No.1 on top, No.5 between the bolts and No.2 in the web).

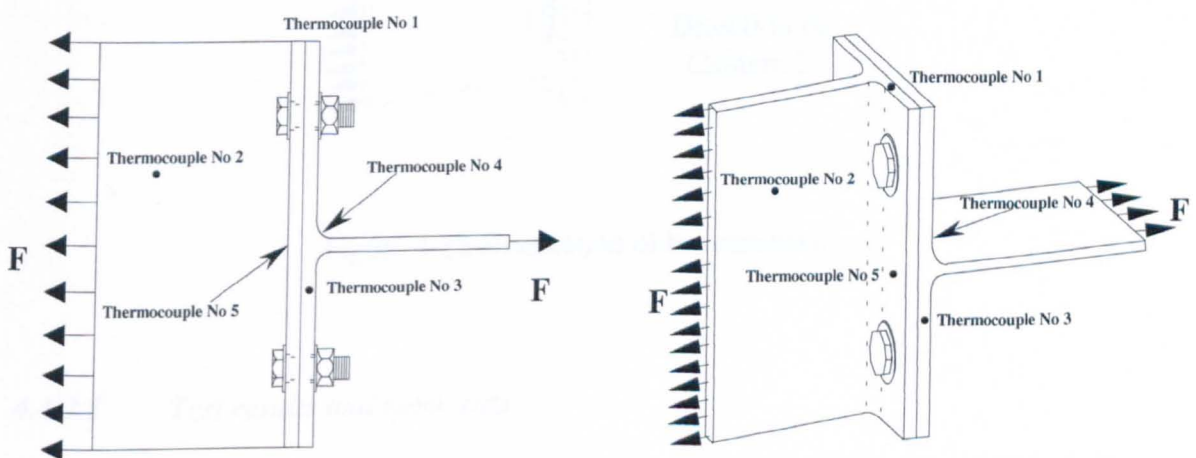


Figure 4.21 Typical T-stub assembly used in *Phase B* and *C* experiments

Phase B included eight tests in total at elevated temperatures, and again was divided into two sub-categories (BA included six tests, using a column section UC203x203x52 and an end plate 200x200x20mm for the two T-stub elements and BB included two tests using an end plate of 200x200x20mm for both T-stub elements). In Figure 4.21 above, the left-hand side represents the column T-stub and the right-hand side the end plate T-stub specimen. Their geometrical and mechanical properties can be found in Appendix B.

In order to carry out these tests three cameras were used. The first camera recorded the displacement of the column T-stub, the second camera recorded the displacement of the end plate T-stub and the third camera recorded the overall behaviour of the column T-stub. The viewing directions of the cameras are shown in Figure 4.22 below.

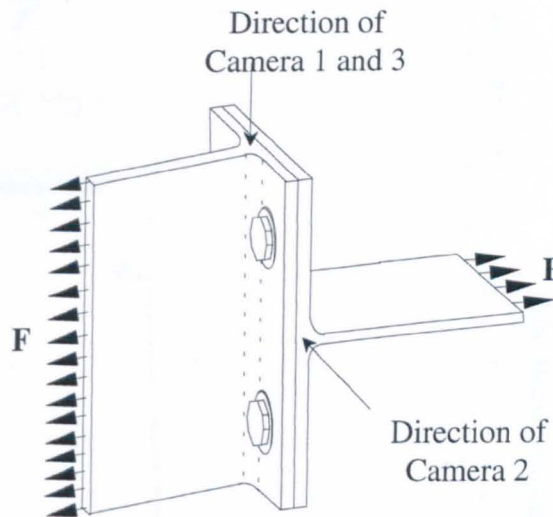


Figure 4.22 Orientation of the cameras

4.4.2.1 Test results and comments

The test results compared with the mathematical model results are presented in Figures 4.23-4.26 for Test Groups BA and BB respectively.

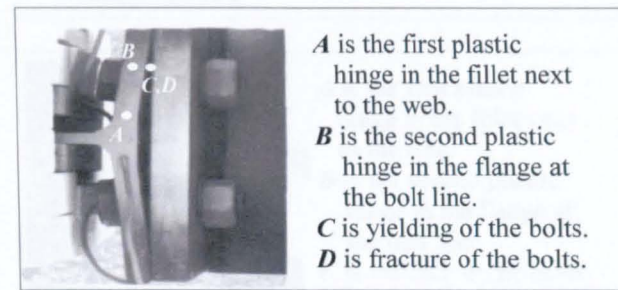
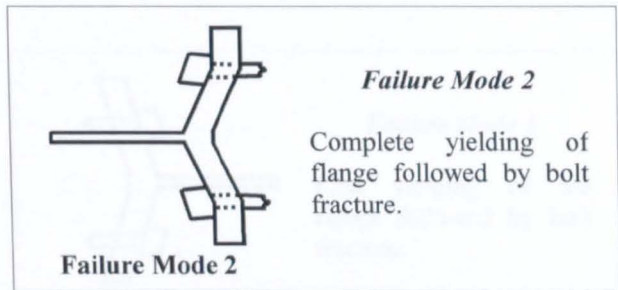
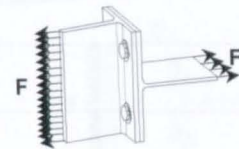
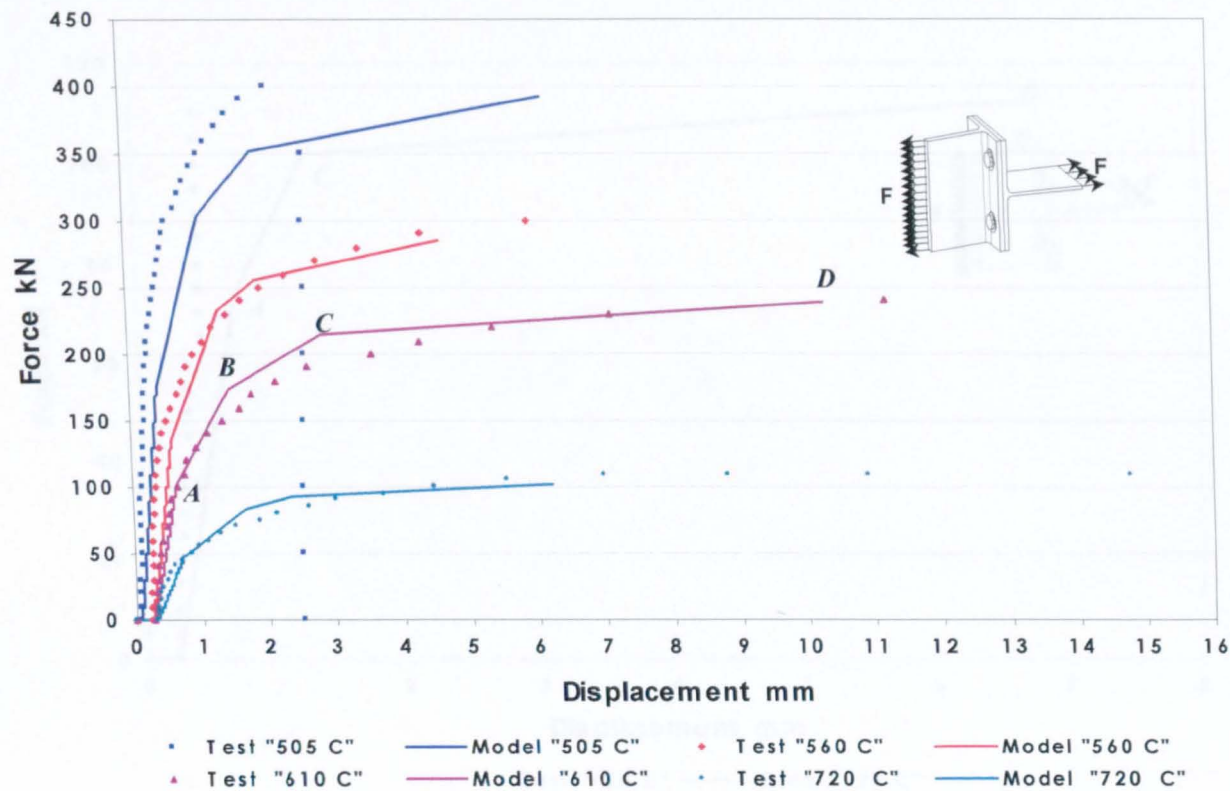


Figure 4.23 Force-deflection curves for the column T-stub for test programme BA.

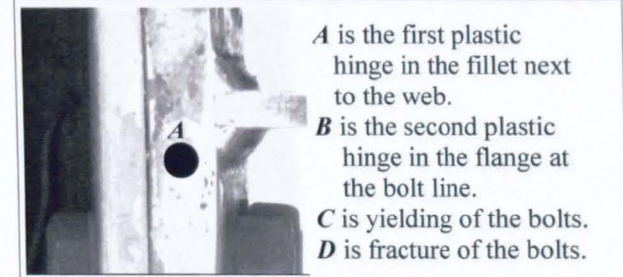
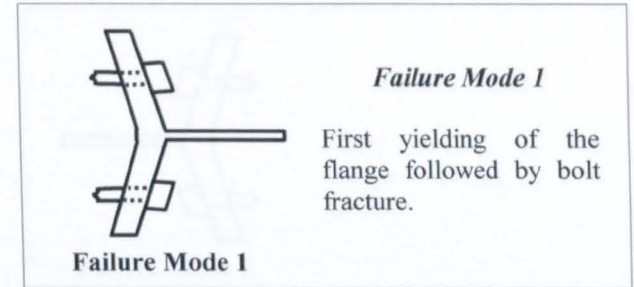
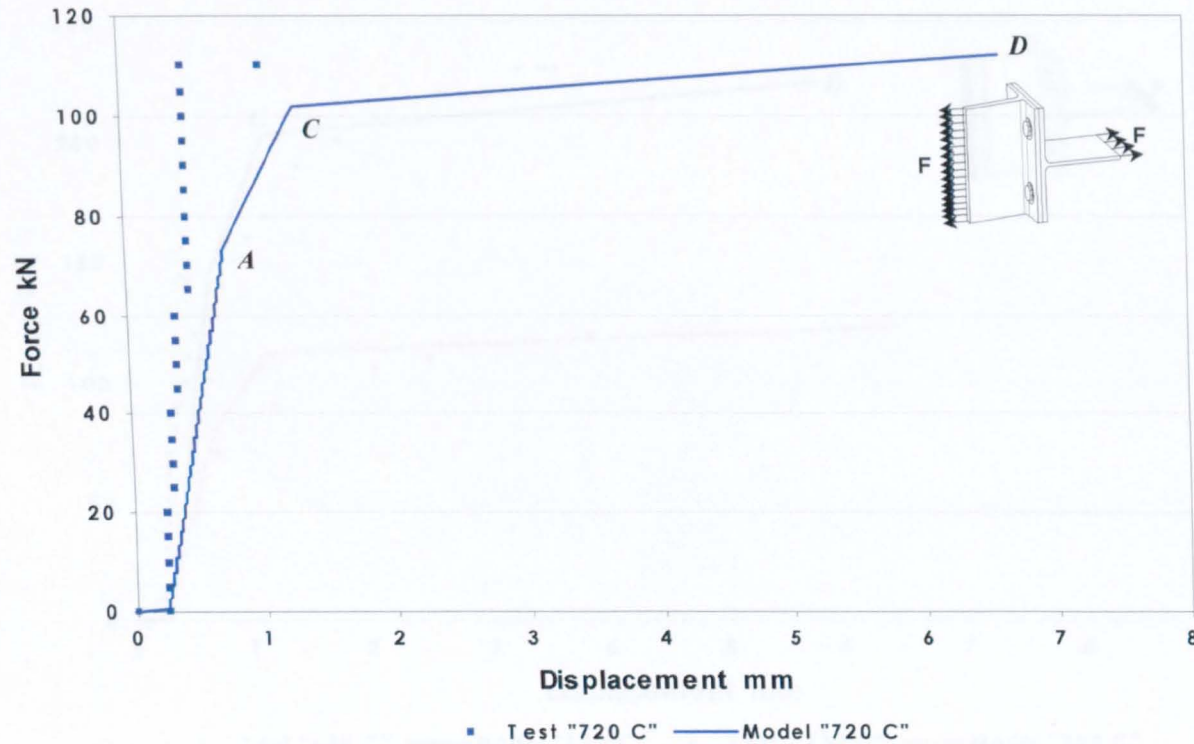


Figure 4.24 Force-deflection curves for end plate T-stub for test programme BA.

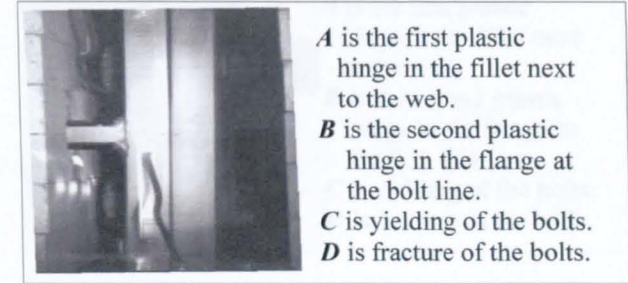
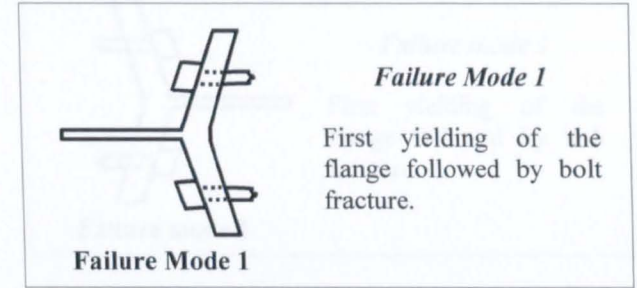
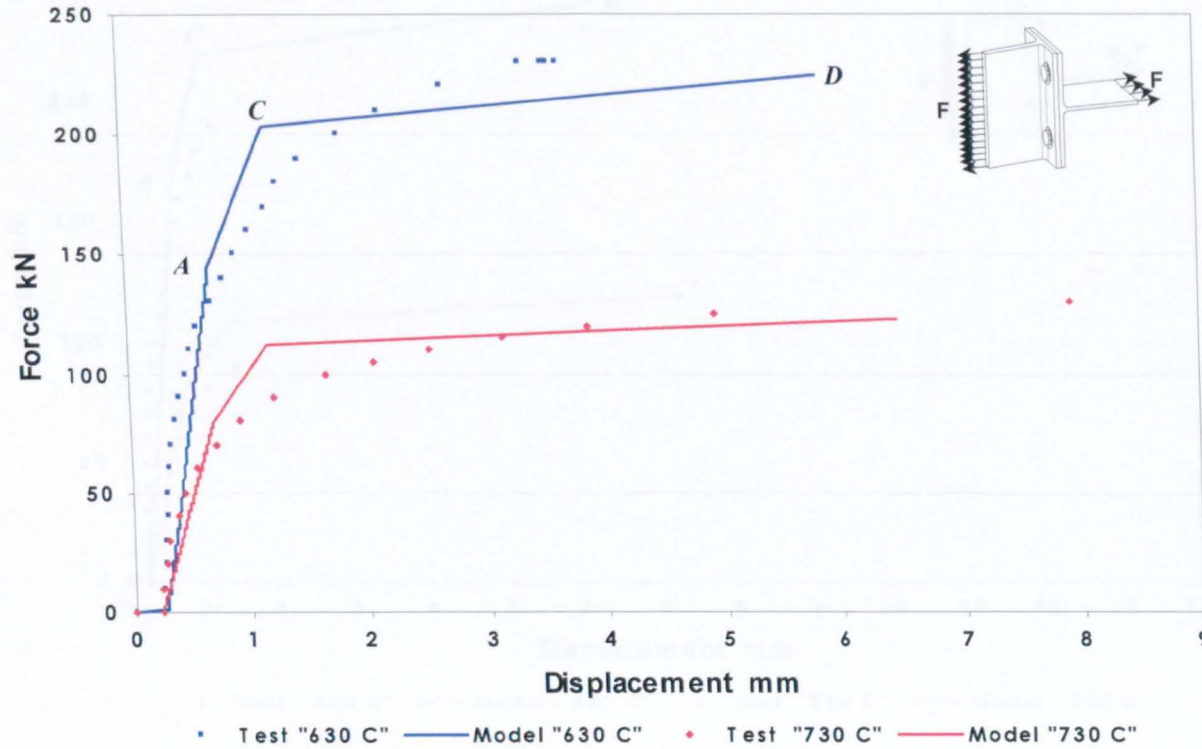


Figure 4.25 Force-deflection curves for the column T-stub for test programme BB.

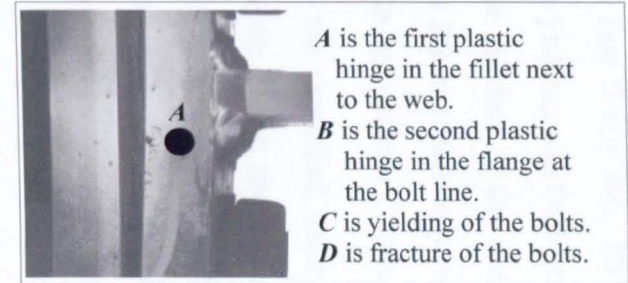
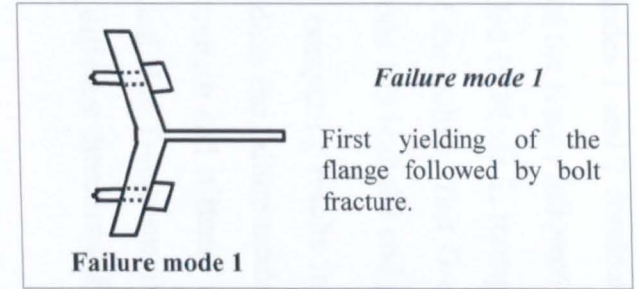
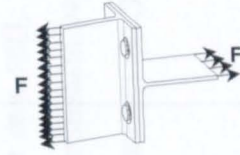
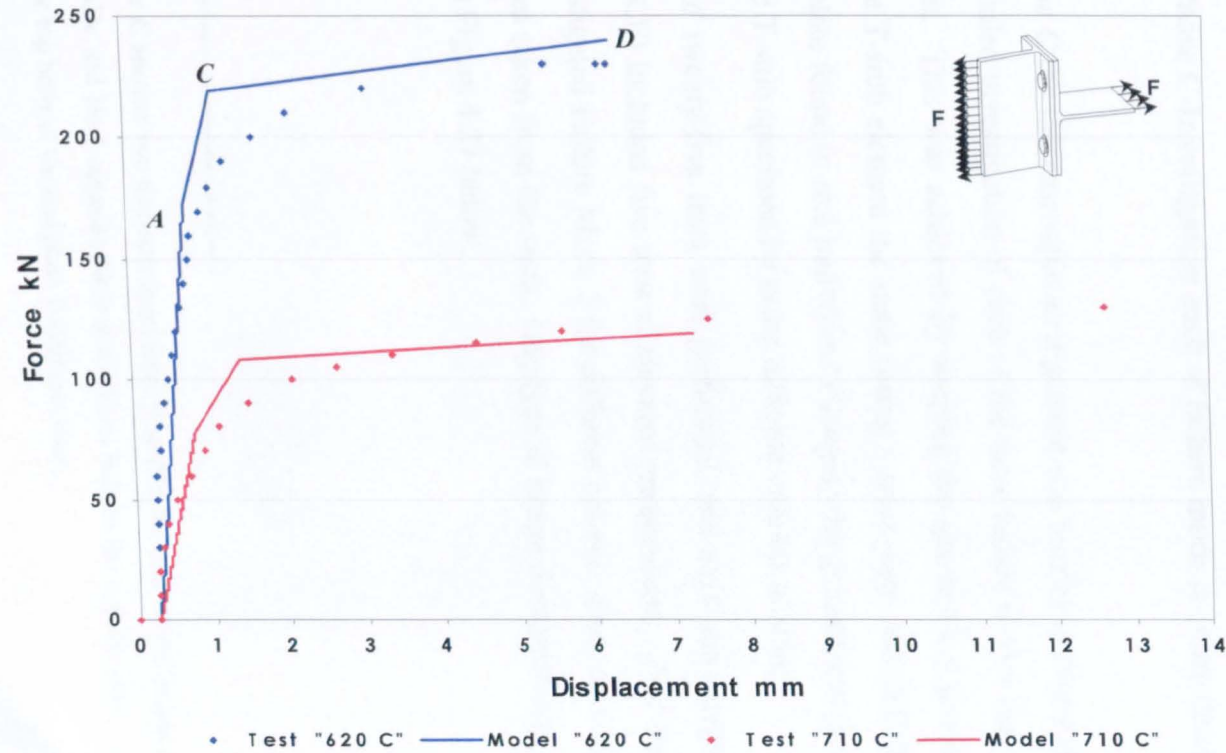


Figure 4.26 Force-deflection curves for end plate T-stub for test programme BB.

Failure Modes 1 and 2 dominated *Test Group BA*. The end plate failed in Mode 1, (yielding of the flange followed by yielding and fracture of the bolts) and the column T-stub failed in Mode 2, (complete yielding of the flange followed by yielding and fracture of the bolts). *Test Group BB* included only two tests, and concentrated on Failure Mode 1 in both the end plate and column T-stub.

Again, by comparing results from the simplified model and tests, it seems that the model predicts the failure mode of the T-stub specimen with reasonable accuracy in terms of strength and stiffness values. It was also observed that the right-hand side and left-hand side T-stub specimens developed their failure mode even if they were aligned in different directions (Figure 4.21).

4.4.3 Phase C-Investigation each of failure mode in more detail

For *Phase C* the thermocouple arrangement was similar to *Phase B^a*. *Phase C* was a more detailed investigation of each of the three failure modes that a T-stub assembly can adopt. This was achieved by keeping the geometrical properties of the right-hand side T-stub element the same (using a steel plate 200x200x20mm to represent the end plate found in real joints) and changing the geometrical properties of the left-hand side T-stub specimen by using different column sections.

A total of twenty-five tests were performed, and each sub-category (CA, CB, CC, CD and CE) included five tests at elevated temperatures. *Test Groups CA, CC and CD* investigated Failure Mode 2 for different column sizes, and this was observed in the images taken from the tests. One typical image demonstrating Failure Mode 1 is shown in Figure 4.27 below.

^a For *Phase C* another two thermocouples were placed in the bolts (No.6 in one of the top bolts on the end plate side and No.7 opposite No.6 at a bottom bolt on the column side). Also No.2 was placed between the top bolts of the end plate T-stub specimen.

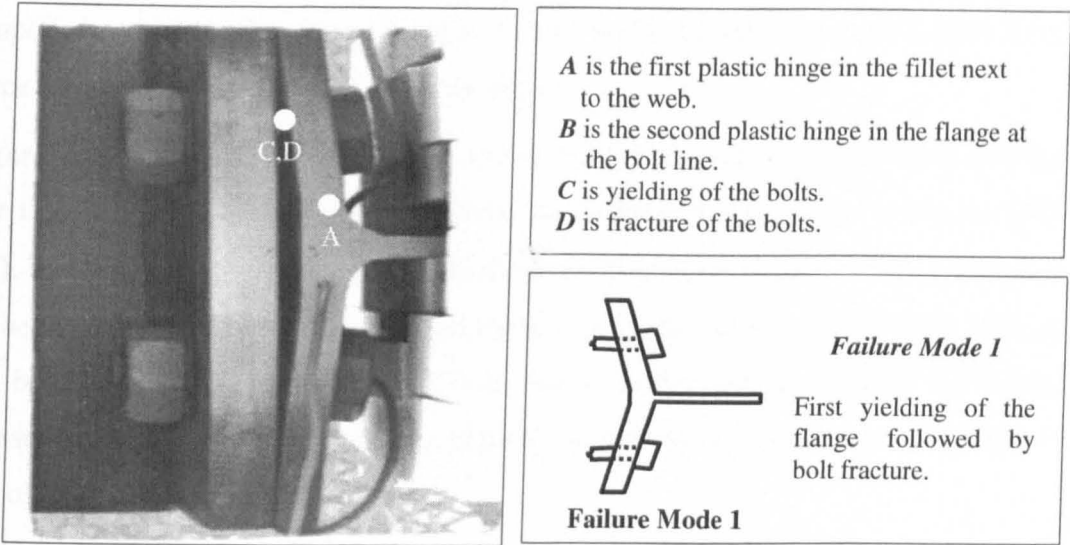


Figure 4.27 Typical image showing Failure Mode 1

Test Group CE investigated Failure Mode 3 at elevated temperatures. In order to achieve complete failure of the bolts without any plastic hinges forming in the T-stub flanges, a smaller bolt size (M12) was used.

Finally Test Group CB examined Failure Mode 2, but because of the extensive deformation of the column T-stub the bolts failed in a combination of shear and tension force. Figure 4.28 shows the failure mechanism of the bolts.

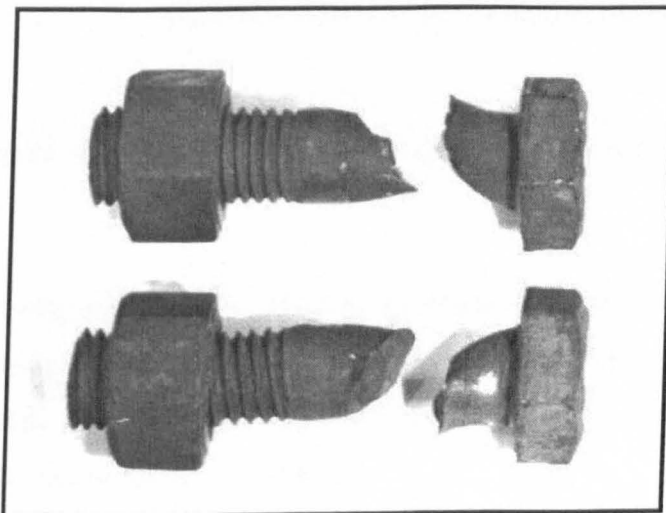


Figure 4.28 Bolt failure in a combination of shear and tension force

In order to include this combined shear and tension bolt failure mechanism in the simplified model the last image from each test was taken and the approximate shear force value applied to the bolts was calculated.

Figure 4.29 shows the last image, just before bolt failure, taken from a test at 650 °C. For this image the actual tension force on the column T-stub flange is known (160 kN). The tensile strength of the bolt is calculated from $2f_{ub,\theta}A_s$ (120.16 kN) where $f_{ub,\theta}$ is the ultimate stress of the bolt at a certain temperature and A_s is the shank area of the bolt. The deformation of the T-stub flange at the bolt line (Figure 4.29) was measured using the image processing software and from that the shear force could be calculated (50.47 kN).

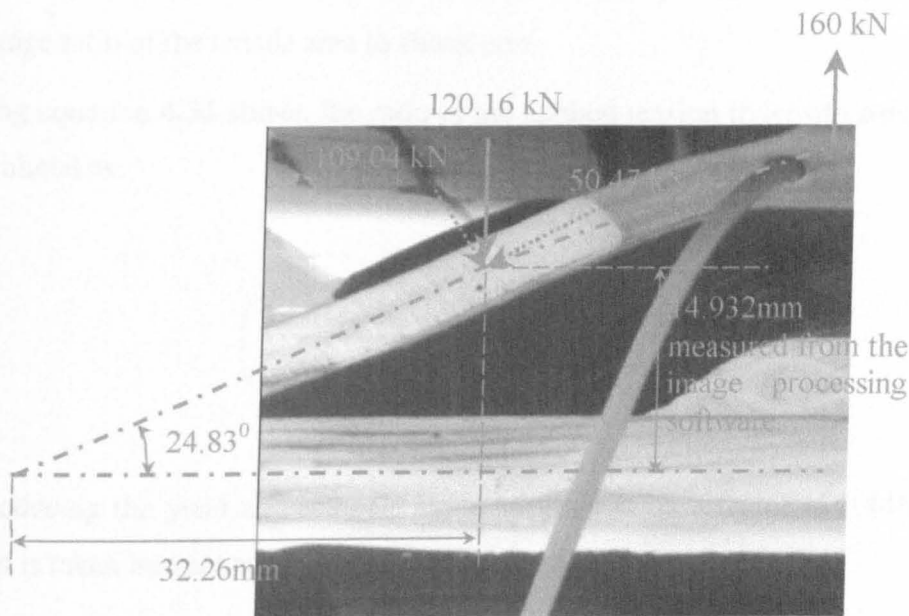


Figure 4.29 Image at 650 °C just before bolt failure at 160 kN

Using the following equation^{4.23}, which is applicable when the threads of the bolt are in the shear plane, the ratio of the applied tension to tensile strength can be calculated and then implemented into the simplified model in order to take into account the shear and tensile forces acting on the bolts.

$$\left(\frac{\text{Applied tension}}{\text{Tensile strength}} \right)^2 + \left(\frac{\text{Applied shear}}{0.63 \times \text{Tensile strength}} \right)^2 = 1.0 \quad \dots 4.32$$

and when the shank of the bolts is in the shear plane:

$$\left(\frac{\text{Applied tension}}{\text{Tensile strength}} \right)^2 + \left(\frac{\text{Applied shear}}{0.79 \times \text{Tensile strength}} \right)^2 = 1.0 \quad \dots 4.33$$

The 0.79 coefficient in the latter equation is simply 0.63/0.80, where 0.8 is the average ratio of the tensile area to shank area.

Using equation 4.32 above, the ratio of the applied tension to tensile strength can be calculated as:

$$\left(\frac{\text{Applied tension}}{\text{Tensile strength}} \right) = 0.846$$

By reducing the yield and ultimate stress of the bolt by a factor of 0.846 the shear effect is taken into account when using the simplified model.

Two tests from *Test Group CB* were conducted using HSFGB bolts and the failure shear plane occurred in the bolt shank (using equation 4.33). For the remaining three tests, Grade 8.8 bolts were used and the shear plane occurred in the bolt threads (using equation 4.32). Using the same procedure the new value of the applied tension to tensile strength can be calculated, which works out as the same value (0.846) as that for HSFGB bolts.

4.4.3.1 Test results and comments

The test results compared with the mathematical model results are presented in Figures 4.30-4.37 for Test Groups CA, CB, CC, CD and CE respectively. Note that

CC, CD and CE the results for column flange failure and end plate failure are shown separately.

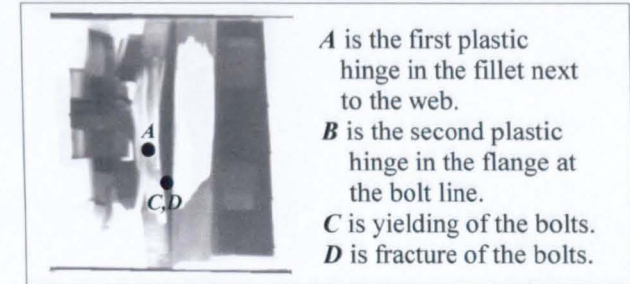
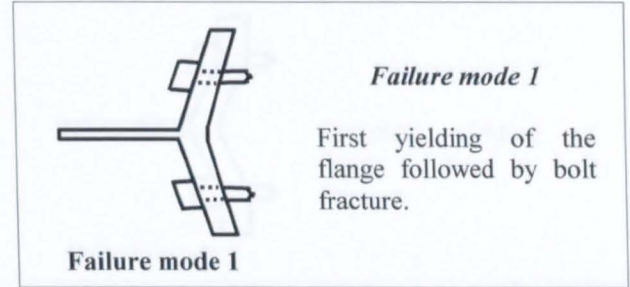
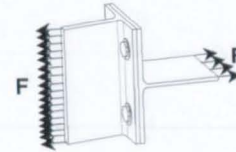
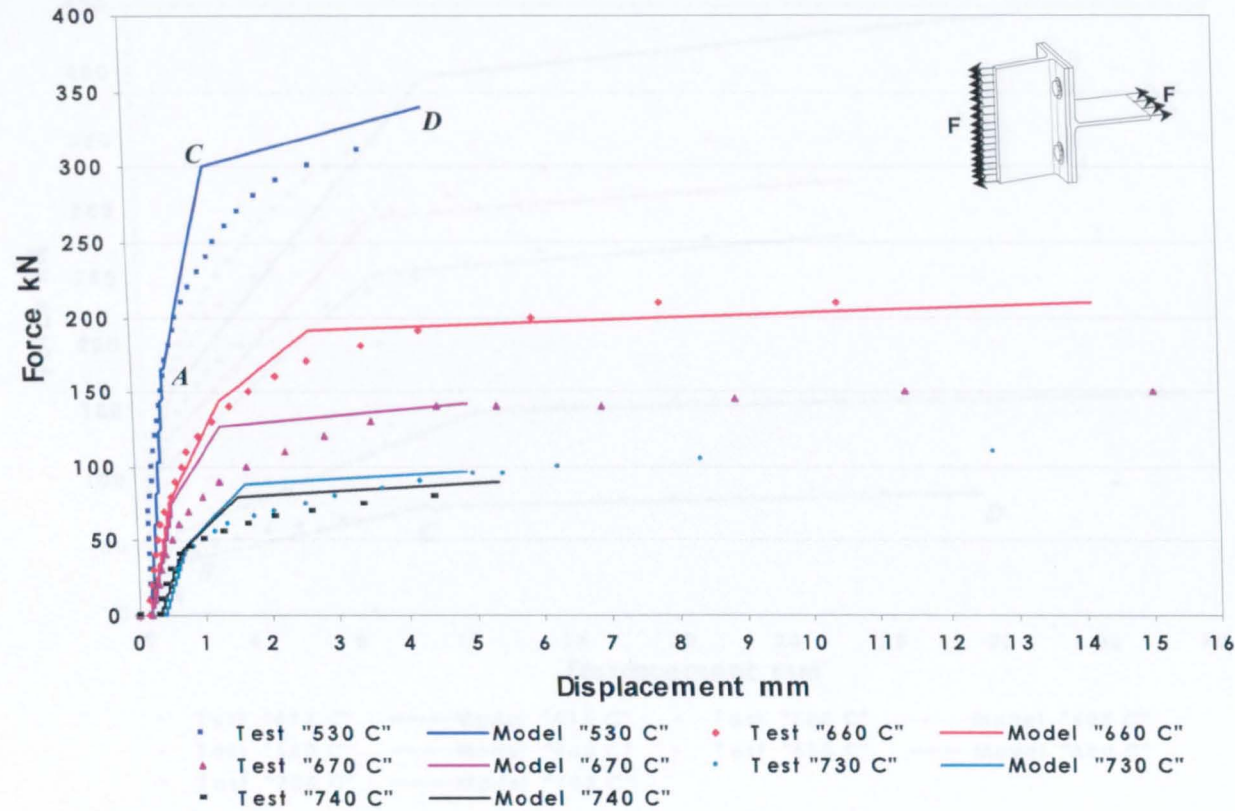


Figure 4.30 Force-deflection curves for the column T-stub for test programme CA

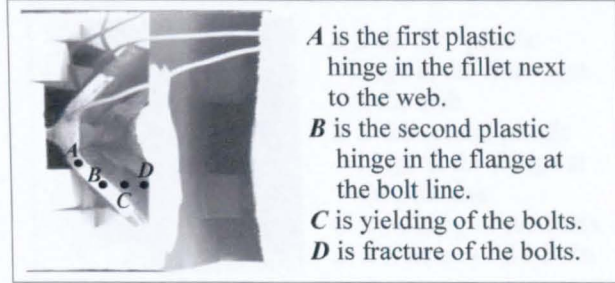
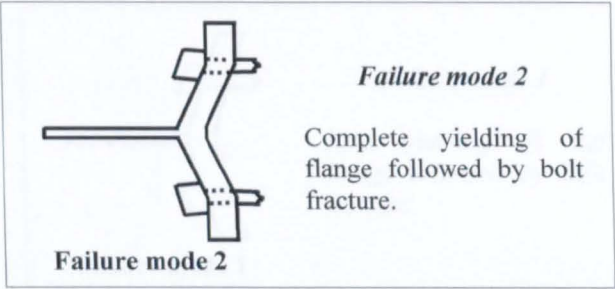
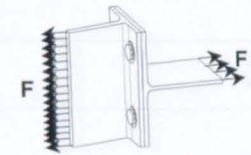
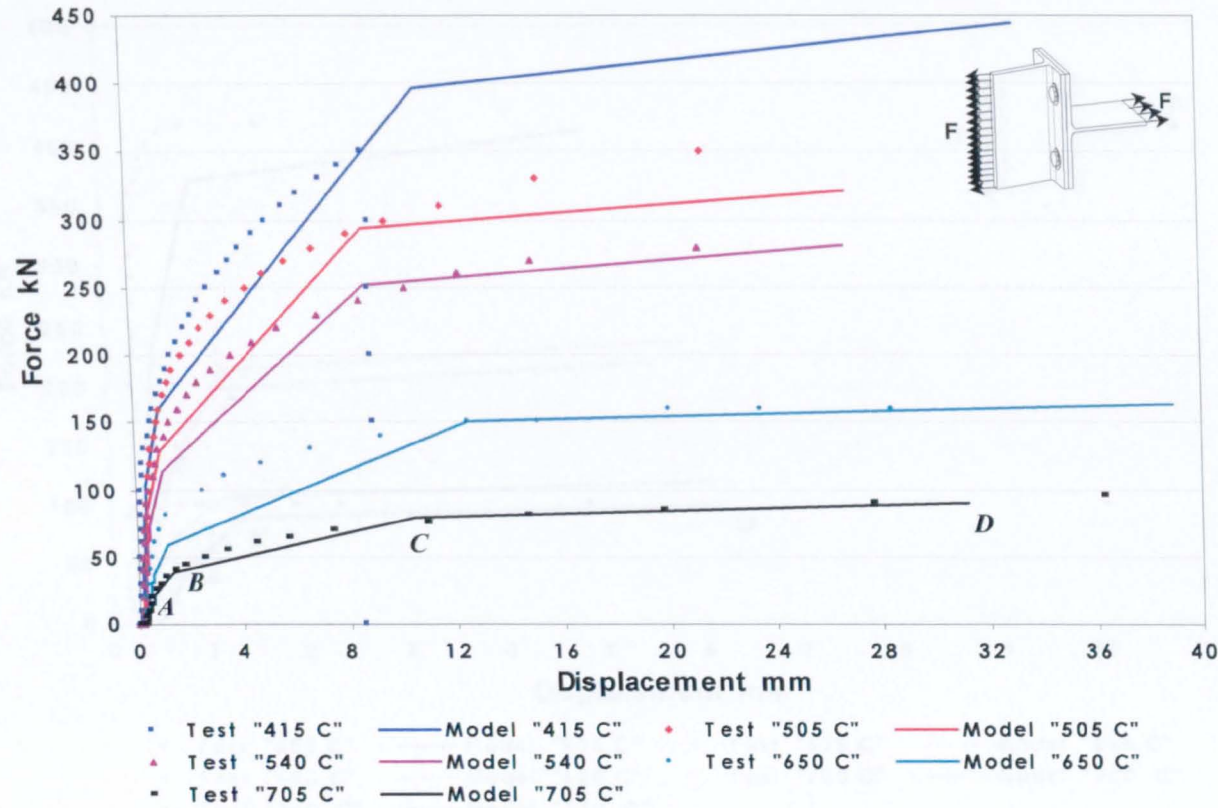


Figure 4.31 Force-deflection curves for the column T-stub for test programme CB

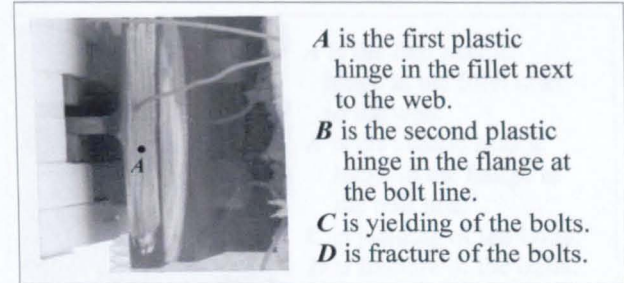
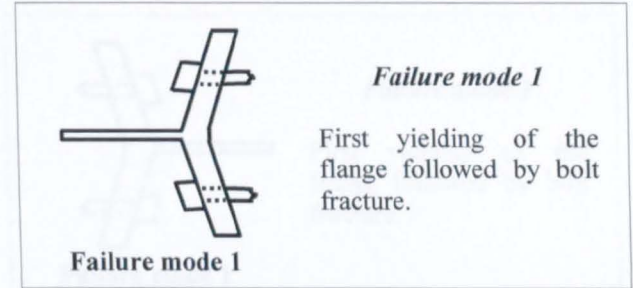
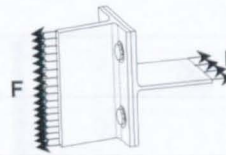
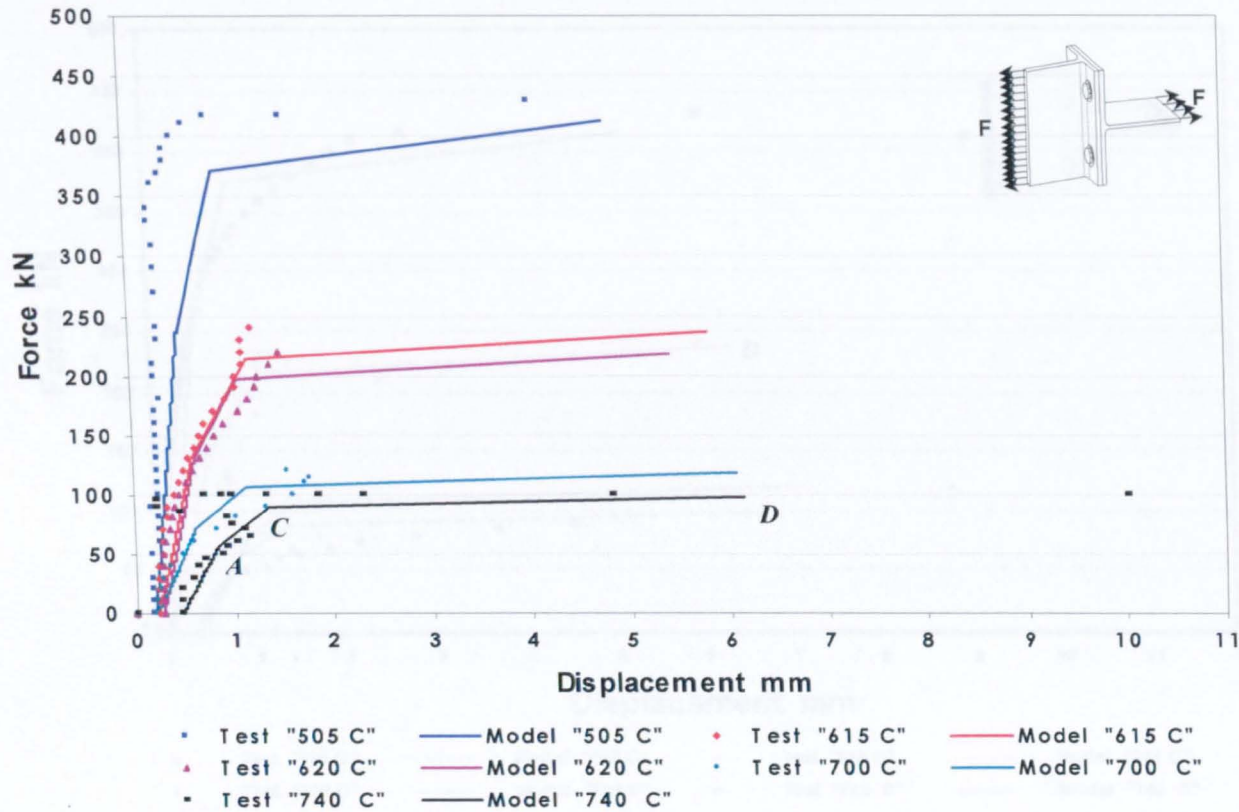


Figure 4.32 Force-deflection curves for the column T-stub for test programme CC

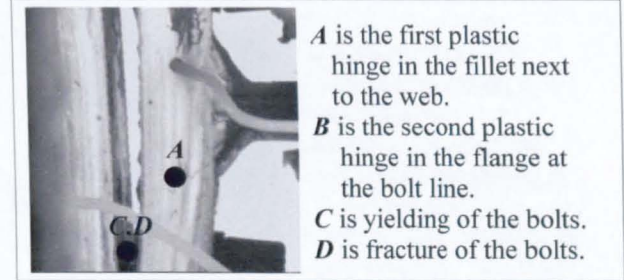
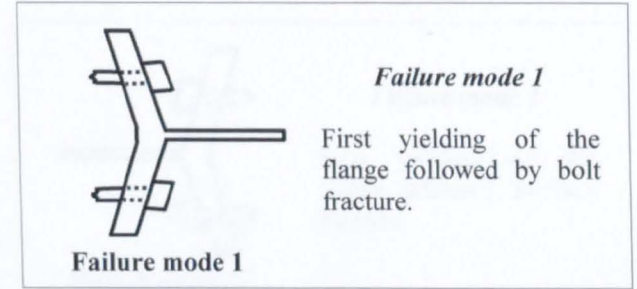
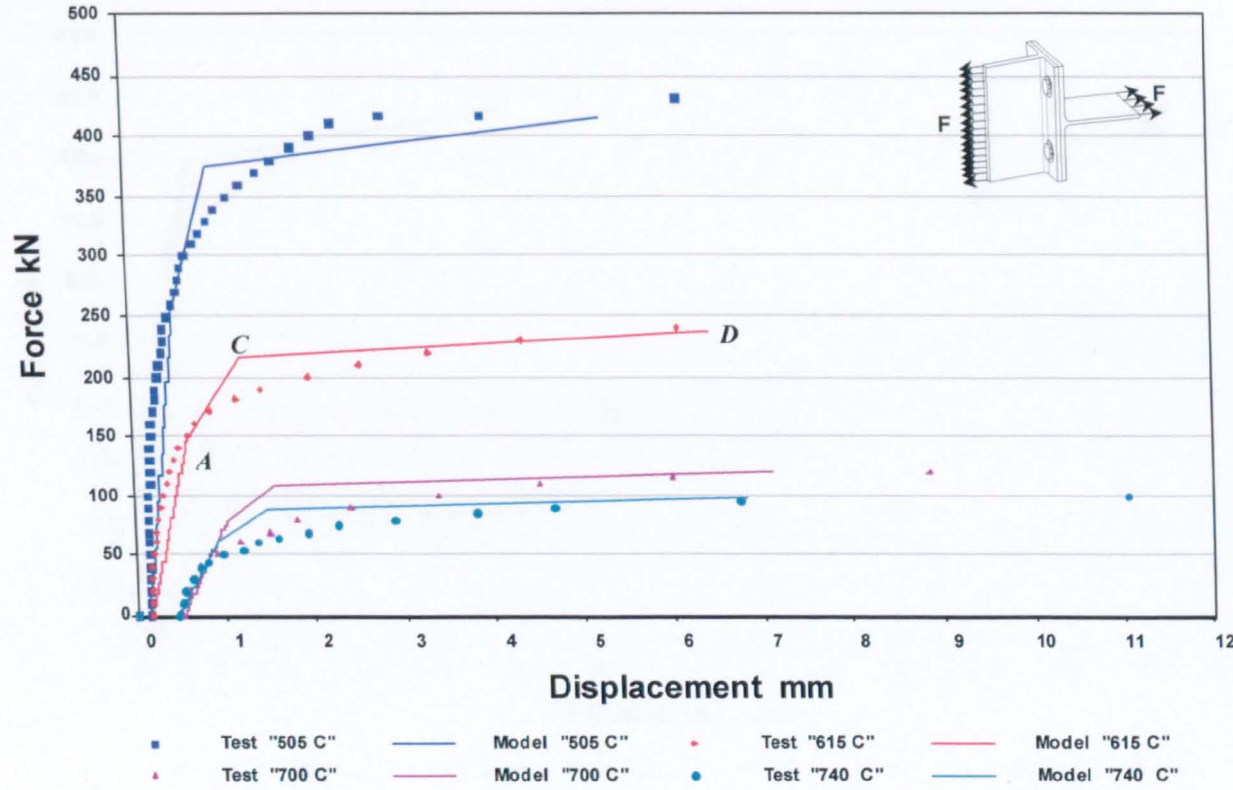


Figure 4.33 Force-deflection curves for end plate T-stub for test programme CC

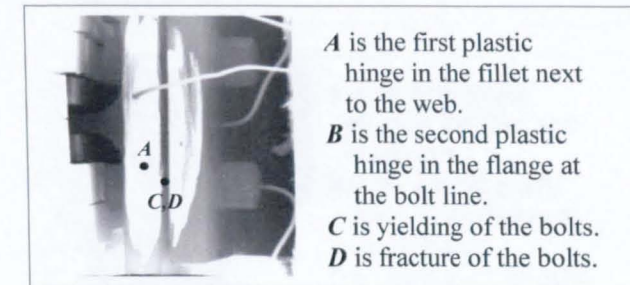
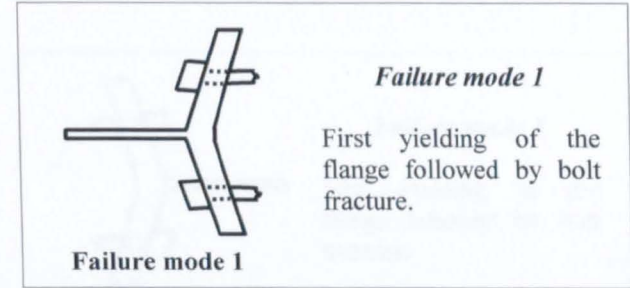
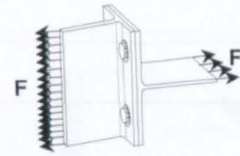
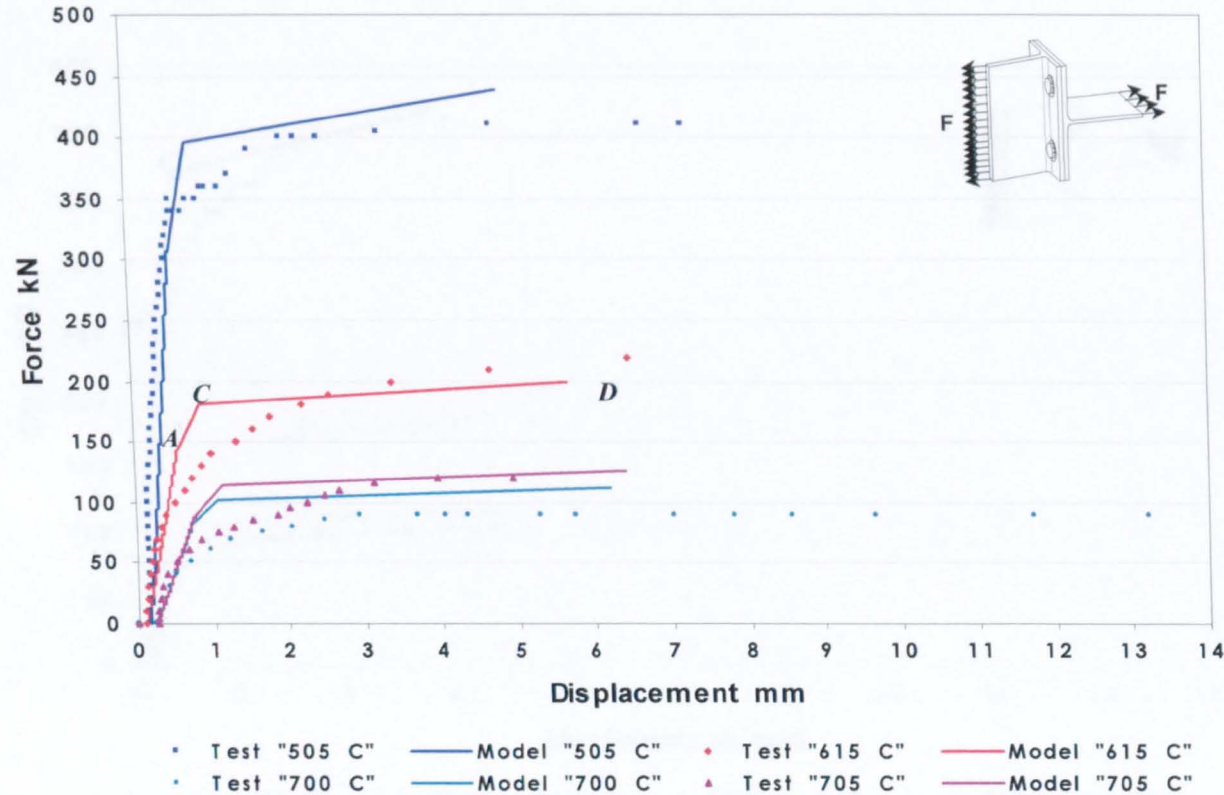


Figure 4.34 Force-deflection curves for the column T-stub for test programme CD

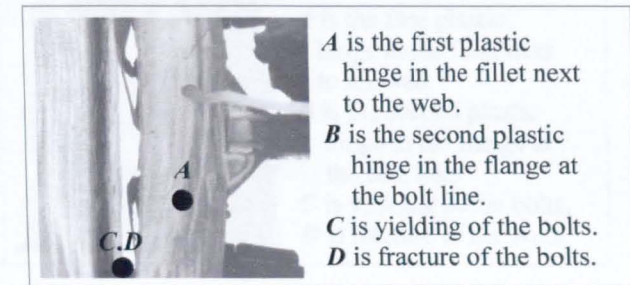
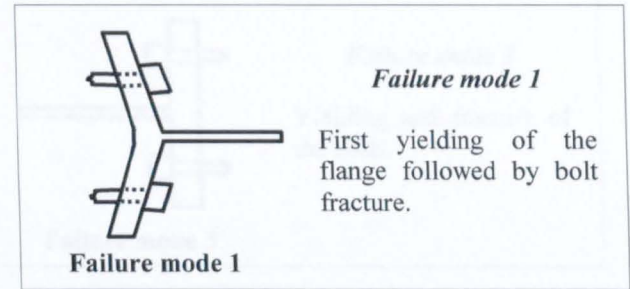
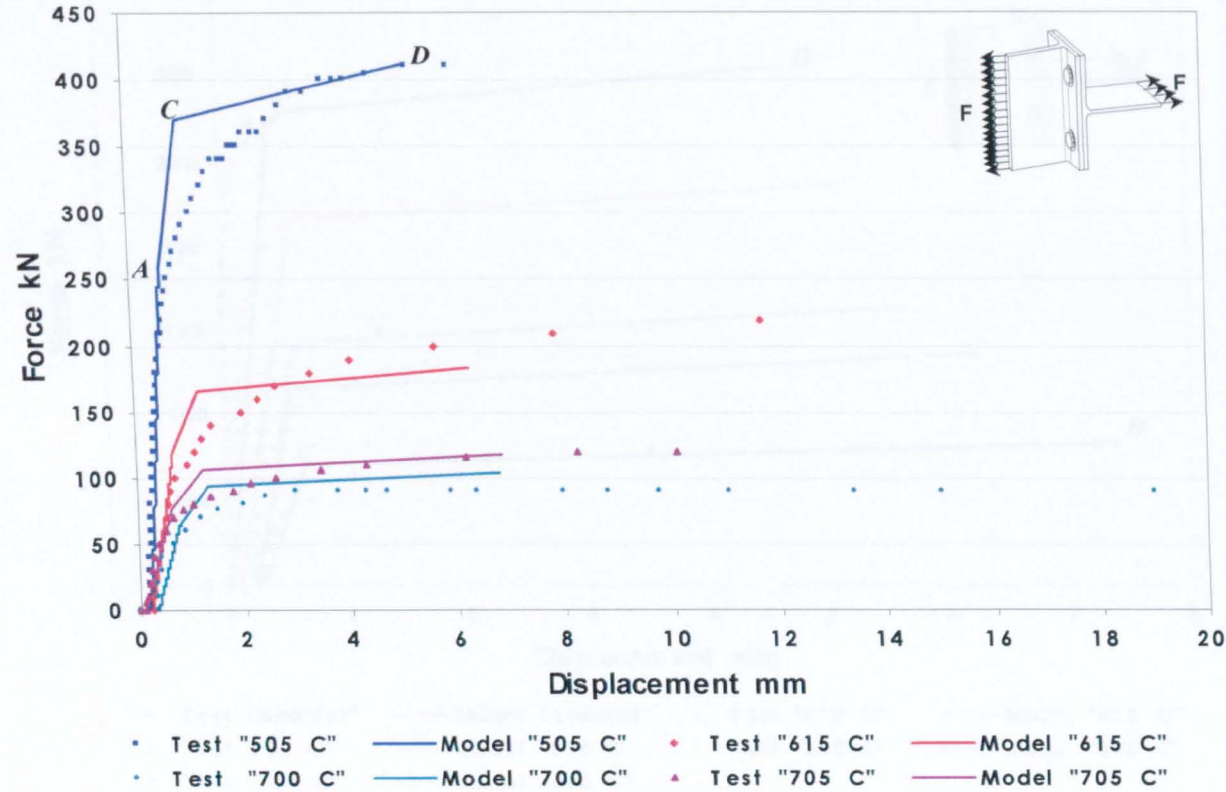


Figure 4.35 Force-deflection curves for end plate T-stub for test programme CD

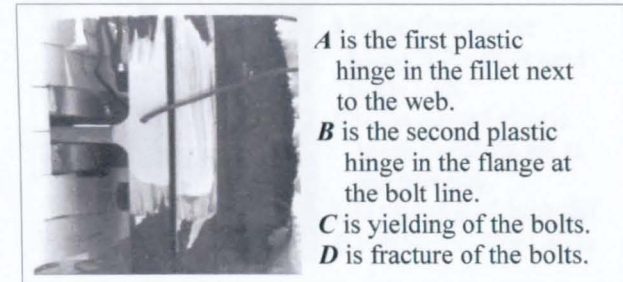
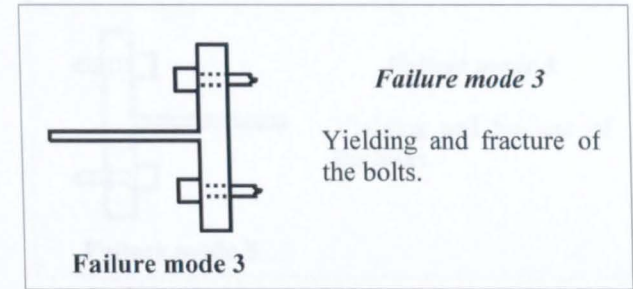
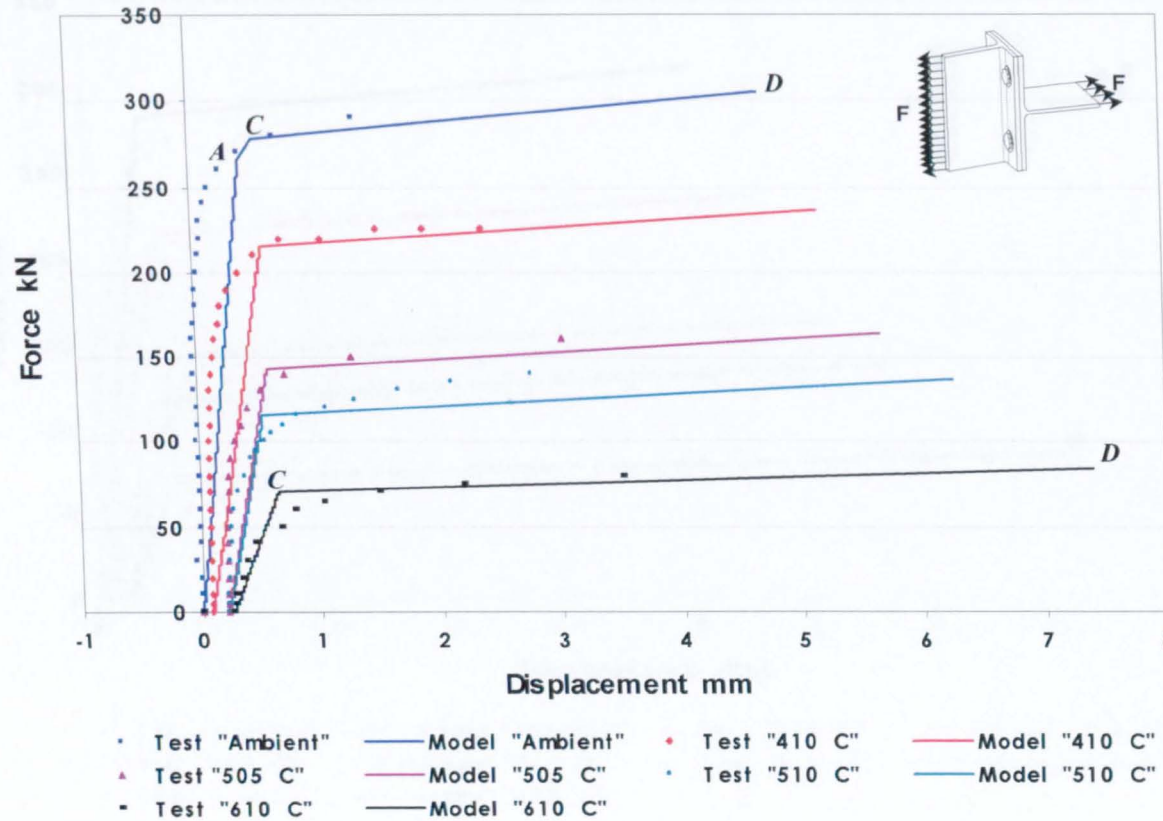


Figure 4.36 Force-deflection curves for the column T-stub for test programme CE

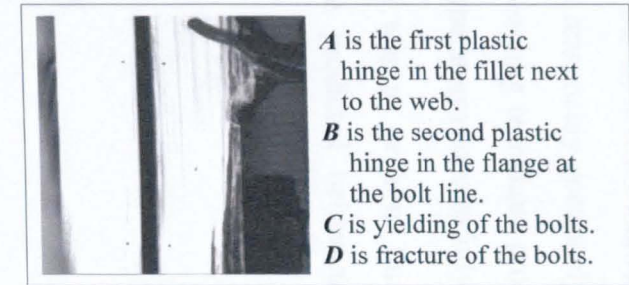
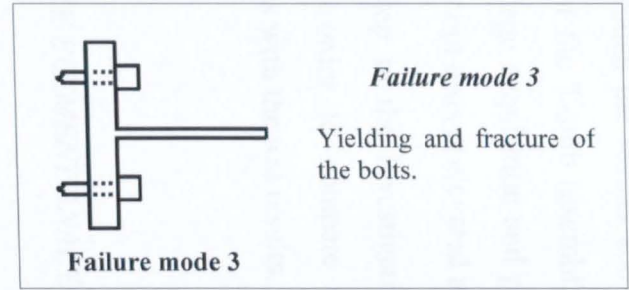
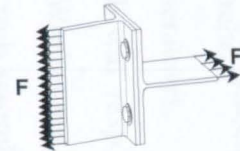
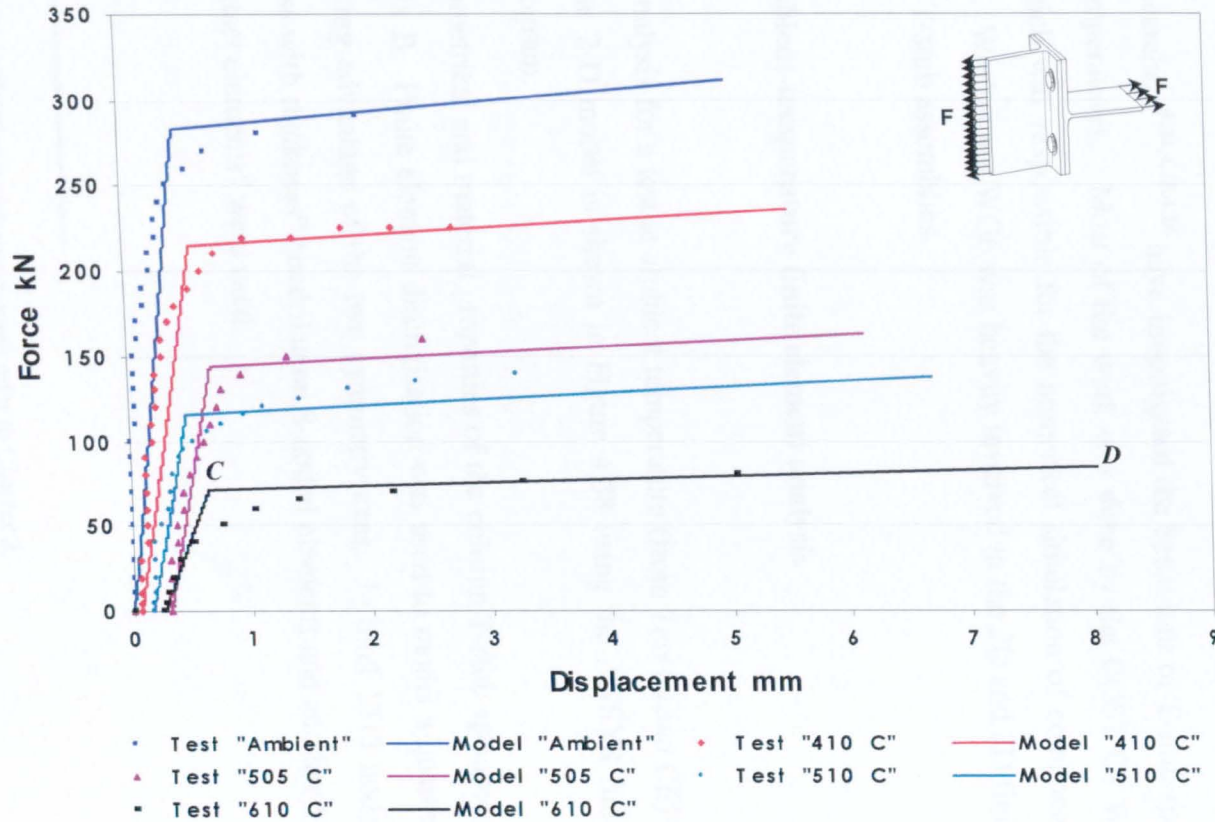


Figure 4.37 Force-deflection curves for end plate T-stub for test programme CE

Looking through the results above the simplified mathematical model predicts the behaviour of the T-stub assemblies reasonably accurately at elevated temperatures. Also the image acquisition and processing technique proves to be a very important tool to carry out tests at elevated temperatures successfully.

The next step in the investigation was to perform finite element analysis using ANSYS in order to compare the predicted behaviour of T-stubs at elevated temperatures with the test results.

4.5 FINITE ELEMENT ANALYSIS

Several researchers^{4.24,4.25,4.26} have investigated the behaviour of T-stub specimens at ambient temperatures. Most of the work was done by the COST C1 Work group No. 6^b, which was responsible for the numerical simulation of components within steel joints. Workgroup WG6 was heavily involved in the 2D and 3D finite element analysis of T-stub assemblies.

4.5.1 Ambient-temperature finite element analysis

A typical analysis for a test at ambient temperature (from *Test Group CE*) is outlined below. The 2-D model is shown in Figure 4.38 using the ANSYS finite element analysis program.

All the geometrical and material properties of the column T-stub specimen are given in Appendix B. Finite element discretisation was used to model a quarter of the T-stub by taking advantage of the two symmetry axes. In total 1313 nodes and 387 “plane stress with thickness” quadrilateral 8-noded elements and another 57 “point to surface contact elements” were used.

^b For details of the COST research programme refer to Chapter 2.

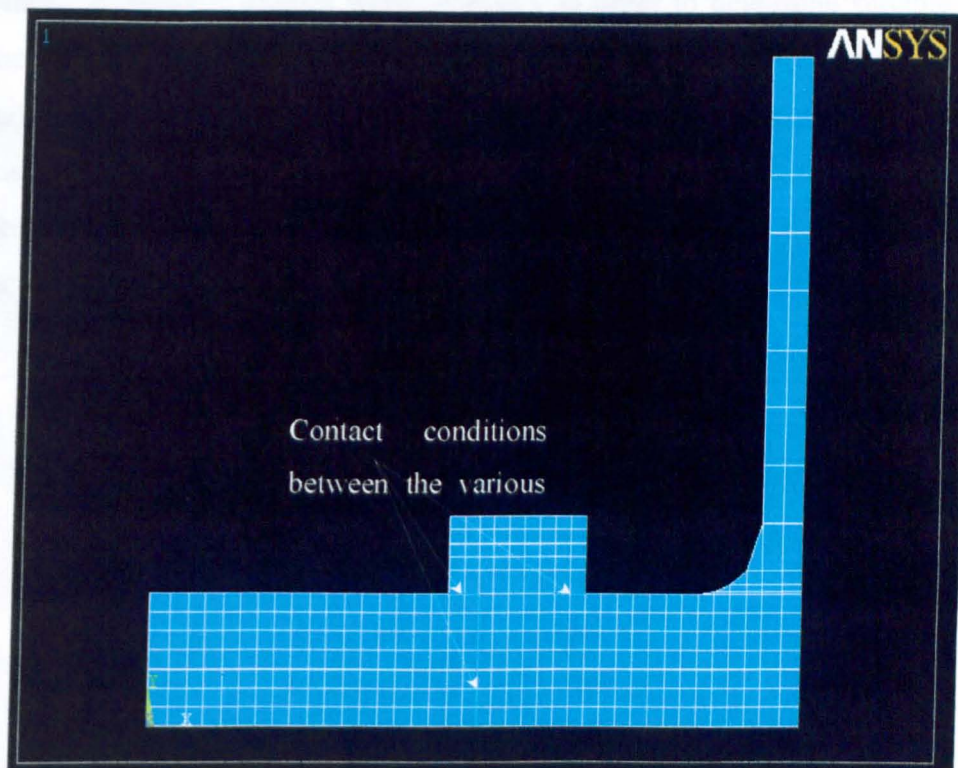


Figure 4.38 Finite element discretisation of the T-stub model

The structure under investigation consists of three different bodies, the bolt, the washer and the column T-stub. The thickness of the plane stress elements was adjusted as shown in Figure 4.39 in order to take into account the three-dimensional properties of the model. A half-thickness of 99.275mm was given to the column T-stub except in the region of the bolthole. For the nut, the shank, the washer and the region of the column T-stub bolthole, the thickness of the corresponding finite elements was assigned according to Figure 4.39.

From the figure above it can be seen that a rough estimation of the thickness was made. In the region of the hole, the two bodies are overlapping. The interaction between these bodies is taken into account by considering contact conditions between them (elements were created between the two contact surfaces). These contact elements have an important influence on the finite element analysis and three parameters need to be input into ANSYS to define their characteristics. These are the normal contact stiffness, the sticking contact stiffness and the penetration

tolerance. Parametric studies were necessary in order to determine suitable values for these coefficients (i.e. to ensure that the bolts stayed in contact with the T-stub flange). It is not practical to include values for these parameters in this section, because they were changed according to the dimensions of the T-stub model and the temperature at which the analysis was performed. Also the parameters for one contact element differed from those of the one next to it.

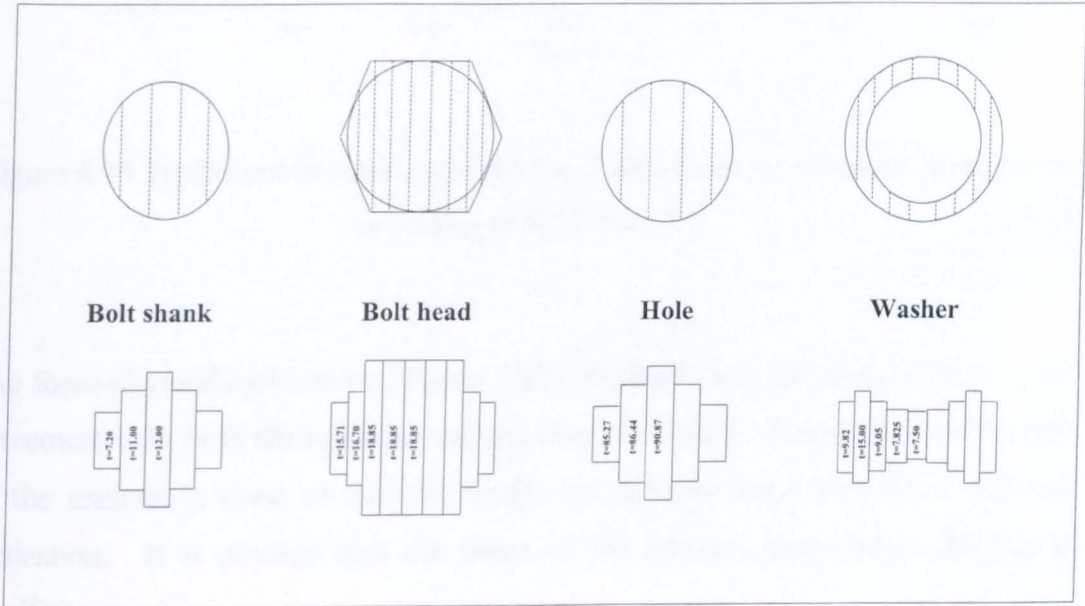


Figure 4.39 Thickness values of the finite element mesh

Typical stress-strain curves for the T-stub flange material at elevated temperatures are shown in Figure 4.40, according to EC3: Part 1.2. Similar curves were produced for the bolts using the reduction factors from Kirby^{4.20} (strength) and EC3: Part 1.2^{4.19} for the modulus. In the finite element analysis the corresponding stress strain curves were used for the T-stub flange and bolts. The model was analysed using symmetry boundary conditions at the mid-web and bolt line, with one support free to move in the x-direction (horizontal) in the region where the prying force is acting. The analysis options included contact surfaces, plasticity and large deformations.

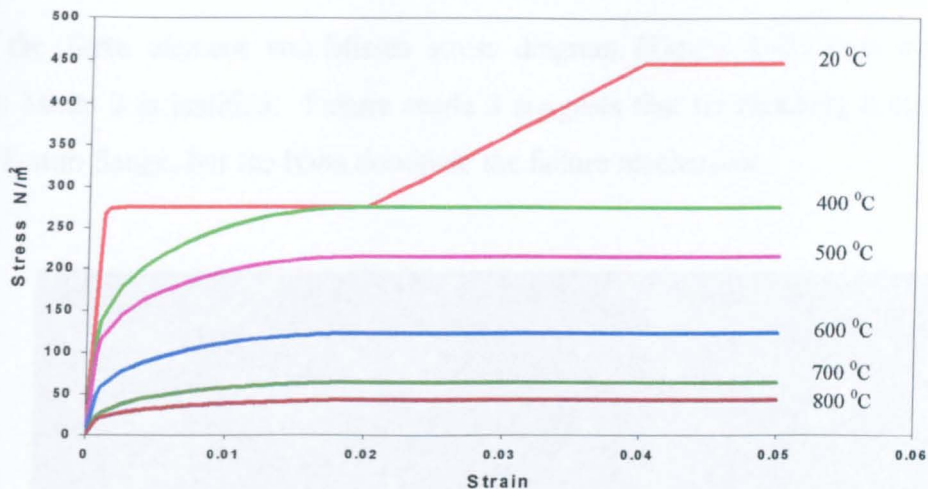


Figure 4.40 Typical stress-strain curve for the T-stub flange at elevated temperatures according to EC3: Part 1.2

The force-displacement curves (Figure 4.41) obtained from the analysis show good agreement with both the experimental and simplified model results. The elastic part of the analysis is close to the test results but the non-linear part has a different inclination. It is obvious that the shape of the adopted stress-strain diagram is significant.

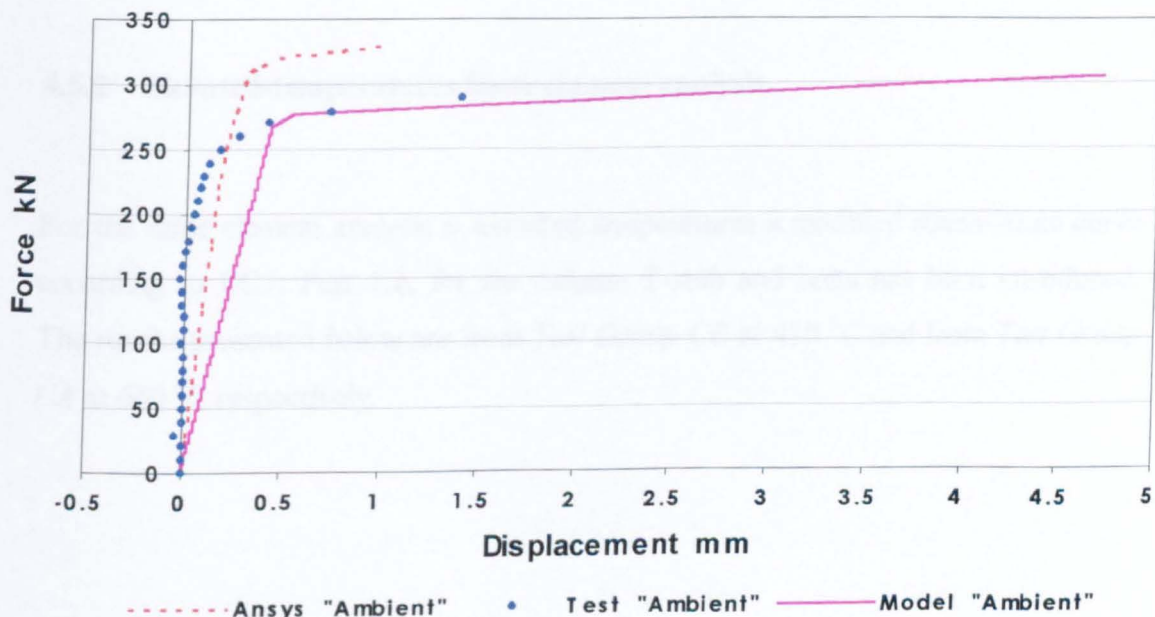


Figure 4.41 Force-deflection curves for a column T-stub from Test Group CE

From the finite element von-Misses stress diagram (Figure 4.42) it is clear that Failure Mode 3 is justified. Failure mode 3 suggests that no plasticity is happening in the T-stub flange, but the bolts dominate the failure mechanism.

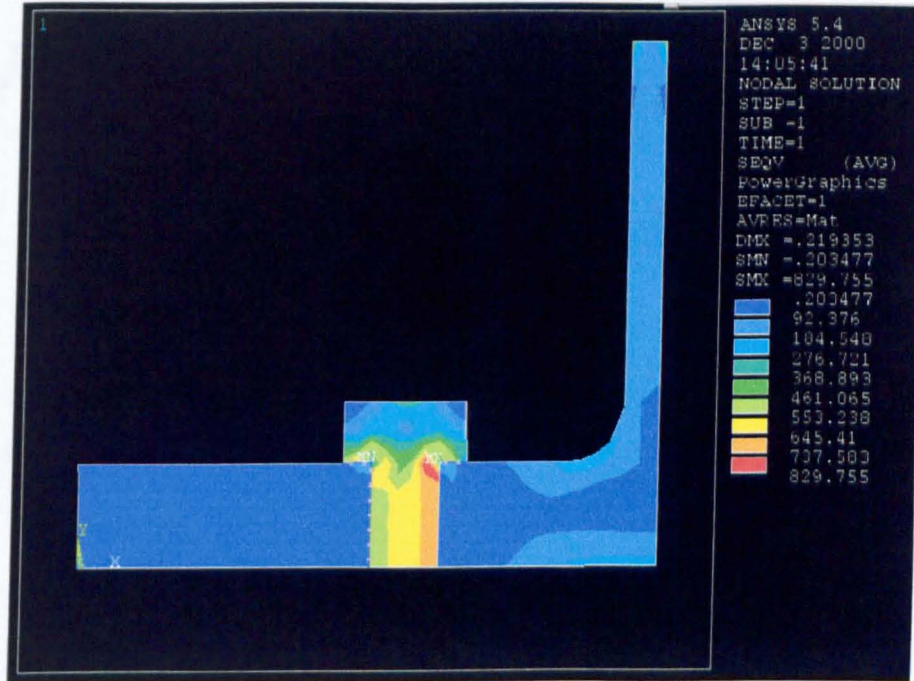


Figure 4.42 Von-Misses stresses for a 240kN tension load

4.5.2 Elevated-temperatures finite element analysis

For the finite element analysis at elevated temperatures a modified stress-strain curve according to EC3: Part 1.2, for the column T-stub and bolts has been introduced. The results presented below are from *Test Group CE* at 410 °C and from *Test Group CA* at 660 °C respectively.

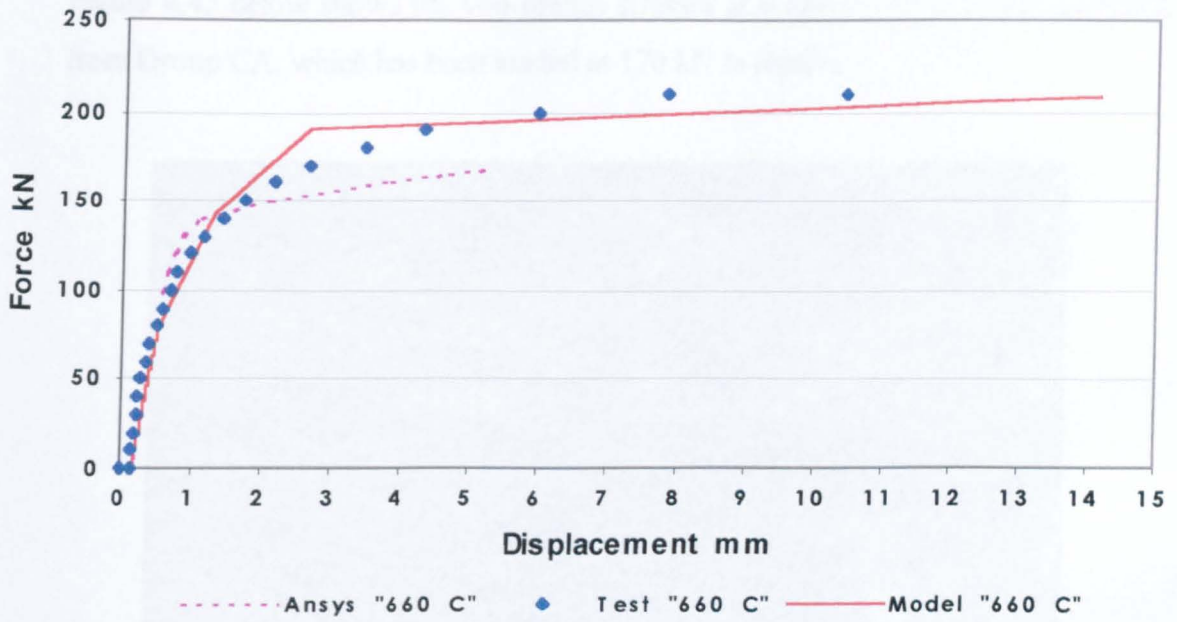


Figure 4.43 Force-deflection curves for a column T-stub at 410 °C from Test Group CE

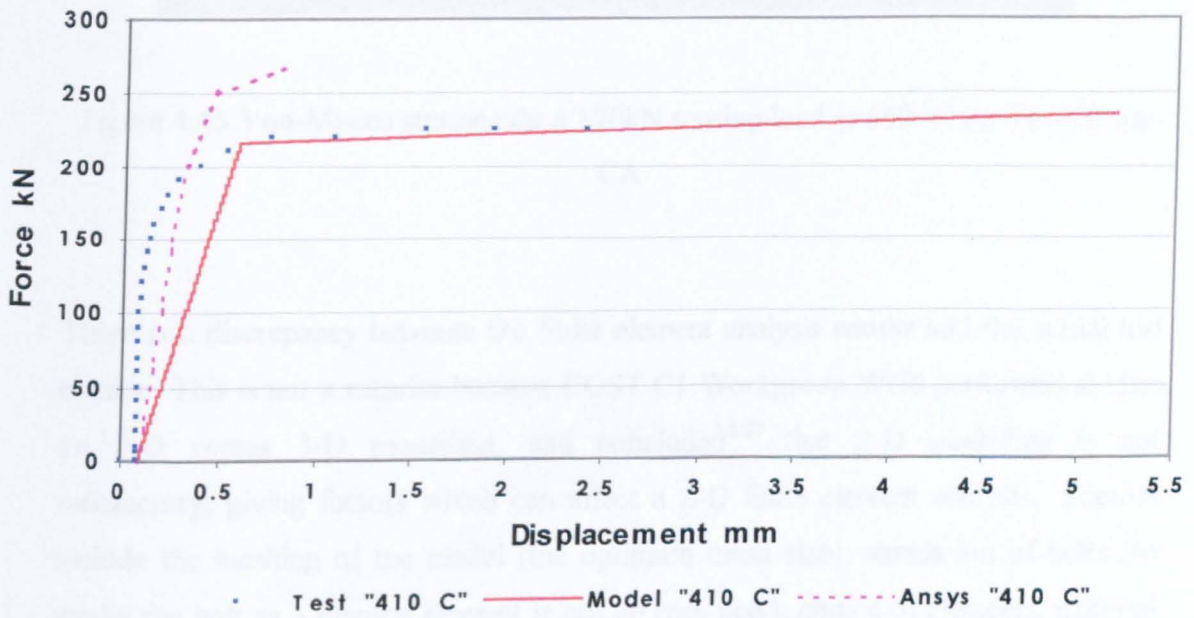


Figure 4.44 Force-deflection curves for a column T-stub at 660 °C from Test Group CA

Figure 4.45 below shows the von-Misses stresses at a 660°C for a T-stub specimen from Group CA, which has been loaded at 170 kN in tension

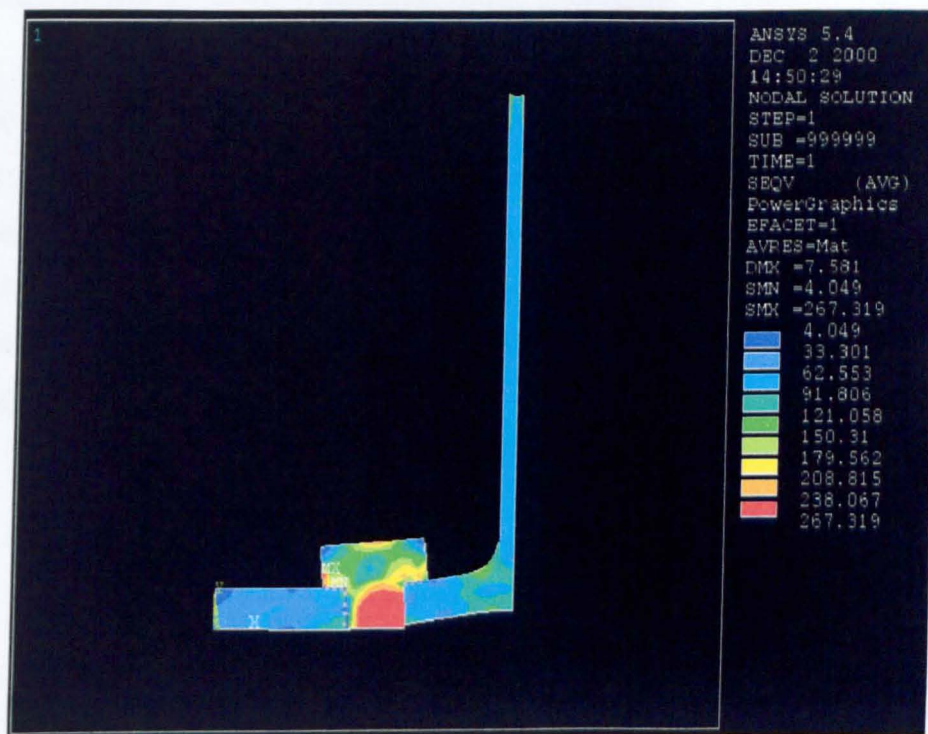


Figure 4.45 Von-Misses stresses for a 170kN tension load at 660°C for Test Group CA

There is a discrepancy between the finite element analysis results and the actual test results. This is not a surprise because COST C1 Workgroup WG6 performed studies on 2-D versus 3-D modelling, and concluded^{4,27} that 2-D modelling is not satisfactory, giving factors which can affect a 2-D finite element analysis. Factors include the meshing of the model (the optimum mesh size), simulation of bolts (to model the bolt as a flexural element is not an easy task), choice of elements, material behaviour, and most importantly the modelling of contact and gap elements.

4.6 DISCUSSION

4.6.1 Image acquisition and processing technique

The accuracy of the image processing software for T-stub tests is adequate for the purpose of studying their deformation response to applied tensile loading. The use of image acquisition and processing techniques has many advantages in comparison with conventional mechanical instruments and could be used for a wide range of testing applications. The benefits of this technique have been listed previously in section 3.6.

4.6.2 Test and Theoretical Results

There is a good correlation between the test results and simplified modelling. During the tests it was observed that, when using Grade 8.8 bolts and nuts, the nuts were failing by stripping their threads as shown in Figure 4.46 below, in which a normal nut is compared against two failed nuts.

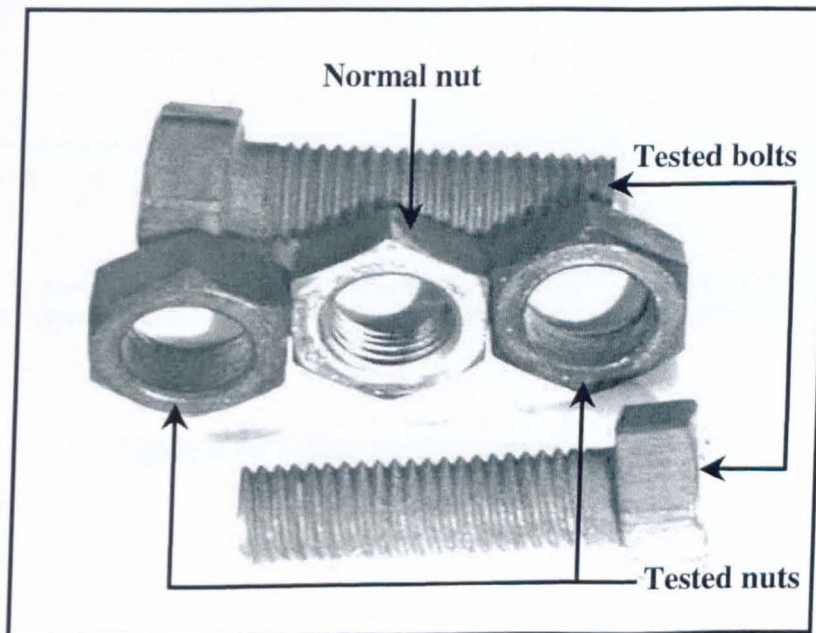


Figure 4.46 Nut stripping failure mechanism

This nut-stripping failure happened in *Test Group CA* for specimens tested at 530 °C and 740 °C. As a result, for all the other tests it was decided to use HSFG nuts in order to avoid this kind of failure.

During the experimental investigation of the tension zone it was very clear from the beginning that bolts could influence the T-stub specimen behaviour significantly. The same behaviour is highlighted by the simplified model results. As a conclusion, the bolt material properties at elevated temperatures need to be modelled correctly.

Another observation from the test and simplified model results is the importance of predicting the failure mode of the T-stub specimen. This is because, according to the failure mode, the total deformation of the T-stub flange varies significantly. This is demonstrated by plotting the three failure modes taken from different test programmes at 505 °C, as shown in Figure 4.47 below.

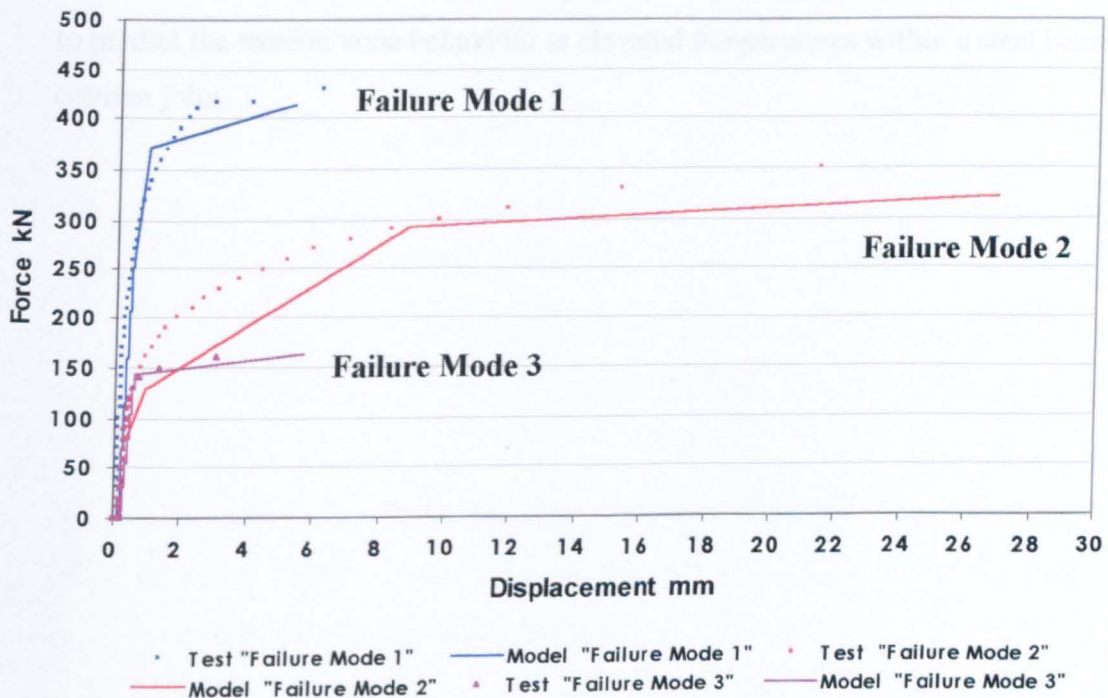


Figure 4.47 Failure modes compared at 505 °C

4.7 CONCLUSION

This study has described the use of an image acquisition and processing technique and the development of a simplified mathematical model for T-stub tests at elevated temperatures. The image acquisition and processing technique is particularly interesting because, aside from obtaining displacement readings at high temperatures, it also records the behaviour of the specimen as soon as the load is applied. This is an advantage because, by careful observation of the recorded test, it is possible to recognise the failure mechanism of the specimen. This information also makes the image acquisition and processing technique attractive for ambient-temperature tensile or compressive tests for steel or concrete.

The simplified model gives acceptable results when compared with test results. It is a mathematical model which can easily be used by designers or researchers in order to predict the tension zone behaviour at elevated temperatures within a steel beam-to-column joint.

4.8 REFERENCES

- 4.1 Yee, Y.L., and Melchers, E., “*Moment-Rotation Curves for Bolted Connections*”, Journal of Structural Engineering, ASCE, Vol. 112, No. 3, 1986.
- 4.2 Weynand, K., Jaspart, J.P., and Steenhuis, M., “*The Stiffness Model of Revised Annex J of Eurocode 3*”, Connections in Steel Structures III, Behaviour Strength and Design, pp. 441-452, 1995.
- 4.3 Sherbourne, A.N., “*Bolted Beam-to-Column Connections*”, The Structural Engineer, Vol. 39, pp. 203-210, 1961.
- 4.4 Zoetemeijer, P., “*A Design Method for the Tension Side of Statically Loaded, Bolted Beam-to-Column Connections*”, Heron, 20, No. 1, pp. 1-59, 1974.
- 4.5 Packer, J.A., and Morris, L.J., “*A Limit State Design Method for the Tension Region of Bolted Beam-to-Column Connections*”, The Structural Engineer Vol. 55, No. 10, pp. 446-458, 1977.
- 4.6 Agerskov, H., “*High-Strength Bolted Connections Subjected to Prying*”, Journal of the Structural Division, ASCE, Vol. 102, No. 1, pp. 161-175, 1976.
- 4.7 Zoetemeijer, P., “*A Design Method for the Tension Side of Statically Loaded, Bolted Beam-to-Column Connections*”, HERON, Vol. 20, No. 1, pp. 1-59, 1974.
- 4.8 “*EC3: Design of Steel Structures, Part 1.1: Revised Annex J Joints and Building Frames*”, (Draft), Document CEN/TC250/SC3 N419E, European Committee for Standardization, 1994.
- 4.9 “*Joints in Steel Construction: Moment Connections*”, The Steel Construction Institute, 1995.
- 4.10 Shi, Y.J., Chan, S.L., and Wong, Y.L., “*Modelling for Moment-Rotation Characteristics for End-Plate Connections*”, Journal of Structural Engineering, Vol. 122, No. 11, pp. 1300-1306, 1996.
- 4.11 Piluso, V., Faella, C., and Rizzano, G., “*Ultimate Behaviour of Bolted T-Stubs. I: Theoretical Model*”, Journal of Structural Engineering, Vol. 127, No. 6, pp. 686-693, 2001.

- 4.12 Piluso, V., Faella, C., and Rizzano, G., "*Ultimate Behaviour of Bolted T-Stubs. II: Model Validation*", Journal of Structural Engineering, Vol. 127, No. 6, pp. 694-704, 2000.
- 4.13 Swanson, A.J., and Leon, T.R., "*Bolted Steel Connections: Tests on T-stub Components*", Journal of Structural Engineering, Vol. 126, No. 1, pp. 50-56, 2000.
- 4.14 Swanson, A.J., and Leon, T.R., "*Stiffness Modelling of Bolted T-stub Connection Components*", Journal of Structural Engineering, Vol. 127, No. 5, pp. 498-505, 2001.
- 4.15 Faella, C., Piluso, V., and Rizzano, G., "*Experimental Analysis of Bolted Connections: Snug Versus Preloaded Bolts*", Journal of Structural Engineering, Vol. 124, No. 7, pp. 765-774, 1998.
- 4.16 Gere J.M., and Timoshenko, S.P., "*Mechanics of Materials*", Second SI Edition, PWS Engineering, Wadsworth International, 1985.
- 4.17 Theodorou, Y., "*Mechanical Properties of Grade 8.8 Bolts at Elevated Temperatures*", MSc. Report, University of Sheffield, UK, 2001.
- 4.18 "BS 5950 Structural Use of Steelwork in Building: Part 8: Code of Practice for Fire Resistance Design", British Standard Institution, London, 1990.
- 4.19 "EC3: Design of Steel Structures, Part 1.2: General rules Structural fire design", (Drafts) Document CEN, European Committee for Standardisation, 1995.
- 4.20 Kirby, R. B., "*The Behaviour of High-strength Grade 8.8 Bolts in Fire*", Journal of Constructional Steel Research, Vol. 33, pp.3-38, 1995.
- 4.21 Plumptre, D.A., "*Realistic Testing and Measurement Techniques at Very High Temperatures Using Quartz Halogen Bulb Furnaces*", Ultra High Temperature Mechanical Testing, Edited by Lohr, R.D., and Steen, M., 1995.
- 4.22 Jaspert, J.P., "*Numerical Simulation of a T-stub-Experimental Data*", COST C1, Numerical Simulation Working Group, Doc. C1WD6/94-09, 1994.
- 4.23 Graham, W.O., and Cheal, B.D., "*Structural Steelwork Connections*", Text book, Published by Butterworth & CO., 1989.

- 4.24 Jaspart, J.P, and Bursi, O.S., “*Calibration of a Finite Element Model for Isolated Bolted End-Plate Steel Connections*”, Journal of Constructional Steel Research, Vol. 44, No. 3, pp. 225-262, 1997.
- 4.25 Jaspart, J.P, and Bursi, O.S., “*Benchmarks for Finite Element Modelling of Bolted Steel Connections*”, Journal of Constructional Steel Research, Vol. 43, Nos. 1-3, pp. 17-42, 1997.
- 4.26 Sherbourne, N. A., and Bahaari, R. M., “*3D Simulation of Bolted Connections to Unstiffened Columns-I. T-stub Connections*”, Journal of Constructional Steel Research, Vol. 40, No. 3, pp. 169-187, 1996.
- 4.27 “Control of the Semi-Rigid Behaviour of Civil Engineering Structural Connections”, Final COST Action C1 Report, EUR 19244, 1999.

Chapter 5

Compression Zone

5.1 INTRODUCTION

The previous chapter outlined an experimental and analytical investigation into the behaviour of components within the tension zone of a steel beam-to-column joint. This chapter investigates the column web subjected to transverse compression forces, which is the most important component within the compression zone of a typical steel joint (Figure 5.1).

At ambient temperatures researchers^{5.1.5.2,5.3} focused on producing simplified models in order to predict the ultimate capacity of a column web subjected to transverse compressive forces and thereby assist engineers to design steel joints efficiently. Another reason for producing these models was to eliminate the use of column web stiffeners, which are expensive to install and interfere with the weak-axis framing of beams into the column.

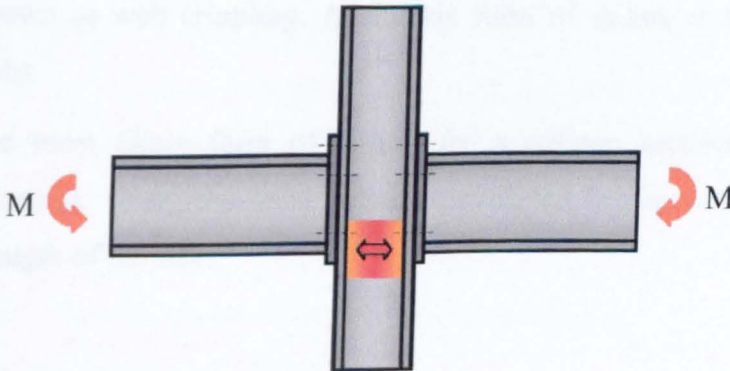


Figure 5.1 Extended endplate joint showing the column web component (shaded)

The resistance to concentrated forces is a problem of a very complex nature in which it is almost impossible to derive closed theoretical solutions. Therefore, studies aiming at predicting the ultimate resistance of column webs to concentrated forces tend towards empirical solutions.

Everything becomes more complicated when another variable, such as temperature, is introduced into the problem. For this reason a closer look into existing empirical models at ambient temperature, contained in design codes and standards, is outlined next with a view to applying the principles at elevated temperatures.

5.2 EXISTING ANALYTICAL MODELS AT AMBIENT TEMPERATURE

When the web of a section is subjected to compressive loads applied through the flanges it may fail in one of three ways:

- a) For webs that are relatively thin compared to their height it is possible that failure could be by buckling as a strut. The resistance to this form of failure may be predicted by considering a portion of the web as a strut and calculating its buckling resistance. Although this form of failure may occur in a beam section subjected to point loading it is unlikely for a column section, as the web height tends to be small compared to the web thickness.
- b) For slender webs some form of local instability may occur. This failure is known as web crippling. Again this form of failure is unlikely in column webs.
- c) The most likely form of failure for a column section is web crushing (bearing). Here the local stresses developed in the web exceed the yield strength of the steel.

5.2.1 British Standard-BS5950

The 1990 edition of BS5950^{5.4} covered crushing (which it referred to as bearing failure) and buckling only; web crippling was not included. In the recent revision to BS5950^{5.5} the web buckling clause has been significantly modified, and is now calculated based on a modification to the bearing capacity. The same formulae are used for both beam webs under concentrated loads and column webs subjected to transverse loads arising from connection moments. Only in cases where the rotation of the web, or lateral movement relative to the flanges, is not assured is the problem addressed as strut buckling. No reductions in crushing or buckling resistance are made to account for axial load in the column.

5.2.1.1 British Standard-BS5950 for column webs

The history of the clauses used for column web buckling and bearing date back to BS449, and they appear to be empirical. For web bearing BS449^{5.6} assumed that the force was distributed through the flange and root of the web at an angle of 30° . According to Morris^{5.7}, when BS5950^{5.8} appeared it followed the American practice for the criterion for yielding (crushing) of the column web when subjected to a compression force arising from an end plate connection. That is, the force from the beam flange is assumed to disperse at a 1:1 gradient within the end plate and at a 1:2.5 slope within the column flange as far as the junction of the root fillet and the web (Figure 5.2).

According to Hendrick *et al*^{5.2} the 1:2.5 dispersion of the compression force was the result of an experimental investigation in the USA (conducted in 1959) which considered the behaviour of column webs within a welded joint. The authors suggested an alternative design criterion for bolted end-plate joints, namely a 1:1 gradient within the end plate and a 1:3 dispersion of the compression force within the column web. The difference was due to the effects of the end plate and the fillet weld connecting the beam to the end plate.

The same recommendation was made by Bose *et al*^{5.1} but in BS5950^{5.4} it remains as a 1:2.5 dispersion of the compression force as shown in Figure 5.2.

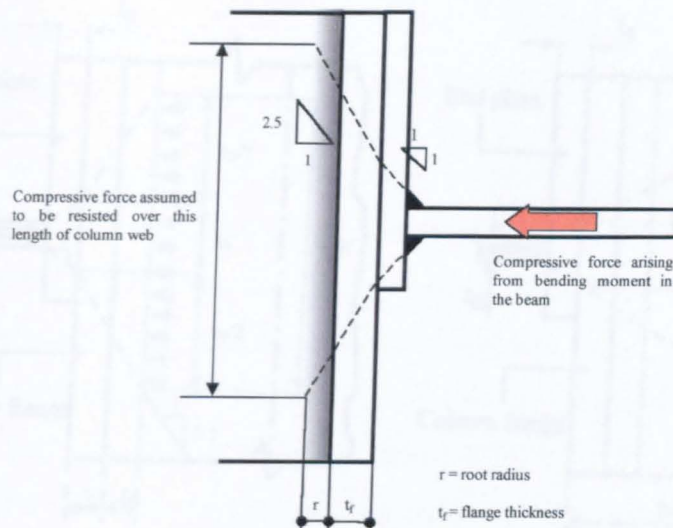


Figure 5.2 Assumed distribution of force for web crushing according to BS5950

The maximum crushing force that can be resisted by the column web is calculated as:

$$P = (b_1 + n_2) t_{wc} p_{yw} \quad \dots 5.1$$

where t_{wc} is the column web thickness, p_{yw} is the yield strength, b_1 is the length of stiff bearing and n_2 is the length obtained by dispersion through the flange to the toe of the fillet, as shown in Figure 5.3 (a) below.

The web buckling resistance is given by:

$$P = (b_1 + n_1) t_{wc} p_c \quad \dots 5.2$$

in which n_1 is the length obtained by dispersion at 45° through half the depth of the section as illustrated in Figure 5.3 (b) below; p_c is the compressive strength as obtained from table 27c of BS5950.

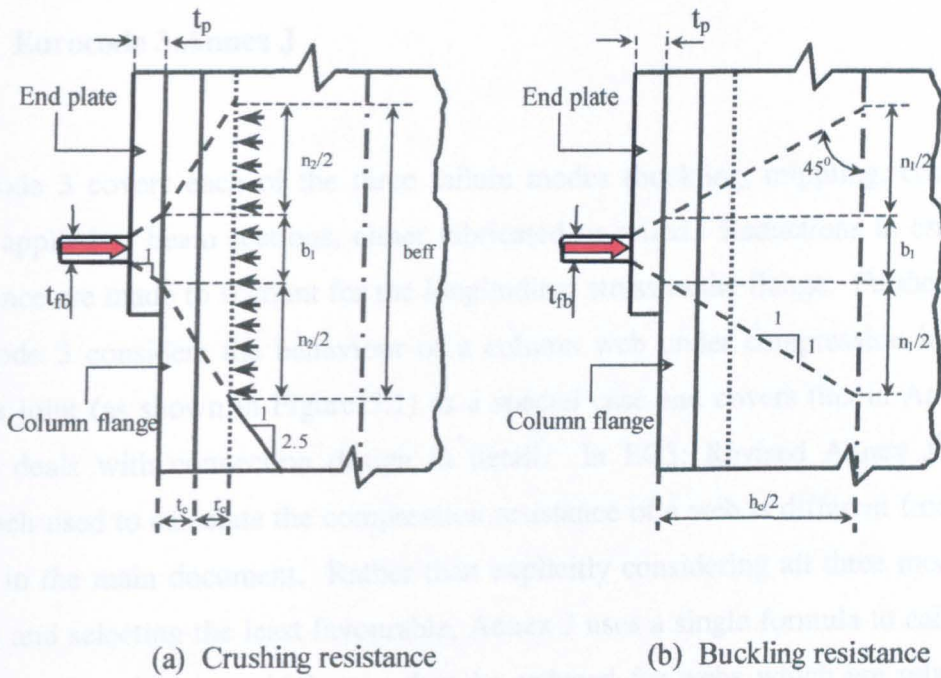


Figure 5.3 Effective breadth for web resistance in BS 5950

The buckling length of the compression member should be determined from the conditions of lateral and rotational restraint at the flanges where the force is applied. In the case of end plate connections, the ends of the web may be assumed as restrained against both rotation and relative lateral movement, and an effective length $l=0.7d_c$ may be considered. The radius of gyration i is given by $\frac{t}{\sqrt{12}}$, and the slenderness ratio λ is determined from

$$\lambda = \frac{l}{i} = \frac{0.7d_c}{t/\sqrt{12}} = 2.42 \frac{d_c}{t} \quad \dots 5.3$$

In BS 5950 a conservative value of $\lambda=2.5d_c/t$ is specified for convenience.

5.2.2 Eurocode 3:Annex J

Eurocode 3 covers each of the three failure modes (buckling, crippling, crushing) when applied to beam sections, either fabricated or rolled. Reductions in crushing resistance are made to account for the longitudinal stress in the flange. Furthermore, Eurocode 3 considers the behaviour of a column web under compression induced from a joint (as shown in Figure 5.1) as a special case and covers this in Annex J, which deals with connection design in detail. In EC3: Revised Annex J^{5,9} the approach used to calculate the compression resistance of a web is different from that found in the main document. Rather than explicitly considering all three modes of failure and selecting the least favourable, Annex J uses a single formula to calculate the crushing resistance, which may then be reduced for webs which are relatively slender, as defined by a plate slenderness parameter. Further reductions in capacity are made when the axial load in the column exceeds 50% of the squash load, and for the effects of panel shear.

5.2.2.1 Eurocode 3:Annex J for column webs

In EC3: Annex J the resistance of an unstiffened column web subjected to transverse compression is given by:

$$F_{c,wc,Rd} = \frac{\rho b_{eff} t_{wc} f_{y,wc}}{\gamma_{M0}} \quad \dots 5.4$$

$$F_{c,wc,Rd} \leq \frac{\rho b_{eff} t_{wc} f_{y,wc}}{\gamma_{M0}} \left[\frac{1}{\bar{\lambda}} \left(1 - \frac{0.22}{\bar{\lambda}} \right) \right] \quad \dots 5.5$$

where

$$\bar{\lambda} = 0.93 \sqrt{\frac{b_{eff} d_c f_{y,wc}}{Et_{wc}^2}} \quad \dots 5.6$$

and if $\bar{\lambda} \leq 0.67$ then equation 5.4 is applied, which gives the crushing resistance of the column web. Otherwise equation 5.5 will give the buckling resistance of the column web. The notation t_{wc} is the column web thickness, $f_{y,wc}$ is the yield strength, E the Young's Modulus, ρ is a reduction factor (taken as 1.0) to do with the shear effects in the column web, γ_{M0} is a material safety factor, d_c is the depth of the column web and $b_{eff} = \sqrt{h_c^2 + s_s^2}$ as shown in Figure 5.4 below.

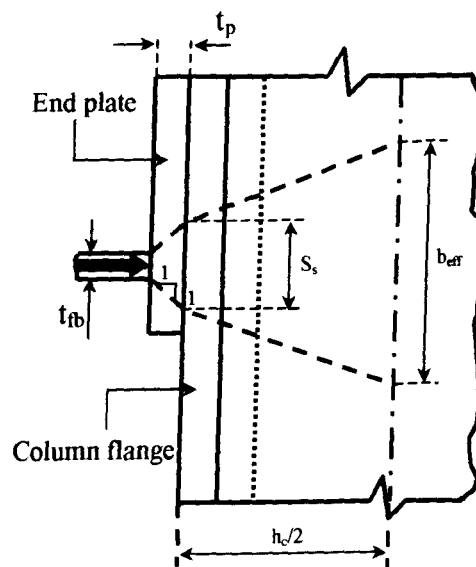


Figure 5.4 Effective breadth for web buckling resistance in Eurocode 3

What is described above are the differences between BS5950 and Eurocode 3 for designing section webs (column or beam) when subjected to compressive loads applied through the flanges. The differences (and similarities) of column web compression in these approaches are highlighted in the Table 5.1.

Table 5.1 Comparison of column web compression resistances (in kN) for a point load (S275 steel)

UC	BS5950:1990		BS5950:2000		Eurocode 3			Annex J	
	Bearing	Buckling	Bearing	Buckling	Crushing	Crippling	Buckling	Resistance	With 70% Axial load
	P_{bw}	P_x	P_{bw}	P_x	$R_{y,Rd}$	$R_{a,Rd}$	$R_{b,Rd}$	$F_{c,wc,Rd}$	
356UC202	1201	1758	1201	1788	1201	1482	868	1201	1081
356UC177	997	1458	997	1328	721	1151	717	997	897
356UC153	784	1117	784	929	567	847	549	761	685
356UC129	604	811	604	634	437	606	400	546	491
305UC283	2741	3232	2741	6063	2741	3921	1613	2741	2467
305UC240	2099	2614	2099	4218	2099	2882	1302	2099	1889
305UC198	1535	2019	1535	2730	1535	1991	1002	1535	1381
305UC158	1127	1571	1127	1760	816	1356	776	1127	1014
305UC137	904	1282	904	1286	654	1031	632	904	814
305UC118	722	1027	722	932	523	776	505	722	650
305UC97	538	735	538	603	389	528	361	506	455
254UC167	1471	1798	1471	2989	1471	2016	896	1471	1324
254UC132	1032	1346	1032	1781	747	1300	667	1032	929
254UC107	754	1037	754	1165	546	895	512	754	679
254UC89	548	750	548	717	397	594	369	548	493
254UC73	411	553	411	473	297	410	272	393	354
203UC86	692	905	692	1231	501	885	449	692	623
203UC71	488	650	488	722	353	568	321	488	439
203UC60	407	581	407	601	295	469	286	407	366
203UC52	318	446	318	410	230	339	219	318	286
203UC46	271	380	271	329	196	277	187	266	239
152UC37	271	395	271	439	196	331	195	271	244
152UC30	196	289	196	274	142	219	142	196	176
152UC23	148	236	148	201	107	157	116	148	133

From the table it is clear that, according to BS5950, crushing controls the compression resistance of the web in all cases. For these column sections, the BS5950:2000 revised calculation of P_x (buckling resistance) results in a smaller value than previously in only a handful of cases (shaded in the table) but these are of academic interest as the controlling factor is the crushing resistance.

Considering the values calculated using EC3, the buckling resistance is the lowest of the three resistances (crushing- $R_{y,Rd}$, crippling- $R_{a,Rd}$, buckling- $R_{b,Rd}$) calculated in accordance with the clauses shown in the main body of the code. However Annex J, which should be used for calculating compression zone resistance gives higher capacities, most of which agree with the BS5950 crushing values. In a few cases (shaded in the table) the Annex J calculation is less than BS5950's P_{bw} (bearing). These are for webs where the plate slenderness of the web^a exceeds 0.673. The final column in the table shows the reduction in compression resistance when the axial load is 70% of the squash load. As shown in the table above, Eurocode 3 Annex J uses essentially the same approach for web crushing

Since the compression resistance in both BS5950 and EC3 is controlled by crushing (bearing) resistance it is obviously important that a design formula accurately predicts this capacity. To verify the accuracy of the formulas described earlier, Bailey *et al*^{5,10} compared test result from a wide range of sources with design results. Figures 5.5 and 5.6 below compare the predicted failure loads with a large number of test results. Considerable scatter exists, with no one method being particularly accurate. Both EC3 and the BS5950 show very conservative results at the d_{wc}/t_{wc} ratios appropriate for rolled column sections (typically below 20). It is suggested that this scatter arises because the EC3 and BS5950 methods of calculating the crushing resistance do not properly account for all the parameters which influence the behaviour.

$$^a \bar{\lambda}_p = \sqrt{\frac{d_{eff, c, wc} d_{wc} f_{y, wc}}{Et^2}}$$

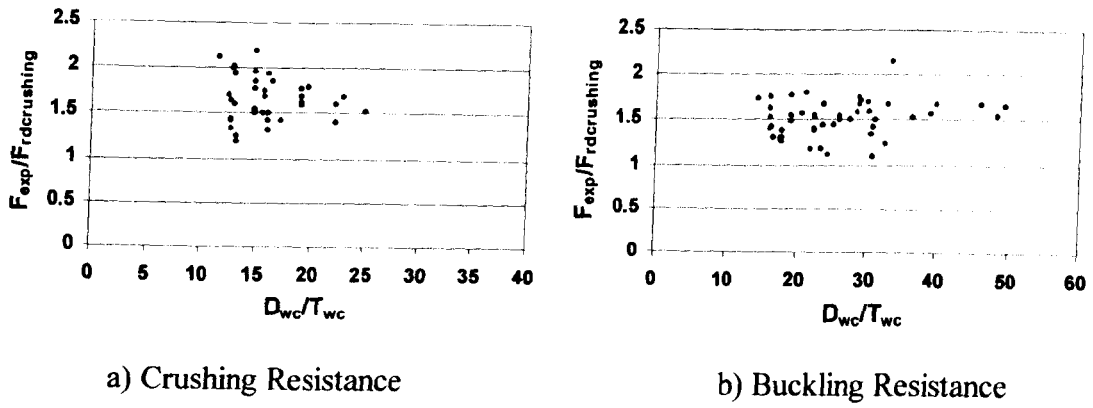


Figure 5.5 Eurocode 3-Annex J results^{5,10}

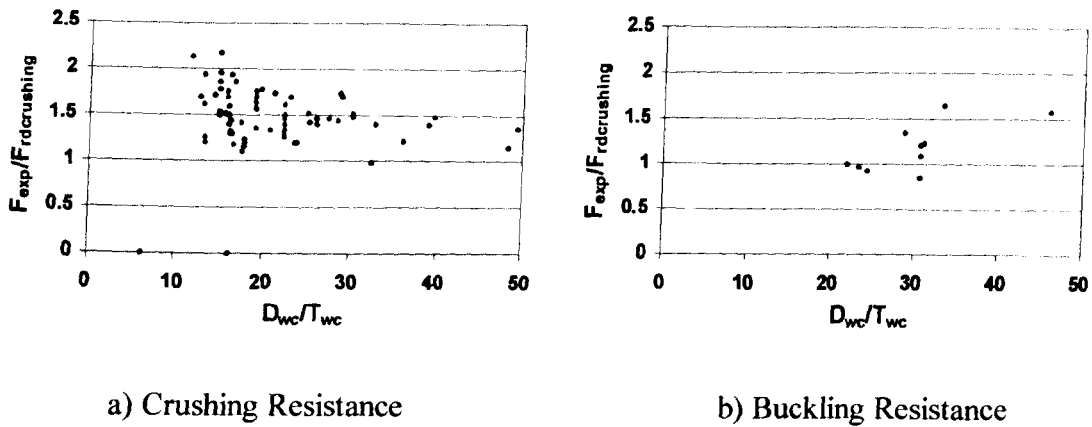


Figure 5.6 BS5950 results^{5,10}

As a concluding remark, the current design codes for the UK and Europe provide a very conservative recommendation for calculating the ultimate resistance of a column web under compression force at ambient temperature. It was decided that a new empirical model should be investigated, which would not only provide the ultimate capacity of the column web at elevated temperatures but also determine the stiffness of the column web in the elastic and plastic regions.

For this reason the experimental investigation was carried out first and then, based on the test observations and results, a simplified empirical model was developed.

5.3 EXPERIMENTAL PROGRAM

The tests were carried out in the purpose-built furnace described in Chapter 3. The procedure followed was to heat the column specimens up to the required temperature, and then continue by applying compression forces and capturing images in order to measure displacements. Figure 5.7 below shows the test arrangement.

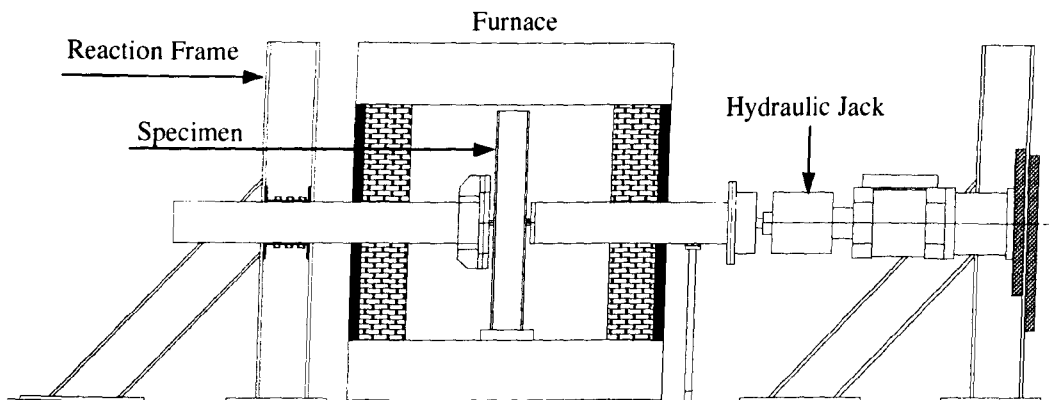


Figure 5.7 Arrangement for compression zone tests

The column specimen was loosely supported on a steel base plate inside the furnace. In order to prevent the specimen from rotating freely in space as soon as the compression force was applied, it was bolted (finger tight) on the reaction frame below the compression force contact point. Figure 5.8 shows the specimen inside the furnace and the details of the support.

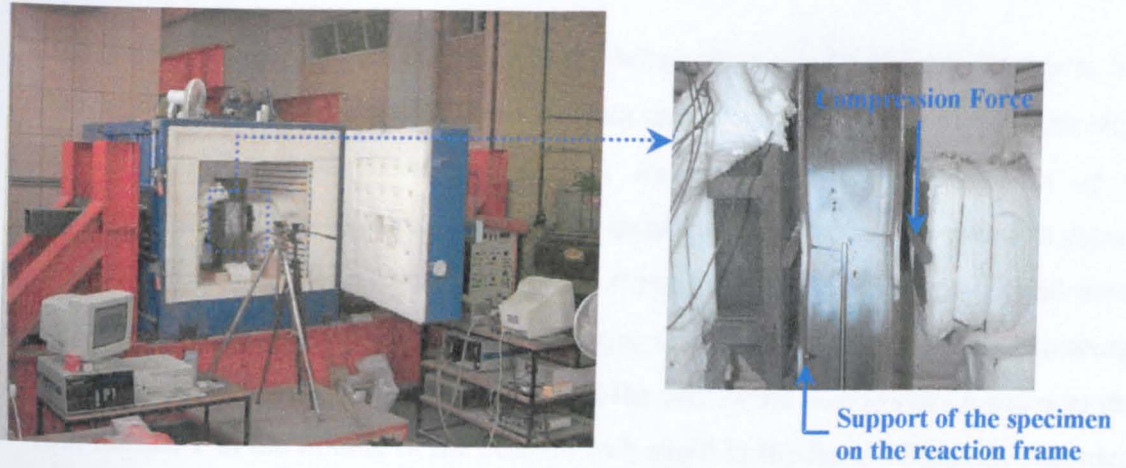


Figure 5.8 Column specimen inside the furnace

Images were taken at different load increments and the out-of-plane (web) and flange displacements were measured. The displacement was then the difference between the targets (made using a 0.5mm diameter drill) for the column web and flanges as shown in Figure 5.9. The distance between the two targets on one steel rod was 5mm. That distance was also measured (using a Vernier) and the average was taken in order to calibrate the image acquisition and processing system.

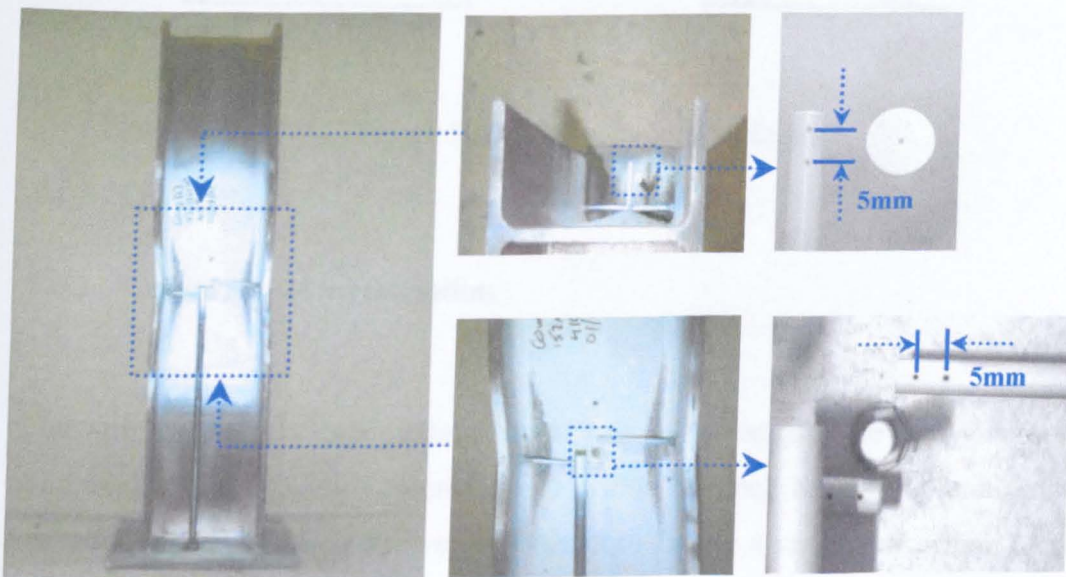


Figure 5.9 Displacement measurement

The final important measurement was the temperature of the column specimen. Six thermocouples were placed on the specimen and another three around the specimen to measure the atmospheric temperature. As soon as the specimen was up to temperature the tests were carried out. The locations of the thermocouples are shown in Figure 5.10. The temperature from each thermocouple was recorded several times during each test and the average temperature was taken as the design temperature. Thermocouples 2 and 5 were placed just at the end of the root radius, 3 and 4 in the root radius, 1 in the middle of the column web and 6 in the flange. From the recorded temperatures it was concluded that thermocouples 2, 5 and 6 had the same temperatures and there was a difference of 15-20 °C between thermocouples 3, 5 and 1.

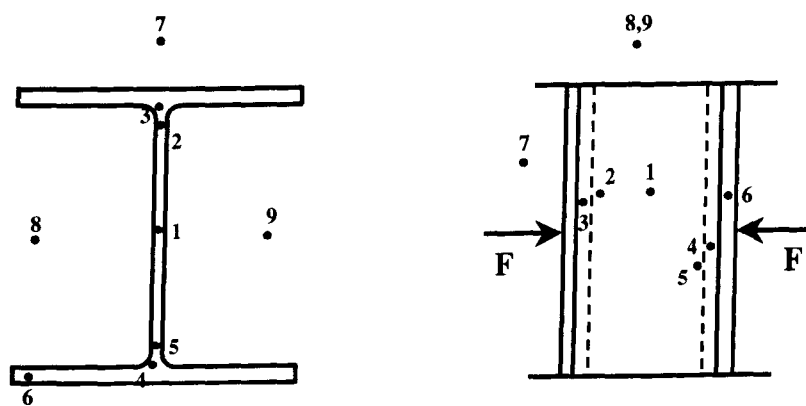


Figure 5.10 Thermocouple positions

5.3.1 Experimental investigation

The purpose of this experimental work was to investigate the behaviour of the compression component (column web) within a steel beam-to-column joint at elevated temperatures. It was very important to choose a variety of column sections, which would have different geometrical properties and as a result might behave differently in terms of strength and stiffness. The important influencing parameters to be investigated were the slenderness of the column web and the thickness of the

flanges. Table 5.2 below shows the different column sections and geometrical properties of the specimens that were tested at elevated temperatures.

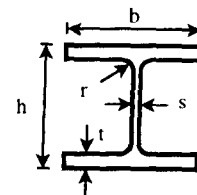


Table 5.2 Different column sections tested at elevated temperatures

Test	Column Sections	Depth of Section h	Width of section b	Thickness of Web s	Thickness of Flange t	Root Radius r	Ratio for web local Buckling d/s	Number of tests
		mm	mm	mm	mm	mm		
A	152UC30	157.6	152.9	6.5	9.4	7.6	19.0	8
B	203UC46	203.2	203.6	7.2	11.0	10.2	22.3	7
C	203UC71	215.8	206.4	10.0	17.3	10.2	16.1	4
D	203UC86	222.2	209.1	12.7	20.5	10.2	12.7	6

In addition to the specimens tabulated above, another one (UC203x203x52) was tested at 600 °C. Another 3 column specimens were tested at ambient temperatures in order to collect a larger number of test results, as the calculation of the ultimate compressive force was not an easy task, even at ambient temperature. The three column sections were UC203x203x86, UC203x203x60 and UC254x254x107. All four additional column specimens were taken from the T-stub investigation at elevated temperatures.

In total 29 tests at ambient and elevated temperatures were investigated and the actual dimensions (average), mechanical properties and experimental data of the column specimens are given in detail in Appendix C.

The actual test results will be presented in the following sections in which an investigation is carried out in order to produce an empirical model for calculating the ultimate strength and stiffness of the compression component (column web). In order to do this, a 2D finite element analysis has been performed to investigate the stress distribution and the behaviour of the column web under transverse compressive forces at elevated temperatures.

5.4 2D-FINITE ELEMENT ANALYSIS

Finite element investigations have been performed by different authors^{5.1,5.2} in order to validate their empirical models for calculating the ultimate capacity of a column web under compression. Several reports^{5.11,5.12} show that the empirical formulation presented in Eurocode 3: Annex J was supported by a 3D finite element analysis performed on a welded joint. The finite element analysis described here has been performed by Block^{5.13} and the purpose was to understand the behaviour of the compression component within a steel beam-to-column joint.

Observations from the experimental tests at elevated temperatures suggested that the column web failure was due to a strength reduction effect rather than a buckling problem. For this reason it was decided to start the finite element analysis with a 2D model as shown in Figure 5.11. Typical finite element results are also included in this section for a UC203x203x46 specimen, although finite element results exist for all of the specimens.

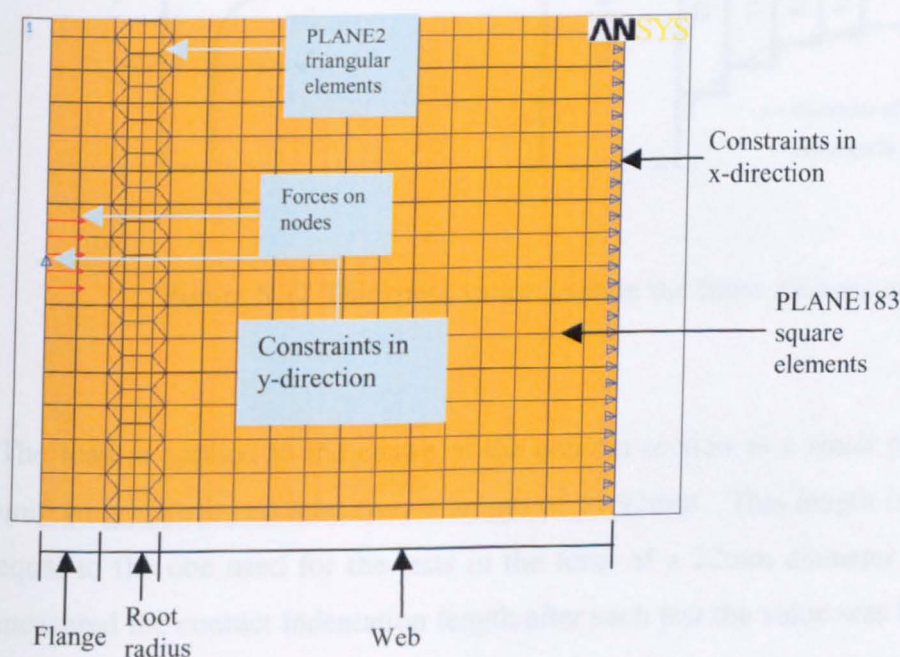


Figure 5.11 Finite element discretisation of the compression model

5.4.1 Finite element model

Taking advantage of symmetry, only half of the UC203x203x46 specimen was modelled. All the geometrical and material properties are given in Tables 4 and 5 in the following section. The model included 8930 nodes and 3133 plane stress elements with thickness. Two types of elements were used:

- a) PLANE183 which are quadrilateral, two-dimensional 8-noded, and
- b) PLANE2 which are triangular 6-noded elements (for the root radius).

“Plane stress with thickness” elements were used in order to take into account the three-dimensional properties of the model. The thickness detail around the root radius is shown in Figure 5.12.

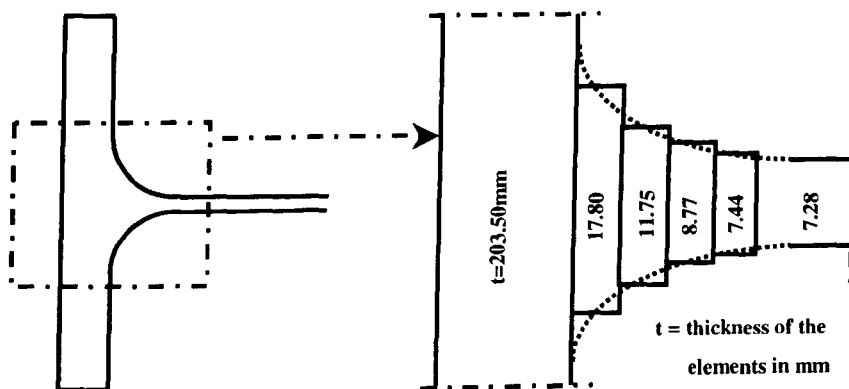


Figure 5.12 Thickness values used in the finite element mesh

The load is applied to the centre of the column section as a small patch area under uniformly distributed load over a length of 11.92mm. This length is approximately equal to the one used for the tests in the form of a 22mm diameter roller. Having measured the contact indentation length after each test the value was between 10 and 13mm.

The stress-strain curves for the particular column section, UC203x203x46, are shown in Figure 5.13. These were calculated from Eurocode 3 Part 1.2. The analysis options included plasticity and large deformations.

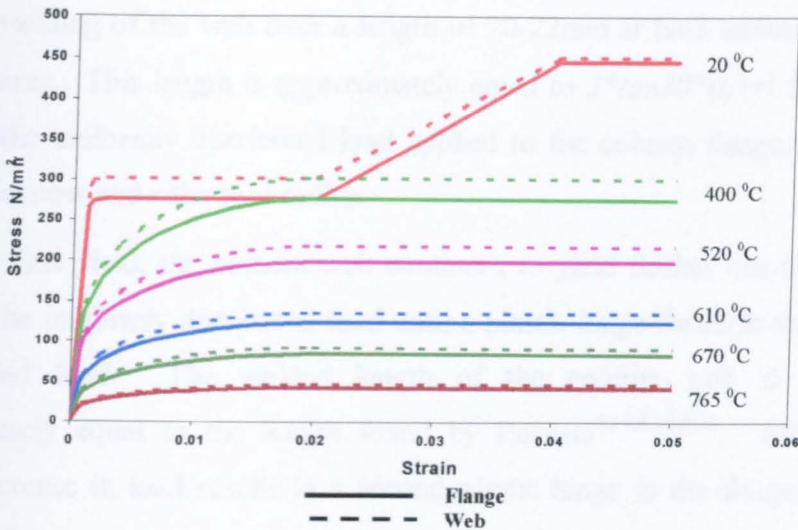


Figure 5.13 The stress-strain curves for the column flange and web

5.4.2 Finite element results

The results from finite element analysis showed yielding first occurred in the column web. Figure 5.4 shows the von-Mises stress distributions for different loading cases.

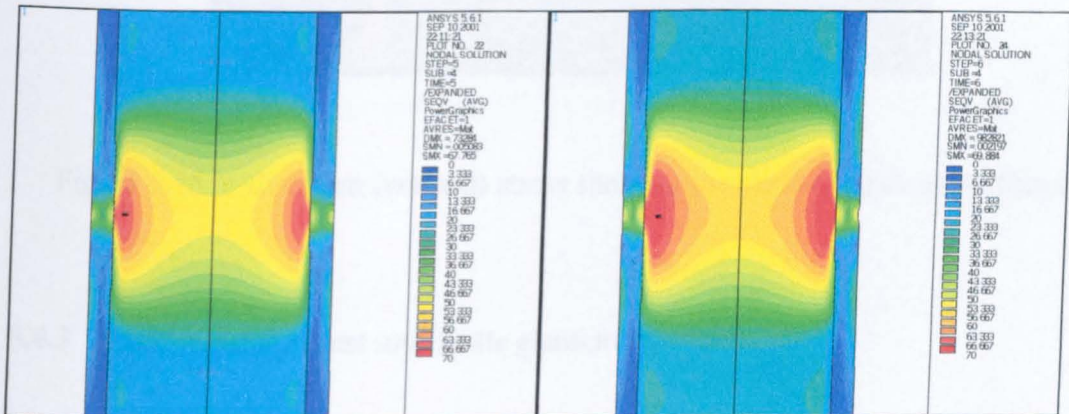


Figure 5.14 Von-Mises stress distributions for 112,5 kN and 125 kN at 610°C

By looking at the stress distribution figures and comparing the stress results from the ANSYS output file at certain elements and nodes it was clear that there was a

uniform yielding of the web over a length of 20-22mm at both ambient and elevated temperatures. This length is approximately equal to $2 \cdot \tan 30^\circ \cdot (t_f + r)$ from the centre point of the uniformly distributed load applied to the column flange, where t_f is the flange thickness and r the root radius.

After the first yield, the column web continues to yield further out from the centre point of the uniformly distributed load until a plastic hinge forms in the flange under the applied load. The yielded length of the column web at this stage is approximately equal to the length found by Roberts^{5,14,5.15,5.16}. After this point, further increase in load results in a second plastic hinge in the flange, as shown in Figure 5.15.

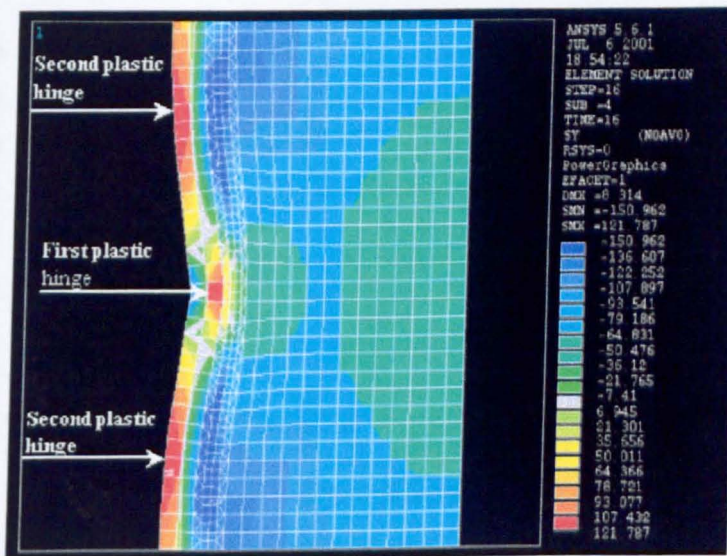


Figure 5.15 Y-direction (vertical) stress showing the plastic hinges in the flange

5.4.3 Comparison of test and finite element results

Typical test and finite element results are presented in Figures 5.16-5.21 for 6 tests on the UC203x203x46 column section at elevated temperatures.

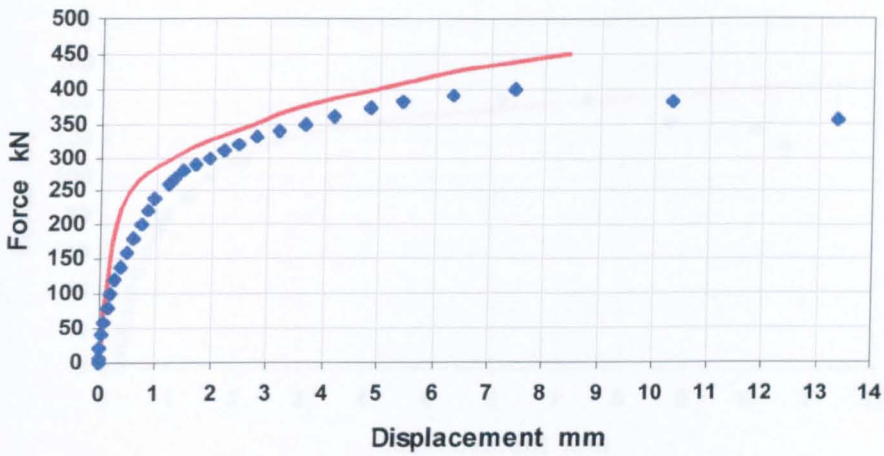


Figure 5.16 ANSYS and test results at ambient temperature

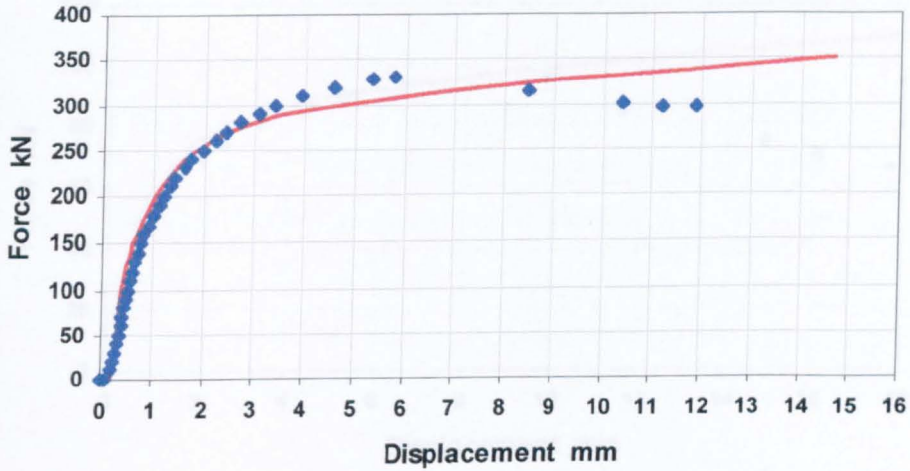


Figure 5.17 ANSYS and test results at 400 °C

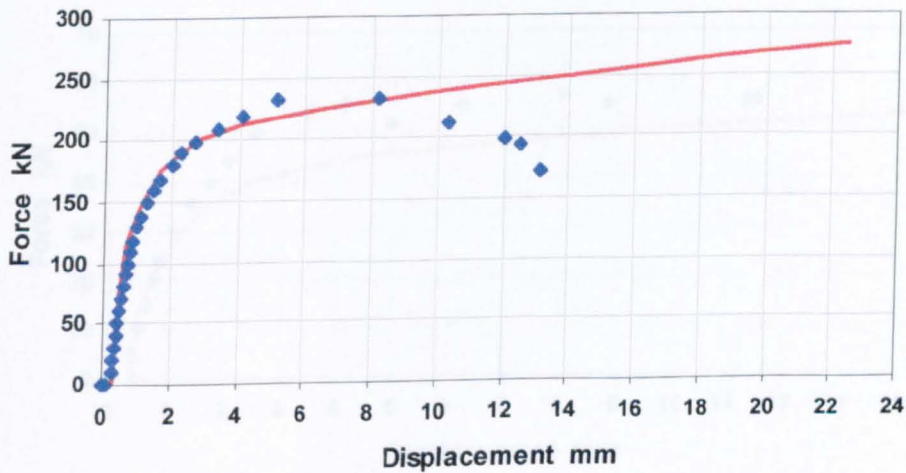


Figure 5.18 ANSYS and test results at 520 °C

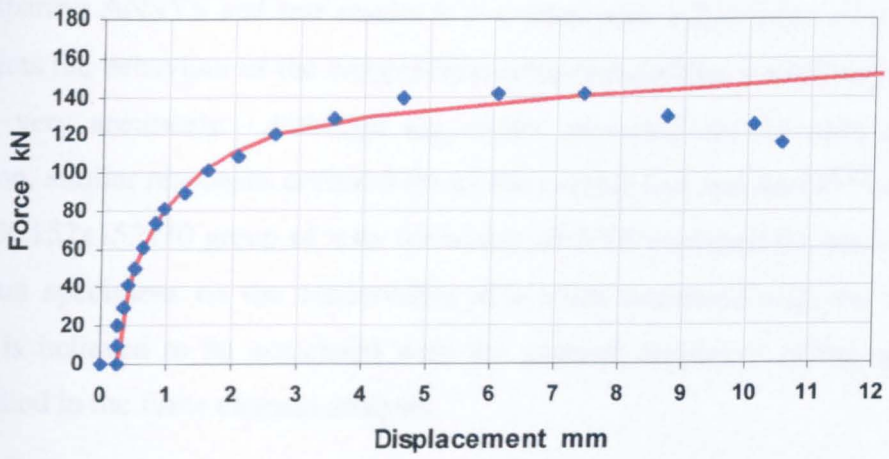


Figure 5.19 ANSYS and test results at 610 °C

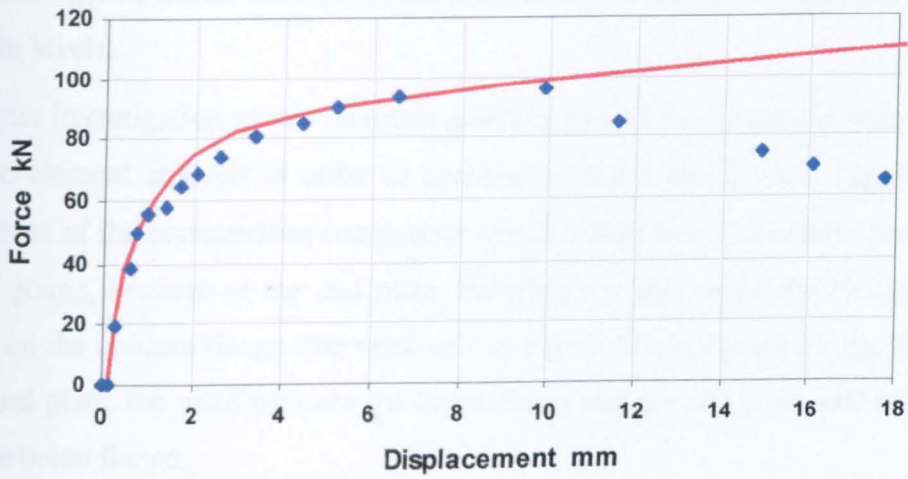


Figure 5.20 ANSYS and test results at 670 °C

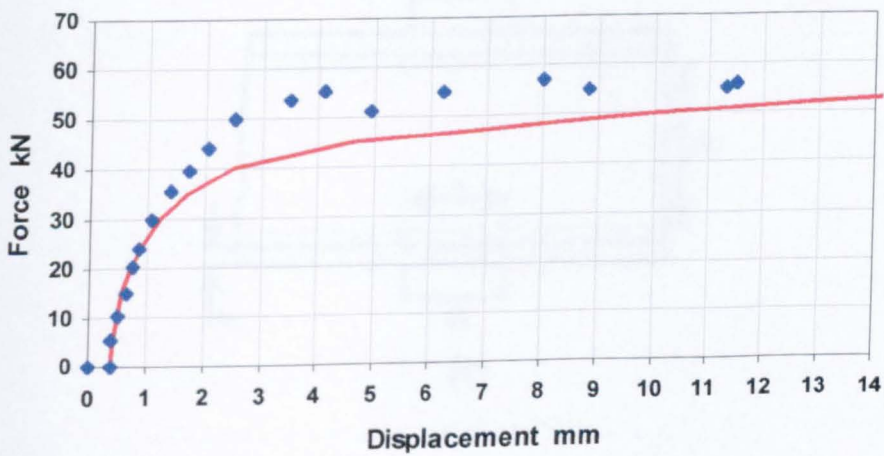


Figure 5.21 ANSYS and test results at 765 °C

Comparing ANSYS and test results it is evident that a 2-D finite element analysis predicts the behaviour of the compression component within a steel beam-to-column joint very accurately. Although the results presented are for only one column section, similar responses occurred for all the column sections tested^{5,13}, except from the UC152x152x30 group of tests for which ANSYS predicted the behaviour of the column specimens on the conservative side when compared with the test results. This is believed to be associated with the material properties of the specimen as modelled in the finite element analysis.

The 2D finite element analysis obviously cannot account for out-of-plane buckling, yet good correspondence with the test results was obtained. This suggests that the major effect is concerned with membrane yielding, and the out-of-plane displacements, which occurred in the tests, were a secondary structural effect at large strain levels.

Further investigation of this complex problem should be carried out with the help of finite element analysis in order to accurately predict the ultimate capacity and the stiffness of the compression component within a steel beam-to-column joint. Within steel joints, because of the end plate, the length of the uniformly distributed patch load on the column flange (the value of c in Figure 5.22) depends on the thickness of the end plate, the weld between the beam flange and the end plate, and the thickness of the beam flange.

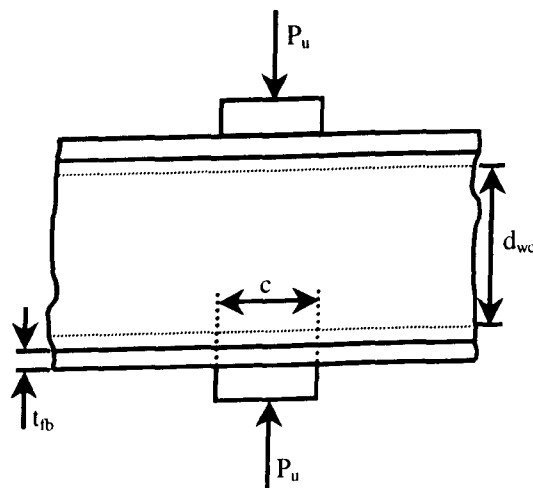


Figure 5.22 Column web subjected to patch loads

A further finite element analysis has already been carried out^{5.13} in order to investigate the effect of changing the value of c in Figure 5.22 on the stiffness and strength of the column section.

The results from this investigation are shown in Figure 5.23.

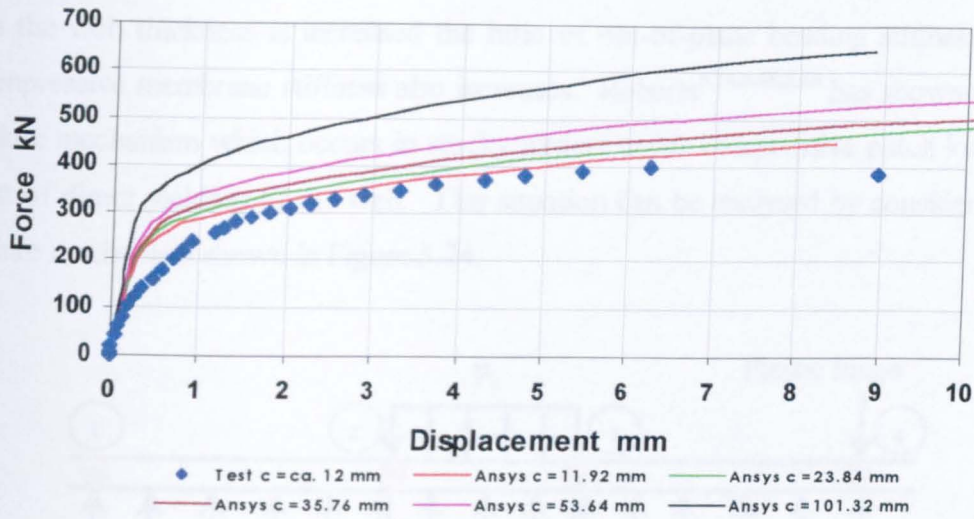


Figure 5.23 Different values of uniform distributed load length c at ambient temperature

From the graph above it is obvious that, by changing the length c of the uniformly distributed load, the stiffness and strength of the column section under investigation are affected. This requires further investigation, but it is important to bear in mind that the contact length c is likely to be small for steel joints (up to 50mm).

5.5 SIMPLIFIED MODEL

The information collected from the 2D finite element analysis and test results was used to produce a simplified model for predicting the behaviour of the column web under compressive forces. Another important source of information was previous research on plate girders subjected to patch loading. The development of an

analytical model to predict column web capacity at elevated temperatures is described in detail below.

5.5.1 Analytical model at elevated temperatures

As the web thickness is increased the ratio of out-of-plane bending stiffness to the compressive membrane stiffness also increases. Roberts^{5.14,5.15,5.16} has shown that the failure mechanism which occurs in stocky girders under compressive patch loading is that of direct yielding of the web. This situation can be analysed by considering the failure mechanism shown in Figure 5.24.

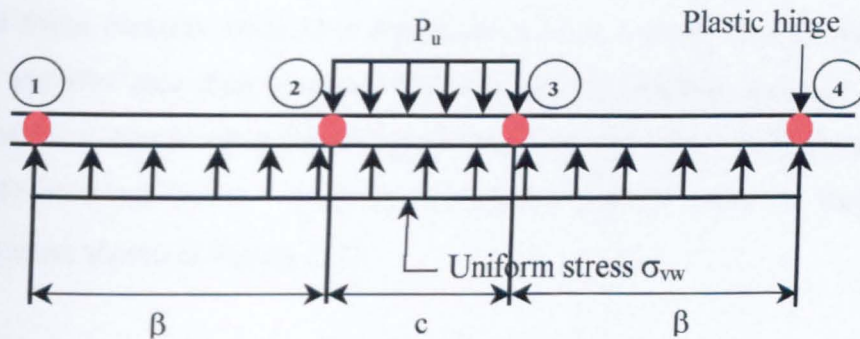


Figure 5.24 Assumed mechanism of web yielding

It is assumed that plastic hinges form in the flange and that the length of web between the outer plastic hinges (hinges 1 and 4) yields in compression. Equating external and internal work as the load moves vertically through a small distance δ_w gives

$$P_u = \left(\frac{4M_{pfc}}{\beta} \right) + \sigma_{yw} t_{wc} (\beta + c) \quad \dots 5.7$$

Energy dissipation around the boundary of the assumed plastic region is neglected. Minimizing P_u with respect to β gives

$$\beta^2 = \frac{4M_{pfc}}{\sigma_{yw}t_{wc}} \quad \dots 5.8$$

where M_{pfc} is the plastic moment of the column flange which is given by $M_{pfc} = (\sigma_{yf} b_{fc} t_{fc}^2) / 4$ and σ_{yf} , σ_{yw} are the column flange and web yield stresses respectively, b_{fc} is the column flange width and t_{fc} and t_{wc} are respectively the column flange and web thicknesses.

The total length of a beam, $L_t = (2\beta + c)$, which is going to be analysed in order to calculate the stiffness of the compression zone, is given by the equations above.

From finite element analysis it was observed that a small area of the web yielded first, and that area then increased until the second yielding occurred in the middle part of the flange (hinges 2 and 3) under the load, and then a third yielding (hinges 1 and 4) occurred further out from the applied load in order to form the failure mechanism shown in Figure 5.24.

a) Yielding (squashing) of the column web

Figure 5.25 shows schematically what happens at the early stages of application of the compressive force, according to the finite element analysis.

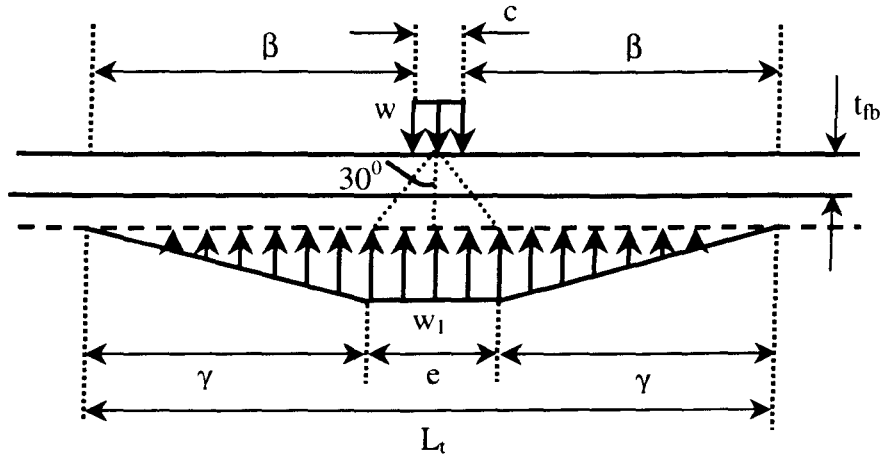


Figure 5.25 First yielding of the column web

An area of web with length e reaches its yield point. The length is approximately equal to $e = 2 \tan 30^\circ (t_{fb} + r)$, where r is the root radius and t_{fb} the flange thickness of the column section.

The initial force $P_I = wc$ required to yield the web is taken to be equal to the reaction created on the web, as shown in Figure 5.25. Hence,

$$P_I = wc = w_1 e + 2 \frac{w_1 \gamma}{2} = w_1 (e + \gamma) = \sigma_{yw} t_{wc} (e + \gamma) \quad \dots 5.9$$

Where w and w_1 are defined in Figure 5.25.

The deflection under this load can be calculated by considering an effective area (taken as $L_{eff} t_{wc}$) of the column web under compression.

$$\delta_1 = \frac{P_I d_{wc}}{E_{wc} A_{wc}} = \frac{\sigma_{yw} t_{wc} (e + \gamma) d_{wc}}{E_{wc} L_{eff} t_{wc}} \quad \dots 5.10$$

where d_{wc} is the depth between the fillets of the column section, E_{wc} is the web Young's Modulus and L_{eff} is as shown in Figure 5.26.

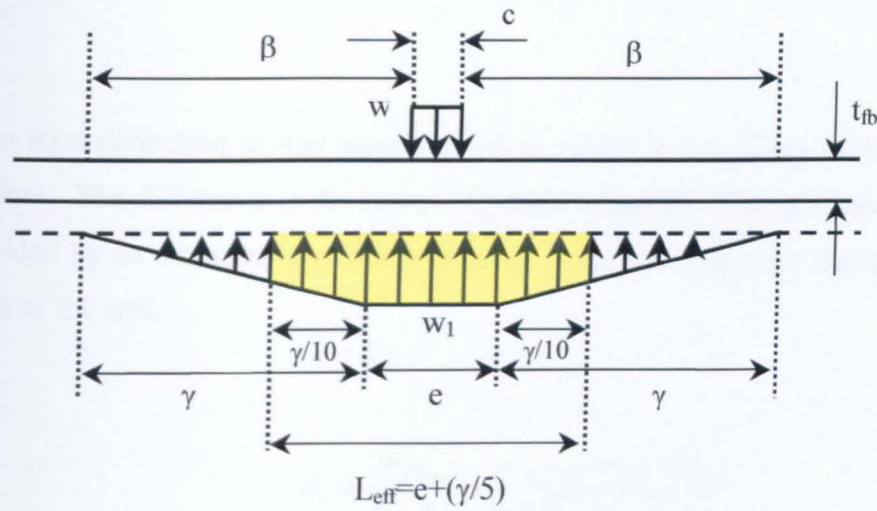


Figure 5.26 Effective length of the compressed web

b) Yielding of the column flange (creating hinges 2 and 3)

After the first yield of the column web, continuing to increase the compression force, the area of the web that is now yielded is approximately equal to $e' = 2 \tan 65^\circ (t_{fb} + r)$. At this stage yield of the column flange has occurred in the middle under the compressive load. The situation now looks like that shown in Figure 5.27.

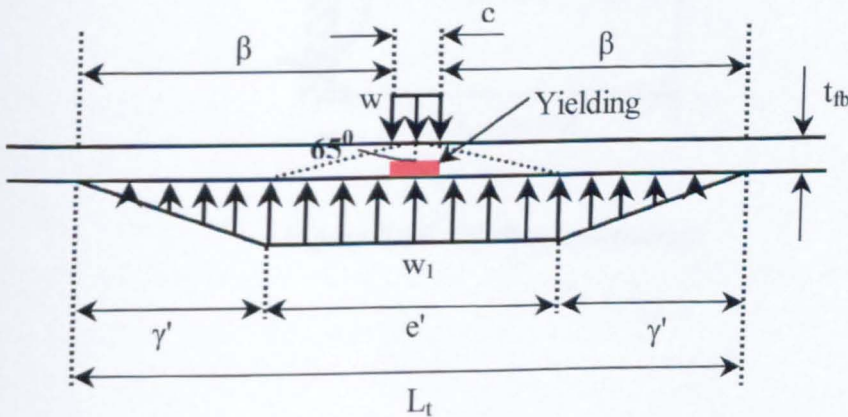


Figure 5.27 Second yielding of the system

$$P_2 = w_1 e' + 2 \frac{w_1 \gamma'}{2} = w_1 (e' + \gamma') = \sigma_{yw} t_{wc} (e' + \gamma') \quad \dots 5.11$$

The total deflection as this second yielding occurs is calculated in the same way as before. The difference in the current formula is that the Young's Modulus has been divided by an empirically derived value, in order to account for the initially yielded area of the web.

$$\delta_2 = \frac{P_1 d_{wc}}{E_{wc} A_{wc}} = \frac{\sigma_{yw} t_{wc} (e + \gamma') d_{wc}}{\left(\frac{E_{wc}}{4}\right) L_{eff}' t_{wc}} \quad \dots 5.12$$

where $L_{eff}' = e' + (\gamma'/5)$

c) Yielding of the column flange (creating hinges 1 and 4)

After causing hinges to form in the flange beneath the patch load, any further increase in the load creates plastic hinges further along the column flange.

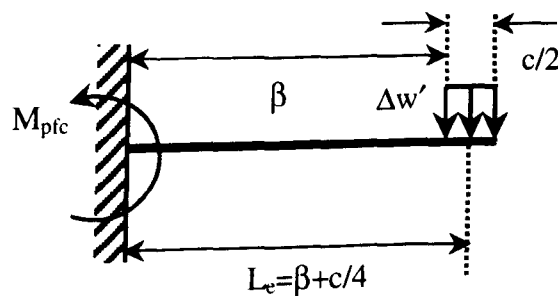


Figure 5.28 Yielding mechanism

By using mechanics and an effective length approximation (Figure 5.28 above) a semi-empirical formula is derived which calculates the force needed in order to create the two final plastic hinges in the flange:

$$P_3 = \frac{2M_{pfc}}{[\beta + (c/4)]} + P_2 \quad \dots 5.13$$

where $M_{pfc} = (\sigma_{yf} b_{fc} t_{fc}^2)/4$ and σ_{yf} is the column flange yield stress, b_{fc} is the column flange width and t_{fc} is the column flange thickness.

The total deflection at this load is given by calculating the incremental deflection derived by assuming the system in Figure 5.28 is a cantilever with a uniformly distributed patch load at its end, plus the deflection derived from the earlier yielding of the column flange δ_2 .

$$\delta_3 = \frac{((P_3 - P_2)/2) [8\beta^3 + 18\beta^2(c/4) + 12\beta(c/4)^2 + 3(c/4)^3]}{24E_{fc}I_{fc}} + \delta_2 \quad \dots 5.14$$

Where $I_{fc} = (b_{fc}t_{fc}^3)/12$ and E_{fc} is the column flange Young's Modulus.

Normally the yielding force P_3 should give the ultimate capacity of the column web under transverse compressive forces. From tests it was observed that the ultimate force was higher than this. The final formula, which gives the ultimate force, is derived from theories on plate girders subjected to patch loading.

The stability problems and ultimate load behaviour of steel plate girders have attracted a lot of attention from research workers^{5.16,5.17,5.18,5.19,5.20}. The behaviour of steel plate girders under patch loading presents complex stability and elasto-plastic problems. Many experimental results and extensive theoretical work have established some empirical and semi empirical formulae for calculating the ultimate capacity of a plate girder subjected to patch loading.

The work of Markovic *et al*^{5.21} gives an assessment of the applicability of existing formulae from different authors for predicting the ultimate load on plate girders subjected to patch loading and the influence of longitudinal stiffeners.

A total of 11 formulae were investigated using a large number of tests (318 girders without longitudinal stiffeners and 133 girders with longitudinal stiffeners), and values of the ratios of predicted to experimental capacity were determined to enable an assessment of the accuracy of these formulae.

All the formulae are for slender plate girders (having values of d_c/t_{wc} around 75) except for one, which is for rather thick plate girder webs^{5.22}. The column specimens tested have d_c/t_{wc} values ranging from 6.10 to a maximum value of 27.9.

The formula^{5.22} by Drdacky is:

$$P_u = 0.55t_{wc}^2 \sqrt{E_{wc} \sigma_{wc}} \sqrt{\frac{t_{fb}}{t_{wc}}} \left[0.9 + \left(\frac{1.5c}{d_{wc}} \right) \right] \quad \dots 5.15$$

Where E_{wc} and σ_{wc} are the Young's Modulus and yield strength respectively of the column web, and t_{wc} is the thickness of the web. All the other parameters are shown in Figure 5.22.

Furthermore equation 5.15 has been compared with a large number (451) of tests and as a result the authors, Markovic *et al* suggested that the mean value for the ratio of predicted to experimental capacity should be equal to 0.72. This means that, instead of using a factor of 0.55 at the beginning of the equation 5.15, a new value of 0.76 could be used.

The above formula gave good correlation with the tests results from the current study, but when compared with finite element results performed in order to investigate the significance of the c value (uniformly distributed patch length) on the behaviour of the column web (Figures 5.22 and 5.23) it was found that equation 5.15 gave un-conservative values for the ultimate capacity of the column web.

For this reason a new empirical formula has been derived, based on the Drdacky formula:

$$P_u = t_{wc}^2 \sqrt{E_{wc} \sigma_{wc}} \sqrt{\frac{t_{fb}}{t_{wc}}} \left\{ 0.65 + \left[\left(\frac{1.6c}{d_{wc}} \right) \left(\frac{2\beta}{2\beta + c} \right) \right] \right\} \quad \dots 5.16$$

and the comparison with experimental results is shown in the next section. Finally the total deflection of the system is given by:

$$\delta_4 = 4.5\delta_3 \quad \dots 5.17$$

The calculation of the final deflection δ_4 is very complicated because of the out-of-plane deflection of the web. Nevertheless, as is shown in the next section equation 5.17 it is not a bad approximation.

Summarising, in this section a new simplified semi-empirical model has been produced to simulate the behaviour of a column web within a steel joint up to the ultimate capacity of the column section under compression. Also a new formula has been derived which estimates the ultimate capacity of the column web taking into account the variation in the length c of the uniformly distributed patch load. The model can be used at ambient temperature, and at elevated temperatures by reducing the strength and Young's Modulus of the steel according to EC3: Part 1.2^{5.23}.

The following section reports the test results and comments on the comparisons with the simplified model.

5.6 RESULTS AND COMMENTS

The reason for developing a new simplified model to predict the behaviour of the compression component at elevated temperatures was because the current codes (BS5950 and EC3:Annex J) underestimate the capacity of the component even at ambient temperature. More attention is given to EC3: Annex J because it uses the principles of the component method in order to predict the response of a beam-to-column steel joint. If this code underestimates the capacity of a column section by a factor of 2.0 as shown in Table 5.3 and Figure 5.29, then inefficient design is inevitable.

Table 5.3 shows the crushing and buckling resistances at ambient temperature calculated from Eurocode 3:Annex J. The lower of these resistances is the design ultimate load. These values were calculated without using the material safety factor γ_{M0} . If this factor is taken into account it will reduce the values further.

Table 5.3 Comparison of tests and EC3: Annex J results at ambient temperature

No.	Column Sections	Tests	Eurocode 3-Annex J			Ratio F_{exp}/F_{rd}
		Ultimate Load	Crushing Resistane	Buckling Resistance	Design Resistance Min.(crushing: buckling)	
		kN	kN	kN	kN	
1	UC152x152x30	320	180.92	197.40	180.92	1.76
2	UC203x203x46	405	251.39	259.17	251.39	1.61
3	UC203x203x60	736	394.45	436.80	394.45	1.86
4	UC203x203x71	844	433.65	483.02	433.65	1.94
5	UC203x203x86	1278	639.53	726.95	639.53	1.99
6	UC203x203x86	1286	635.53	722.15	635.53	2.02
7	UC203x203x86	1125	577.80	656.19	577.80	1.94
8	UC254x254x107	1158	656.17	722.10	656.17	1.76

When reduction factors for strength and stiffness are used in the Eurocode 3:Annex J ambient temperature formula, the results found are also very conservative compared with the elevated temperature tests, as seen in Figure 5.29.

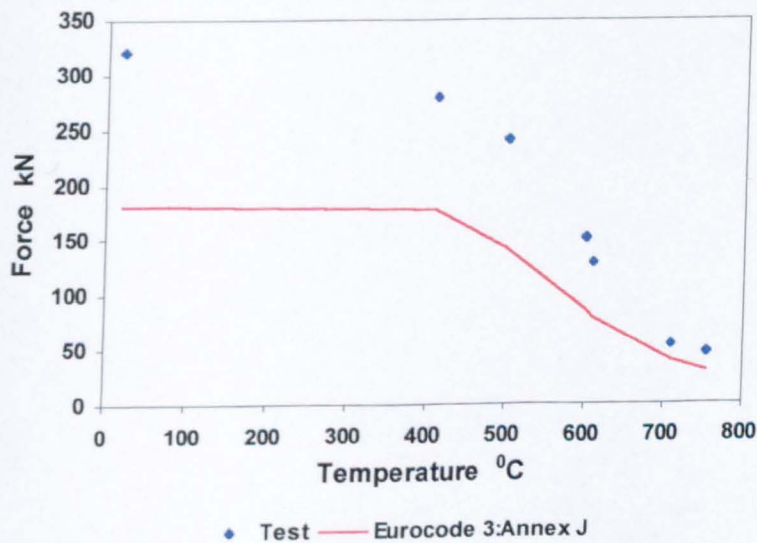


Figure 5.29 Typical test and Eurocode 3:Annex J results for UC152x152x30

Furthermore, for some tests at elevated temperatures the results from the above calculation procedure predicted that the column web will fail by buckling, which did not occur. Because of the stockiness of the column web, its bearing capacity (crushing) rather than buckling governs the design.

Another important comparison is between equation 5.15 giving the ultimate capacity of a plate girder under patch loading and the new empirical equation 5.16 derived by the author to predict the ultimate capacity of the compression component within a steel joint. Figures 5.30-5.33 show this comparison, giving the conclusion that the new empirical formula can predict the ultimate capacity with acceptable accuracy for the purposes of the current study.

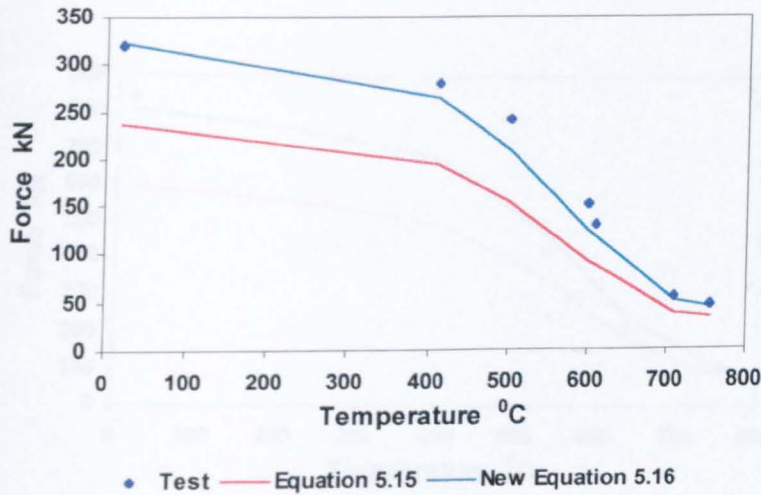


Figure 5.30 Test, Equation 5.15 and new Equation 5.16 results for UC152x152x30

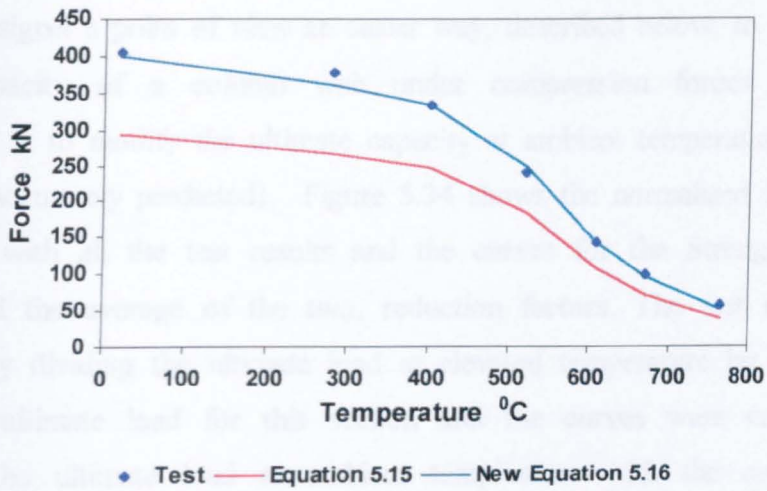


Figure 5.31 Test, Equation 5.15 and new Equation 5.16 results for UC203x203x46

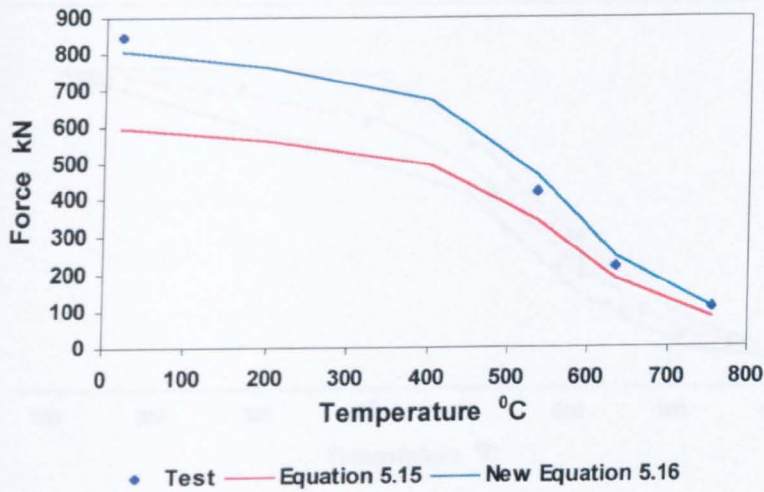


Figure 5.32 Test, Equation 5.15 and new Equation 5.16 results for UC203x203x71

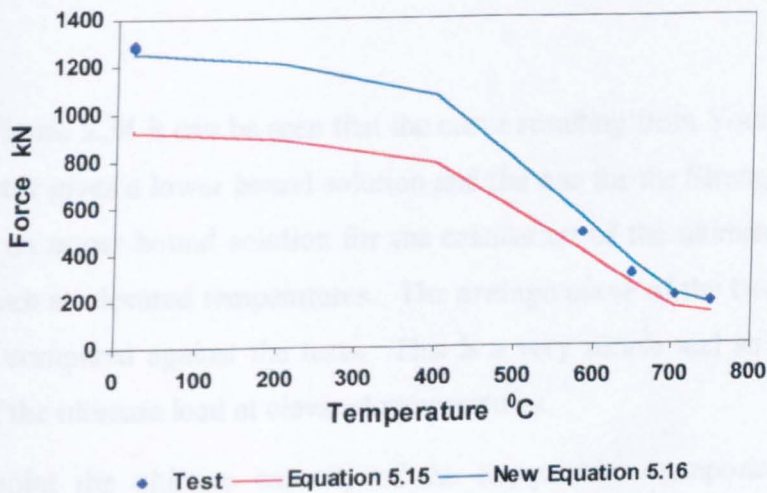


Figure 5.33 Test, Equation 5.15 and new Equation 5.16 results for UC203x203x86

From the designer's point of view an easier way, described below, to calculate the ultimate capacity of a column web under compression forces at elevated temperatures is to modify the ultimate capacity at ambient temperature (assuming this can be accurately predicted). Figure 5.34 shows the normalised force against temperature with all the test results and the curves for the Strength, Young's Modulus and the average of the two, reduction factors. The test results were normalised by dividing the ultimate load at elevated temperature by the ambient temperature ultimate load for this section and the curves were calculated by multiplying the ultimate load at ambient temperature with the corresponding reduction factor at elevated temperatures. The reduction factors were taken from Eurocode 3 Part 1.2^{5.23}.

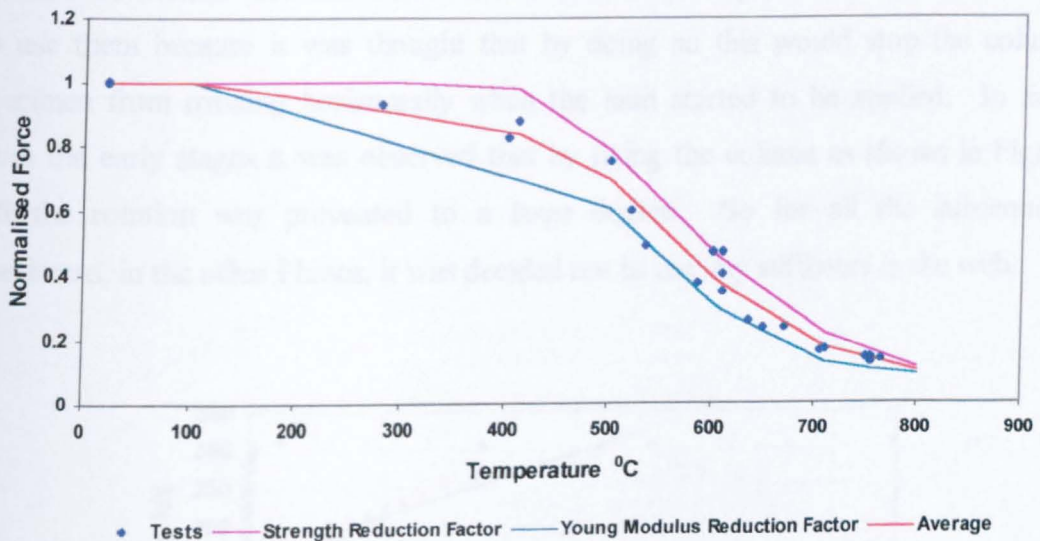


Figure 5.34 Normalised force against temperature

Looking at Figure 5.34 it can be seen that the curve resulting from Young's Modulus reduction factor gives a lower bound solution and the one for the Strength Reduction Factor gives an upper bound solution for the calculation of the ultimate capacity of the column web at elevated temperatures. The average curve of the two gives good results when compared against the tests. This is a very simple and straightforward calculation of the ultimate load at elevated temperatures.

Up to this point the ultimate capacity of the compression component has been compared against the empirical formula at elevated temperatures. The next step is to

compare the full response (strength and stiffness) of the compression component, derived from the simplified model, against the test results at elevated temperatures.

5.6.1 Phase A Test Results

Phase A included eight tests at elevated temperatures on a UC152x152x30 column section. Each graph shows the out-of-plane displacements of the web, the column flange displacements and the displacements calculated from the simplified model. These tests were the first to be made at elevated temperatures so some of them included stiffeners in the column web. These stiffeners were placed at a minimum distance of 170mm each side from the centerline of the applied load. It was decided to use them because it was thought that by doing so this would stop the column specimen from rotating horizontally when the load started to be applied. In fact, from the early stages it was observed that by fixing the column as shown in Figure 5.8 the rotation was prevented to a large degree. So for all the subsequent specimens, in the other Phases, it was decided not to use any stiffeners in the web.

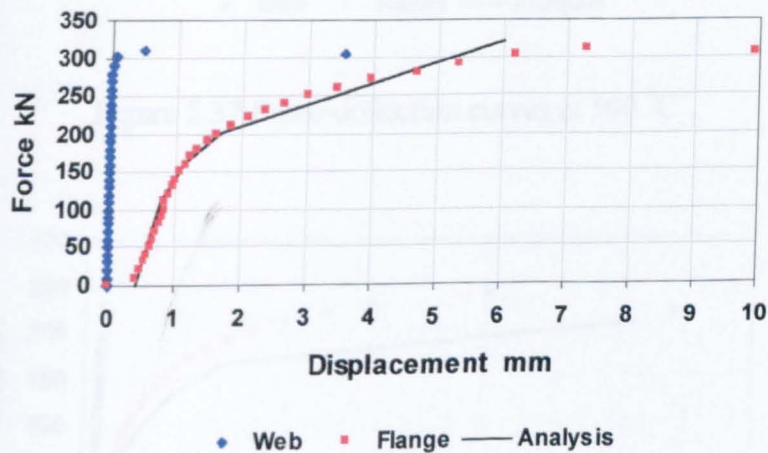


Figure 5.35 Force-deflection curves at 20 °C

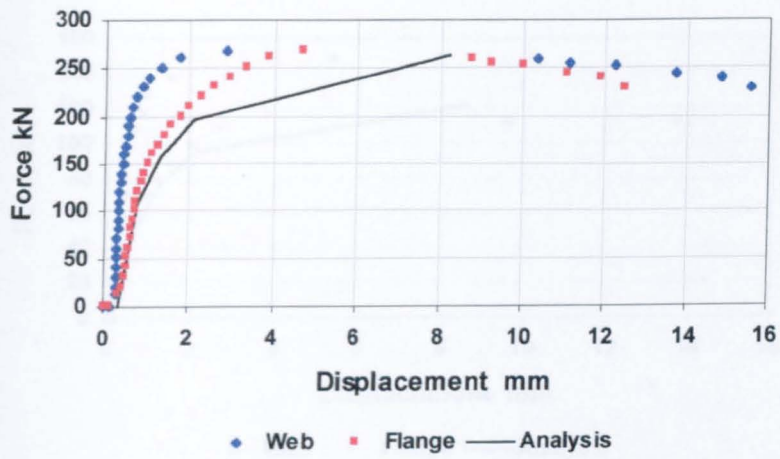


Figure 5.36 Force-deflection curves at 410 °C

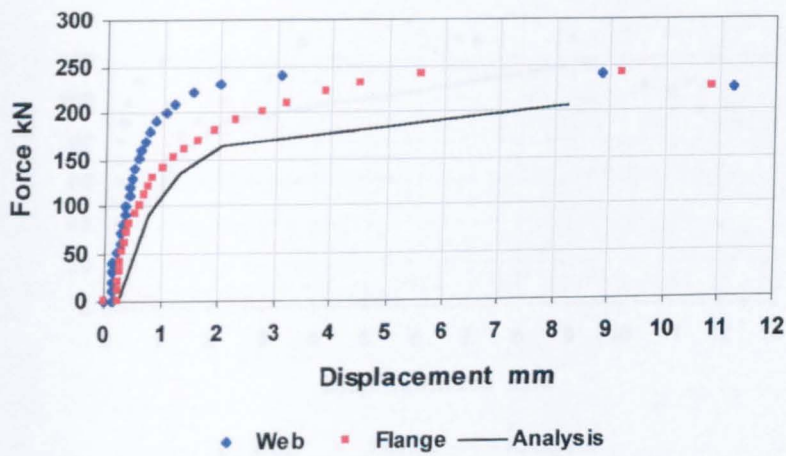


Figure 5.37 Force-deflection curves at 500 °C

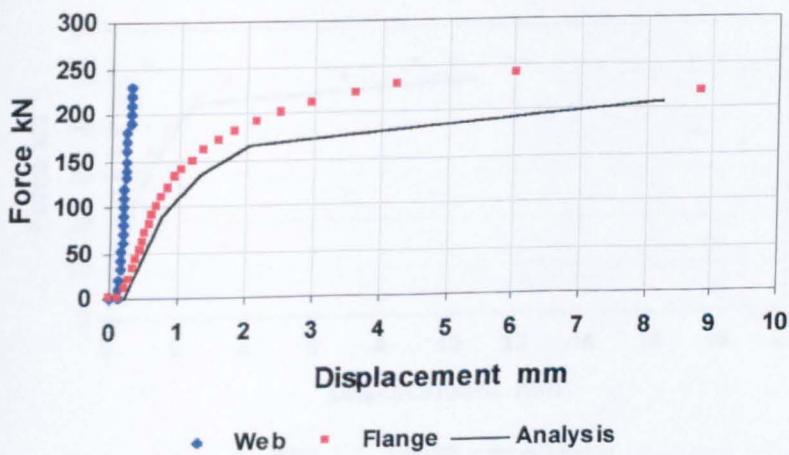


Figure 5.38 Force-deflection curves at 500 °C

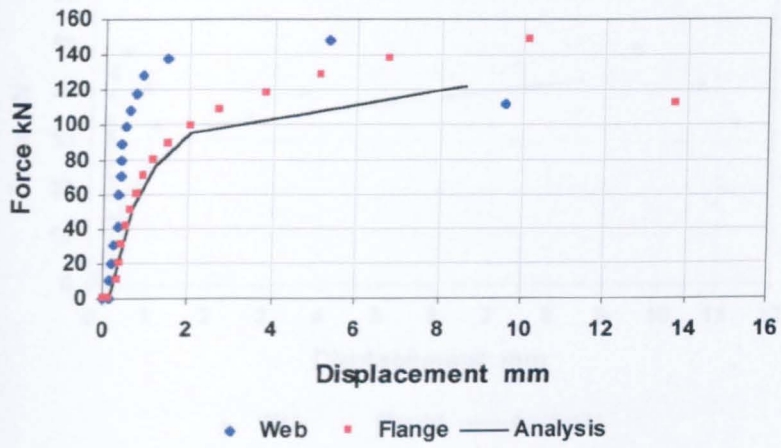


Figure 5.39 Force-deflection curves at 600 °C

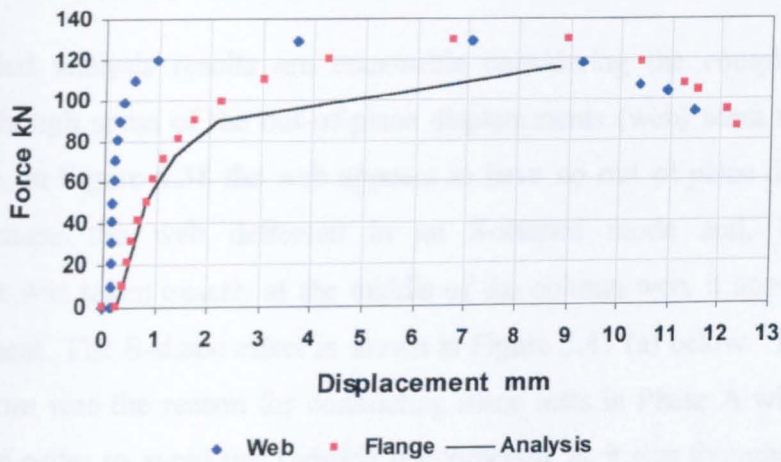


Figure 5.40 Force-deflection curves at 610 °C

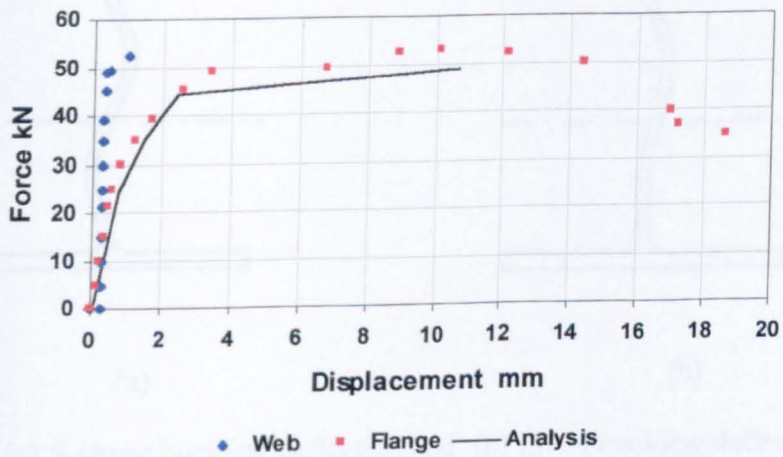


Figure 5.41 Force-deflection curves at 710 °C

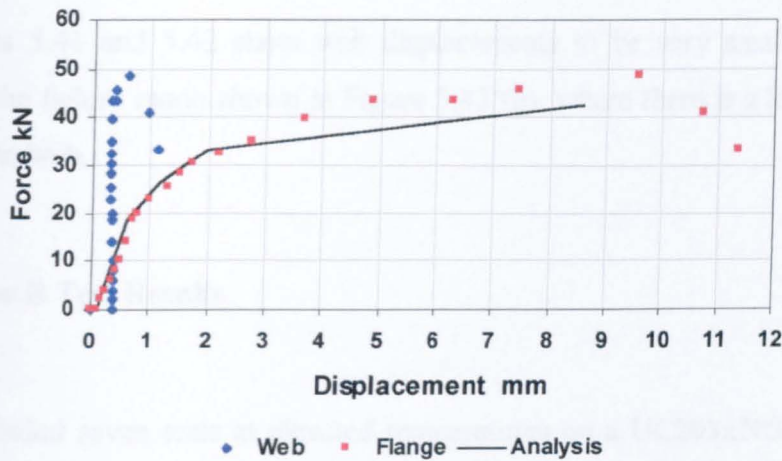


Figure 5.42 Force-deflection curves at 755 °C

The simplified analysis results are reasonable considering the complexity of the problem, although some of the out-of-plane displacements (web) seem very strange. For example, in Figure 5.38 the web appears to have no out of plane displacement. This is because the web deflected in an S-shaped mode and, because the measurement was taken exactly at the middle of the column web, it appears to have no displacement. The S-shape effect is shown in Figure 5.43 (a) below. This S-shape mode of failure was the reason for conducting some tests in Phase A with stiffeners on the web in order to avoid this twisting phenomenon, as it was thought at the time that the behaviour occurred was because the web was not properly restrained.

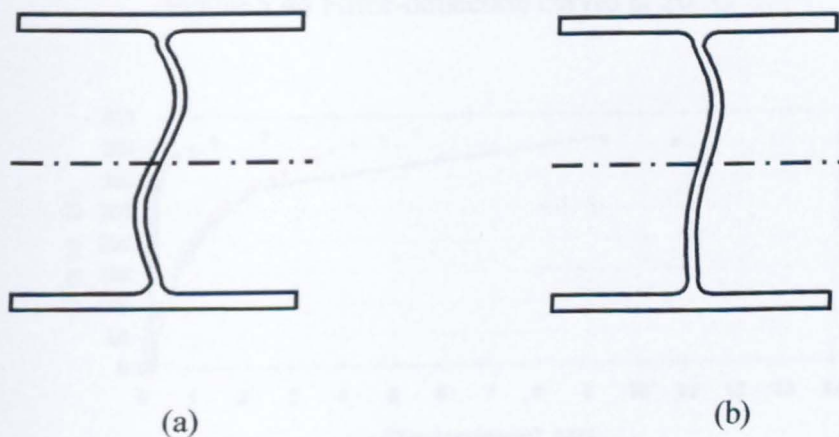


Figure 5.43 (a) S-shape buckling deflection and (b) Local buckling deflection of the column web

Also Figures 5.41 and 5.42 show web displacements to be very small, and this is because of the failure mode shown in Figure 5.43 (b), where there is a local buckling of the column web.

5.6.2 Phase B Test Results

Phase B included seven tests at elevated temperatures on a UC203x203x46 column section, the results of which are illustrated in Figures 5.44-5.50.

(Note: the vertical axes in these figures are shown at different scales for clarity. There was a very significant reduction in capacity as temperatures were increased)

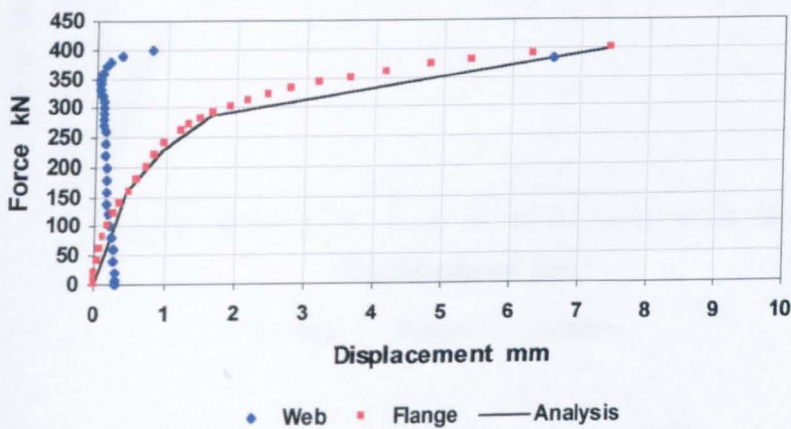


Figure 5.44 Force-deflection curves at 20 °C

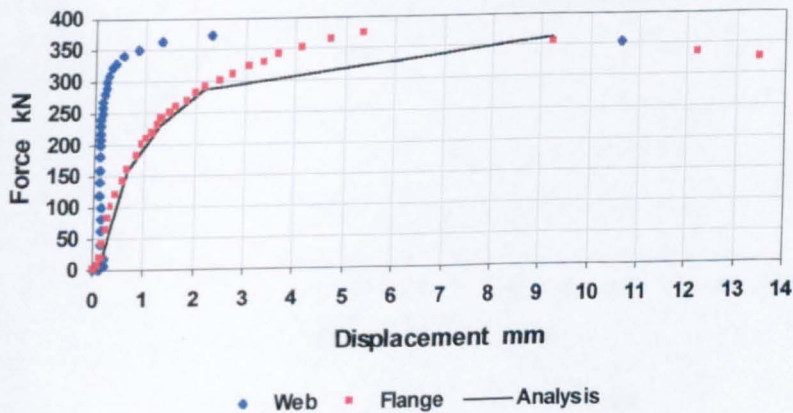


Figure 5.45 Force-deflection curves at 280 °C

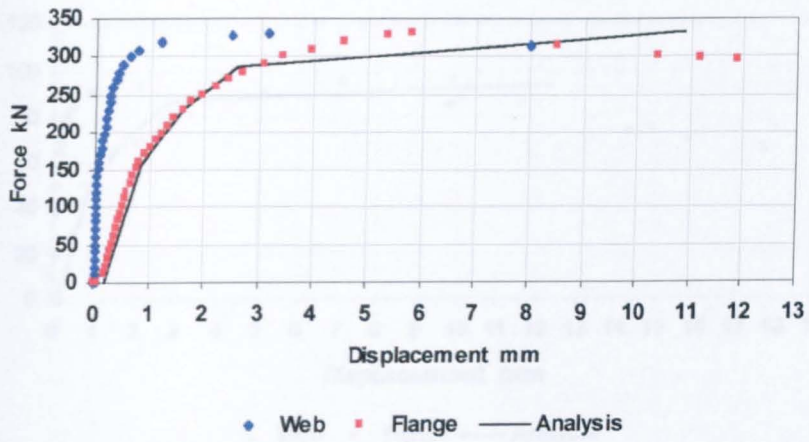


Figure 5.46 Force-deflection curves at 400 °C

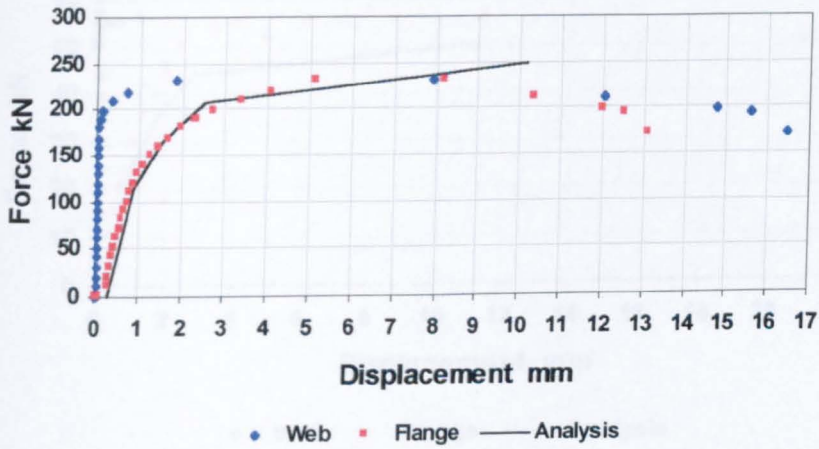


Figure 5.47 Force-deflection curves at 520 °C

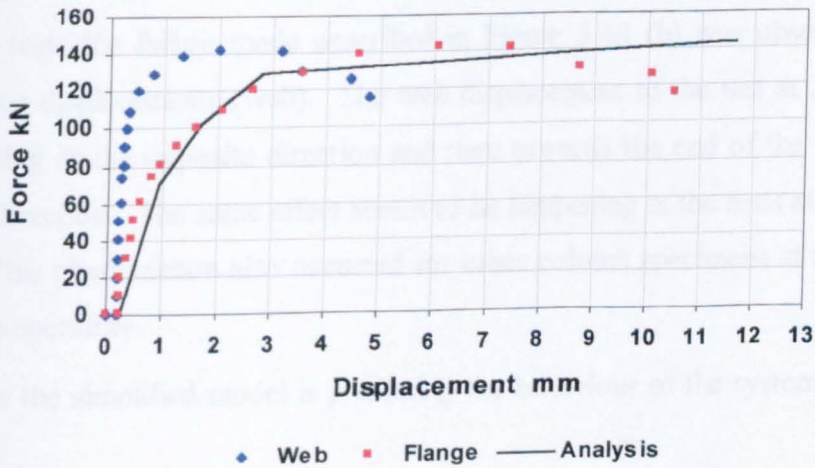


Figure 5.48 Force-deflection curves at 610 °C

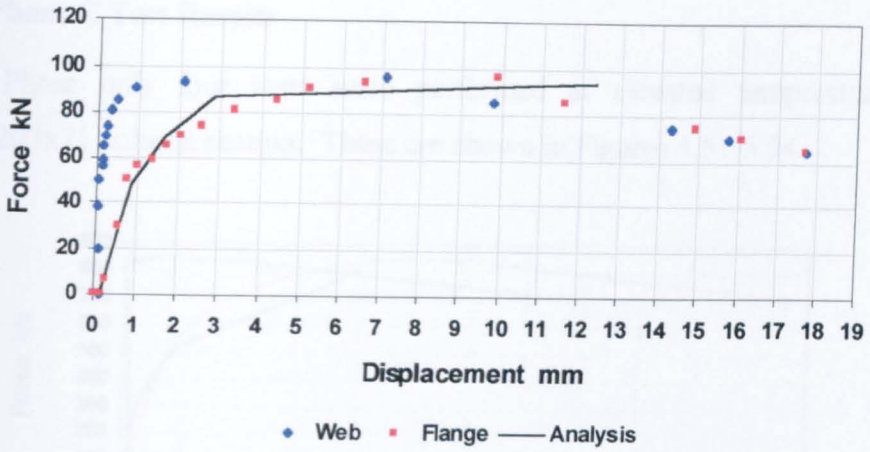


Figure 5.49 Force-deflection curves at 670 °C

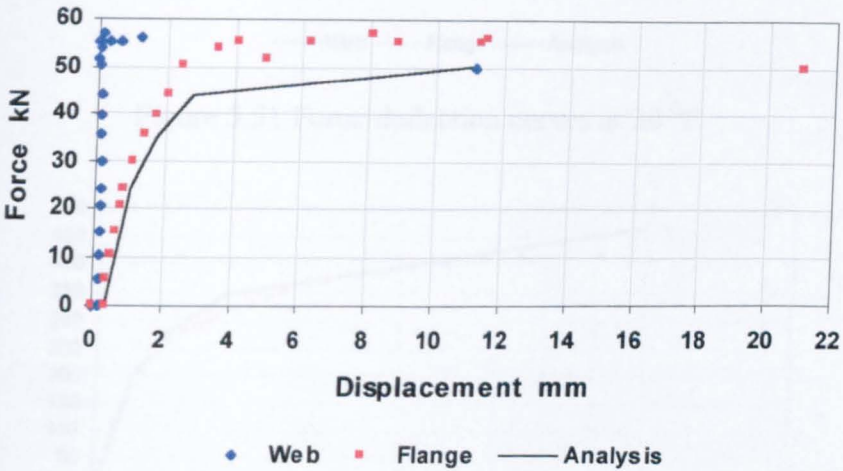


Figure 5.50 Force-deflection curves at 765 °C

For some tests the failure mode described in Figure 5.43 (b) was observed for the out-of-plane displacements (web). The web displacement of the test at 20 °C seems to be starting in the opposite direction and then towards the end of the test turns in the other direction. The same effect seems to be happening in the tests at 280 °C and 765 °C. This phenomenon also occurred for other column specimens at ambient and elevated temperature.

Once again the simplified model is predicting the behaviour of the system reasonably accurately.

5.6.3 Phase C Test Results

In this Phase only four tests were performed at elevated temperatures on a UC203x203x71 column section. These are shown in Figures 5.51-5.54.

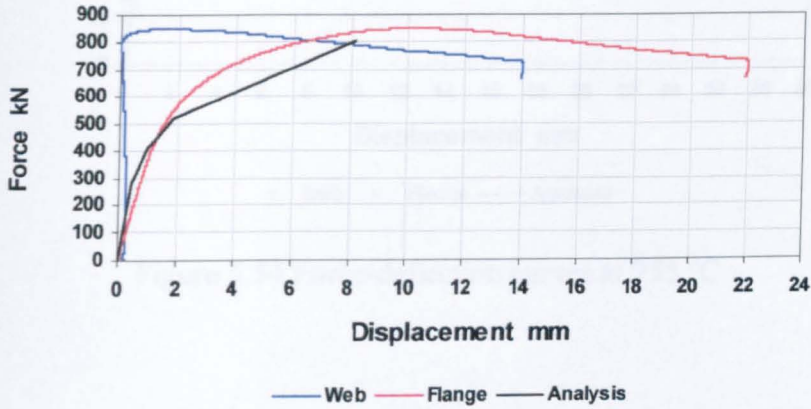


Figure 5.51 Force-deflection curves at 20 °C

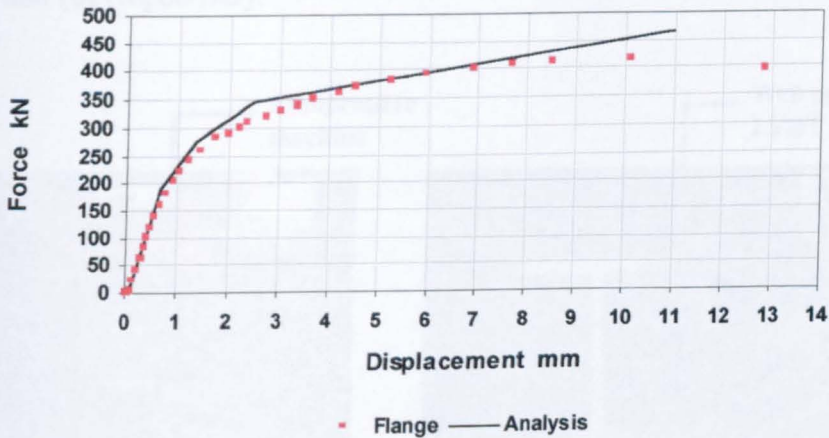


Figure 5.52 Force-deflection curves at 535 °C

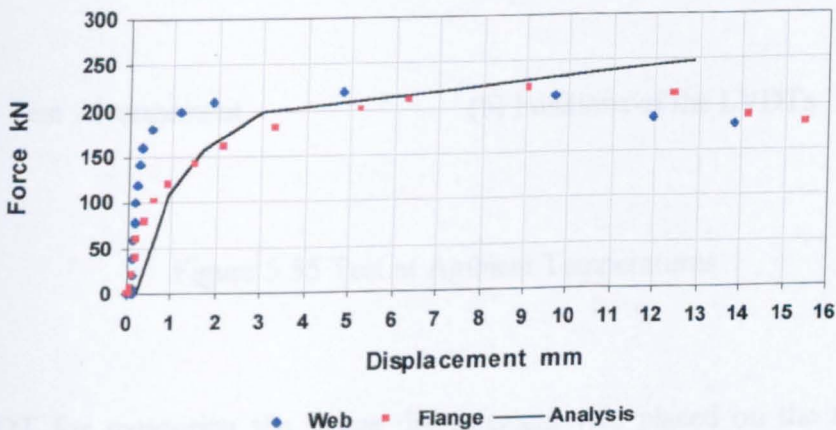


Figure 5.53 Force-deflection curves at 635 °C

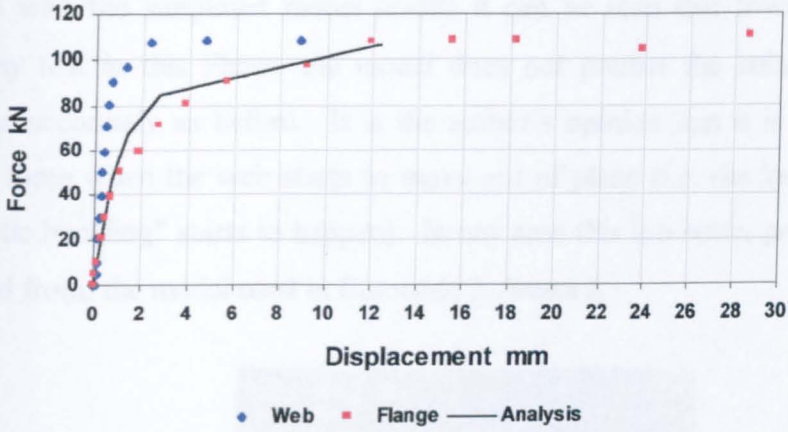


Figure 5.54 Force-deflection curves at 755 °C

The tests at ambient temperature were performed in a universal compression-testing machine and the displacements were measured using LVDT's as shown in Figures 5.55 (a) and (b) respectively.

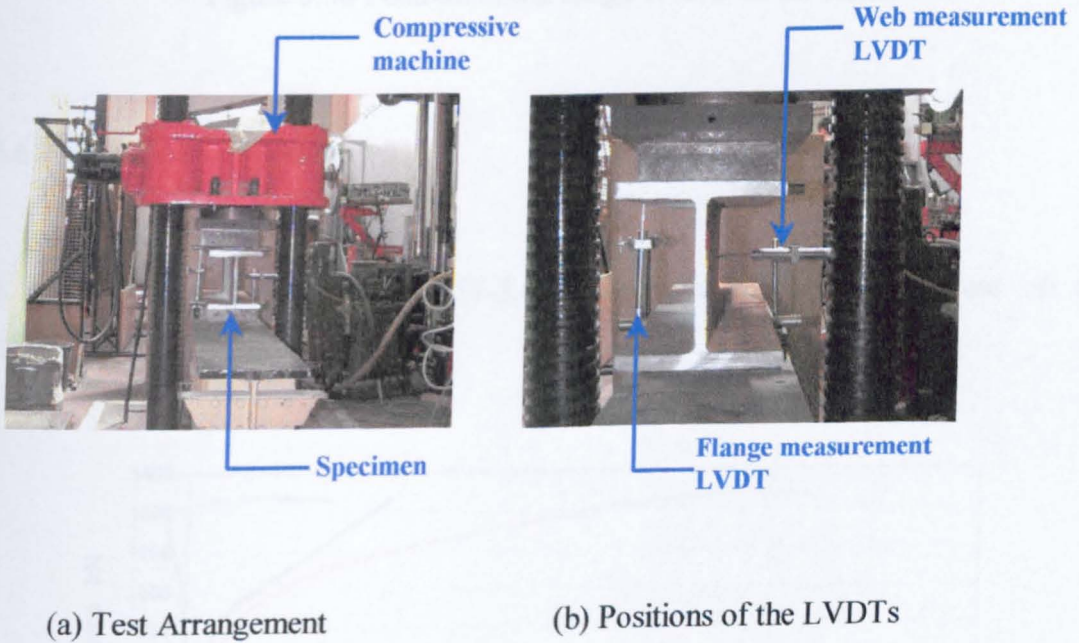


Figure 5.55 Test at Ambient Temperatures

The LVDT for measuring the flange displacement was placed on the roller which was used to apply the compressive force, as shown in Figure 5.56. Comparing the

test results with the simplified model results it can be seen that towards the final steps of any test in this Phase, the model does not predict the behaviour of the specimen as accurately as before. It is the author's opinion that it is necessary to predict the force when the web starts to move out of plane (i.e. the load where so-called "plastic buckling" starts to happen). In any case this is a better prediction, and step forward from, the model used in Eurocode 3-Annex J.

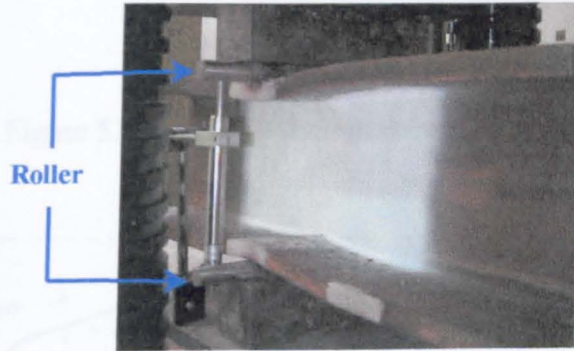


Figure 5.56 Position of the flange LVDT on the roller

5.6.4 Phase D Test Results

A total of six tests (Figures 5.57-5.62) were performed in this Phase on a UC203x203x86 column section.

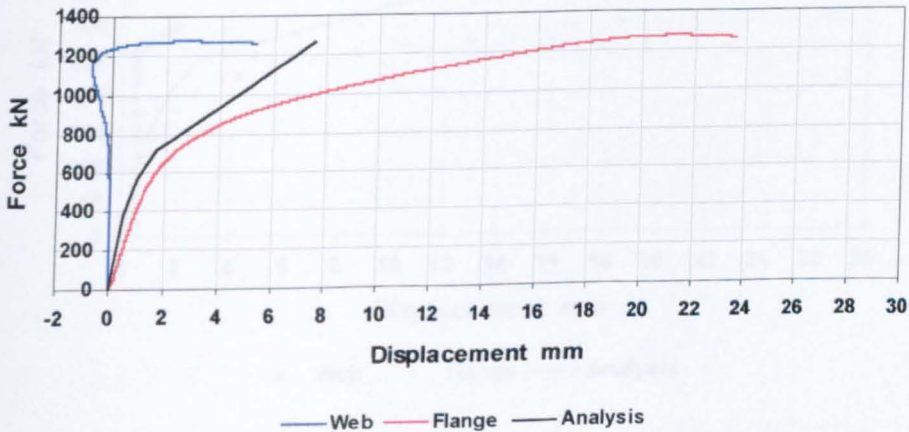


Figure 5.57 Force-deflection curves at 20 °C

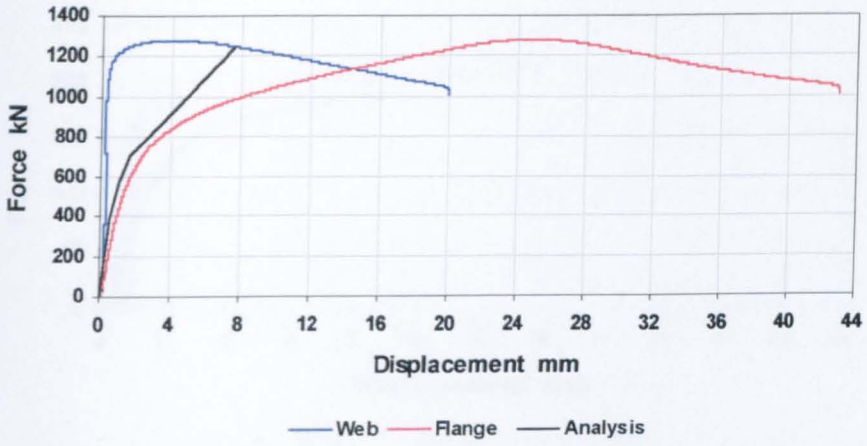


Figure 5.58 Force-deflection curves at 20 °C

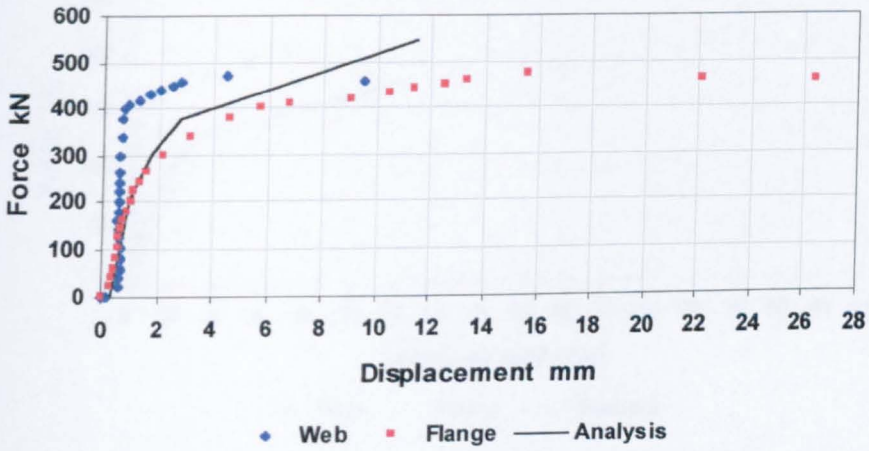


Figure 5.59 Force-deflection curves at 585 °C

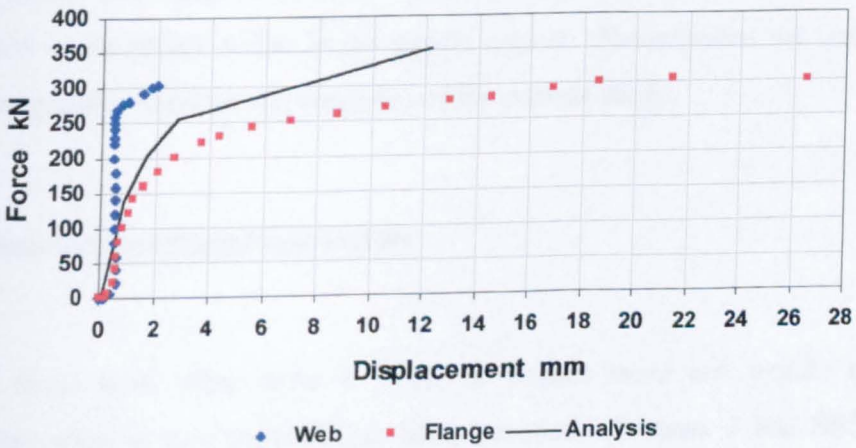


Figure 5.60 Force-deflection curves at 650 °C

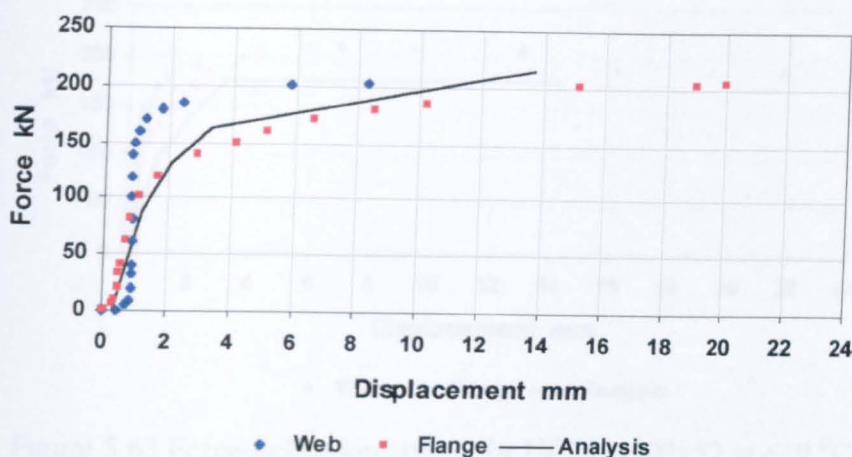


Figure 5.61 Force-deflection curves at 705 °C

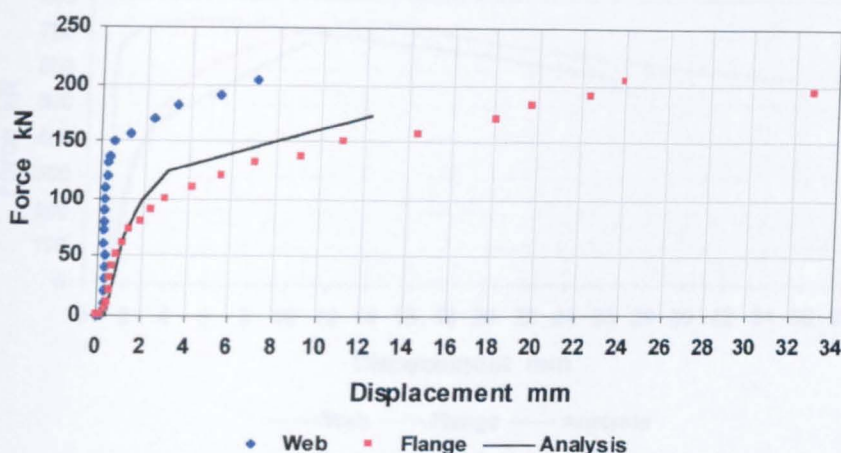


Figure 5.62 Force-deflection curves at 750 °C

In this phase the simplified model predicts the behaviour of the compression component to be rather stiffer in the plastic region. Nevertheless the comparison is within acceptable limits for the purposes of the current study.

5.6.5 Random specimens test results

Most of these tests were done in order to collect more test results at ambient temperature after it was realized that both Eurocode 3:Annex J and BS5950 were under-predicting the ultimate capacity of the column web under compressive forces at ambient temperature.

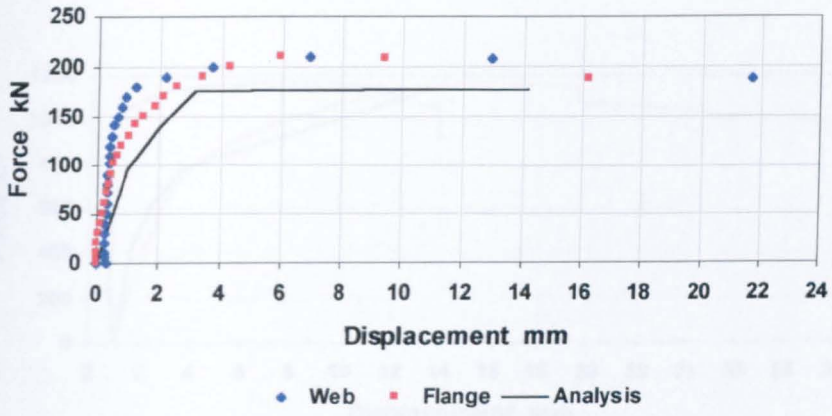


Figure 5.63 Force-deflection curves for UC203x203x52 at 610 °C

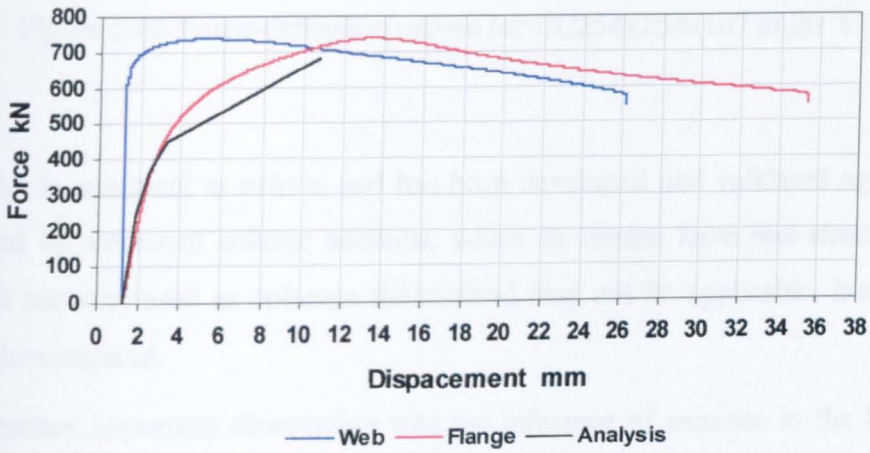


Figure 5.64 Force-deflection curves for UC203x203x60 at 20 °C

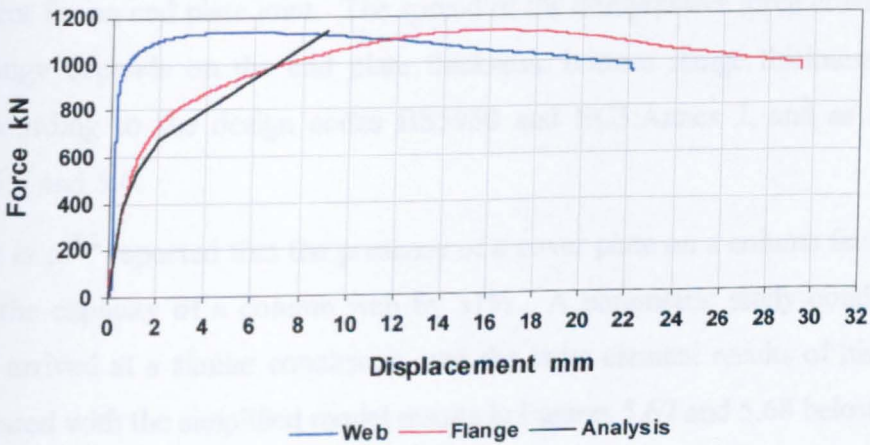


Figure 5.65 Force-deflection curves for UC203x203x86 at 20 °C

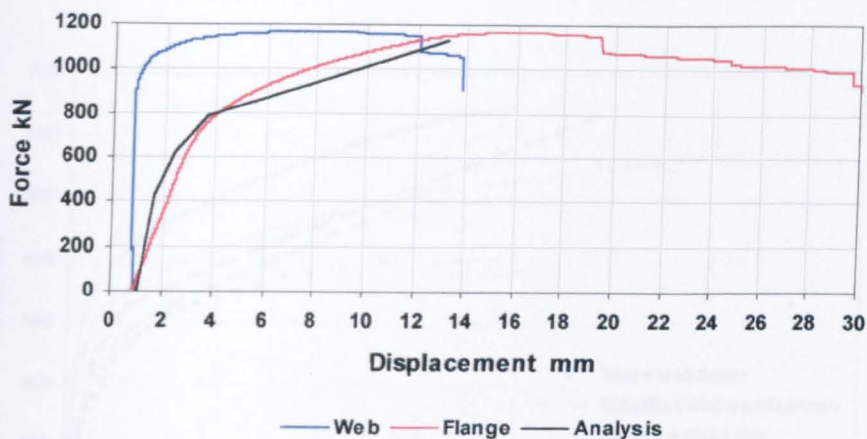


Figure 5.66 Force-deflection curves for UC254x254x107 at 20 °C

The model is empirical in nature, and has been developed and validated against test data based on universal column sections, which by design have non-slender webs. For beam sections used as columns the method may not be applicable, but this has not been investigated.

Finally another important observation was the influence of increase in the length of the uniformly distributed compressive load patch on the column flange (c value as shown in Figures 5.22 and 5.23). It has been mentioned before that this is an important value when calculating the ultimate capacity of the compression component for an end plate joint. The spread of the compressive force created by the beam flange depends on the end plate thickness, bottom flange thickness and the weld, according to the design codes BS5950 and EC3:Annex J, and as shown in Figures 5.3 and 5.4.

Hendrick *et al*^{5.2} reported that the presence of a cover plate on a column flange could increase the capacity of a column web by 31%. A parametric study conducted by Block^{5.13} arrived at a similar conclusion, and the finite element results of his analysis are compared with the simplified model results in Figures 5.67 and 5.68 below.

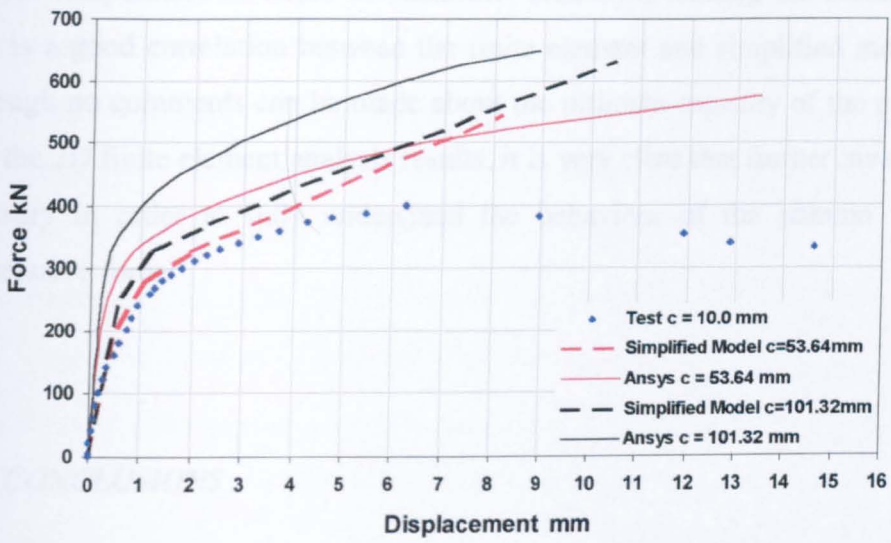


Figure 5.67 Influence of the c value on the UC203x203x46 specimen at ambient temperature

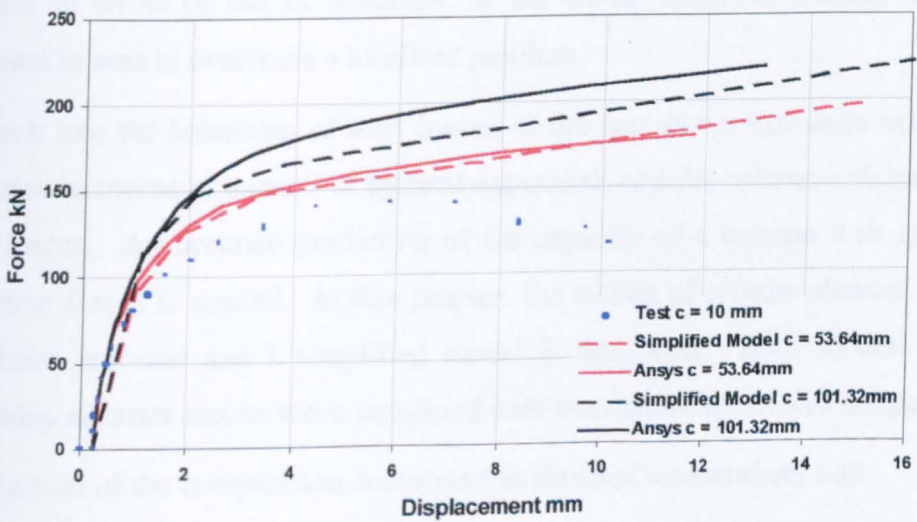


Figure 5.68 Influence of the c value on the UC203x203x46 specimen at 610 °C

From the figures above it is clear that the simplified model is not so accurate at ambient temperature in terms of stiffness. However, looking the results at 610⁰C there is a good correlation between the finite element and simplified model results. Although no comments can be made about the ultimate capacity of the column web from the 2D finite element analysis results, it is very clear that further investigation is necessary in order to fully understand the behaviour of the column web under compressive force.

5.7 CONCLUSIONS

In joint design it is necessary to ensure ductility and therefore failure in the compression zone must be avoided. Where a column web is unstiffened, the web resistance may be critical. In such cases the designer has two options; to use a heavier column section to ensure that an alternative more ductile failure mode becomes critical, or to strengthen the web using stiffeners or web plates. Strengthening the column adds considerable cost to fabrication and is not recommended. Increasing the column weight may avoid the problem but is not efficient in terms of use of materials, as the whole length of column has to be increased in area to overcome a localised problem.

Research into the behaviour of steel frames in fire has shown that large axial forces may arise in beams as a result of thermal expansion, and the column web must resist these forces. An accurate prediction of the capacity of a column web to sustain transverse forces is needed. In this chapter, the results of a finite element analysis have been reported and a simplified model is described. Both models provide reasonably accurate results when compared with test results at elevated temperatures.

Investigation of the compression component at elevated temperatures has:

- a) For the first time produced experimental results for column webs under transverse compressive forces at elevated temperatures,
- b) Shown discrepancies between the current standards and the calculated and tested column web capacities, even at ambient temperature,

- c) Demonstrated that 2D finite element analysis gives good correlation with the test results at elevated temperatures, which makes further investigation into the compression component easier, less expensive and less time consuming,
- d) Led to a simplified empirical model that predicts not only the ultimate capacity of the column web under compression but also the full behaviour of the component in terms of strength and stiffness,
- e) Illustrated the influence of increase of the uniformly distributed load patch length on calculated compressive resistance,
- f) Proved the image acquisition and processing technique to be a very useful tool for carrying out elevated-temperatures tests.

In the author's opinion, the most important achievement from this part of the current study was the prediction of the ultimate capacity of the column web under compressive forces at ambient and elevated temperatures.

5.8 REFERENCES

- 5.1 Bose, S.K., McNeice, G.M., and Sherbourne, A.N., "Column webs in steel beam to column connections Parts I and II", *Computers and Structures*, Vol. 2, pp. 253-279, 281-301, 1972.
- 5.2 Hendrick, A., and Murray, T., "Column web compression strength at end plate connections", *AISC, Engineering Journal*, 3rd Quarter, pp. 161-169, 1984.
- 5.3 Bose, B., "Design resistance of unstiffened column web subject to transverse compression in beam to column joints", *Journal of Constructional Steel Research*, Vol. 45, No. 1, pp 1-15, 1998.
- 5.4 British Standards Institution, *BS5950: Part 1: Structural use of steelwork in building: Code of practice for design: rolled and welded sections*, BSI, London, England, 1990.
- 5.5 British Standards Institution, *BS5950-1:2000 Structural use of steelwork in building Part 1 : Code of practice for design: rolled and welded sections*, BSI, 2000.
- 5.6 BS449: Part 2: 1969 Specification for the use of structural steel in building, British Standards Institution.
- 5.7 Morris, L.J., "Design Rules for Connections in the United Kingdom", *Journal of Constructional Steel Research*, Vol. 10, pp. 375-413, 1988.
- 5.8 British Standards Institution, *BS5950: Part 1: Structural use of steelwork in building*. BSI, London, England, 1985.
- 5.9 ENV 1993-1-1:1992/prA2:1994, *Eurocode 3: Part 1.1, Revised Annex J: Joints in buildings frame*, European Committee for Standardization (CEN).
- 5.10 Bailey, C. G., and Moore, D. B., "The influence of local and global forces on column design", Final report for DETR, Partners in Technology Contract No. CC1494, September 1999.

- 5.11 “*Semi-Rigid Action in Steel Frame Structures*”, Technical Reports No. 2, and No. 4, C.E.C Agreement No. 7210-SA/507, Luxembourg, 1988-1989.
- 5.12 Guisse, S., and Jaspart, J.P., “*Influence on Structural Frame Behaviour on Joint Design*”, Connections in Steel Structures III: Behaviour, Strength & Design, Proceedings of the Third International Workshop, Italy, 1995.
- 5.13 Block, F., “*2D and 3D Finite Element Analysis of a Column Web under Transverse Compressive Forces at Elevated Temperatures*”, Internal Report, University of Sheffield, 2001.
- 5.14 Roberts T.M., and Rockey K.C., “*A mechanism solution for predicting the collapse loads of slender plate girders when subjected to in-plane patch loading*”, Proc. Instn Civ. Engrs, Part 2, 67, pp. 155-175, 1979.
- 5.15 Roberts T.M., “*Slender plate girders subjected to edge loading*”, Proc. Instn Civ. Engrs, Part 2, 71, pp. 805-819, 1981.
- 5.16 Roberts T.M., and Newark A.C.B., “*Strength of webs subjected to compressive edge loading*”, Journal of Structural Engineering, Vol. 123, No. 2, pp. 176-183, 1997.
- 5.17 Shimizu, S., Horii, S., and Yoshida, S., “*The Collapse Mechanism of Patch Loaded Web Plates*”, Journal of Constructional Steel Research, Vol. 14, pp. 321-337, 1989.
- 5.18 Shimizu, S., Yabana, H., and Yoshida, S., “*A new Collapse Model for Patch Loaded Web Plates*”, Journal of Constructional Steel Research, Vol. 13, pp. 61-73, 1989.
- 5.19 Johansson, B., and Lagerqvist, O., “*Resistance of Plate Edges to Concentrated Forces*”, Journal of Constructional Steel Research, Vol. 32, pp. 69-105, 1995.
- 5.20 Johansson, B., and Lagerqvist, O., “*Resistance of I-girders to Concentrated Loads*”, Journal of Constructional Steel Research, Vol. 39, pp. 87-119, 1996.

- 5.21 Markovic, N., and Hajdin, N., “A contribution to the analysis of the behaviour of plate girders subject to patch loading”, *Journal of Constructional Steel Research*, Vol. 21, pp. 163-173, 1992.
- 5.22 Drdacky, M., and Novotny, R., “*Partial Edge Loading-Carrying Capacity Tests of Thick Plate Girder Webs*”, *Acta Technika CSAV*, Vol. 5, pp. 614-20, 1977.
- 5.23 “*EC3:Design of Steel Structures, Part 1.2:General Rules for Structural Fire Design*”, (Draft), ENV 1993-1-2, European Committee for Standardization, 1995.

Chapter 6

Steel Joint Modelling

6.1 INTRODUCTION

The importance of considering semi-rigid joint action when analysing the behaviour of a steel frame has already been discussed in a previous chapter. In early studies of steel frame response the most appropriate means of including the effects of semi-rigid joint action relied on representations of test data. Whilst this is the best way of representing the joint response, and in early studies that resulted in a better understanding of the role of the steel joints within a steel frame, there are several limitations associated with the use of experimentally derived joint characteristics:

- a) Expense associated with testing,
- b) Wide range of steel joint types commonly adopted,
- c) Limited availability of carefully documented existing test data.

As a result there is a real need to consider ways in which joint characteristics may be generated analytically.

Forms of joint modelling range from simple curve fitting, through semi-empirical relationships, to finite element analysis. Existing models for both bare-steel and composite joints are commonly classified according to their theoretical basis into three main categories:

- a) Global models,
- b) Mechanical models,
- c) Finite element analysis.

The various forms of model described have been discussed by several authors^{6.1,6.2,6.3,6.4,6.5}. A summary, based on their reports is outlined in the following sections.

6.1.1 Global models

Global models can be further classified into two categories:

i) Mathematical expressions

These approaches are based on fitting mathematical expressions to experimentally obtained data for the considered joint type. Initial attempts to model experimental work by Baker^{6.6} and Rathburn^{6.7} date back to the 1930s, and a single straight line corresponding to the initial tangent-stiffness (Z) of the joint was used.

$$Z = \Phi / M \quad \dots 6.1$$

The linear modelling of joint behaviour may be satisfactory for ambient-temperature studies in which joint characteristics might be expected to remain within the elastic range of response. At elevated temperatures it may be anticipated that the joint would enter the plastic range of response at low levels of moment.

It was not until the 1970s that bi-linear representations were introduced^{6.8,6.9}, recognising the reduced stiffness of joints at high levels of rotation. Bi-linear forms of curve fit typically consist of a linear portion following the initial tangent stiffness, which is intersected by a line of reduced plastic stiffness. This assumption of a constant plastic stiffness may result in an un-conservative assessment of moment capacity at high levels of rotation.

In the early 1980s tri-linear relationships^{6.10} were proposed as a result of these limitations. Initial and strain-hardening slopes of the moment-rotation curve were connected by the addition of an intermediate linear branch between the elastic limit and yield moment.

At a similar time to the introduction of bi-linear forms of curve-fit, polynomial models^{6.11} were developed in an attempt to account for the curved nature of the moment rotation relationship.

$$\theta = c_1(kM) + c_2(kM)^3 + c_3(kM)^5 \quad \dots 6.2$$

where k depends on the main geometrical parameters of the particular joint type under consideration, and c_1 , c_2 and c_3 are curve fitting constants. The limitation of this method is that it may sometimes yield negative values of joint stiffness, which is physically unacceptable.

As a result of the above limitation, B-spline techniques^{6.12} were developed in the early 1980s, in which continuity was enforced for the first and second derivatives at the intersections of experimental data. This technique represents the joint response very closely but on the other hand a large quantity of experimental data is required to achieve an acceptable fit.

As an alternative, a Ramberg and Osgood^{6.13} expression developed to define the non-linear nature of stress-strain curves in terms of three simple parameters, may replace the polynomial of equation 6.2. Ang and Morris^{6.14} extended the expression to describe moment-rotation characteristics and El-Rimawi^{6.15} modified the expression to include high temperatures. When applied to moment-rotation curves, the model has the advantage of always yielding a positive slope, corresponding with the tangent-stiffness of the joint. The modified version of the Ramberg-Osgood expression states that:

$$\Phi_c = \frac{M_c}{A} + 0.01 \left(\frac{M_c}{B} \right)^n \quad \dots 6.3$$

Where Φ_c is the joint rotation, M_c is the corresponding level of moment, and A , B and n are temperature-dependent factors.

The above equation 6.3 has been used by Leston-Jones^{6.3} and Al-Jabri^{6.4} to express their test data for bare steel and composite joints at elevated temperatures. It can be applied at elevated temperatures by modifying the terms A and B , which control the stiffness and capacity of the joint respectively, and index n which defines the shape of the moment-rotation curve.

The limitations of the above expression are that a considerable amount of test data is needed in order to accurately represent the joint behaviour at elevated temperatures and it is not possible from this type of curve-fit to define the ultimate moment capacity or rotation limit of the joint. The models already described are based on calibration against experimental data.

ii) Simplified analytical models

These are based on *prediction* of the key parameters within the joint response, such as initial stiffness and moment capacity, and fitting a curve through these points. The initial stiffness is calculated by elastic analysis of the most flexible component and the joint moment capacity is calculated by plastic mechanism analysis of the same key component. For this reason simplified analytical models are typically restricted to the more flexible arrangements where deformation may easily be attributed to an isolated component.

In the early 1950s an elastic model was developed for prediction of the initial flexibility of double-web-cleat joints, whilst ignoring all forms of deformation other than bending of the cleats. The expression given by Lothers^{6.16} was:

$$K_{\theta} = \frac{Eht^3 y^2 (4g + g_1)}{6g^3 (g + g_1)} \quad \dots 6.4$$

Where E is the Young's Modulus for steel, g and g_1 are the gauge lengths of the angle legs, t is the angle thickness and y relates the neutral axis to the depth h of the joint.

In the late 1960s formulae were developed for the initial elastic and final plastic phases of the load-deformation behaviour of double web-angle segments, concentrating on the response of the angles under tension^{6.17}.

Almost twenty years later another model^{6.18} was developed which considered the behaviour of web-cleats, flange-cleats, and combined web-and-flange-cleat joints, utilising a power expression, as shown in equation 6.5, to generate the resultant moment-rotation response.

$$M = \frac{k_l \theta}{\left[1 + \frac{\theta}{\theta_o^n}\right]^n} + k_p \theta \quad \dots 6.5$$

Where k_p is the plastic stiffness of the joint, $k_l = k_i - k_p$, k_i is the elastic stiffness, θ_o is the plastic rotation and n is a shape parameter derived from test data. The above model focuses attention on the flexibility of the connecting components (angle T-stubs only), assuming that the connected members are themselves rigid. However, with today's knowledge of the overall behaviour of steel joints, deformation of the column components (flange and web) is known to take place, contributing to the joint flexibility. If it is assumed that the interaction between different joint components does not affect considerably the response of a single component, the overall behaviour of a joint may be obtained by super imposing the flexibilities of the joint components.

Recognising the influence of connectivity to a "flexible" column on the response of a flush end plate joint, a model was developed in the early 1980s^{6.19}. The joint response was expressed in terms of initial stiffness and plastic capacity, with the simplified assumption of an elastic-perfectly plastic form of curve-fit.

Yee and Melchers^{6.20} developed a method, based on the same principles, for the analysis of bolted end plate eaves connections. The exponential representation:

$$M = M_p \left[1 - \exp\left(\frac{-(K_i - K_p + C\Phi)\Phi}{M_p} \right) \right] + K_p \Phi \quad \dots 6.6$$

was assumed, where M_p is the plastic joint resistance, K_i and K_p define the initial and strain-hardening stiffnesses respectively, and C is an empirical coefficient for calibrating the equation against test data.

Methods based on simplified analyses of the main joint components show that it is possible to estimate the moment-rotation curves without resorting to testing. Eurocode 3:Annex J^{6.21} contains a simplified analytical model for predicting the joint behaviour. Mechanical models have been developed to calculate the ultimate joint capacity and empirical equations adopted for the description of the elasto-plastic joint stiffnesses.

6.1.2 Mechanical models

This group of models can represent the joint behaviour throughout the whole range of the moment-rotation curve, relying only on theoretical considerations. This can be achieved by assembling the contributions of sets of rigid and deformable components which exist in a joint arrangement. The non-linearity of the whole joint is then accounted for by analytically derived inelastic force-displacement relationships. The accuracy with which mechanical models can predict joint response is related to the number of components incorporated.

Wales and Rossow^{6.22} considered the major zones (tension, compression) within a double-web-angle joint and developed a component-based model. The joint was idealised as two rigid bars linked by a homogeneous continuum of independent non-linear springs, which simulate segments of the double web-angle. The trilinear load-displacement relationships for the tension and compression springs were determined by simply analysing the segments under tension and compression forces. The model incorporates the coupling effects between moment and axial force applied to the joint. The ability of the model to account for axial forces is an important feature,

since it may influence the characteristics of the moment-rotation curve, especially at elevated temperatures when these forces are unavoidable.

Treating the tension and compression zones as a T-stub model, Kennedy and Hafez^{6.23} describe the response of a partial-depth end plate joint. The analytical formulation derived for the T-stub models was validated against test data. In order to define the moment-rotation characteristics of the joint, a trial and error location of the centre of rotation was carried out. When compared with test results, conducted by the same researchers, a close agreement in terms of ultimate capacity occurred, but in terms of the corresponding level of rotation the results were rather erratic.

Towards the mid-1980s the model by Wales and Rossow had been extended to predict the behaviour of all types of angle joints, subjected to bending and shear. The angle segments within the joint were modelled using mathematical expressions (in the form of equation 6.5) and then calibrated by curve fitting against experimental results. A limitation of the approach is that the validity of the results is restricted to the range of the calibration data.

Tschemmerneegg *et al.*^{6.24,6.25} used the component-based approach in combination with empirical functions in order to describe the behaviour of steel and composite joints. The model consisted of an arrangement of springs describing the tension, compression and shear zones within a joint. The springs were calibrated against experimental data. By superposition of the deformability of the springs the moment-rotation curve was obtained.

Madas^{6.2} has developed a series of spring-stiffness models for a range of both bare steel and composite joints. The form of model adopted was similar to that described by Wales, Rossow and Tschemmerneegg *et al.* but also included the effects of axial forces developed as a result of a cyclic loading. A close correlation was observed with existing test data in terms of both the overall form of response and the observed mechanisms of failure.

De Stefano *et al.*^{6.26} developed a mechanical model in order to simulate the behaviour of double-angle joints subjected to large inelastic cyclic bending. The model is purely mechanical and needs only the stress-strain law of the material and the geometric properties of the joint. The joint is simulated by a series of rigid and deformable elements, where the constitutive relationship of the deformable elements

is derived from the response of beam elements subjected to bending. By using the kinematic hardening rule the model was extended into the cyclic range.

In EC3: Part 1.1 Annex J^{6.21} the component-based model is used for defining key parameters which control the joint behaviour. These parameters are the initial stiffness, moment and rotational capacity. However, due to the lack of experimental data to describe the component or even the joint response at elevated temperatures, elevated-temperature component-based models are limited and restricted to single joint types. Based upon EC3 component approach, Leston-Jones^{6.3} and Al-Jabri^{6.4} proposed a component model for bare steel and composite flush end-plate joints at elevated temperatures.

6.1.3 Finite element analysis

Finite element analysis of steel joints at ambient or elevated temperatures is the most accurate way of representing the joint characteristics. The use of finite element analysis models permits the complex representation of components and the full non-linear joint response, incorporating the influence of welds and contact zones. However, its application is complex and requires careful construction of the finite element joint representation. The effects of bolt slippage or contact surfaces between bolts and flange are complex to model and require a new finite element formulation (Baniotopoulos^{6.27}). Nevertheless, the method has the potential to describe in great detail the joint behaviour. The use of finite element modelling for studying the joint behaviour started in the early 1970s, as the application of computers in solving structural problems developed.

Initially Bose *et al.*^{6.28,6.29} studied the behaviour of fully welded beam-to-column joints at ambient temperature. It was considered that the column web under compression was the critical component, and it was analysed in isolation as a plate strength problem for internal and external joints. The effects of strain-hardening, buckling and material plasticity were accounted for in the analysis and the results compared against experimental results in terms of critical loads only.

The investigation of the column web under compressive forces, using finite element analysis, attracted the attention of other researchers. Hendrick and Murray^{6.30}

performed a 2D inelastic finite element analysis in order to determine stress distributions and yield patterns in the column web of an end plate joint. Patel and Chen^{6.31} investigated the behaviour of joints where the beam was either fully or partially welded to the unstiffened column. The joints were analysed using a general-purpose finite element package (NONSAP) in a 2D model with plane stress isoparametric elements. Three-dimensional finite element analyses were conducted by Atamiaz and Frey^{6.32} on unstiffened welded joints using shell elements. The studies compared satisfactorily against experimental results, suggesting that finite element analysis presents a tool of sufficient accuracy to model the response of welded joints.

When considering bolted connections within steel joints, the finite element analysis becomes more complicated. The reason lies in the influence of complex boundary conditions, including friction, slip and interface contact, all of which interact in a manner that is not yet fully understood and remains difficult to monitor experimentally. An attempt to tackle the problem was performed by Richard *et al.*^{6.33} who considered the response of a single web-plate joint, modelling the response of the joint in its entirety, along with the connected beam. An inelastic finite element was developed to simulate bolt behaviour based on statistical evaluation of tests on single bolts.

The contact surfaces generated by the tensile force action in a bolted joint create the need to use more complex bolt models. Krishnamurthy^{6.34} developed a sophisticated finite element model that incorporates the influence of changes in the contact zone between end plate and an idealized rigid support, and bolt pre-loading. The close correlation between the numerical results and experimental data demonstrated the importance of including the bolt heads and welds in the numerical models in order to define accurately the joint response.

More recently various software companies have developed codes that have the ability to model the behaviour of joints in terms of complex boundary conditions such as slip, friction and interface contact between elements. Sherbourne and Bahaari^{6.35} developed a methodology based on finite element modelling to investigate the behaviour of bolted joints using the ANSYS code for equivalent 3D analysis. The model was examined for end plate joints with commonly used end plate thicknesses and the predicted results were within the range of accuracy of experimental values.

Choi and Chung^{6.36} used the ADINA code to model extended end plate joints with and without stiffeners in the column web. The effect of bolt pretensioning and the shapes of the bolt shank, head and nut were taken into consideration in the modelling. A simple yet efficient algorithm with a new gap element was employed to simulate the interaction between the end plate and column flange. Again the analytical results were compared against test results and the conclusion was that the proposed model could properly simulate the actual behaviour of end plate joints.

Bursi and Jaspart^{6.37} used ABAQUS, initially for calibration of finite element analysis against test data and then to set up a 3D model to predict both the displacement and stress fields of isolated extended end plate steel connections. The numerical results, which were compared with the experimental ones in terms of stiffness and strength, allow the reliability of finite element models to be assessed and commented upon. A similar analysis was performed by Troup *et al.*^{6.38} using ANSYS. Simplified bi-linear stress-strain curves for the steel sections and bolt shank were adopted. Material non-linearity has been considered for steel members and connecting components, together with geometric non-linearity due to the changing area of contact between faces of the end plate or T-stubs. An encouraging correlation between the model and test was observed, with good comparisons of the stiffnesses in both thick and thin plate conditions.

In terms of modelling the behaviour of different joints at elevated temperatures the work conducted so far is limited, due to the large number of parameters which need to be considered and due to the small number of fire tests conducted to date.

Based on an ambient-temperature end plate model, Liu^{6.39,6.40} developed an elevated temperature model incorporating material plasticity and deterioration with temperature, non-uniform thermal expansion across a section, and large deformation at high temperatures. The response of bolts and the contact 'link' between the column flange and end plate was simulated using a beam element with special characteristics to take into account the behaviour of bolts during the course of expansion at elevated temperatures. Verification of the described model was based mainly on two tests of extended end plate joints by Lawson^{6.41}. A reasonable simulation of joint response was achieved for both joints, and failure was defined by the joint rotation exceeding 100 millirads. The cause of any discrepancy between the

results was suggested as being the limited information about temperature distributions and actual stress-strain relationships.

More recently El-Houssieny^{6,42} has performed analytical studies to evaluate the moment-rotation stiffness, bolt forces and stresses for semi-rigid extended end plate joints at ambient and elevated temperatures. The objective was to develop simple prediction equations, which would contribute to the understanding of the behaviour of different joint components at elevated temperatures. These equations could be used for design of common joint types under the effect of different thermal loads with considerable accuracy.

6.1.4 Summary of joint modelling techniques and approaches methods

The behaviour of steel joints may be represented by various types of models. These have been considered in some detail for two reasons:

- a) It is necessary to incorporate the non-linear form of moment-rotation response observed for joints within numerical frame analysis models, to ascertain the resultant influence on frame behaviour. The models must be sufficiently accurate, and compatible with the frame analysis tools.
- b) Due to the difficulties in performing actual steel joint tests, especially at elevated temperatures, there is a need to develop forms of joint models which can predict the moment-rotation response of a broad range of commonly used steel joint types without recourse to testing.

Global models result in expressions which describe joint behaviour very accurately, but the limitation is that they cannot be used outside the range of their calibration data. In addition, because they are calibrated against specific test data, it is very difficult to follow a different failure mode when the material and geometrical properties of the joint are changed. Nevertheless, global models are very effective for design purposes as well as for implementation in frame analysis programs.

Existing *mechanical models* are, in principle, the most suitable provided that the load-deformation characteristics of the key components within steel joints are known. Their advantage over global models is that moment-rotation curves can be

predicted for a range of joint parameters, without using experimental data. To date the application of spring-stiffness models at elevated temperatures has not been considered. It is felt that the use of spring-stiffness models compares favourably with other forms of modelling due to the combination of efficiency and the ability to accurately follow the full non-linear range of joint response.

In terms of joint complexity, *finite element analysis models* can lead to accurate results, taking into account the complex interaction between joint components, bolt action, boundary conditions and contact zones. Therefore, modelling of joints by finite elements can save money and time against actual testing for collecting data over a wide range of joints. However, for frame analysis the use of finite element models, including the joints, would be prohibitively expensive in time and money. Mathematical relationships can be implemented more easily in frame analysis programs. Recent work by Liu has extended the scope of finite element modelling to include the effects of temperature. The results from experimental fire tests^{6.3,6.4} compared with his finite element results have demonstrated the applicability of the model. The down-side of this kind of modelling is its complexity and computational requirements, which make its use in design very limited.

6.2 ELEVATED-TEMPERATURE SPRING STIFFNESS MODEL

As already discussed, the component-based approach compares favourably with all other analytical methods since it combines economy with effective and predictive application. As explained earlier in Chapter 2 the joint behaviour can be modelled by assembling the contributions of individual components, representing the joint as a set of rigid and deformable elements. The behaviour of a joint as a whole may be obtained by super imposing the stiffnesses of individual components in the compression and tension zones, if it is assumed that the interaction between connected components has a negligible effect on the response of individual components. As a result, the components are analysed in isolation as described in Chapters 4 and 5, and due to their non-linear response it is then possible to predict variations in joint failure modes and deformations resulting from changes in

geometry, material properties and temperature distributions. At elevated temperatures, the influence of thermal expansion is neglected (this will be investigated and discussed in a later chapter in this study). The joint model to be presented applies to a balanced two-sided joint, in which there is no shear deformation due to out-of-balance moments.

The joint is modelled principally as a two-dimensional problem and the rotation is assumed to occur about the centre-line of the lower beam flange. Individual springs are used to simulate the stiffnesses of the individual components, and in order to simplify the solution process the stiffnesses of all components acting in the tension zone are grouped and considered as a single spring of equivalent stiffness. The idealised representation of a flush end plate joint is illustrated in Figure 6.1, where the components contributing towards overall joint stiffness may be summarised as in Table 6.1 below:

Table 6.1 Principal zones within a steel joint

<i>Tension Zone (K_t)</i>	<i>Compression Zone (K_c)</i>
<i>First bolt row T-stub stiffness, K_1 (Bolt, end plate and column flange stiffness)</i>	<i>Column web stiffness, K_c</i>
<i>Second bolt row T-stub stiffness, K_2 (Bolt, end plate and column flange stiffness)</i>	

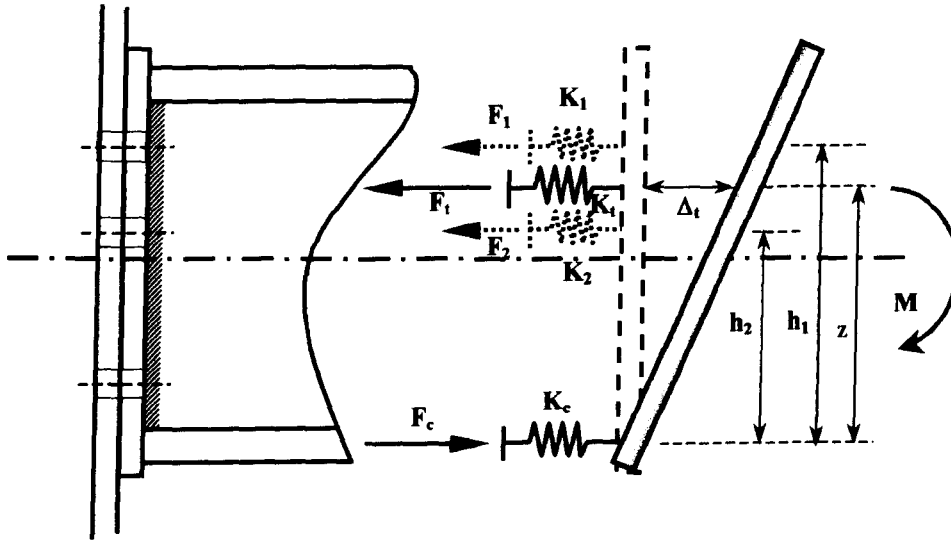


Figure 6.1 Idealised bare-steel spring stiffness model

According to EC3:Annex J^{6.21} the final step in the procedure, as described in Chapter 2, is the assembly of the components in order to determine the moment-rotation characteristics of the joint. This means calculating the ultimate resistance of the joint, which is given by:

$$M_{ult} = \min(P_t, P_c)z \quad \dots 6.7$$

where z is the lever arm corresponding to the equivalent tension spring as shown in Figure 6.1 and given by the equation below:

$$z = \frac{\sum_{i=1}^n (K_i h_i^2)}{\sum_{i=1}^n (K_i h_i)} \quad \dots 6.8$$

The overall rotation of the joint is expressed by:

$$\Phi = \frac{\sum_{i=1}^n \Delta_i}{z} \quad \dots 6.9$$

According to the EC3:Annex J component model, which is based on linear-perfectly plastic behaviour of a steel joint, it is inevitable that some discrepancies between the actual non-linear test results and predicted values will occur. This is not the case for the current model simply because the component models were developed up to failure and exhibit non-linear behaviour.

The component model results have been validated against test results performed by Leston-Jones^{6.3} and Al-Jabri^{6.4} in studies of bare-steel flush end plate joints at elevated temperatures. Details of the comparisons are presented in the following section.

6.3 VALIDATION OF JOINT MODEL

Al-Jabri performed several tests on bare steel and composite joints at elevated temperatures. A cruciform arrangement was used consisting of two 254x102x22UB Grade 43 beams 1700mm long, symmetrically framing into the flanges of a single 152x152x23 UC Grade 43 column 2700mm in length as shown in Figure 6.2 below. The test programme included flush end plate joints; these tests were used for comparison with the component model.

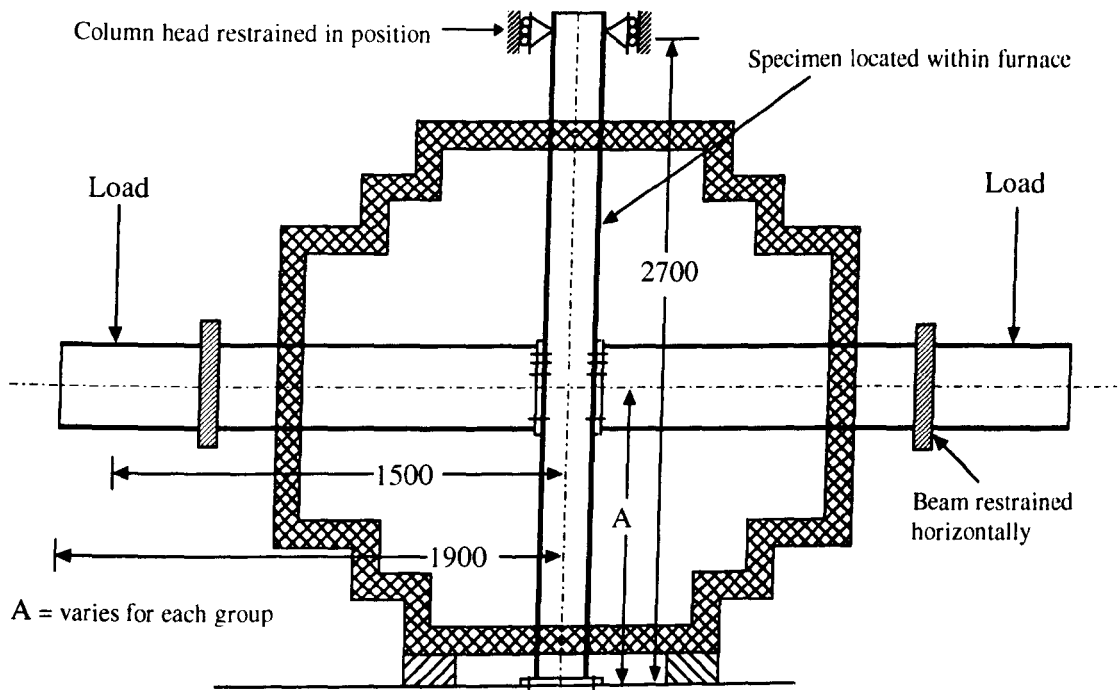


Figure 6.2 Elevated temperature flush end plate joint test arrangement^{6.3,6.4}

This is a popular type of joint, being simple to fabricate and neatly contained within the beam depth. In order to obtain an accurate representation of the joint characteristics over a reasonable range of temperatures, four tests were conducted at constant load levels (4, 8, 13 and 17 kNm respectively) where the temperature was constantly increasing by $10^{\circ}\text{C}/\text{minute}$. The load levels were selected based on the calculated moment capacity according to EC3:Annex J. Al-Jabri carried out the tests by applying a constant moment, and then applied temperature by following a standard fire curve. During the fire tests rotations were measured using inclinometers and displacement transducers, and temperatures were measured using thermocouples attached at different locations in the joint. The moment applied on each side of the joint was kept constant. The geometrical details of the joints are shown in Figure 6.3 below and full details of the tests are given by the Al-Jabri^{6.4,6.43}.

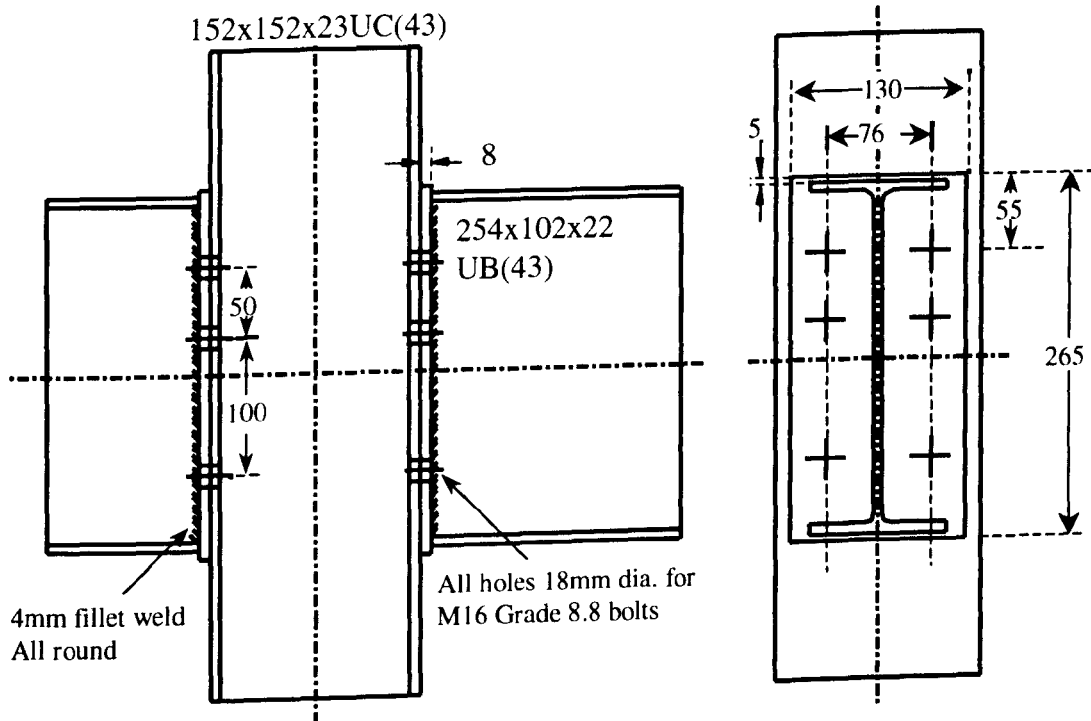


Figure 6.3 Bare steel flush end plate joint detail^{6.3,6.4}

A simplified model analysis was carried out on T-stubs, as described in Chapter 4, taking into account the difference in temperatures between the flange and the bolts. The T-stubs were analysed as arrangements with four bolts (Figure 6.3, two top bolt rows), as shown in Figure 6.4 below. The column T-stub arrangements treated in the analysis, consisted of the column flange and web, and for the end plate consisted of the end plate and beam web. In order to calculate the resisting forces and deflections, the concept of effective length was used as given in EC3:Annex J^{6.21}. The response of the column web under compressive forces was also determined as described in Chapter 5.

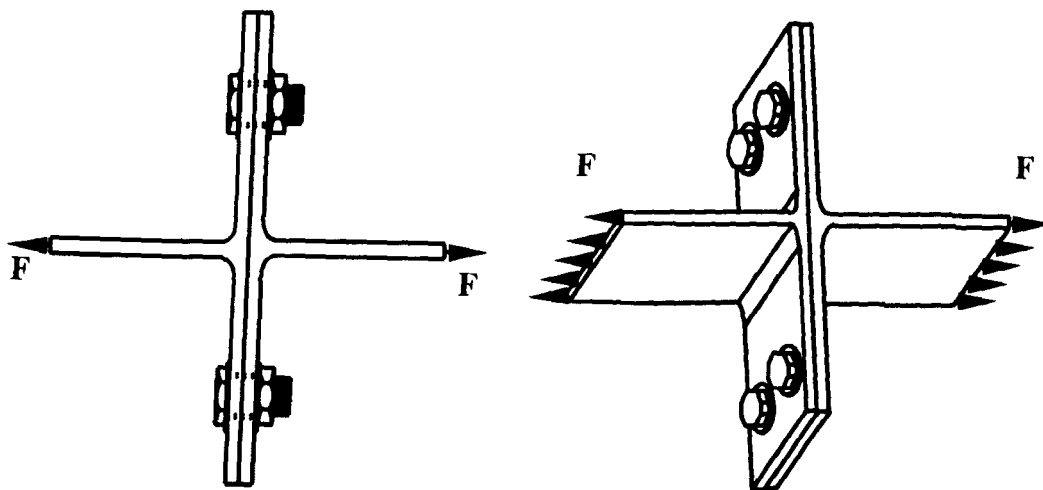


Figure 6.4 Plan and overall view of the effective T-stub arrangements used for the simplified analysis

As explained earlier, the test results were presented in terms of rotation and temperature at a constant moment on both sides of the joint, eliminating the effects of shear in the column web. By taking into account the four components emerging from the joint arrangement (Table 6.2), three in the tension zone and one in the compression zone, the joint response could be determined by the analytical procedure.

Table 6.2 Principal components within the compression and tension zone of a steel joint

<i>Tension Zone</i>	<i>Compression Zone</i>
<i>Column web in bending (bolts in tension)</i>	<i>Column web in compression</i>
<i>End plate in bending (bolts in tension)</i>	
<i>Column web in tension</i>	

The comparison between the component model and the test results are presented in Figure 6.5, and it can be seen that there is a good correlation between them. From the comparison it can also be seen that initially the simplified model over-predicts

the joint response, but actually the maximum difference from all the tests, if it is translated into overall deflections, is 0.375mm. In test FB14 (under a moment of 17kNm) there is a small sudden increase in the rotation at a temperature around 300 °C. According to Ivanyi^{6.44} this is due to bolt slip in the clearance holes.

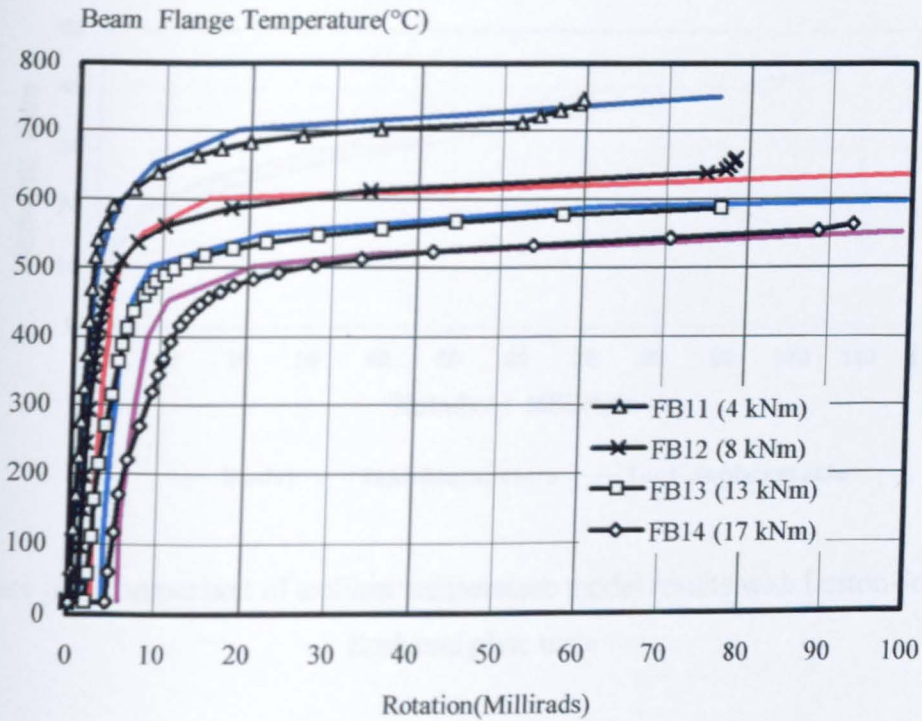


Figure 6.5 Comparison of the actual test and simplified model results from Al-Jabri fire tests on bare-steel flush end plate joints

Similar tests on flush end plate joints were performed by Leston-Jones^{6.3,6.45,6.46}. The major difference from Al-Jabri's tests was that Leston-Jones used a 12mm thick end plate instead of 8mm. The schedule of his experimental investigations on flush end plate joints was as follows:

- One test at ambient temperature, driving the rotation up to 100 millirads and recording maximum capacity of 40 kNm,
- One in an unloaded state subjected to various rates of heating,
- Five at different constant load levels (5, 10, 15, 20 and 25 kNm respectively) where the temperature was constantly increasing by 10 °C/minute.

The results obtained from the component model at ambient temperature are shown in Figure 6.6 below. Two test curves are shown; one relates to rotations measured directly using an inclinometer and the other is the rotation calculated from displacement readings.

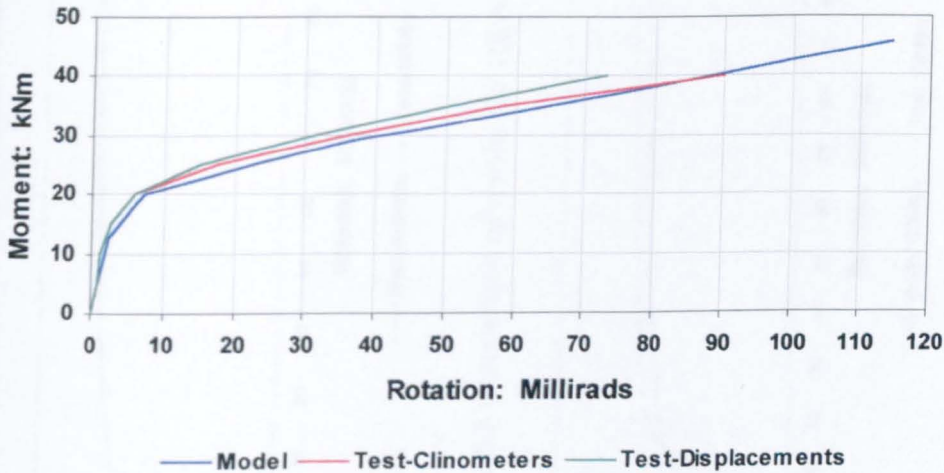


Figure 6.6 Comparison of ambient temperature model results with Leston-Jone's flush end plate tests

It is obvious that there is a good agreement between the results over the full range (elastic and elasto-plastic regions) of the joint response. In Figures 6.7-6.11 the results at elevated temperatures are plotted against the component model results. The accuracy seems to be within acceptable limits for design purposes. Once again, where the moment is large (15, 20 and 25 kNm), slip appears to have occurred.

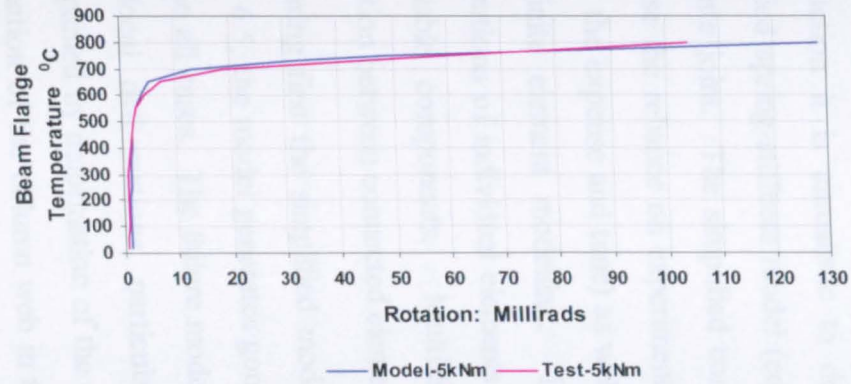


Figure 6.7 Comparison of results for 5kNm moment

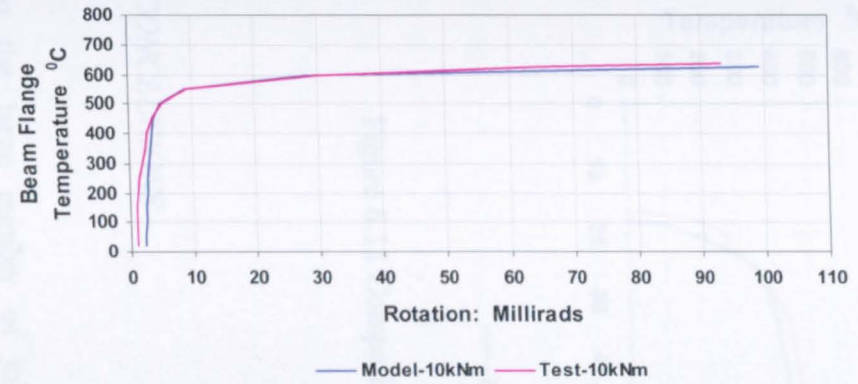


Figure 6.8 Comparison of results for 10kNm moment



Figure 6.9 Comparison of results for 15kNm moment



Figure 6.10 Comparison of results for 20kNm moment

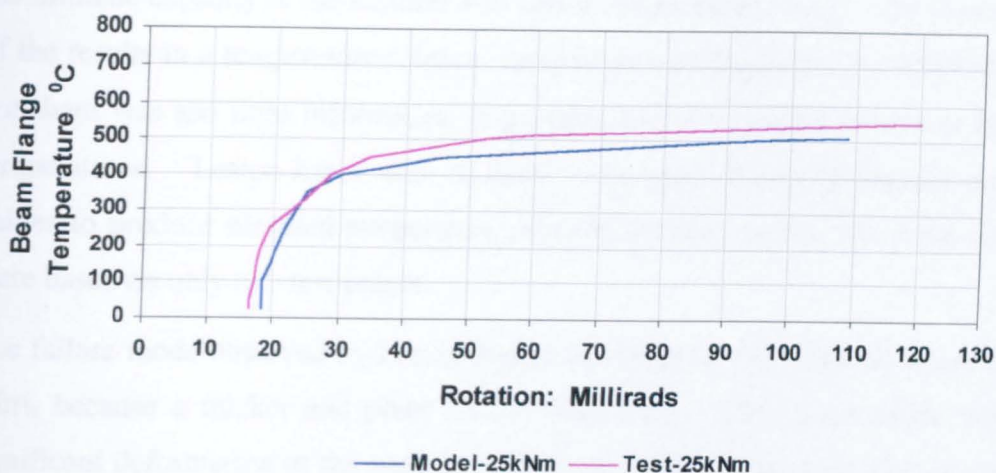


Figure 6.11 Comparison of results for 25kNm moment

6.4 CONCLUSIONS

Due to the large number of joint types and arrangements used in building construction it is unrealistic to develop characteristics for each by testing. A simplified spring-stiffness model (component model) has been presented for a flush end plate joint. The simplified component model offers an alternative solution to minimise the reliance on experimentation to investigate the joint response (and thus reduce the expense and time) as well as easing the numerical complexities associated with finite element modelling. The model was assembled by considering the contributions of individual elements and representing the joint as a set of rigid and deformable components. Multi-linear modelling was adopted, neglecting the interaction between connected elements.

Comparing first the simplified model results with Al-Jabri's fire tests, as shown in Figure 6.5, the model generates good results, and also accurately predicts the failure mode in all cases. The failure mode observed from the actual fire tests included end plate local deformations, particularly around the top bolt row, and this was accompanied by deformation of the column flange in the tension zone and significant deformation of the column web in the compression zone. The model predicted the same failure mode. The ultimate temperature that each test could sustain was due to

the ultimate capacity of the column web under compressive forces. The presentation of the results in a temperature-rotation curve form (see Figure 6.5) is rather unusual, but there was too little information to produce moment-rotation curves at elevated temperatures. Leston-Jones and Al-Jabri both gave Ramberg-Osgood curve-fit values to produce elevated-temperature moment-rotation curves, but some of these were based on only two test points.

The failure mode observed by Leston-Jones was different from that observed by Al-Jabri, because a thicker end plate (12mm) was used. The failure mode included significant deformation of the column web in the compression zone and the column flange in the tension zone, whilst there was little damage either to the beams or the end plate. The simplified model was able to show the same failure mode. From the test results shown in Figures 6.6-6.11 it is obvious that the accuracy of the simplified model is within acceptable limits for design purposes.

The novelty of this simplified model is that it can predict the ultimate capacity and also, with acceptable accuracy, the rotations within a steel flush end plate joint at elevated temperatures. It is also worth mentioning that it provides a better representation of the joint behaviour if it is compared with EC3:Annex J analysis at ambient temperature. In EC3: Annex J the ultimate moment capacity of this particular flush end plate joint was calculated to be 19 kNm with unlimited rotation capacity. Using the current model this is 45 kNm. In fact the actual joint reached a moment of 40kNm and around 100 millirads rotation. In contrast some fire tests were conducted with moments above 19 kNm (Leston-Jone's tests; one at 20 kNm and one at 25 kNm constant moment).

A further attraction of this model is that different temperatures can be used for the elements in the simplified model (i.e. bolts, column flange, end plate and column web). Therefore, when the components are assembled in order to predict the overall moment-rotation behaviour, the actual temperature profile measured around the joint during a fire test may be used.

The use of component-based models has proved desirable due to their simplicity, efficiency and the advantage that they can easily be modified to account for alternative arrangements.

6.5 REFERENCES

- 6.1 Nethercot, D.A., and Zandonini, R., "*Methods of Prediction of Joint Behaviour: Beam-to-Column Connections*", Structural Connections, Stability and Strength, Narayanan, R., ed., Elsevier Applied Science Publishers, pp. 23-62, London, 1989.
- 6.2 Madas, J.P., "*Advanced Modelling of Composite Frames Subjected to Earthquake Loading*", PhD. Thesis, Civil Engineering Department, Imperial College Science, Technology and Medicine, University of London, 1993.
- 6.3 Leston-Jones, L.C., "*The Influence of Semi-Rigid Connections on the Performance of Steel Framed Structures in Fire*", Ph.D. Thesis, Department of Civil and Structural Engineering, University of Sheffield, 1997.
- 6.4 Al-Jabri, K.S., Lennon, T., Burgess, I.W., Plank, R.J., "*Behaviour of Steel and Composite Beam-Column Connections in Fire*", Journal of Constructional Steel Research, Vol. 46, No. 1-3, 1998.
- 6.5 Sherbourne N.A., and Bahaari, R.M., "*Finite Element Prediction of End Plate Bolted Connection Behaviour Part I and II: Parametric Study, Analytical Formulation*", Journal of Structural Engineering, Vol. 123, No. 2, pp. 157-164, 165-175, 1997.
- 6.6 Baker, J.F., *Second Report*, Steel Structures Research Committee, Department of Scientific and Industrial Research, HMSO, London, 1934.
- 6.7 Rathburn, J., "*Elastic Properties of Riveted Connections*", Trans. American Society of Civil Engineers, Vol. 101, pp. 524-563, 1936.
- 6.8 Lionberger, S.R., and Waver, W., "*Dynamic Response of Frames with Non-rigid Connections*", Journal of Engineering Mechanics Division, ASCE, Vol. 95 (EM1), pp. 95-114, 1969.
- 6.9 Romstad, K.M., and Subramanian, C.V., "*Analysis of Frames with Partial Connection Rigidity*", Journal of Structural Division, ASCE, Vol. 96 (ST11), pp. 2283-2300, 1970.

- 6.10 Moncarz, P.D., and Gerstle, K.H., "Steel Frames with Non-Linear Connections", Journal of Structural Division, ASCE, Vol. 107 (ST8), pp. 1427-1441, 1981.
- 6.11 Frye, M.J., and Morris, G.A., "Analysis of Flexibly Connected Steel Frames", Canadian Journal of Civil Engineering, Vol. 2, pp. 280-291, 1975.
- 6.12 Jones, S.W., Kirby, P.A., and Nethercot, D.A., "Modelling of Semi-Rigid Connection Behaviour and its Influence on Steel Column Behaviour", In Joints in Structural Steelwork (ed. J.H. Howlett *et al.*), Pentech Press, London, pp. 5.73-5.87, 1981.
- 6.13 Ramberg, W., and Osgood, W.R., "Description of Stress-Strain Curves by Three Parameters", National Advisory Committee for Aeronautics, Technical Report 902, 1943.
- 6.14 Ang K.M., and Morris, G.A., "Analysis of 3-Dimensional Frames with Flexible Beam-Column Connections", Canadian Journal of Civil Engineering, Vol. 11, pp. 245-254, 1984.
- 6.15 El-Rimawi, J., "The Behaviour of Flexural Members Under fire Conditions", PhD. Thesis, Department of Civil Engineering, University of Sheffield, 1989.
- 6.16 Lothers, J.E., "Elastic Restraint Equations for Semi-Rigid Connections", ASCE, Vol. 1, pp. 480-502, 1951.
- 6.17 Lewitt, C.W., Chesson, E., and Munse, W., "Restraint Characteristics of Flexible Riveted and Bolted Beam-to-Column Connections", Bulletin No. 500, Engineering Experiment Station, University of Illinois, Chicago, 1969.
- 6.18 Chen, W.F., and Kishi, N., "Moment-Rotation Relation of Top and Seat Angle Connections", Department of Structural Engineering, Purdue University, Report CE-STR-87-4, 1987.
- 6.19 Johnson, R.P., and Law, C.L.C., "Semi-Rigid Joints for Composite Frames", In Joints in Structural Steelwork (ed. J.H. Howlett *et al.*), Pentech Press, London, pp. 3.3-3.19, 1981.

- 6.20 Yee, Y.L., and Melchers, R.E., "*Moment-Rotation Curves for Bolted Connections*", Journal of Structural Engineering, Vol. 112, No. 3, pp. 615-635, 1986.
- 6.21 "*EC3: Design of Steel Structures, Part 1.1: Revised Annex J Joints and Building Frames*", (Draft), Document CEN/TC250/SC3 N419E, European Committee for Standardization, 1994.
- 6.22 Wales, W.M., and Rossow, C.E., "*Coupled Moment-Axial Force Behaviour in Bolted Joints*", Journal of Structural Engineering, ASCE, Vol. 109, No. 5, pp. 1250-1266, 1983.
- 6.23 Kennedy, D.J.L., and Hafez, M.A., "*A Study of End-Plate Connections for Steel Beams*", Canadian Journal of Civil Engineering, Vol. 11, No.2, pp. 139-149, 1984.
- 6.24 Tschemmernegg, F., "*On the Nonlinear Behaviour of Joints in Steel Frames*", Connections in Steel Structures: Behaviour, Strength and Design (ed. R. Bjorhovde *et al.*), Elsevier Applied Science Publishers, pp. 158-165, 1988.
- 6.25 Tschemmernegg, F., and Queiroz, G., "*Mechanical Modelling of Semi-Rigid Joints for the Analysis of Framed Steel and Composite Structures*", Connections in Steel Structures III: Behaviour, Strength and Design (ed. R. Bjorhovde *et al.*), Proceedings of the Third International Workshop, Pergamon Publishers, pp. 237-247, 1995.
- 6.26 De Stefano, M., De Luca, A., and Astaneh-Asl, A., "*Modelling of Cyclic Moment-Rotation Response of Double-Angle Connections*", Journal of Structural Engineering, Vol. 120, No. 1, pp. 212-229, 1994.
- 6.27 Baniotopoulos, C.C., lecture notes from "*Semi-Rigidity in Connections of Structural Steelworks: Theory, Analysis and Design*", Advance Professional Training, Italy, 1999.
- 6.28 Bose, K.S., McNeice, M.C., and Sherbourne, A.N., "*Column Webs in Steel Beam-to-Column Connections, Part I-Formulation and Verification*", Computers and Structures, Vol. 2, pp. 253-279, 1972.

- 6.29 Bose, K.S., McNeice, M.C., and Sherbourne, A.N., "Column Webs in Steel Beam-to-Column Connexions, Part II-Design Recommendations", Computers and Structures, Vol. 2, pp. 281-301, 1972.
- 6.30 Hendrick, A., and Murray, M.T., "Column Web Compression Strength at End-Plate Connections", AISC, Engineering Journal, 3rd Quarter, pp. 161-169, 1984.
- 6.31 Patel, K.V., and Chen, W.F., "Non-Linear Analysis of Steel Moment Connections", ASCE, Journal of Structural Engineering, Vol 110 (ST8), pp. 1861-1875, 1984.
- 6.32 Atamiyaz Sibai, W., and Frey, F., "Numerical Simulation of the Behaviour up to Collapse of Two Welded Unstiffened One-Side Flange Connections", Connections in Steel Structures: Behaviour, Strength and Design (ed. R. Bjorhovde *et al.*), Elsevier Applied Science Publishers, pp. 85-92, 1988.
- 6.33 Richard, R.M., Gillet, P.E., Kreigh, I.D., and Lewis, B.A., "The Analysis and Design of Simple Plate Framing Connections", Engineering Journal, American Institute of Steel Construction, Vol. 17, No. 2, pp. 38-52, 1980.
- 6.34 Krishnamurthy, N., "Modelling and Prediction of Steel Bolted Connection Behaviour", Computers and Structures, Vol. 11, No. 2, pp. 75-82, 1980.
- 6.35 Sherbourne, N.A., and Bahaari, R.M., "3D Simulation of End Plate Connections", Journal of Structural Engineering, Vol. 120, No. 11, pp. 3122-3136, 1994.
- 6.36 Choi, C.K., and Chung, G.T., "Refined Three-Dimensional Finite Element Model for End-Plate Connection", Journal of Structural Engineering, Vol. 122, No. 11, pp. 1307-1316, 1996.
- 6.37 Bursi, S.O., and Jaspart, P.J., "Calibration of a Finite Element Model for Isolated Bolted End-Plate Steel Connections", Journal of Constructional Steel Research, Vol. 44, No. 3, pp. 225-262, 1997.

- 6.38 Troup, S., Xiao, Y.R., and Moy, J.S.S., "*Numerical Modelling of Bolted Steel Connections*", Journal of Constructional Steel Research, Vol. 46, No. 1-3, Paper No. 362, 1998.
- 6.39 Liu, T.C.H., and Morris, L.J., "*Theoretical Modelling of Steel Bolted Condition Under Fire Exposure*", Proc. of Int. Conf. on Comp. Mech., Vol. 1, 1994.
- 6.40 Liu, T.C.H., "*Finite Element Modelling of Behaviour of Steel Beams and Connections in Fire*", Journal of Constructional Steel Research, Vol. 36, No. 3, pp. 181-199, 1996.
- 6.41 Lawson, R.M., "*Behaviour of Steel Beam-to-Column Connections in Fire*", The Structural Engineer, Vol. 68, No. 14, pp. 263-271, 1990.
- 6.42 El-Houssieny, O.M., Abdel Salam, S., Attia, G.A.M., and Saad, A.M., "*Behaviour of Extended End Plate Connections at High Temperature*", Journal of Constructional Steel Research, Vol. 46, No.1- 3, 1998.
- 6.43 Al-Jabri, "*Behaviour of Steel and Composite Beam-Column Connections in Fire-Test Results*", Internal Report DCSE/97/F/7, University of Sheffield, 1997.
- 6.44 Ivanyi, M., lecture notes from "Semi-Rigidity in Connections of Structural Steelworks: Theory, Analysis and Design", Advance Professional Training, Italy, 1999.
- 6.45 Leston-Jones, C.L., and Lennon. T., "*Elevated Temperature Moment-Rotation Tests on Steelwork Connections*", Research Report DCSE/95/F/8, University of Sheffield, 1995.
- 6.46 Leston-Jones, C.L., "*Material and Geometrical properties for Elevated Temperatures Beam-Column Tests*", Research Report DCSE/96/F/02, University of Sheffield, 1996.

Chapter 7

Steel Joint Moment-Rotation-Thrust Response

7.1 INTRODUCTION

In the analysis of a frame, joints are routinely idealised as being either perfectly rigid or perfectly pinned. However, the real behaviour of a joint (the semi-rigid response) cannot be incorporated into an analysis unless it can be quantified accurately, which has proved to be a difficult task.

Studies of the response of steel frames to loading, not only at ambient temperature but also at elevated temperatures, have required experimental and analytical investigations of the behaviour of steel joints. It is well known that a complete structure behaves better than its individual members in isolation due to the influence of frame continuity. Unfortunately new fire resistance design codes have posed their basic calculation methods in terms of isolated members, and as a result the issue of restraint to thermal expansion has not been addressed at all. They do, however, allow designers to establish fire resistance, within their general principles, using validated procedures or suitable software. To examine the differences in behaviour between isolated members and members as parts of a completed frame, in particular the effect of restraint to thermal expansion, an 8-storey full-scale building frame was constructed in 1994 at BRE's Large Building Test Facility at Cardington^{7.1,7.2,7.3}.

Observations during the fire tests at Cardington suggest that it is inadequate to place reliance solely on the purely rotational characteristics of steel or composite joints, as found from furnace tests or numerical modelling. Local inelastic buckling of the lower flanges of the steel beams was seen on several occasions in heated zones which experience combined hogging action and axial compression due to restraint to thermal expansion. In some cases, again in zones of high restraint to thermal

expansion, partial-depth end plates have fractured adjacent to the weld during cooling when a member, which has undergone considerable compressive strain due to restrained thermal expansion in heating, contracts as it regains stiffness. The axial forces developed in the beam due to restraint to thermal expansion can change dramatically the frame response and it has become clear that the rotational behaviour of a joint depends on the local responses to the net axial forces in its parts, which provide the greatest contributions to strength and stiffness.

The main objectives of this chapter are to highlight and describe:

- a) The influence that an axial force can have on the moment-rotation characteristics of a steel joint,
- b) The frame response resulting from a finite element analysis that takes into account moment-rotation-thrust characteristics for the joints.

To fulfil the above objectives, first a simplified component-based model was developed to predict the moment-rotation-thrust characteristics for a steel joint, and secondly a finite element analysis was performed on a 2D frame, using the finite element package VULCAN, developed at the University of Sheffield in order to model frame behaviour in fire conditions. The two different joint configurations that were taken into account in the finite element analysis are shown in Figure 7.1 below.

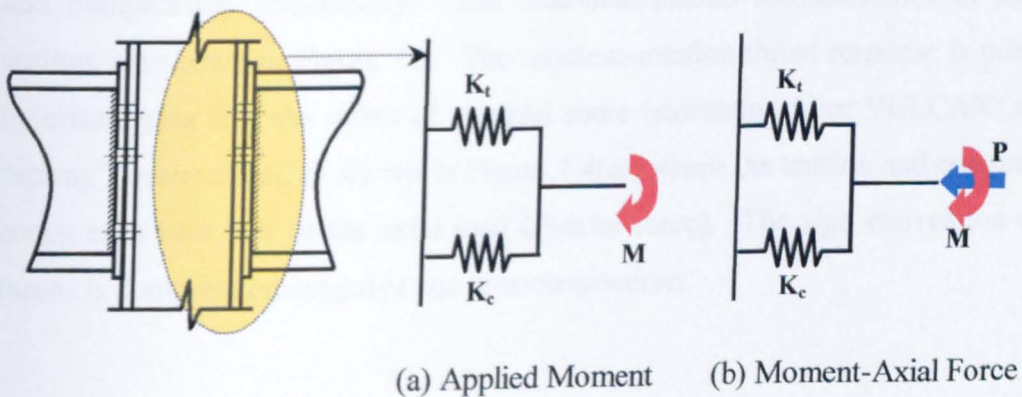


Figure 7.1 Moment-Rotation and Moment-Rotation-Thrust configuration of a steel joint

7.2 MOMENT-ROTATION-THRUST MODEL

When considering frame response at elevated temperatures it is necessary to consider axial forces which are developed due to the restraint to expansion of the heated beam because of the adjacent cooler frame elements. These axial forces are transferred through the joints, resulting in modification of their moment-rotation characteristics.

One simple way to include these axial forces into the component-based model (as described in Chapter 6) is outlined next. Ideally, an analysis would permit the use of non-linear horizontal "springs" directly in modelling of structural sub frames, rather than using them to attempt to construct four-dimensional moment-rotation-thrust-temperature surfaces for each type of steel joint. However, in the finite element program VULCAN used to observe the response of a steel sub frame under fire conditions, it was necessary to input a moment-rotation curve, modified if necessary for the effects of temperature and axial force.

Considering the joint arrangement described in Chapter 6, the component-based model (as shown in Figure 7.2) idealises the beam-to-column joint as two rigid bars connected by two non-linear springs simulating the tension and the compression zones. In this figure K_t and K_c are the tension and compression zone spring stiffnesses respectively, z is the lever arm and the subscripts t and c denotes tension and compression respectively. The load-deformation characteristics of the two springs are shown in Figure 7.3. The moment-rotation-thrust response is predicted by considering first the effect of an axial force (calculated from VULCAN) on the "spring" arrangement, as shown in Figure 7.4(a), where the tension and compression zones each take half of the axial load (P -axial force). The sign convention of the forces is compression=negative and tension=positive.

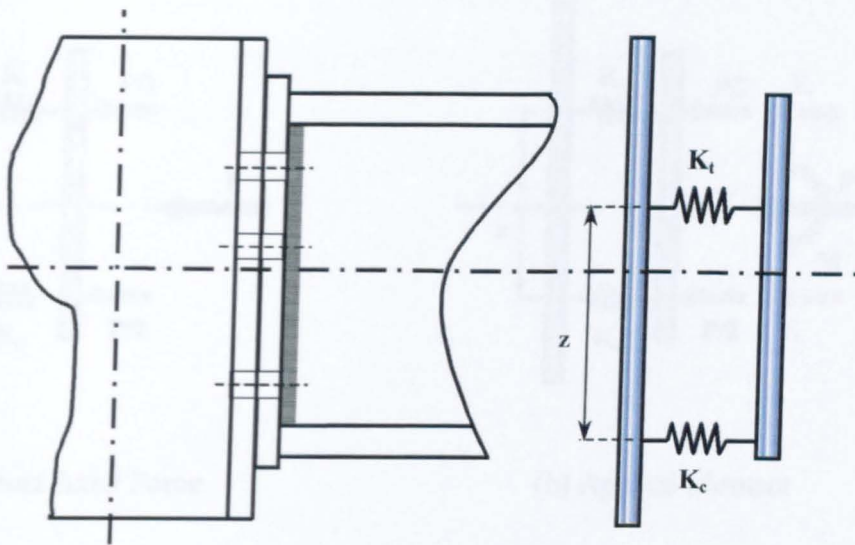


Figure 7.2 Idealised bare-steel spring stiffness model

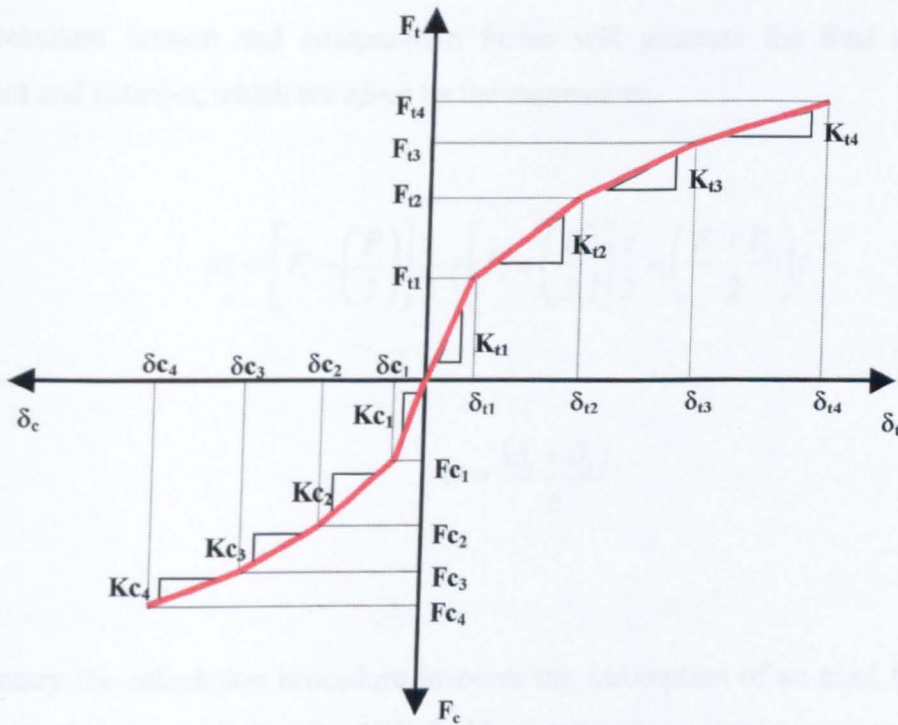


Figure 7.3 Load-deformation characteristics of the tension and compression zones

The next step is to consider an applied moment, which generates another set of tension and compression forces as shown in Figure 7.4(b).

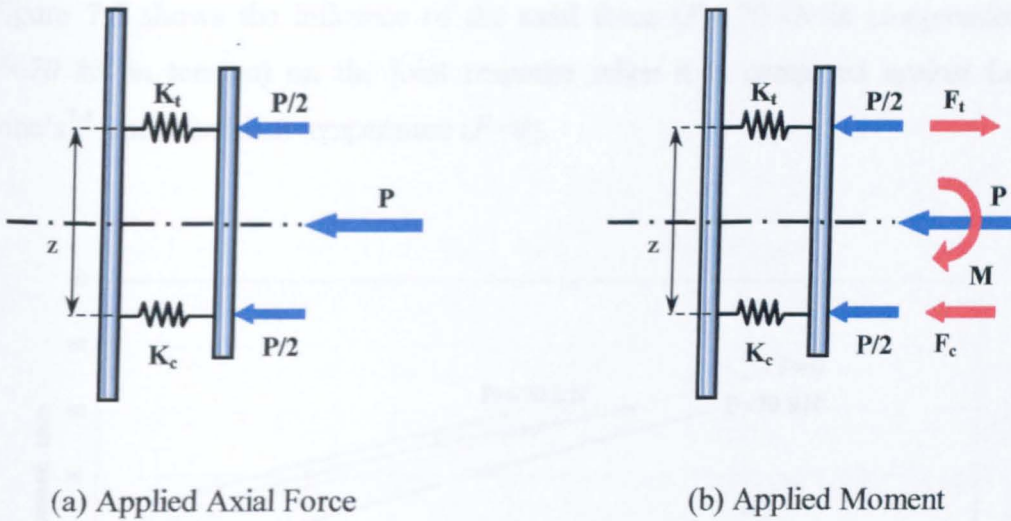


Figure 7.4 Idealised bare-steel moment-axial force model

The resultant tension and compression forces will generate the final steel joint moment and rotation, which are given by the expressions:

$$M = \left[F_t - \left(\frac{P}{2} \right) \right] \frac{z}{2} + \left[F_c + \left(\frac{P}{2} \right) \right] \frac{z}{2} = \left(\frac{F_t + F_c}{2} \right) z \quad \dots 7.1$$

$$\Phi = \frac{(\delta_t + \delta_c)}{z} \quad \dots 7.2$$

In summary the calculation procedure involves the assumption of an axial force (or an estimate from an analysis using VULCAN) and then for a given moment value the resultant tension and compression forces can be calculated. The displacements corresponding to those forces are predicted from the Load-Deformation characteristics of each zone (Figure 7.3) within a joint, and finally the rotation is calculated according to those displacements.

Figure 7.5 shows the influence of the axial force ($P=-70$ kN in compression and $P=70$ kN in tension) on the joint response when it is compared against Leston-Jone's^{7.4} test at ambient temperature ($P=0$).

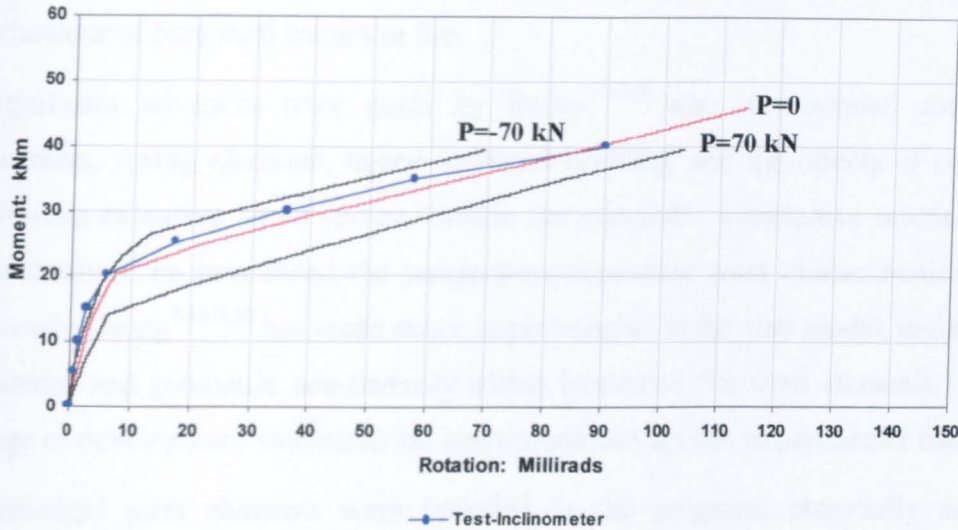


Figure 7.5 Influence of axial force on rotation behaviour at ambient temperature

It is obvious from Figure 7.5 that the axial force P has a significant influence on the moment-rotation characteristics of the joint. The differences are in terms of stiffness, ultimate moment and rotational capacity of the joint.

7.3 DESCRIPTION OF THE FINITE ELEMENT PROGRAM VULCAN

Despite the availability of general-purpose finite element packages that can simulate the effect of joints within structural frames at elevated temperatures, research-oriented models are often preferable due to their reduced computing requirements. During the last few years, significant advances have been made at the University of Sheffield in two and three-dimensional computer modelling of structural frame behaviour under fire conditions using the finite element program developed by Bailey^{7.5}.

The program was originally based on an existing two-dimensional program, INSTAF, developed by El-Zanaty and Murray^{7.6} to investigate the response of steel frames at ambient temperatures, incorporating geometrical non-linearity and the spread of yield. It was subsequently extended by Saab^{7.7} in 1990 to include elevated temperature material properties and Najjar^{7.8} proceeded to include three-dimensional behaviour of bare steel frames in fire.

Significant advances were made by Bailey^{7.5,7.9} who incorporated simple slab elements, spring elements, lateral torsional buckling and the effects of cooling by allowing extensive strain reversal within the material's constitutive relationship^{7.10}. Furthermore he introduced the temperature-dependent joint characteristics. More recently Haung^{7.11,7.12} has made major improvements to the slab model, incorporating material and geometric non-linearity within laminated flat shell elements. At each stage of development validation has been conducted against experimental data.

Semi-rigid joint elements were included in the program, essentially as spring elements to which non-linear characteristics could be assigned to any degree of freedom at a node and which could degrade with temperature. So far only rotational characteristics have been assigned to these joint elements in frame modelling. The same spring elements have been used in the current parametric study which investigates steel frame response at elevated temperatures, but the moment-rotation characteristics were calculated using the component model as described in Chapter 6, except that on this occasion the axial forces due to thermal expansion of the beam were taken into account.

7.3.1 Parametric studies on sub-frame arrangement

The analysis of sub-frames, as opposed to complete structures, is preferable in terms of computational requirements. Also the number of runs required to investigate fully the influence of semi-rigid joint characteristics on sub-frame behaviour is smaller than for a complete frame. For these reasons, when conducting a parametric study it is very useful to consider "representative" sub-frames instead of a complete frame.

A number of sub-frames have been suggested as being suitable for modelling beam response in rigidly jointed frames in BS5950^{7.13} as shown in Figure 7.6.

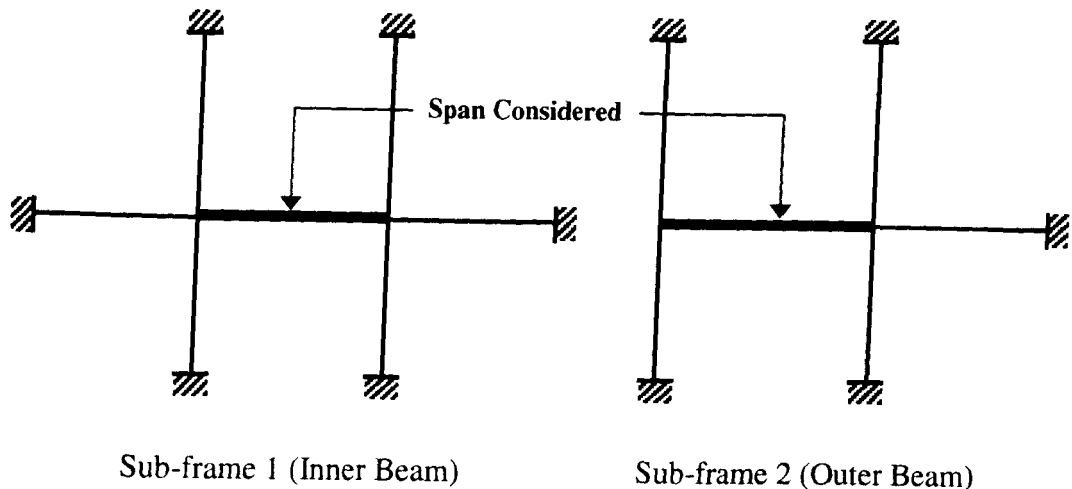


Figure 7.6 Sub-frame idealisations considered in BS5950

El-Rimawi^{7.14} performed analytical studies to demonstrate that the forms of sub-frames shown in Figure 7.6 are capable of producing results that are reasonably comparable with those from full-frame analysis, based on studies of the response of the Cardington full-scale frame^{7.1} subjected to elevated temperatures.

Further extensive parametric studies have been conducted^{7.4,7.6,7.15} using similar sub-frame arrangements to investigate the influence of joint characteristics on beam performance at elevated temperatures, using either experimental or postulated moment-rotation characteristics.

A sub-frame layout used in an experimental and analytical study conducted by Sheffield and Manchester Universities^{7.16,7.17}, which investigated the behaviour of axially restrained steel beams in fire, has been adopted in the present study in order to observe the influence of coupling between axial force and moment on the behaviour of the frame under increasing temperatures.

The experimental investigation was performed on a “rugby” goal-post structure arrangement, shown in Figure 7.7. The main objective was to measure axial forces due to the restraint to expansion of the heated steel beam, so the columns and joints were well protected against temperature rise to avoid local failures. The tests did not provide enough information to compare the test results with the current finite element results, taking into account the joint moment-rotation-thrust characteristics.

However it was considered an advantage to use the same joint configurations because the magnitudes of the beam axial force obtained from the elevated temperature tests had been validated against VULCAN finite element results.

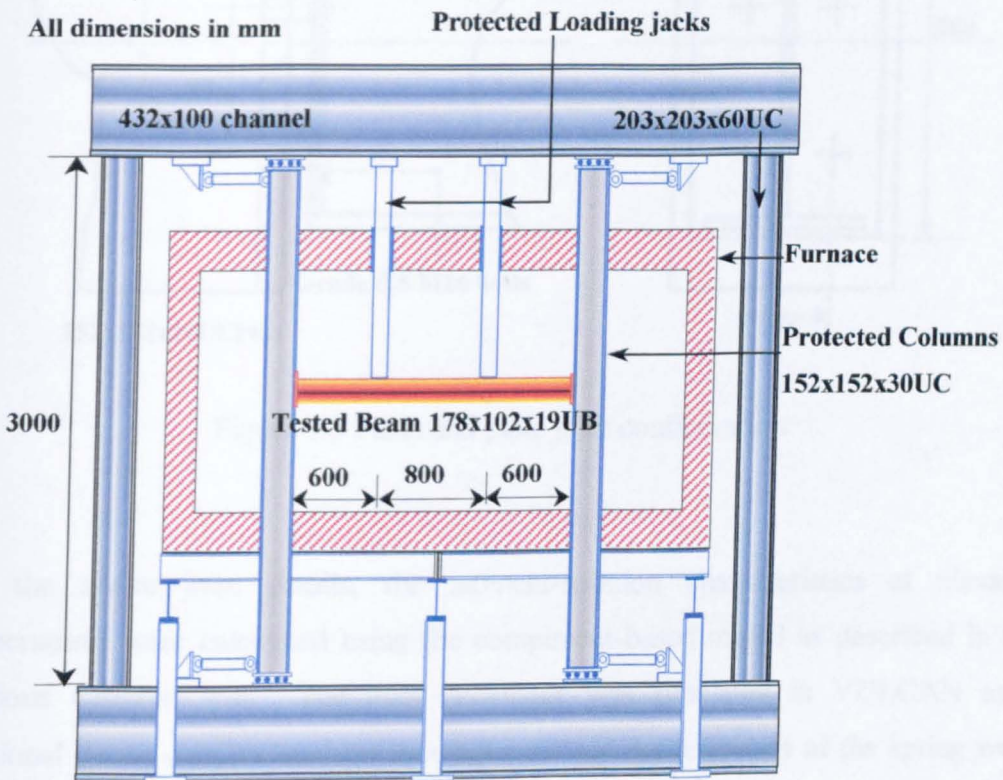


Figure 7.7 Testing arrangement

The columns of the “rugby” goal-post structure arrangement were secured in position at the top and bottom by four pin load-cells and the transverse load on the beam was applied using two independent hydraulic jacks. The joint configuration used in the experimental investigation is shown in Figure 7.8.

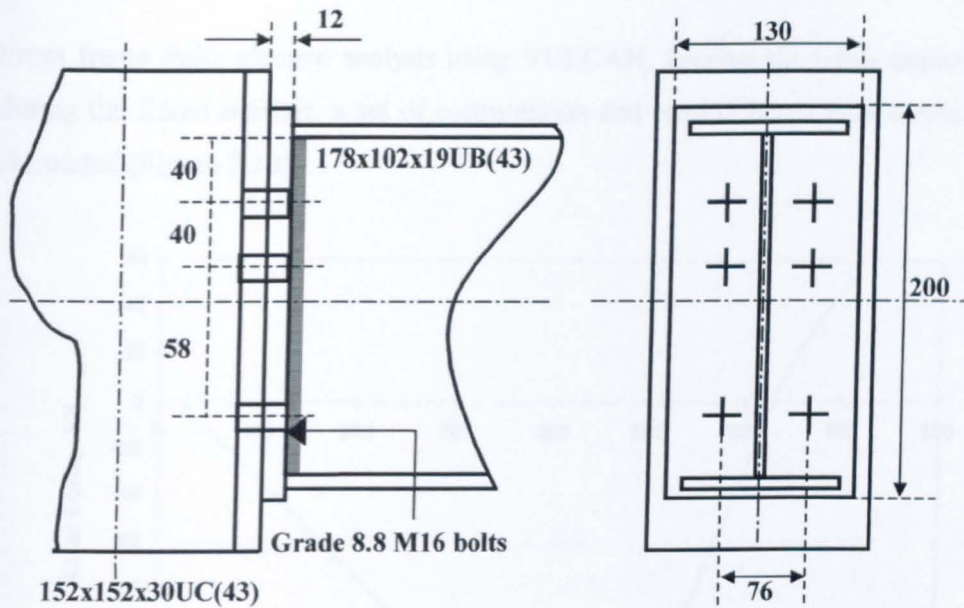


Figure 7.8 Flush end plate joint configuration

For the above joint details, the moment-rotation characteristics at elevated temperatures were calculated using the component-based model as described in the previous Chapters 4-6. The joint behaviour was simulated in VULCAN as a rotational spring element, and the moment-rotation characteristics of the spring were presented as Ramberg-Osgood functions, shown in Figure 7.9.

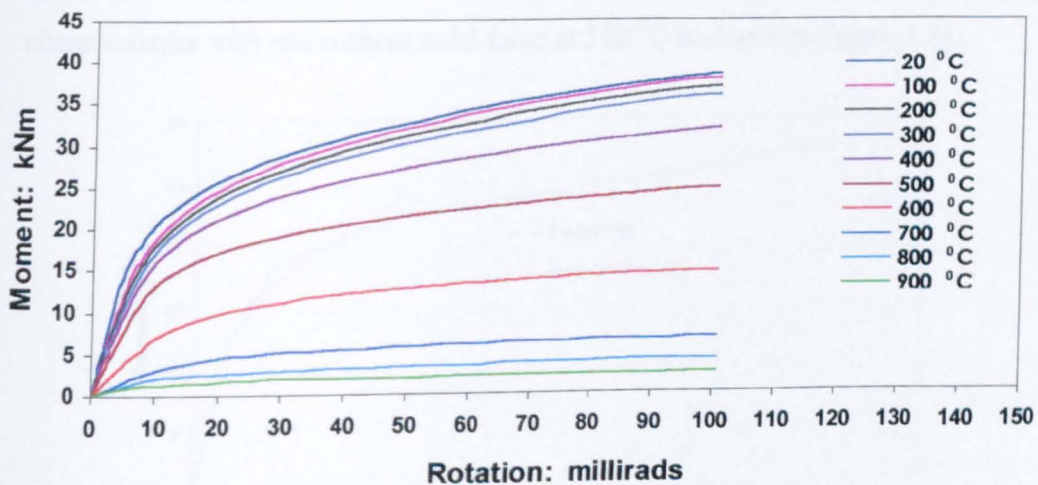


Figure 7.9 Ramberg-Osgood curves at elevated temperatures

From frame finite element analysis using VULCAN, keeping the joints unprotected during the frame analysis, a set of compression and tension beam axial forces were calculated (Figure 7.10).

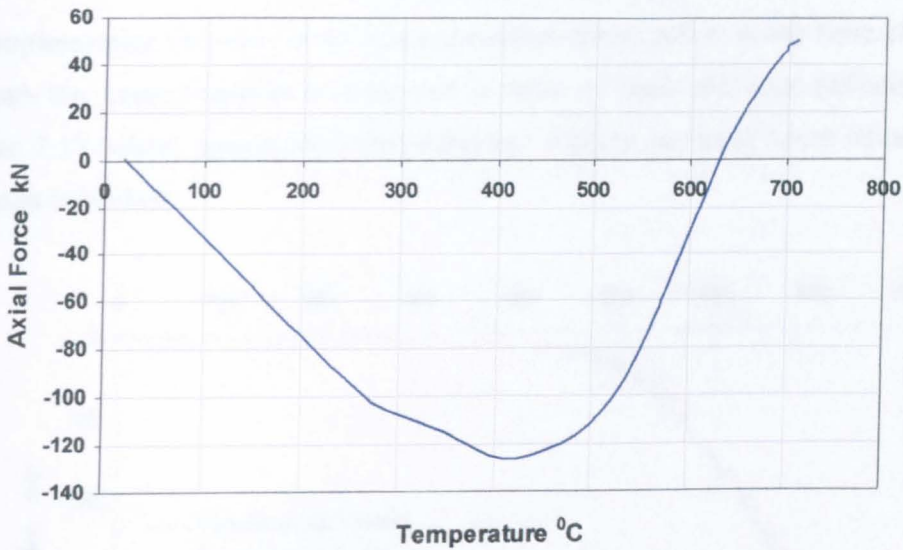


Figure 7.10 Axial forces in beam at elevated temperatures (Positive=tension)

Using these axial forces in the component-based model described earlier in this chapter, which takes into account the axial forces, a new set of moment-rotation-thrust curves were predicted at elevated temperatures. A typical comparison of joint characteristics with and without axial force at 500 °C is shown in Figure 7.11.

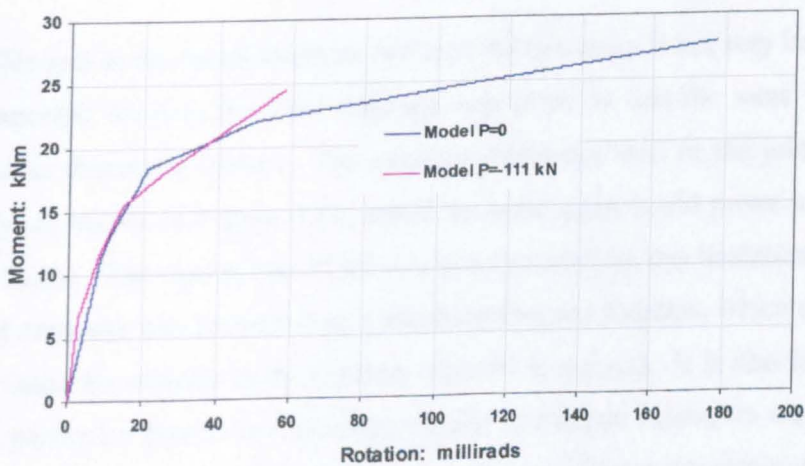


Figure 7.11 Influence of axial force on joint behaviour at 500 °C

From the comparison above it is obvious that for this particular joint there is no significant difference in the joint stiffness when the axial compression force of $P=-111$ kN is considered. The differences are more obvious in terms of ultimate moment capacity and, more importantly, in terms of joint rotational capacity.

By implementing the new set of moment-rotation-thrust curves in the finite element analysis the frame response is compared in terms of beam mid-span deflections in Figure 7.12 below, against the frame behaviour without any axial forces influencing the joint behaviour.

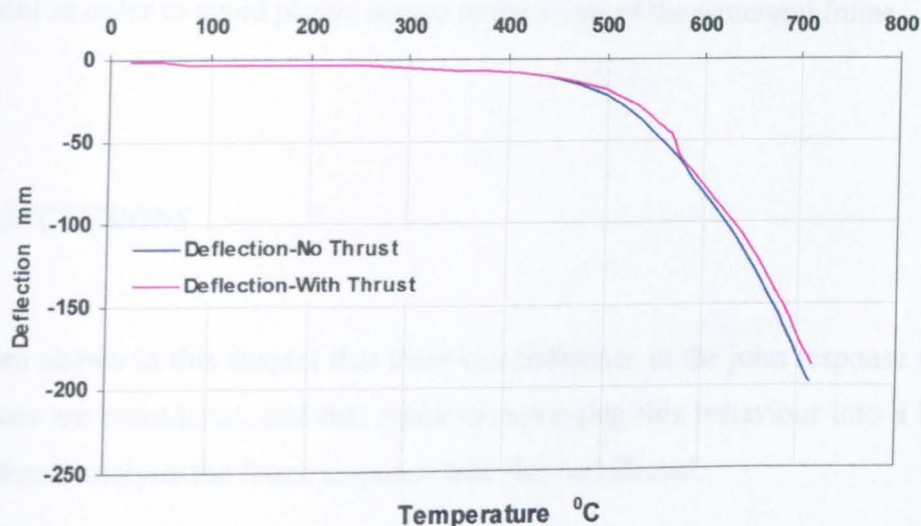


Figure 7.12 Comparison of frame response when axial forces are considered

The difference in the frame response between the two cases is not very large, but this is as expected because the joint response was more or less the same in terms of stiffness as described earlier. The obvious difference was in the joint rotational capacity, as shown in Figure 7.11, which in some cases could prove to be a very critical factor. The reason that VULCAN is not picking up this limitation is because the joint response was presented as a Ramberg-Osgood function, which results in an infinite value for rotation as the ultimate capacity is reached. It is also believed that for this particular frame, in which the restraint to thermal expansion was prevented only by the bending stiffness of the columns, the axial forces developed in the beam

(Figure 7.10) were not of sufficient magnitude to create a significant change in the overall behaviour of the frame under fire conditions.

The failure mode for this particular joint, predicted from the component analysis, was by yielding of the column web under transverse compressive forces. It is very important to notice the rotational capacity of the joint, which is limited to 58 *millirads* when $P = -111.48 \text{ kN}$ (compressive force) is applied to the joint. From the designer's point of view it is very important to recognise these limitations in order to be in a position to decide whether to fire-protect the column web or any other critical component in order to avoid plastic hinges in the joints of the structural frame.

7.4 CONCLUSIONS

It has been shown in this chapter that there is a difference in the joint response when axial forces are considered, and that when incorporating this behaviour into a finite element frame analysis the frame response will also be affected.

It is very important to consider rotational capacity when simulating moment-rotation-thrust joint characteristics, because in some cases this could prove to be a limiting factor in the overall frame response. These limitations should be avoided, and the advantage of using a component-based model is that it can predict the failure mode of a joint with reasonable accuracy so that the critical components can be identified and fire-protected in real fire scenarios.

As a concluding remark, further finite element studies should be performed, with and without fire-protected joints, in order to understand better the overall behaviour of a structural frame. The use of non-linear horizontal "springs", to represent the major zones within a joint, would in fact be a better simulation of a joint if used directly in a finite element analysis of structural sub frames, rather than using only one rotational spring element per joint.

7.5 REFERENCES

- 7.1 Armer, G.S.T., and Moore, D.B., "*Full-Scale Testing on Complete Multi-Storey Structures*", *The Structural Engineer*, Vol. 72, No. 2, pp. 30-11, 1994.
- 7.2 Moore, D.B., and Lennon, T., "*Fire Engineering Design of Steel Structures*", *Progress in Structural Engineering and Materials*, Vol. 1, No. 1, pp. 4-9, 1997.
- 7.3 Bailey, C.G., Lennon, T., and Moore, D.B., "*The Behaviour of Full-Scale Steel-Framed Buildings Subjected to Compartment Fires*", *The Structural Engineer*, Vol. 77, No. 8, pp. 15-21, 1999.
- 7.4 Leston-Jones, L.C., "*The Influence of Semi-Rigid Connections on the Performance of Steel Framed Structures in Fire*", Ph.D. Thesis, Department of Civil and Structural Engineering, University of Sheffield, 1997.
- 7.5 Bailey, C.G., "*Simulation of the Structural Behaviour of Steel-Framed Buildings in Fire*", Ph.D. Thesis, Department of Civil and Structural Engineering, University of Sheffield, 1995.
- 7.6 El-Zanaty, M.H., and Murray, D.W., "*Non-Linear Finite Element Analysis of Steel Frames*", *Journal of Structural Division, ASCE*, Vol. 109(ST2), pp. 353-368, 1983.
- 7.7 Saab, H.A., "*Non-Linear Finite Element Analysis of Steel Frames in Fire*", Ph.D. Thesis, Department of Civil and Structural Engineering, University of Sheffield, 1990.
- 7.8 Najjar, S.R., "*Three-Dimensional Analysis of Steel Frames and Sub-Frames in Fire*", Ph.D. Thesis, Department of Civil and Structural Engineering, University of Sheffield, 1994.
- 7.9 Bailey, C.G., Burgess, I.W., and Plank, R.J., "*Computer Simulation of a Full-Scale Structural Fire Test*", *The Structural Engineer*, Vol. 74, No. 6, pp. 93-100, 1996.

- 7.10 Bailey, C.G., Burgess, I.W., and Plank, R.J., "*Analyses of the Cooling and Fire Spread on Steel-Framed Buildings*", Fire Safety Journal, Vol. 26, pp. 273-293, 1996.
- 7.11 Haung, Z., Burgess, I.W., and Plank, R.J., "*Finite Element Modelling of Composite Frame Behaviour Subjected to Fire*", Proceedings 2nd European Conference on Steel Structures (EUROSTEEL99), Prague, May 26-29, pp. 611-614, 1999.
- 7.12 Haung, Z., Burgess, I.W., and Plank, R.J., "*Three-Dimensional Analysis of Composite Steel-Frame Buildings in Fire*", Journal of Structural Engineering, Vol. 126, No. 3, pp. 389-397, 2000.
- 7.13 "*BS5950 Structural Use of Steelwork in Building: Part 1: Code of Practise for Design in Simple and Continuous Construction*", British Standard Institution, London, 1985.
- 7.14 El-Rimawi, J.A., Burgess, I.W., and Plank, R.J., "*Modelling the Behaviour of Steel Frames and Sub-Frames with Semi-Rigid Connections in Fire*", Research Report DCSE/93/S/02, Department of Civil and Structural Engineering, University of Sheffield, April 1993.
- 7.15 Al-Jabri, K.S., Lennon, T., Burgess, I.W., Plank, R.J., "*Behaviour of Steel and Composite Beam-Column Connections in Fire*", Journal of Constructional Steel Research, Vol. 46, No. 1-3, 1998.
- 7.16 Allam, A.M., Fahad, M.K., Liu, T.C.H., Burgess, I.W., Plank, R.J., and Davies, J.M., "*Effects of Restraint on the Behaviour of Steel Frames in Fire*", Eurosteel Conference, No. 64, Turkey, 2000.
- 7.17 Liu, T.C.H., Fahad, M.K., and Davies, J.M., "*Experimental Investigation of Behaviour Axially Restrained Steel Beams in Fire*", In press.

Chapter 8

Conclusions and Further Recommendations

8.1 INTRODUCTION

To date the provision of adequate fire resistance for steel and composite framed structures has involved the use of insulating material for the protection of structural members such as beams, columns, slabs etc. Engineers design the structural frame for normal conditions and then apply fire protection, resulting in an increase of the structure's overall cost. This is analogous to designing a building to withstand wind loading by enclosing it within a four-sided wall.

It is more logical from an engineering perspective to design the structure to withstand fire. A new design approach is emerging in which buildings are designed on the basis of the real strength of the structure under fire conditions, as is done for other limit states. This design approach comes under the new Fire Safety Engineering concept and as Green *et al.*^{8.1} highlights, the potential benefits are many and varied:

- a) Opportunities to reduce capital cost whilst maintaining safety,
- b) The development of design solutions that enable the speed of construction to be increased,
- c) Improvement of safety in the most cost effective way,
- d) Opportunity to create a closer relationship and synergy between the design and the management of a building,
- e) Support for the concept of construction as a manufacturing process,
- f) A simple means for construction and for clients to innovate.

In the last two decades this concept has been applied to investigations on different isolated structural elements under fire conditions. It was soon realised that real

frames, both bare-steel and composite, survive better under fire scenarios than the responses of isolated members would suggest. This is partly because structural members such as beams, columns and floor slabs interact with each other, enhancing the frame resistance.

The above remark indicates the importance of structural joints on the overall response of a frame under fire conditions, and when one considers that the behaviour of a joint is still the product of the responses of different zones within it under the effects, basically, of horizontal tension or compression, it becomes apparent that a breakdown of the joint into “components” (EC3: Annex J^{8.2}) would be very advantageous.

The current study has concentrated on investigating *experimentally* and *analytically* the different zones and the components within these zones in order to develop a component-based model to represent the behaviour of end-plate joints in fire conditions. The principles will establish the initial steps in a modelling technique for other types of joints, avoiding large numbers of tests in order to collect data on one particular joint arrangement.

8.2 EXPERIMENTAL AND ANALYTICAL INVESTIGATION ON COMPONENTS

Initially a series of furnace tests were carried out on simple components representative of the major zones of tension and compression within a typical end-plate joint. These were kept fairly small, and were not very complex to perform, being tested in uniaxial tension or compression. The complex part was to develop an efficient testing arrangement and a robust instrumentation layout in order to carry out the large number of high-temperature component tests.

8.2.1 Instrumentation and testing arrangement

The experimental investigation was carried out using a testing arrangement and instrumentation which were purpose-designed by the author. Although initially

designed specifically for the current high-temperature study, the instrumentation system provides a good alternative for ambient-temperature testing as well.

To date, testing of structural elements or frames at elevated temperatures has involved the use of displacement transducers, dial gauges, “dumb bells” or inclinometers in order to measure displacements and rotations. The advantage of using these devices is that they provide accurate and sensitive measurements. On the other hand much effort and time has been devoted to fire protection, not only of the actual device but also of the wiring which connects the device to the data logger, and often several devices are lost during a fire test due to the hostile environment found inside a furnace.

For this reason a displacement measurement device^{8.3,8.4} which is new to fire engineering testing was investigated and applied. This gave the accuracy, sensitivity and robustness needed to carry out successfully the numerous elevated-temperature component tests. The image acquisition and processing technique involved taking images at different load steps, for a particular high-temperature component test, and then processing the images using image processing software, and finally recording the displacement results in an output file.

In order to use this technique, the furnace needed to be purpose-built and designed, to give a clear view of the specimen and to accommodate the video cameras for capturing the images. An electric furnace capable of reaching 1100 °C was used, with one cubic metre capacity and view-ports in front and on top for the video cameras. It also included a fan, which helped to keep the temperature inside the furnace uniform. The tension and compression forces were applied, using a hydraulic jack having 500 kN capacity, driven by a Kelsey controller. The actual testing procedure was to take the specimen up to temperature, and then to apply the load steps and at the same time capture the images.

This technique works in favour of long-term elevated-temperature testing because no devices are placed inside the furnace so that they are not exposed to the very high temperatures, and also nothing is attached to the specimen which could alter the properties of the specimen.

The advantages of using the image acquisition and processing technique are:

- a) The availability of information in two directions, so it is possible to measure displacements in the transverse direction simultaneously, if needed,
- b) The entire testing procedure can be video-recorded, making it possible to go back and collect more information by re-examining the behaviour of the specimen,
- c) It offers the possibility of better long-term stability than contacting methods (no creep of rods).

The technique worked well, performing reliably and accurately throughout the whole experimental investigation. It also provides extra information, such as the failure path of the specimen, by reviewing the images at different load steps. This information would otherwise be difficult to capture.

Another important remark concerning the instrumentation and testing arrangement was the development of the halogen lamp furnace, which was used to study the behaviour of Grade 8.8 bolts at elevated temperatures^{8.5}. The furnace was very cheap to construct and was able to reach a specimen temperature of around 1200 °C. Although it was developed for an MSc. project and could perform only isothermal tests, (where the specimen was subjected to a constant temperature, stabilized, and then tensile load was applied) the furnace has the potential for development and further calibration, using a temperature controller and a voltage-control dimmer, in order to follow a standard fire curve. In this way an anisothermal (transient) test could be performed, where the specimen is subjected to a constant load and the temperature is increased at a pre-determined-rate, with the resulting strains being recorded.

8.2.2 Tension zone

The first elevated temperature tests were performed on T-stub specimens which simulate the tension zone within a steel joint. The three major components within a tension zone are:

- a) End plate in bending,
- b) Column flange in bending,

c) Bolts in tension.

In total 45 specimens were tested at elevated temperatures, the main objective being to investigate the three failure modes shown in Figure 8.1.

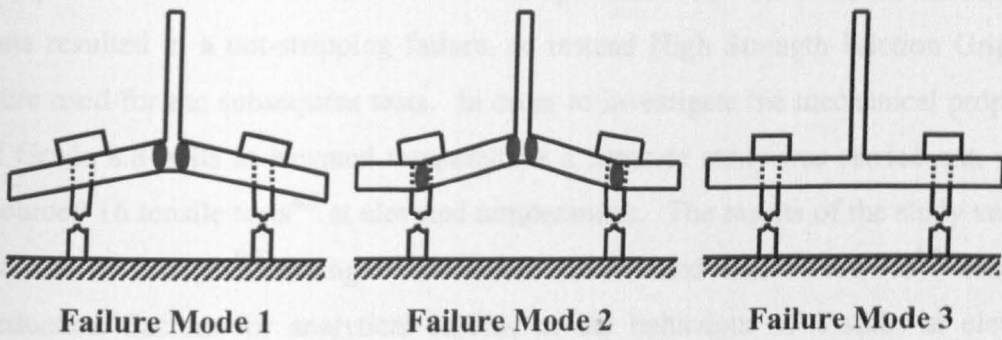


Figure 8.1 Failure modes for the T-stub flange

The specimen temperatures ranged from 20 °C to 800 °C and were measured using Type K thermocouples placed at different positions within the flange and bolts. The last 25 T-stub specimens were connected in the arrangement shown in Figure 8.2 below, that could be found in a real frame.

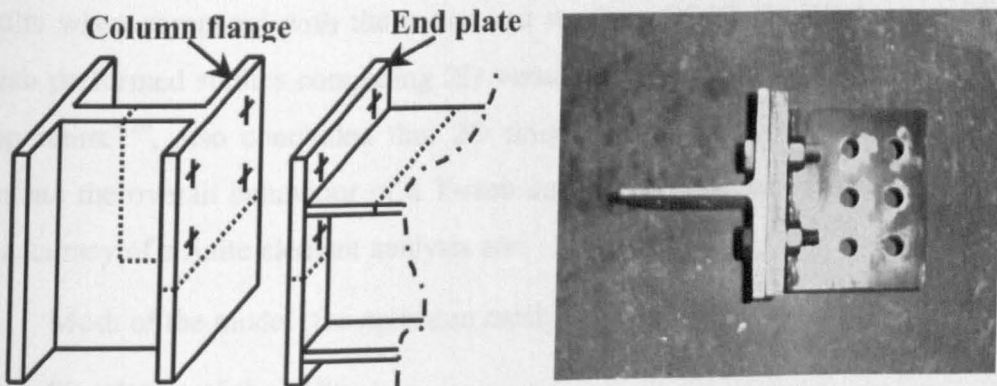


Figure 8.2 T-stub identification and orientation for extended end-plate joint

With the above arrangement prying forces can still be developed, and due to the different geometrical and mechanical properties of the end plate and column flange

T-stubs, the failure modes can sometimes be different between them. These failure modes were recorded and measured, in both directions, by the use of the image acquisition and processing technique.

From the first tests at elevated temperatures it was obvious that bolt flexibility was a key parameter in the behaviour of a T-stub specimen. The use of Grade 8.8 bolts and nuts resulted in a nut-stripping failure, so instead High Strength Friction Grip nuts were used for the subsequent tests. In order to investigate the mechanical properties of Grade 8.8 bolts at elevated temperatures a separate study was carried out, which included 16 tensile tests^{8.5} at elevated temperatures. The results of the study verified the use of Kirby's^{8.6} Strength Reduction Factors and EC3's:Part 1.2^{8.7} Stiffness Reduction Factors for analytical studies of the behaviour of T-stubs at elevated temperatures.

From the analytical part of the investigation, a simplified model has been developed using plastic theory and mechanics^{8.8,8.9}. The model has been extended to predict the three failure modes of the T-stub specimen from the geometrical and mechanical properties at ambient and elevated temperatures. Furthermore the load-deflection results, when compared against the actual elevated-temperature tests, were in acceptable agreement considering the complexity of the problem resulting from the interaction of flange and bolt forces and the added elevated-temperature factor.

In contrast the 2D finite element analysis using ANSYS did not generate very good results when compared with the actual test results. COST C1 Workgroup (WG6), which performed studies comparing 2D versus 3D modelling on T-stubs at ambient temperature^{8.10}, also concluded that 2D finite element analysis is not adequate to simulate the overall behaviour of a T-stub under tension force. Factors influencing the accuracy of a finite element analysis are:

- a) Mesh of the model (the optimum mesh size),
- b) Simulation of the bolts,
- c) Choice of elements,
- d) Material behaviour,
- e) The contact and gap element simulation between bolts and flange (the most important factor).

8.2.3 Compression zone

One of the most important components when investigating steel joints at elevated temperatures is the column web under transverse compression forces.

The main objective during the compression component investigation was to determine the ultimate capacity and observe the behaviour of the column web under fire conditions. For this reason a total of 29 column tests were performed at ambient and elevated temperatures covering a broad range of web local buckling ratios (d/s , where d is the depth between fillets and s is the web thickness) from 12.7 to 22.3^{8.11}. By the early stages of this experimental investigation it was realized that the ultimate load capacity of the column web was determined by the strength characteristics of the specimen. The column sections have thick webs compared to their height, so elastic buckling was unlikely to happen.

It was also realized that the current design codes, BS5950^{8.12} and EC3:Annex J^{8.13} gave very conservative results for the ultimate capacity of the column section under compression forces at ambient temperature when compared with test results. That was a major disadvantage, especially when it was proven later in the experimental investigation that the ultimate capacity of a column section at elevated temperatures could be calculated by multiplying the ultimate force at ambient temperature by the average value of the two reduction factors, one for strength (at 2% strain) and the second for stiffness, given in EC3:Part 1.2^{8.9}.

As a result of the discrepancies between the current design codes and the test results, a simplified semi-empirical model has been described in Chapter 5, which predicts the overall behaviour of the column web at ambient and elevated temperatures. A revised empirical formula has also been proposed, based on the results from studies of partial edge loading on thick plate girder webs^{8.14}. The formula predicts the ultimate web capacity, and correlates well with the actual elevated-temperature test results.

Most importantly the results from a 2D finite element analysis^{8.15} of column webs under transverse compressive forces highlighted the advantage of using 2D models in order to predict accurately the behaviour of the column web component at elevated temperatures, without resorting to expensive and complex testing.

8.3 JOINT MODELLING AND FRAME RESPONSE

Defining a suitable expression to represent the joint characteristics at elevated temperatures is important for incorporation within analytical analysis. The form of expression should represent the joint response in terms of the main parameters, such as initial stiffness and moment capacity, and should have the capability of representing the entire non-linear moment-rotation response.

Having investigated experimentally and analytically the main components within the tension and compression zones, the principles of the component-based model were applied to predict the moment-rotation behaviour of a joint at elevated temperatures. The behaviour of a joint as a whole may be obtained by superposing the stiffnesses of individual components in the compression and tension zones. This assumes that the interaction between connected components has a negligible effect on the response of individual components.

The moment-rotation results obtained from the component-based model, when compared against ten elevated-temperature tests conducted by Al-Jabri^{8.16} and Leston-Jones^{8.17}, were very encouraging. Two flush end plate joint arrangements were tested, and these arrangements represent a large percentage of joints used in real steel frame buildings.

The joint components were tested and analytically investigated up to their failure point, giving an advantage to the component-based model in accurately predicting the failure mechanism and the level of moment and rotation that a particular joint can sustain.

Another advantage of analysing a steel joint at elevated temperatures by dividing the different zones into components is that a full temperature profile can be implemented into the component-based model, making the representation of moment-rotation characteristics more accurate and realistic.

Finally the influence of axial forces on joint response and overall frame behaviour is highlighted in Chapter 7. It is important to consider these tensile or compressive axial forces when predicting steel joint behaviour, because they could reduce the rotational ductility of the joint and limit the ductility of the structural frame. The problem is more pronounced at elevated temperatures where high axial compression

forces could be developed in the initial stages of a fire scenario and thus reduces joint ductility to a minimum. It is very important for designers to recognise these critical ductile components in order to fire-protect them and thus avoid premature failure of the steel joints when frame analysis is carried out at elevated temperatures. The component-based model, described in this study, is capable of providing this information with acceptable accuracy.

8.4 RECOMMENDATIONS FOR FURTHER WORK

The current study was the first step in demonstrating the potential for incorporating component-based models in order to predict steel joint behaviour at elevated temperatures. Having the advantage of being able to predict the behaviour of any joint arrangement under fire conditions from geometrical and mechanical properties minimises the need to carry out costly, time consuming and complex tests at elevated temperatures.

Major components within a steel joint, in the tension and compression zones, were tested and analytically investigated. Furthermore load-deformation characteristics for individual or groups of components at elevated temperatures have been collected for the first time. There remain other components, which will need experimental and analytical investigation. These are the beam flange in compression, the beam web in tension and compression, and finally the column panel in shear.

The influence of compressive axial force on joint response is very important, especially when this force could result in column web or beam bottom flange local inelastic buckling failure. The latter failure has been observed in the Cardington fire tests in several cases, proving that high axial compression forces can be developed at elevated temperatures. This local inelastic buckling of the lower flange of the beam needs to be further investigated experimentally and analytically because in some cases it could limit the ductility of a steel joint.

The assessment of the influence of joint response on the frame behaviour has been limited by the quantity of available test data, although initial studies based on postulated moment-rotation-temperature characteristics concluded that this would be

beneficial to the fire resistance of steel structures due to the rigidity of “simple” joints. Future experimental and analytical research into the response of joints at elevated temperatures should take into consideration the effects of structural continuity and restraint to thermal expansion. Also analytical studies on the frame response under fire conditions should be carried out considering the zones involved within a joint arrangement (tension, compression and shear zone) as “springs” with predetermined force-deflection characteristics resulting from component studies as shown in Figure 8.3 below.

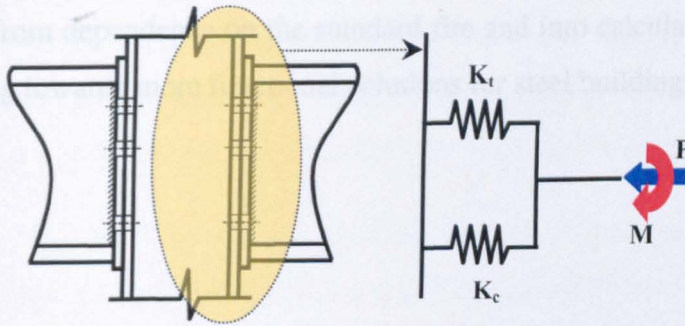


Figure 8.3 Joint modelling for finite element analysis of frames under fire conditions

Future developments could also be made in the image acquisition and processing technique. With today's fast technological advances in video camera and digital imaging it is feasible to build a system within a reasonable budget and benefit from a very fast image acquisition frame grabber, obtaining frames very quickly, and most importantly having the advantage of high resolution imaging which results in better accuracy when displacement or rotation measurements are considered. It is also possible to fully automate the tests by making the frame grabber, which is responsible for triggering the video cameras, to interact with the hydraulic jack controller in order to follow a certain load or displacement controlled path. The most advanced development would be the use of photogrammetry principles in order to produce three-dimensional data on deformations from purely two-dimensional images. This could prove to be an advantage when local buckling is investigated at ambient or elevated temperatures.

The use of commercial finite element programs such as ANSYS and ABAQUS in modelling joints at ambient and elevated temperature have become popular in recent

years. These models could provide good predictions for the joint response at elevated temperatures. It is envisaged that the use of such programs could offer a cheap alternative to testing, providing improved understanding of the joint behaviour by studying the influence of various parameters. Results from such models can also enrich the database of joint behaviour at elevated temperatures.

A future development of the Fire Safety Engineering concept, as reported by Dowling^{8,18}, is the development of methods which allow engineers to calculate the actual temperatures which steel sections are likely to reach in a real fire and implement different fire scenarios into finite element packages. This moves fire design away from dependence on the standard fire and into calculation based on real events, moving towards more functional solutions for steel buildings in fire.

8.5 REFERENCES

- 8.1 Green, M., and Butterworth, N., "*Steel and Fire: Designing for Value*", New Steel Construction, Vol. 9, No. 1, pp.30-31, January/February, 2001.
- 8.2 "*EC3: Design of Steel Structures, Part 1.1: Revised Annex J Joints and Building Frames*", (Draft), Document CEN/TC250/SC3 N419E, European Committee for Standardization, 1994.
- 8.3 Spyrou, S., Davison, J.B., and Burgess, I.W., "*Experimental and Analytical Studies of Steel T-stubs at Elevated Temperatures*", Abnormal Loading on Structures: Experimental and Numerical Modelling, Edited by Viridi, K.S., Matthews, R.S., Clarke, J.L., and Garas, F.K., E&FN Spon, London, 2000.
- 8.4 Spyrou, S., and Davison, J.B., "*Displacement Measurements in Studies of Steel T-stub Connections*", Journal of Constructional Steel Research, Vol. 57, No. 6, pp. 647-659, 2001.
- 8.5 Theodorou, Y., "Mechanical Properties of Grade 8.8 Bolts at Elevated Temperatures", MSc. Report, University of Sheffield, UK, 2001.
- 8.6 Kirby, R. B., "*The Behaviour of High-strength Grade 8.8 Bolts in Fire*", Journal of Constructional Steel Research, Vol. 33, pp.3-38, 1995.
- 8.7 "*EC3: Design of Steel Structures, Part 1.2: General rules Structural fire design*", (Drafts) Document CEN, European Committee for Standardisation, 1995.
- 8.8 Gere J.M., and Timoshenko, S.P., "*Mechanics of Materials*", Second SI Edition, PWS Engineering, Wadsworth International, 1985.
- 8.9 Popov. E.P., "*Mechanics of Materials: SI Version*", Second Edition, Prentice-Hall, Inc., New Jersey, 1978.
- 8.10 "Control of the Semi-Rigid Behaviour of Civil Engineering Structural Connections", Final COST Action C1 Report, EUR 19244, 1999.

- 8.11 “*Structural Sections to BS4:Part 1 and BS4848:Part4*”, British Steel, January, 1996.
- 8.12 British Standards Institution, *BS5950: Part 1: Structural use of steelwork in building: Code of practice for design: rolled and welded sections*, BSI, London, England, 1990.
- 8.13 ENV 1993-1-1:1992/prA2:1994, *Eurocode 3: Part 1.1, Revised Annex J: Joints in buildings frame*, European Committee for Standardization (CEN).
- 8.14 Drdacky, M., and Novotny, R., “*Partial Edge Loading-Carrying Capacity Tests of Thick Plate Girder Webs*”, Acta Technica CSAV, Vol. 5, pp. 614-20, 1977.
- 8.15 Block, F., “*Numerical and Analytical Investigation of a Column Web under Transverse Compressive Forces at Elevated Temperatures*”, Internal Report, University of Sheffield, 2001.
- 8.16 Al-Jabri, K.S., Burgess, I.W., Plank, R.J., “*The Behaviour of Steel and Composite Beam-Column Connections in Fire*” Ph.D. Thesis, Department of Civil and Structural Engineering, University of Sheffield, 1999.
- 8.17 Leston-Jones, L.C., “*The Influence of Semi-Rigid Connections on the Performance of Steel Framed Structures in Fire*”, Ph.D. Thesis, Department of Civil and Structural Engineering, University of Sheffield, 1997.
- 8.18 Dowling, J., “*Fire Resistance of Steel Structures-The Future*”, New Steel Construction, Vol. 9, No. 1, pp.32-33, January/February, 2001.

Appendix A

Test Apparatus for Elevated Temperature Testing

A.1 Testing Arrangement

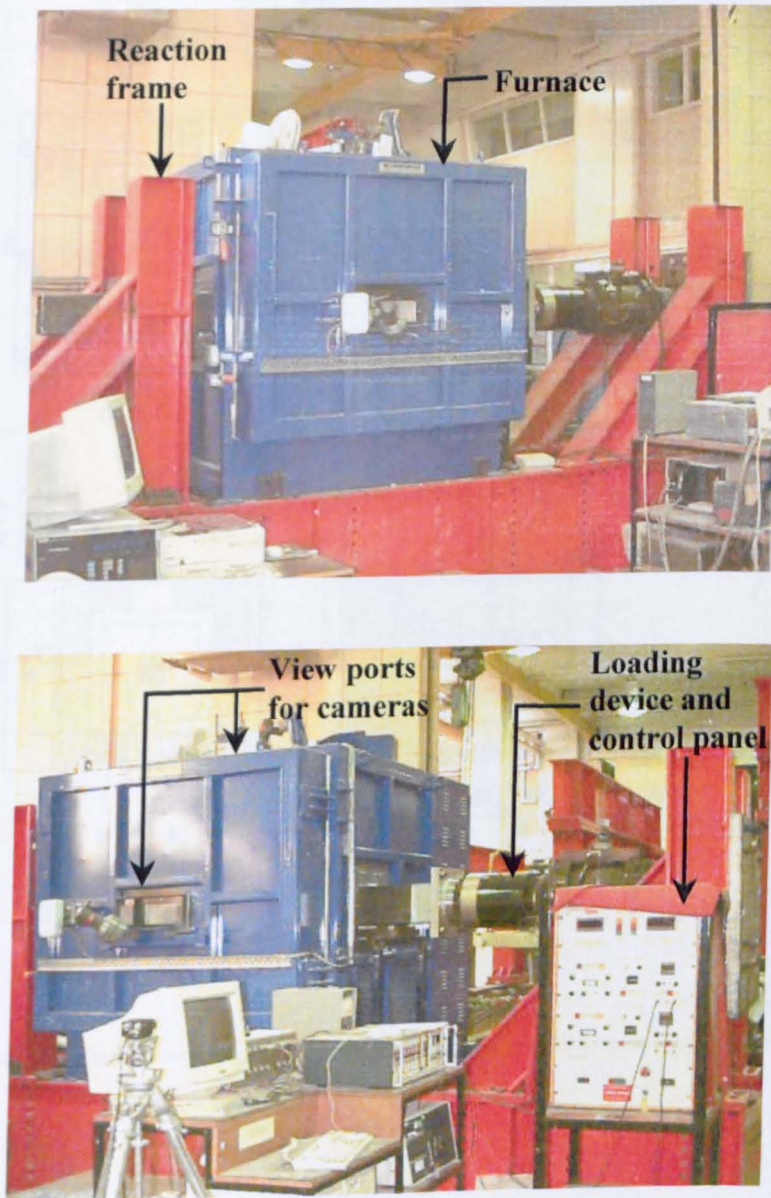


Figure A.1 (a) Furnace and reaction frame layout (b) Loading device and view ports for the video cameras arrangement

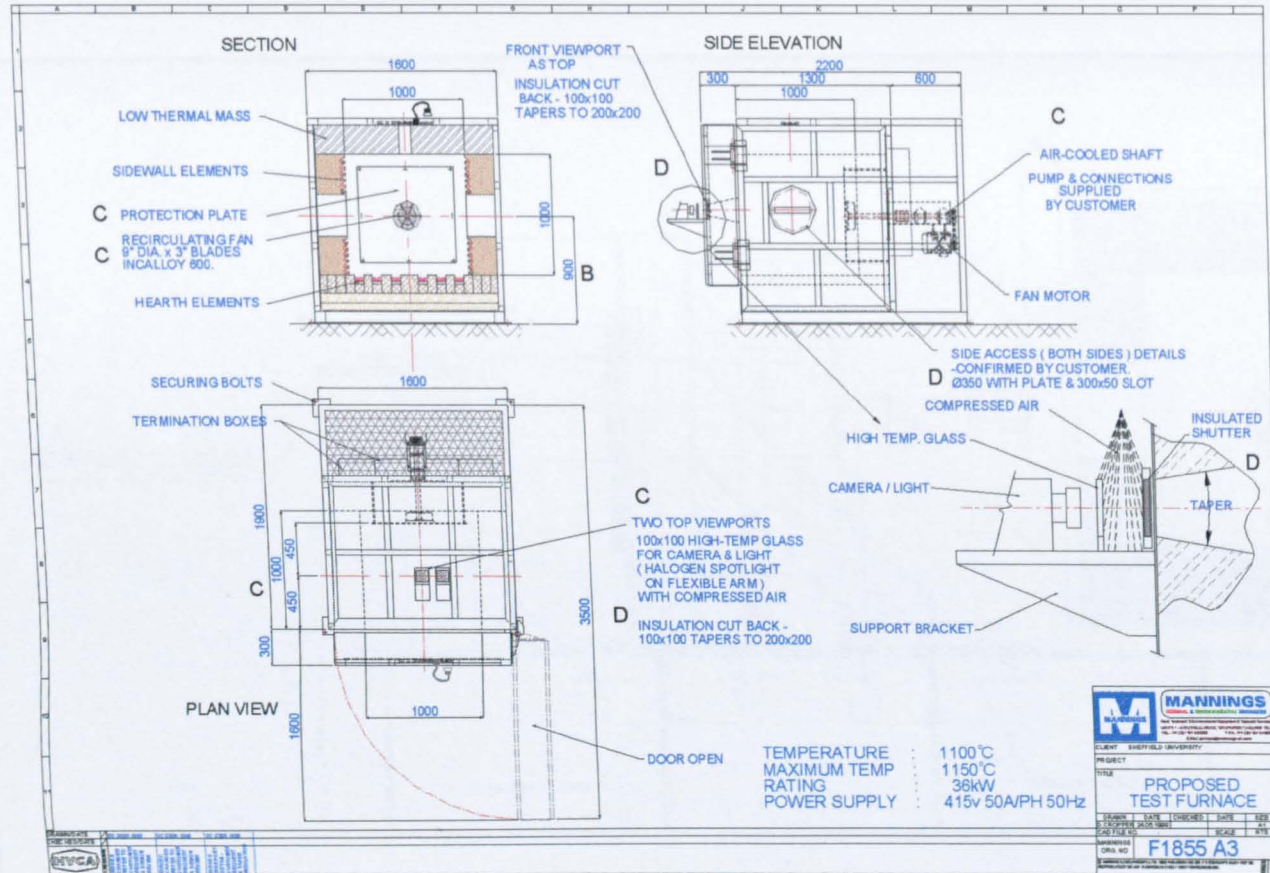


Figure A.2 Electric furnace specifications and fabrication drawings

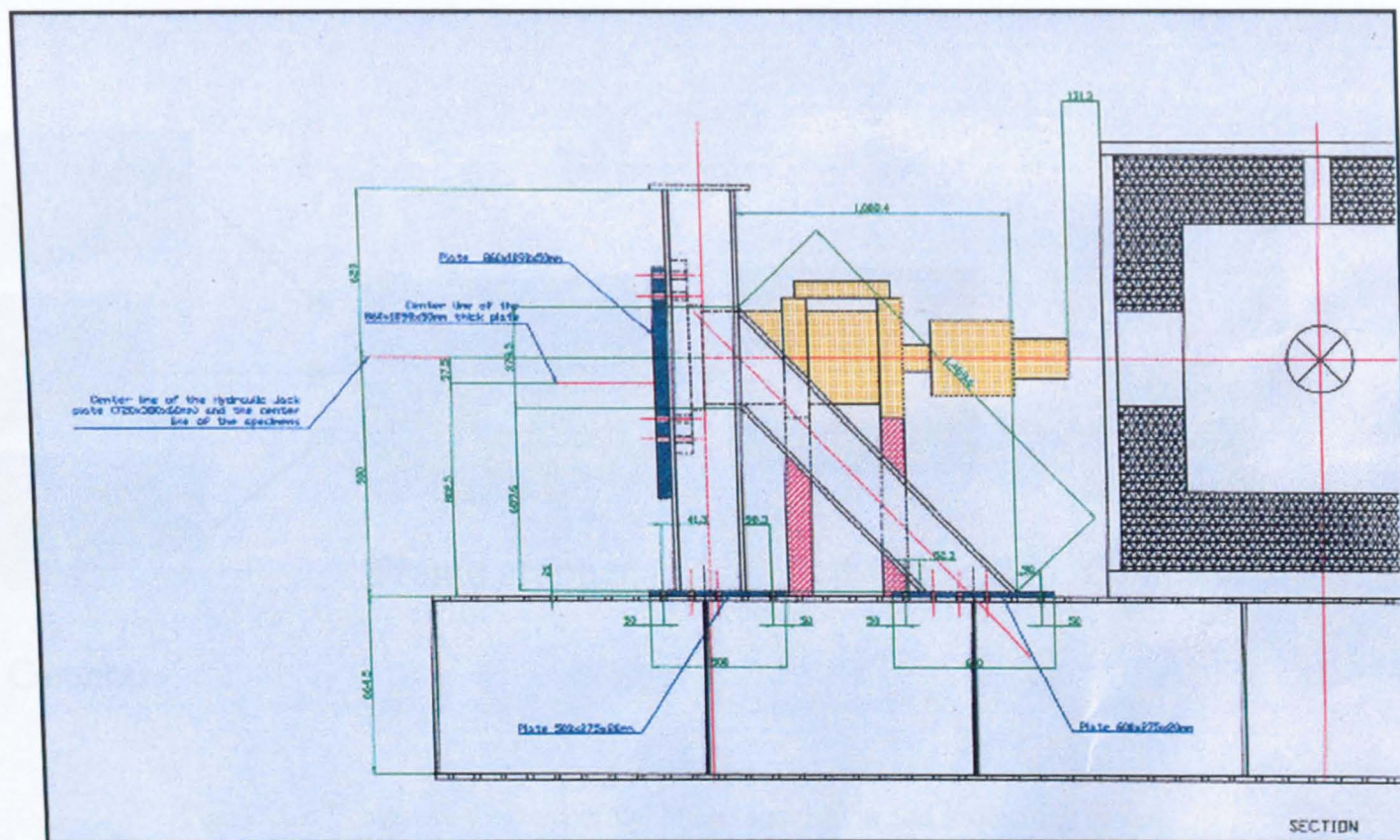


Figure A.3 Reaction frame and hydraulic jack fabrication details

A.2 Image acquisition and processing system details and specifications

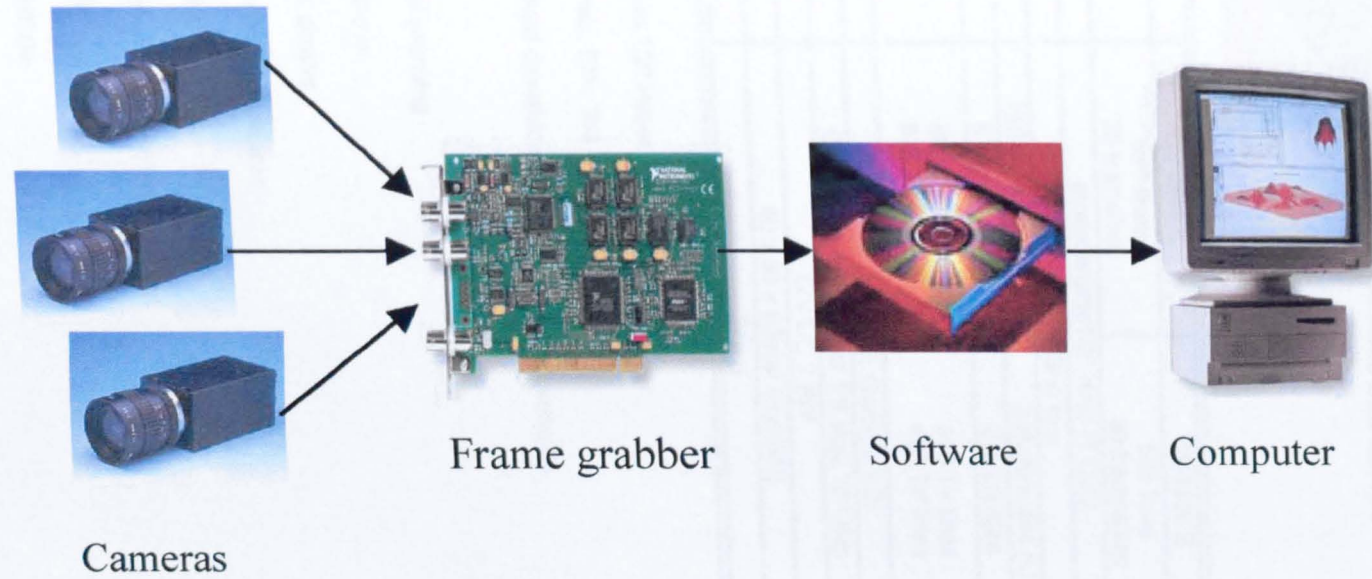


Figure A.4 Schematic diagram of the image acquisition and processing system

Table A.1 Monochrome video cameras specifications

Monochrome Cameras JAI CV-M50



Industrial Monochrome CCD Camera

	CV-M50 C	CV-M50 E
Scanning system	625 lines 25 frame/sec	525 lines 30 frames/sec
CCD Sensor	monochrome 1/2" HAD IT CCD	
Sensing area:	6.6(h) x 4.8(v) mm	
Picture elements eff.	752 (h) x 582 (v)	768 (h) x 494 (v)
Cell size:	8.6 x 8.3 μ m	8.4 x 9.8 μ m
Resolution:		
horizontal	560 TV lines	570 TV lines
vertical	575 TV lines	485 TV lines
S/N ratio	>56 dB (AGC off, Gamma 1.0)	
Video output	Composite VBS signal 1.0 Vpp, 75 Ohm	
Power	12V DC 2.5W	
Dimensions	40 x 50 x 80mm (HxWxD)	
Weight	245 g	

Features

- 3 High resolution monochrome 1/2" Hyper HAD IT CCD sensor
- 4 CCIR: 752 (h) x 582 (v) pixels. EIA: 768 (h) X 494 (v) pixels
- 5 Extreme sensitivity • Improved dynamic range and smear performance
- 6 High S/N ratio >56 dB
- 7 Interlaced or non-interlaced scanning
- 8 Field or frame integration mode
- 9 Electronic or asynchronous shutter
- 10 Long time exposure with external VD pulses
- 11 HD/VD synchronization input or output. – TTL level
- 12 Exposure enable (EEN) and write enable (WEN) output
- 13 Sub-pixel accuracy possible
- 14 Frame grabber friendly interface
- 15 Rugged and compact construction

Table A.2 Frame Grabber specifications

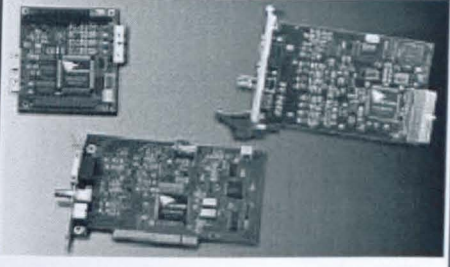
Frame Grabber PXC200	
	<p>The PXC200 Color Frame Grabber combines high quality color and monochrome video capture with a Peripheral Component Interface (PCI) at an unusually affordable price. High accuracy, low pixel jitter and other leading features offer solid support for the most demanding industrial and commercial applications.</p>
<p>FEATURES & BENEFITS</p>	
<ul style="list-style-type: none"> • Compact, PCI short card, PC/104-Plus core module and CompactPCI3U • PCI bus master design for real-time image capture • Support for YCrCb, RGB and Y8 (gray scale) output formats • High color accuracy with low pixel jitter • Standard capture resolutions of 640 x 480 (NTSC) and 768 x 576 (PAL) • Four multiplexed video inputs (NTSC/PAL/S-video) • Real-time image scaling with interpolation, plus horizontal and vertical cropping • Continuous, software-initiated and triggered capture of frames • External TTL-level trigger • +12 VDC camera power supply • Simple software interface • Software development support for DOS, Watcom DOS/4GW extender, Windows 3.1, Windows 95, Windows NT applications, QNX • Support for C/C++, Visual Basic and Delphi • Software and manual included • DAC reference generator eliminates inconsistency of AGC 	
<p>Acting as a PCI bus master, the PXC200 achieves real-time video capture to system memory. It handles data transfers while the main CPU is free to run other parts of your application or other applications. Image data can be transferred to a buffer in main memory or directly to another PCI device.</p> <p>Four multiplexed video inputs can accept color video from NTSC and PAL video sources. One of these can also be reserved for S-video. Color output formats supported include YCrCb and RGB, while Y8 is supported for monochrome applications. Also included are real-time image scaling with interpolation, plus horizontal and vertical cropping to minimize memory and bus bandwidth requirements.</p>	

Table A.3 C-Mount Lenses specifications

Standard C Mount Lenses



Ideal for most standard resolution cameras standard C mount lenses for machine vision use glass elements and a rugged construction. Firstsight have detailed specification data on all our C mount lenses, for further details please contact sales.

- Fitted with Locking Screws
- Typical MTF at centre of 60-100 lp/mm
- Typical MTF at format edge 30-50 lp/mm
- Typical Distortion 1-3% at format edge
- Thread for attaching filters

Below is a selection guide for lenses

Model	Manufacturer	Focal Length (mm)	Aperture Range (C=Close)	Iris & Focus Operation	Minimum Object Distance (mm)	Max Format	Filter Thread (0.5)	Max. Dia. (mm)	Overall Length (mm)
VC3514	VORTEX	3.5	F1.4-C	Manual/Lock	200	1/2"	None	31	39
VC4514	VORTEX	4.5	F1.4-C	Manual/Lock	200	1/2"	M25.5	31	37.6
VC6514	VORTEX	6	F1.4-C	Manual/Lock	200	2/3"	M27	30	30
VC8013	VORTEX	8	F1.3-C	Manual/Lock	200	2/3"	M25.5	29	34.5
219HB	TAMRON	8	F1.4-16	Manual/Lock	300	2/3"	M25.5	29	27
VC1214	VORTEX	12	F1.4-C	Manual/Lock	300	2/3"	M27	30	34.5
25HB	TAMRON	12	F1.8-16	Manual/Lock	300	2/3"	M25.5	29	27
17HF	TAMRON	16	F1.4-16	Manual/lock	300	2/3"	M25.5	30.5	25
VC1614	VORTEX	16	F1.4-C	Manual/lock	400	2/3"	M27	30	24.5
20HC	TAMRON	25	1.6~16	Manual/lock	250	1/2"	M25.5	30.5	25.5
VC2514	VORTEX	25	F1.4-C	Manual/Lock	500	2/3"	M27	30	24.5
VC3514	VORTEX	25	F1.4-C	Manual/Lock	500	2/3"	M30.5	35	37.5
21HC	TAMRON	50	2.8~22	Manual/lock	500	1/2"	M25.5	30.5	38.5
VC5018	VORTEX	50	F1.8-C	Manual/Lock	1000	2/3"	M30.5	32	37.5
1A1HB	TAMRON	75	3.9~32	Manual/lock	500	1/2"	M25.5	30.5	65.5
VC7527	VORTEX	75	F2.7-c	Manual/lock	1000	2/3"	M30.5	32	42.5
VC10035	VORTEX	100	F3.5-c	Manual/lock	1000	2/3"	M30.5	32	44.2

The image processing software was purpose built and calibrated against the image acquisition equipment used in the current study. It is based on the Edison, general purpose 32 bit image processing package for Windows 95/NT, which can be downloaded for free from the <http://www.inventions.u-net.com/> web page.

Geometrical, Mechanical Properties and Test Data for the T-Stub Specimens

Geometrical Properties

The geometrical properties for each T-Stub specimen are given in Table 11.1. Figures 11.1-11.3 and Tables 11.1-11.3.



Figure 11.1 Arrangement of the T-Stub specimens

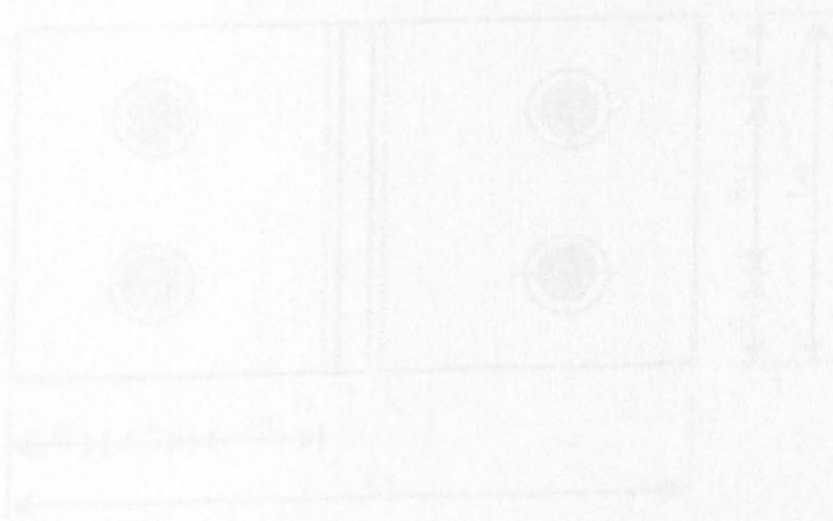


Figure 11.2 Plan view arrangement of the T-Stub specimens

Appendix B

Geometrical, Mechanical Properties and Test Data for the T-Stub Specimens

B.1 Geometrical Properties

The geometrical properties for each T-stub specimen and bolts are given below in Figures B.1-B.3 and Tables B.1-B.7.

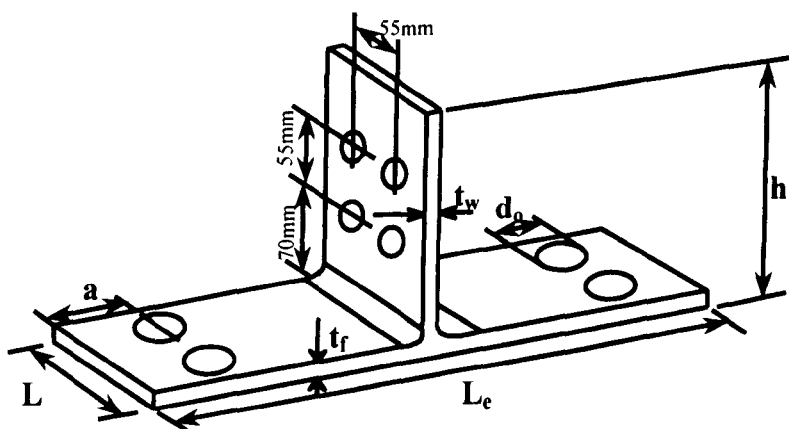


Figure B.1 Arrangement of the T-stub specimen

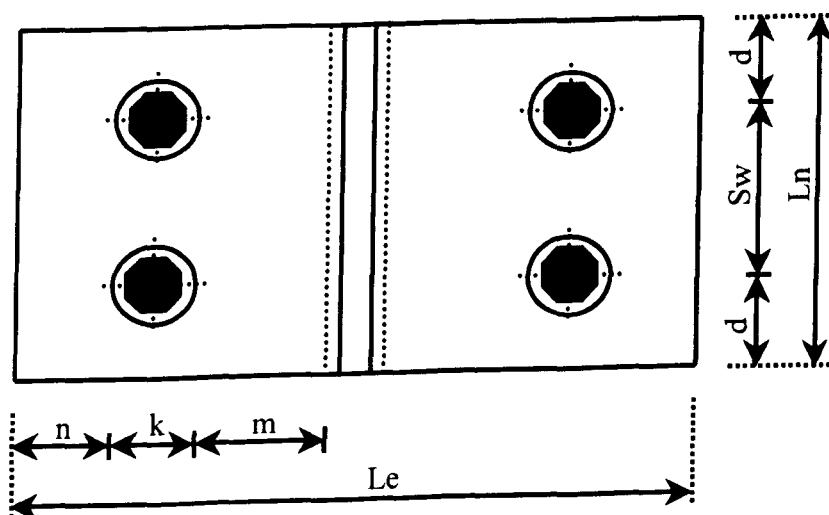


Figure B.2 Plan view arrangement of the T-stub specimen

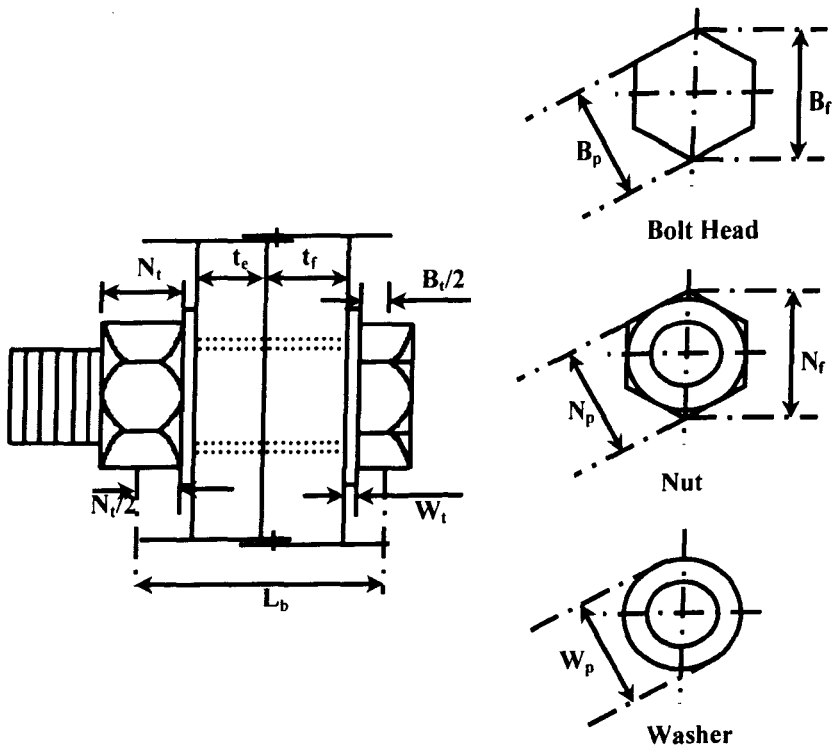
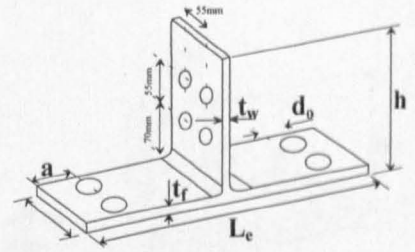


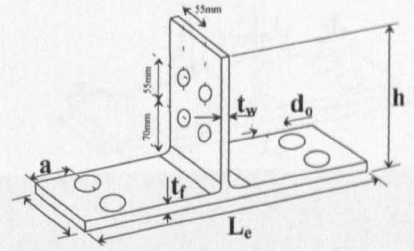
Figure B.3 Bolts, Nuts and Washers

Table B.1 Geometrical Properties of specimens for Phase A



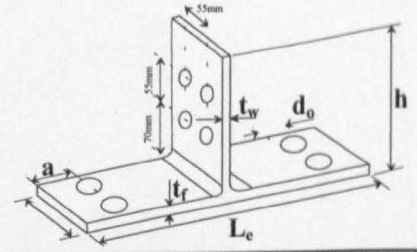
Test Program		h mm	L _e mm	d _b mm	a mm	t _w mm	t _r mm	Root Radius mm	Weld a _r mm	
Phase A	Flange 1 (UB305x 165x40)	AA1	153.00	165.60	22.00	25.00	6.60	9.60	8.90	No
		AA2	153.55	165.50	22.00	25.00	6.55	9.60	8.90	No
		AA3	153.00	165.80	22.00	25.00	6.70	9.50	8.90	No
		AA4	153.20	166.30	22.00	25.00	6.55	9.80	8.90	No
	Flange 2 (UB305x 165x40)	AA1	153.00	165.60	20.00	25.00	6.60	9.60	8.90	No
		AA2	153.55	165.50	22.00	25.00	6.55	9.60	8.90	No
		AA3	153.00	165.80	22.00	25.00	6.70	9.50	8.90	No
		AA4	153.20	166.30	22.00	25.00	6.55	9.80	8.90	No
	Flange 1 (UB305x 165x40)	AB1	153.00	166.00	18.00	45.00	6.60	9.67	8.90	No
		AB2	153.00	166.00	18.00	45.00	6.65	9.50	8.90	No
		AB3	153.00	165.85	18.00	45.00	6.90	9.50	8.90	No
		AB4	153.00	166.20	18.00	45.00	6.75	9.52	8.90	No
		AB5	153.00	166.17	18.00	45.00	6.82	9.60	8.90	No
	Flange 2 (UB305x 165x40)	AB1	153.00	166.00	18.00	45.00	6.60	9.67	8.90	No
		AB2	153.00	166.00	18.00	45.00	6.65	9.50	8.90	No
		AB3	153.00	165.85	18.00	45.00	6.90	9.50	8.90	No
		AB4	153.00	166.20	18.00	45.00	6.75	9.52	8.90	No
		AB5	153.00	166.17	18.00	45.00	6.82	9.60	8.90	No
	Flange 1 (UB305x 165x40)	AC1	153.00	165.55	18.00	25.00	6.80	9.52	8.90	No
		AC2	153.00	166.00	18.00	25.00	6.75	9.52	8.90	No
		AC3	153.00	165.85	18.00	25.00	6.60	9.50	8.90	No
	Flange 2 (UB305x 165x40)	AC1	153.00	165.55	18.00	25.00	6.80	9.52	8.90	No
		AC2	153.00	166.00	18.00	25.00	6.75	9.52	8.90	No
		AC3	153.00	165.85	18.00	25.00	6.60	9.50	8.90	No

Table B.2 Geometrical Properties of specimens for Phase B



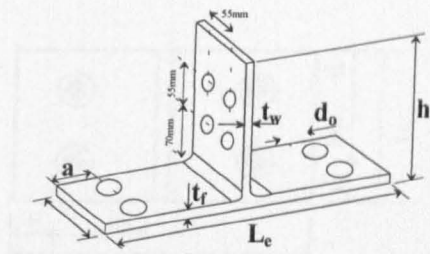
Test Program		h mm	L_e mm	d_o mm	a mm	t_w mm	t_f mm	Root Radius mm	Weld a_f mm	
Phase B	Column (UC203x 203x52)	BA1	160.40	205.85	22.40	57.15	7.42	12.03	10.20	No
		BA2	161.25	205.70	22.20	57.30	7.42	12.10	10.20	No
		BA3	160.35	206.00	22.17	57.75	7.55	12.15	10.20	No
		BA4	160.65	206.05	22.22	56.92	7.65	12.15	10.20	No
		BA5	159.65	205.90	22.45	57.65	7.55	12.25	10.20	No
		BA6	159.80	205.85	22.30	57.67	7.50	11.90	10.20	No
	End plate (200x 200x20)	BA1	196.05	201.90	22.00	50.00	10.25	19.20	No	10.00
		BA2	193.45	200.70	22.50	50.00	10.00	19.50	No	10.00
		BA3	193.50	201.00	22.50	50.00	9.90	19.55	No	10.00
		BA4	193.60	202.30	22.75	50.00	9.95	19.65	No	10.00
		BA5	193.45	200.70	22.50	50.00	10.00	19.55	No	10.00
		BA6	196.20	200.60	23.00	50.00	10.10	19.50	No	10.00
	Column (200x 200x20)	BB1	168.55	201.42	23.10	50.00	11.80	19.55	No	10.00
		BB2	168.20	200.20	22.80	55.00	11.85	19.60	No	10.00
	End plate (200x 200x20)	BB1	198.80	200.90	23.04	55.00	11.95	20.20	No	10.00
		BB2	199.30	200.00	22.70	50.00	11.90	20.32	No	10.00

Table B.3 Geometrical Properties of specimens for Phase C



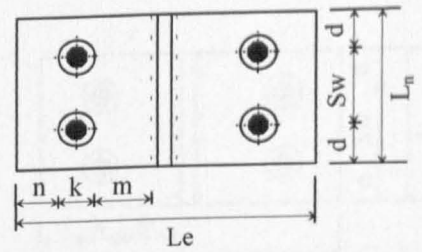
Test Program		h mm	L _e mm	d _o mm	a mm	t _w mm	t _f mm	Root Radius mm	Weld a _r mm	
Phase C	Column (UC203x 203x60)	CA1	174.25	203.95	22.00	56.97	10.00	13.70	10.20	No
		CA2	174.49	203.25	22.15	56.50	9.90	13.90	10.20	No
		CA3	173.96	203.35	22.12	56.55	9.95	13.90	10.20	No
		CA4	174.92	203.25	22.45	56.25	9.96	13.90	10.20	No
		CA5	173.35	203.20	22.25	56.22	9.90	13.80	10.20	No
	End Plate (200x 200x20)	CA1	194.16	196.00	22.00	47.75	10.20	20.20	No	11.00
		CA2	193.95	195.65	22.30	47.75	10.25	20.20	No	11.00
		CA3	194.58	195.65	22.20	47.75	10.27	20.16	No	11.00
		CA4	194.29	195.78	22.36	47.59	10.32	20.22	No	11.00
		CA5	194.22	196.25	22.20	47.85	10.20	20.15	No	11.00
	Column (UC152x 152x30)	CB1	157.02	153.66	22.22	32.26	6.15	9.15	7.6	No
		CB2	157.06	153.60	22.05	31.92	6.15	9.20	7.6	No
		CB3	156.90	153.65	22.10	31.70	6.20	9.15	7.6	No
		CB4	156.82	153.75	22.10	31.85	6.10	9.20	7.6	No
		CB5	156.82	154.00	22.10	32.23	6.10	9.15	7.6	No
	End Plate (200x 200x20)	CB1	194.05	196.34	22.10	48.02	10.28	20.15	No	11.00
		CB2	194.00	195.73	22.20	47.81	10.15	20.15	No	11.00
		CB3	194.30	196.10	22.10	47.74	10.26	20.15	No	11.00
		CB4	193.95	196.05	22.10	48.29	10.32	20.15	No	11.00
		CB5	194.12	195.68	22.20	47.93	10.22	20.17	No	11.00
	Column (UC203x 203x86)	CC1	179.00	204.55	22.25	57.49	12.45	19.12	10.20	No
		CC2	179.02	204.62	22.35	57.22	12.30	19.02	10.20	No
		CC3	179.55	204.05	22.30	56.92	12.25	19.46	10.20	No
		CC4	179.60	204.65	22.25	57.26	12.35	19.26	10.20	No
		CC5	178.80	203.70	22.25	56.60	12.30	19.47	10.20	No
	End Plate (200x 200x20)	CC1	194.06	196.00	22.20	48.03	10.25	20.10	No	11.00
		CC2	193.92	196.70	22.45	48.35	10.20	20.10	No	11.00
		CC3	194.65	196.25	22.15	48.55	10.20	20.10	No	11.00
		CC4	194.15	196.70	22.05	47.98	10.25	20.15	No	11.00
		CC5	194.40	195.20	22.20	47.13	10.40	20.15	No	11.00
Column (UC254x 254x107)	CD1	180.70	255.61	22.25	83.22	12.80	21.12	12.70	No	
	CD2	180.02	255.10	22.15	82.46	12.85	21.14	12.70	No	
	CD3	181.83	258.35	22.20	84.30	12.80	20.80	12.70	No	
	CD4	181.52	258.55	22.20	84.00	12.75	20.85	12.70	No	
	CD5	181.39	258.45	22.25	84.16	12.75	20.82	12.70	No	
End Plate (200x 200x20)	CD1	194.08	196.36	22.25	47.94	10.25	20.20	No	11.00	
	CD2	194.25	195.85	22.25	47.51	10.40	20.25	No	11.00	
	CD3	194.80	195.85	22.15	47.48	10.35	20.30	No	11.00	
	CD4	194.20	195.65	22.28	47.89	10.32	20.16	No	11.00	
	CD5	194.30	196.00	22.25	47.93	10.35	20.22	No	11.00	
Column (UC203x 203x86)	CE1	179.90	204.70	14.50	57.42	12.30	19.21	10.20	No	
	CE2	179.95	204.75	14.35	57.35	12.45	19.37	10.20	No	
	CE3	180.17	204.10	14.45	57.22	12.40	19.66	10.20	No	
	CE4	179.60	204.25	14.45	57.02	12.35	19.46	10.20	No	
	CE5	180.37	204.50	14.40	57.40	12.38	19.30	10.20	No	

Table B.3 Continue



Test Program		h mm	L _e mm	d _o mm	A Mm	t _w mm	t _f mm	Root Radius mm	Weld a _f mm	
<i>Phase C</i>	End Plate (200x 200x20)	CE1	193.80	195.76	14.35	47.88	10.22	20.10	No	11.00
		CE2	194.05	195.70	14.20	47.57	10.38	20.20	No	11.00
		CE3	194.00	195.65	14.20	47.54	10.40	20.20	No	11.00
		CE4	194.05	195.82	14.32	47.86	10.25	20.10	No	11.00
		CE5	194.10	195.40	14.20	47.52	10.38	20.25	No	11.00

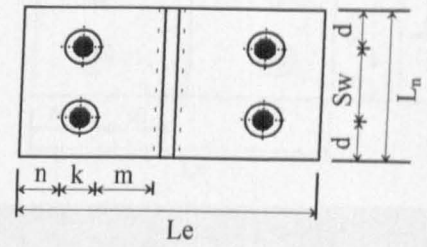
Table B.4 Geometrical Properties of specimens for Phase A



Test Program		n mm	k mm	m mm	d mm	L_n mm	Bolt Size	Strength		
								Bolt	Nut	
Phase A	Flange 1 (UB305x 165x40)	AA1	6.85	36.30	29.23	25.00	101.00	M20	G 8.8	HSFG
		AA2	6.85	36.30	29.70	25.00	100.00	M20	G 8.8	HSFG
		AA3	6.85	36.30	29.28	25.00	100.80	M20	G 8.8	HSFG
		AA4	6.85	36.30	29.60	25.00	100.50	M20	G 8.8	HSFG
	Flange 2 (UB305x 165x40)	AA1	6.85	36.30	29.23	25.00	101.00	M20	G 8.8	HSFG
		AA2	6.85	36.30	29.70	25.00	100.00	M20	G 8.8	HSFG
		AA3	6.85	36.30	29.28	25.00	100.80	M20	G 8.8	HSFG
		AA4	6.85	36.30	29.60	25.00	100.50	M20	G 8.8	HSFG
	Flange 1 (UB305x 165x40)	AB1	30.17	29.65	12.75	35.00	140.00	M16	HSFG	HSFG
		AB2	30.17	29.65	12.73	35.00	141.28	M16	HSFG	HSFG
		AB3	30.17	29.65	12.53	35.00	141.20	M16	HSFG	HSFG
		AB4	30.17	29.65	12.78	35.00	138.60	M16	HSFG	HSFG
		AB5	30.17	29.65	12.70	35.00	142.85	M16	HSFG	HSFG
	Flange 2 (UB305x 165x40)	AB1	30.17	29.65	12.75	35.00	140.00	M16	HSFG	HSFG
		AB2	30.17	29.65	12.73	35.00	141.28	M16	HSFG	HSFG
		AB3	30.17	29.65	12.53	35.00	141.20	M16	HSFG	HSFG
		AB4	30.17	29.65	12.78	35.00	138.60	M16	HSFG	HSFG
		AB5	30.17	29.65	12.70	35.00	142.85	M16	HSFG	HSFG
	Flange 1 (UB305x 165x40)	AC1	10.17	29.65	32.43	40.00	218.70	M16	HSFG	HSFG
		AC2	10.17	29.65	32.58	40.00	219.50	M16	HSFG	HSFG
		AC3	10.17	29.65	32.50	40.00	219.00	M16	HSFG	HSFG
	Flange 2 (UB305x 165x40)	AC1	10.17	29.65	32.43	40.00	218.70	M16	HSFG	HSFG
		AC2	10.17	29.65	32.58	40.00	219.50	M16	HSFG	HSFG
		AC3	10.17	29.65	32.50	40.00	219.00	M16	HSFG	HSFG

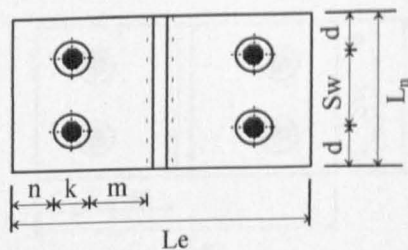
Where HSFG is High Strength Friction Grip and G 8.8 is Grade 8.8 bolts and nuts.

Table B.5 Geometrical Properties of specimens for Phase B



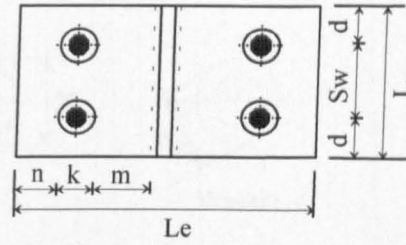
Test Program		n mm	k mm	m mm	d mm	L_n mm	Bolt Size	Strength		
								Bolt	Nut	
Phase B	Column (UC203x 203x52)	BA1	39.00	36.30	15.75	50.00	200.70	M20	HSFG	HSFG
		BA2	39.15	36.30	15.53	50.00	200.35	M20	HSFG	HSFG
		BA3	39.60	36.30	15.16	50.00	199.80	M20	HSFG	HSFG
		BA4	38.77	36.30	15.96	50.00	200.65	M20	HSFG	HSFG
		BA5	39.50	36.30	15.21	50.00	199.50	M20	HSFG	HSFG
		BA6	39.52	36.30	15.19	50.00	200.00	M20	HSFG	HSFG
	End plate (200x 200x20)	BA1	31.85	36.30	16.36	55.00	201.55	M20	HSFG	HSFG
		BA2	31.85	36.30	15.88	55.00	201.10	M20	HSFG	HSFG
		BA3	31.85	36.30	16.08	55.00	201.00	M20	HSFG	HSFG
		BA4	31.85	36.30	16.71	55.00	202.20	M20	HSFG	HSFG
		BA5	31.85	36.30	15.88	55.00	200.60	M20	HSFG	HSFG
		BA6	31.85	36.30	15.78	55.00	200.50	M20	HSFG	HSFG
	Column (200x 200x20)	BB1	31.85	36.30	15.34	55.00	202.00	M20	HSFG	HSFG
		BB2	36.85	36.30	9.71	50.00	201.30	M20	HSFG	HSFG
	End plate (200x 200x20)	BB1	36.85	36.30	10.01	50.00	200.70	M20	HSFG	HSFG
		BB2	31.85	36.30	14.58	55.00	202.50	M20	HSFG	HSFG

Table B.6 Geometrical Properties of specimens for Phase C



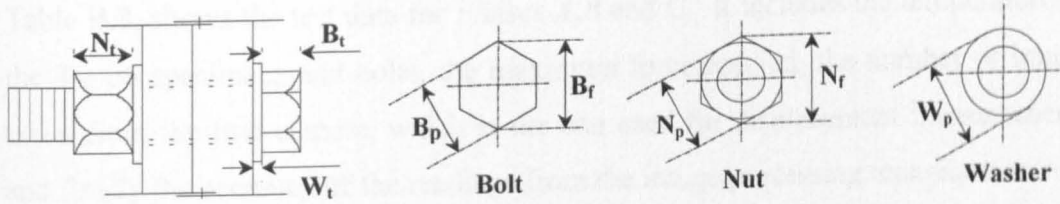
Test Program		n mm	k mm	m mm	d mm	L_n mm	Bolt Size	Strength		
								Bolt	Nut	
Phase C	Column (UC203x 203x60)	CA1	38.82	36.30	13.69	49.22	198.45	M20	HSFG	HSFG
		CA2	38.35	36.30	13.86	49.50	199.00	M20	G 8.8	HSFG
		CA3	38.40	36.30	13.84	49.80	199.60	M20	HSFG	HSFG
		CA4	38.82	34.85	14.81	49.87	199.33	M20	G 8.8	G 8.8
		CA5	38.79	34.85	14.84	49.77	199.55	M20	G 8.8	G 8.8
	End Plate (200x 200x20)	CA1	29.60	36.30	14.55	54.27	198.55	M20	HSFG	HSFG
		CA2	29.60	36.30	14.35	54.10	198.70	M20	G 8.8	HSFG
		CA3	29.60	36.30	14.34	54.30	198.60	M20	HSFG	HSFG
		CA4	30.17	34.85	15.26	54.48	198.60	M20	G 8.8	G 8.8
		CA5	30.42	34.85	15.30	54.14	198.70	M20	G 8.8	G 8.8
	Column (UC152x 152x30)	CB1	14.83	34.85	17.99	49.56	198.90	M20	HSFG	HSFG
		CB2	14.50	34.85	18.29	49.67	199.70	M20	G 8.8	HSFG
		CB3	14.27	34.85	18.52	49.55	199.35	M20	G 8.8	HSFG
		CB4	14.42	34.85	18.47	50.15	200.30	M20	G 8.8	HSFG
		CB5	14.80	34.85	18.21	49.29	199.30	M20	HSFG	HSFG
	End Plate (200x 200x20)	CB1	30.59	34.85	15.14	54.30	199.00	M20	HSFG	HSFG
		CB2	30.39	34.85	15.10	54.21	198.70	M20	G 8.8	HSFG
		CB3	30.32	34.85	15.30	53.96	198.50	M20	G 8.8	HSFG
		CB4	30.86	34.85	14.70	54.25	198.70	M20	G 8.8	HSFG
		CB5	30.50	34.85	14.93	54.15	198.40	M20	HSFG	HSFG
	Column (UC203x 203x86)	CC1	40.07	34.85	12.96	49.77	198.95	M20	G 8.8	HSFG
		CC2	39.80	34.85	13.35	48.10	196.60	M20	G 8.8	HSFG
		CC3	39.49	34.85	13.39	49.53	199.30	M20	G 8.8	HSFG
		CC4	39.83	34.85	13.30	49.79	199.30	M20	HSFG	HSFG
		CC5	39.17	34.85	13.51	49.02	198.20	M20	G 8.8	HSFG
	End Plate (200x 200x20)	CC1	30.60	34.85	14.97	53.95	198.65	M20	G 8.8	HSFG
		CC2	30.92	34.85	15.03	54.30	198.82	M20	G 8.8	HSFG
		CC3	31.12	34.85	14.60	54.15	198.65	M20	G 8.8	HSFG
		CC4	30.55	34.85	15.37	53.79	198.65	M20	HSFG	HSFG
		CC5	29.70	34.85	15.40	54.17	198.75	M20	G 8.8	HSFG
	Column (UC254x 254x107)	CD1	65.79	34.85	10.59	50.58	200.90	M20	G 8.8	HSFG
		CD2	65.03	34.85	11.08	50.10	200.25	M20	G 8.8	HSFG
		CD3	66.87	34.85	10.89	50.48	200.55	M20	HSFG	HSFG
		CD4	66.57	34.85	11.31	50.17	200.55	M20	G 8.8	HSFG
		CD5	66.73	34.85	11.10	50.46	200.70	M20	G 8.8	HSFG
	End Plate (200x 200x20)	CD1	30.52	34.85	15.24	54.65	198.53	M20	G 8.8	HSFG
		CD2	30.08	34.85	15.34	53.97	198.60	M20	G 8.8	HSFG
		CD3	30.06	34.85	15.39	54.33	198.75	M20	HSFG	HSFG
		CD4	30.46	34.85	14.90	53.96	198.60	M20	G 8.8	HSFG
		CD5	30.50	34.85	15.02	54.54	199.62	M20	G 8.8	HSFG
	Column (UC203x 203x86)	CE1	45.75	23.35	18.94	48.36	197.20	M12	G 8.8	HSFG
		CE2	45.67	23.35	18.96	48.82	198.60	M12	HSFG	HSFG
		CE3	45.55	23.35	18.79	48.65	198.30	M12	G 8.8	HSFG
		CE4	45.35	23.35	19.09	48.43	197.45	M12	G 8.8	HSFG
		CE5	45.72	23.35	18.82	49.13	198.55	M12	G 8.8	HSFG

Table B.6 Continue



Test Program		n mm	k mm	m mm	d mm	L_n Mm	Bolt Size	Strength		
								Bolt	Nut	
<i>Phase C</i>	End Plate (200x 200x20)	CE1	36.20	23.35	20.77	54.40	198.55	M12	G 8.8	HSFG
		CE2	35.90	23.35	20.96	54.21	198.50	M12	G 8.8	HSFG
		CE3	35.87	23.35	20.96	54.41	199.02	M12	HSFG	HSFG
		CE4	36.19	23.35	20.79	54.51	198.25	M12	G 8.8	HSFG
		CE5	35.85	23.35	20.86	54.16	198.60	M12	G 8.8	HSFG

Table B.7 Bolt Geometrical Properties for all the specimens



Test Program		Bolt			Nut			Washer	
		B_f	B_p	B_t	N_f	N_p	N_t	W_p	W_t
Phase A	AA1	33.82	29.65	12.60	35.70	31.60	18.40	36.30	2.55
	AA2	33.00	29.60	12.70	35.65	31.55	18.50	36.30	2.50
	AA3	33.20	29.55	12.96	35.70	31.55	18.50	36.30	2.45
	AA4	33.20	29.80	12.80	35.80	31.55	18.65	36.30	2.50
	AB1	30.10	26.80	9.35	30.30	26.80	14.80	29.65	2.00
	AB2	30.15	26.70	10.40	30.25	26.90	14.75	29.65	2.00
	AB3	30.20	26.90	9.95	30.30	27.00	14.90	29.65	1.90
	AB4	30.20	27.00	10.00	30.30	27.10	14.75	29.65	2.00
	AB5	30.20	26.85	10.20	30.30	26.95	14.85	29.65	2.00
	AC1	30.30	26.70	9.45	30.30	26.80	14.90	29.65	1.98
	AC2	30.30	26.70	9.95	30.30	26.70	14.85	29.65	2.00
	AC3	30.25	27.00	9.85	30.25	27.00	14.85	29.65	2.00
Phase B	BA1	35.55	31.08	12.45	35.90	31.20	18.70	36.30	2.42
	BA2	35.62	31.16	12.50	36.00	31.65	17.40	36.30	2.46
	BA3	35.55	31.15	12.45	35.95	31.50	17.45	36.30	2.40
	BA4	35.68	31.20	12.50	36.10	31.70	17.55	36.30	2.55
	BA5	35.60	31.20	12.25	36.00	31.65	17.58	36.30	2.45
	BA6	35.55	31.15	12.50	36.00	31.66	17.60	36.30	2.55
	BB1	35.70	31.25	12.25	36.05	31.60	17.80	36.30	2.55
	BB2	35.65	31.05	12.40	35.90	31.55	17.55	36.30	2.45
Phase C	CA1	35.55	31.10	12.30	36.05	31.40	17.85	36.30	2.55
	CA2	32.85	29.60	12.90	35.82	31.40	17.90	36.30	2.35
	CA3	35.50	31.07	12.40	35.85	31.65	17.60	36.30	2.50
	CA4	33.05	29.45	12.85	34.30	29.85	15.70	34.85	3.13
	CA5	32.88	29.40	12.92	34.30	29.85	15.75	34.85	3.19
	CB1	35.44	31.09	12.35	35.70	31.40	17.80	34.85	3.25
	CB2	32.70	29.30	12.85	35.70	31.30	17.78	34.85	3.25
	CB3	32.80	29.50	13.07	35.65	31.20	18.02	34.85	3.25
	CB4	32.85	29.55	12.90	35.65	31.20	18.00	34.85	3.22
	CB5	35.40	31.01	12.30	35.50	31.15	18.00	34.85	3.25
	CC1	34.10	29.80	12.65	35.85	31.60	17.85	34.85	3.25
	CC2	34.00	29.75	12.65	35.88	31.55	17.85	34.85	3.25
	CC3	33.95	29.80	12.65	35.85	31.55	17.80	34.85	3.25
	CC4	35.90	31.30	12.90	35.95	31.55	17.90	34.85	3.25
	CC5	33.95	29.65	12.58	36.05	31.63	17.85	34.85	3.20
	CD1	33.75	29.60	12.55	35.85	31.55	17.80	34.85	3.23
	CD2	33.95	29.65	12.50	35.90	31.50	17.90	34.85	3.25
	CD3	36.00	31.32	13.00	35.80	31.40	18.10	34.85	3.23
	CD4	33.95	29.63	12.55	35.95	31.55	17.80	34.85	3.22
	CD5	33.98	29.65	12.45	35.87	31.47	17.85	34.85	3.25
	CE1	21.30	18.83	7.90	24.50	21.65	11.20	23.35	3.30
	CE2	21.43	18.80	7.95	24.65	21.75	11.15	23.35	3.40
	CE3	25.10	22.00	8.29	24.70	21.72	11.15	23.35	3.35
	CE4	21.25	18.65	7.85	24.35	21.65	10.98	23.35	3.32
	CE5	21.45	18.85	7.95	24.68	21.73	11.20	23.35	3.35

B.2 *Actual Test Data and Material Properties*

Table B.8, shows the test data for *Phases A,B and C*. It includes the temperatures of the T-stub specimens and bolts, the maximum force applied, the number of images taken from the first camera, which is the one used for displacement measurements, and finally the accuracy of the readings from the image processing technique without any sub-pixel division.

Table B.9 shows the material properties for the column and end plate T-stub specimens and for the bolts. These values were taken from the actual coupon tests performed on each set of T-stub specimens. A private company called Allvac Ltd performed the coupon tests.

Table B.8 Test Data

Test Program	Temperature °C		Maximum Force (kN)	Total Images (Nr)	Accuracy without Sub-pixel division (µm)		
	T-stub	Bolt			Column	End plate	
Phase A	AA1	570 °C	NO	68	65	40.15	No readings
	AA2	415 °C	NO	135	94	40.85	No readings
	AA3	745 °C	NO	24	24	37.75	No readings
	AA4	200 °C	NO	175	64	39.13	No readings
	AB1	Ambient	NO	250	52	34.00	No readings
	AB2	540 °C	NO	175	28	38.28	No readings
	AB3	320 °C	NO	250	60	35.78	No readings
	AB4	660 °C	NO	87.5	28	37.75	No readings
	AB5	460 °C	NO	245	39	39.25	No readings
	AC1	Ambient	NO	205	53	31.15	No readings
	AC2	360 °C	NO	200	45	34.11	No readings
	AC3	610 °C	NO	90	29	35.65	No readings
	Phase B	BA1	Ambient	NO	440	56	37.82
BA2		610 °C	NO	240	26	39.47	123.10
BA3		505 °C	NO	400	50	38.03	118.86
BA4		715 °C	NO	120	26	No readings	No readings
BA5		720 °C	NO	110	27	38.14	119.18
BA6		560 °C	575 °C	300	32	36.90	120.24
BB1		630 °C	630 °C	230	30	37.28	128.46
BB2		730 °C	705 °C	130	19	37.91	130.56
Phase C	CA1	660 °C	630 °C	220	25	40.22	No readings
	CA2	670 °C	670 °C	150	23	36.28	No readings
	CA3	730 °C	725 °C	110	21	38.28	No readings
	CA4	530 °C	530 °C	320	34	37.60	No readings
	CA5	740 °C	747 °C	85	14	36.40	No readings
	CB1	650 °C	640 °C	160	21	37.39	No readings
	CB2	540 °C	540 °C	280	30	38.57	No readings
	CB3	415 °C	415 °C	350	44	36.60	No readings
	CB4	705 °C	705 °C	95	20	37.79	No readings
	CB5	505 °C	510 °C	350	35	36.38	No readings
	CC1	620 °C	630 °C	230	24	36.12	115.01
	CC2	700 °C	698 °C	125	16	37.44	130.65
	CC3	505 °C	505 °C	430	46	38.15	124.33
	CC4	615 °C	619 °C	250	26	39.54	112.80
	CC5	740 °C	746 °C	100	25	38.76	116.46
	CD1	615 °C	618 °C	220	24	36.67	112.86
	CD2	700 °C	703 °C	90	25	34.83	107.68
	CD3	705 °C	707 °C	120	21	35.21	95.81
	CD4	505 °C	507 °C	410	55	35.73	98.05
	CD5	800 °C	803 °C	90	34	No readings	No readings
	CE1	610 °C	614 °C	80	14	38.76	115.55
	CE2	510 °C	515 °C	140	22	34.63	120.61
	CE3	505 °C	508 °C	160	19	35.48	122.49
	CE4	410 °C	414 °C	225	29	34.76	118.37
	CE5	Ambient	Ambient	300	31	28.27	111.77

Table B.9 Material Properties

Test Program	Actual Yield Stress (N/mm ²)		Young Modulus (kN/mm ²)		Bolts			
	Column	End Plate	Column	End Plate	Actual Stress (N/mm ²)		Young Modulus (kN/mm ²)	
					0.2% Yield	Ultimate stress		
Phase A	AA1	345	345	209.55	209.55	811	886	215
	AA2	345	345	209.55	209.55	811	886	215
	AA3	345	345	209.55	209.55	811	886	215
	AA4	345	345	209.55	209.55	811	886	215
	AB1	345	345	209.55	209.55	635	750	205
	AB2	345	345	209.55	209.55	635	750	205
	AB3	345	345	209.55	209.55	635	750	205
	AB4	345	345	209.55	209.55	635	750	205
	AB5	345	345	209.55	209.55	635	750	205
	AC1	345	345	209.55	209.55	635	750	205
	AC2	345	345	209.55	209.55	635	750	205
	AC3	345	345	209.55	209.55	635	750	205
Phase B	BA1	365	324	202.10	236.20	835	906	201
	BA2	365	324	202.10	236.20	835	906	201
	BA3	365	324	202.10	236.20	835	906	201
	BA4	365	324	202.10	236.20	835	906	201
	BA5	365	324	202.10	236.20	835	906	201
	BA6	365	324	202.10	236.20	835	906	201
	BB1	324	324	236.20	236.20	835	906	201
	BB2	324	324	236.20	236.20	835	906	201
Phase C	CA1	304	284	204	192	826	887	208
	CA2	304	284	204	192	811	886	215
	CA3	304	284	204	192	826	887	208
	CA4	304	284	204	192	811	886	215
	CA5	304	284	204	192	811	886	215
	CB1	285	284	198	192	826	887	208
	CB2	285	284	198	192	811	886	215
	CB3	285	284	198	192	811	886	215
	CB4	285	284	198	192	811	886	215
	CB5	285	284	198	192	826	887	208
	CC1	258	284	201.10	192	811	886	215
	CC2	258	284	201.10	192	811	886	215
	CC3	258	284	201.10	192	811	886	215
	CC4	258	284	201.10	192	835	906	201
	CC5	258	284	201.10	192	811	886	215
	CD1	288	284	189.30	192	811	886	215
	CD2	288	284	189.30	192	811	886	215
	CD3	288	284	189.30	192	835	906	201
	CD4	288	284	189.30	192	811	886	215
	CD5	288	284	189.30	192	811	886	215
	CE1	258	284	201.10	192	635	750	205
	CE2	258	284	201.10	192	635	750	205
	CE3	258	284	201.10	192	766	869	209.40
	CE4	258	284	201.10	192	843	924	207
	CE5	258	284	201.10	192	843	924	207

Appendix C

Geometrical, Mechanical Properties and Test Data for the Column Web specimens

C.1 Geometrical, Mechanical and Experimental Data

The geometrical mechanical properties and experimental data for each column specimen tested are given below in Figures C.1 and Tables C.1-C.3.

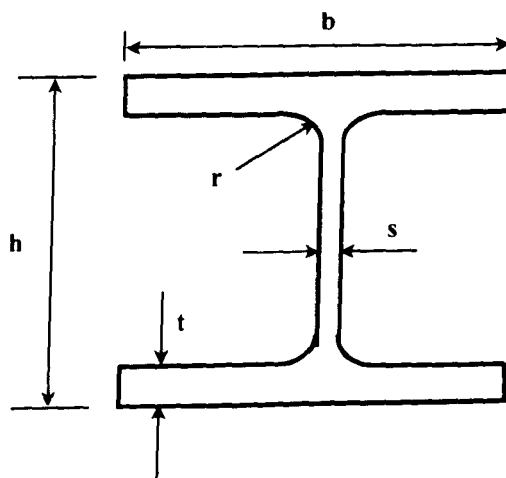
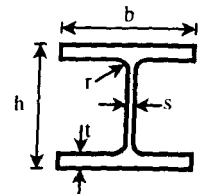


Figure C.1 Universal Column Section

Table C.1 Geometrical Data



Phase	Column Sections	Depth of Section	Width of section	Thickness of Web	Thickness of Flange	Root Radius	Ratio for web local Buckling	Temperature
		h	b	s	t	r		d/s
A	UC152x152x30	159.00	151.61	6.60	8.85	7.60	19.10	20
		160.70	151.60	6.35	9.09	7.60	20.05	410
		156.90	153.75	6.10	9.10	7.60	20.24	500
		157.10	152.40	6.65	8.95	7.60	18.64	500
		158.20	152.05	6.60	8.90	7.60	18.96	600
		158.55	152.01	6.75	9.10	7.60	18.54	610
		159.90	151.60	6.40	9.15	7.60	19.75	710
		160.70	151.75	6.33	9.01	7.60	20.14	755
B	UC203x203x46	203.85	203.58	7.22	11.20	10.20	22.30	20
		204.03	203.54	7.22	11.20	10.20	22.33	280
		203.95	203.39	7.26	11.16	10.20	22.20	400
		202.20	203.41	7.29	11.23	10.20	21.85	520
		203.05	203.66	7.27	11.10	10.20	22.07	610
		202.75	203.50	7.56	11.05	10.20	21.19	670
		203.90	203.51	7.18	11.12	10.20	22.45	765
C	UC203x203x71	216.02	205.62	9.94	17.36	10.20	16.18	20
		215.65	205.24	9.95	17.46	10.20	16.11	535
		215.73	205.21	10.13	17.41	10.20	15.84	635
		215.84	204.74	9.86	17.08	10.20	16.35	755
D	UC203x203x86	223.70	208.47	12.66	19.97	10.20	12.90	20
		223.68	208.58	12.71	20.02	10.20	12.84	20
		223.86	208.52	12.60	20.03	10.20	12.96	585
		223.44	208.52	12.70	20.07	10.20	12.82	650
		223.26	208.46	12.63	20.13	10.20	12.87	705
		223.59	208.43	12.65	20.02	10.20	12.89	750
1	UC203x203x52	210.77	206.02	7.65	12.20	10.20	21.69	610
2	UC203x203x60	212.30	206.15	9.95	13.72	10.20	16.52	20
3	UC203x203x86	223.71	207.54	12.61	19.55	10.20	13.02	20
4	UC254x254x107	267.37	260.34	12.87	20.95	12.70	15.54	20

Table C.2 Mechanical Properties

Phase	Column Sections	Web			Flange		
		Yield Strength	Ultimate Strength	Young Modulus	Yield Strength	Ultimate Strength	Young Modulus
		N/mm ²	N/mm ²	kN/mm ²	N/mm ²	N/mm ²	kN/mm ²
A	UC152x152x30	293	474	233	274	467	227
B	UC203x203x46	301	450	234	275	445	230
C	UC203x203x71	294	500	230	273	481	220
D	UC203x203x86	312	492	225	265	492	220
1	UC203x203x52	365	519	202.10	-	-	-
2	UC203x203x60	304	527	204	-	-	-
3	UC203x203x86	285	501	201.10	-	-	-
4	UC254x254x107	288	488	189.30	-	-	-